

MICROWAVE ELECTRONICS

**INVESTIGATIONS ON A MICROSTRIP EXCITED
RECTANGULAR DIELECTRIC RESONATOR ANTENNA**

A thesis submitted by

MRIDULA.S

in partial fulfilment of the requirements for the degree of

DOCTOR OF PHILOSOPHY

Under the guidance of

Prof.P.Mohanan

DEPARTMENT OF ELECTRONICS

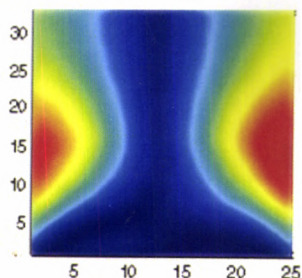
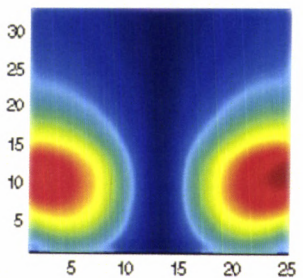
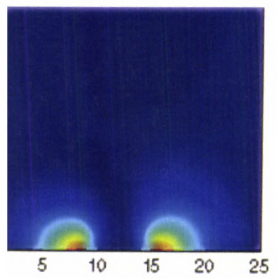
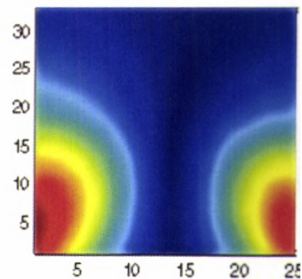
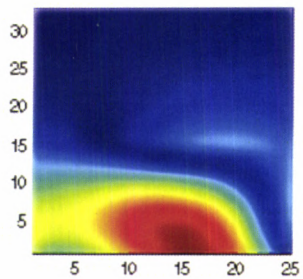
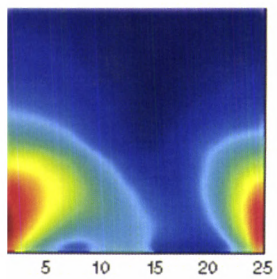
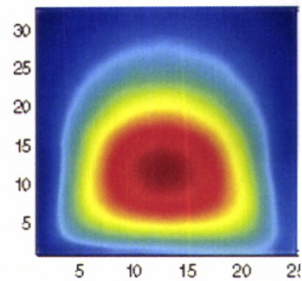
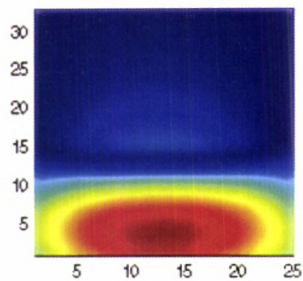
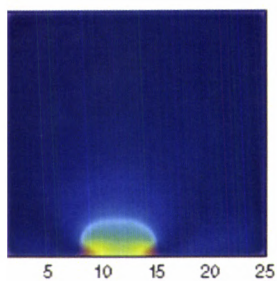
FACULTY OF TECHNOLOGY

COCHIN UNIVERSITY OF SCIENCE AND TECHNOLOGY

KOCHI 682 022, INDIA

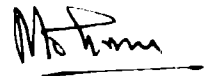
JULY 2005

To The Almighty for helping me sail through....



CERTIFICATE

This is to certify that this thesis entitled "**INVESTIGATIONS ON A MICROSTRIP EXCITED RECTANGULAR DIELECTRIC RESONATOR ANTENNA**" is a bona fide record of the research work carried out by **Smt. Mridula.S** under my supervision in the Department of Electronics, Cochin University of Science and Technology. The results presented in this thesis or parts of it have not been presented for the award of any other degree.



Dr.P.MOHANAN

(Supervising Teacher)

Professor

Department of Electronics

Cochin University of Science and Technology

Kochi - 682 022

7th July 2005

DECLARATION

I hereby declare that the work presented in this thesis entitled **"INVESTIGATIONS ON A MICROSTRIP EXCITED RECTANGULAR DIELECTRIC RESONATOR ANTENNA"** is based on the original research work carried out by me under the supervision of **Dr.P.Mohanan**, in the Department of Electronics, Cochin University of Science and Technology. The results presented in this thesis or parts of it have not been presented for the award of any other degree.

Kochi - 682 022

7th July 2005



MRIDULA.S

ACKNOWLEDGEMENT

I remember with gratitude....

My supervising guide Dr P. Mohanan, Professor, Department of Electronics, Cochin University of Science and Technology for introducing me to the fascinating world of Microwave Antennas. His sincerity, devotion to work and tremendous support has been a steady source of inspiration to me. I was able to persevere, complete the research and deliver this document because of his able guidance. I shall forever cherish the period of my research work under his supervision.

Dr.K.G.Nair, Director, Centre for Science in Society, Cochin University of Science and Technology and former Head, Department of Electronics, Cochin University of Science and Technology for his blessings and good wishes. I gratefully acknowledge his advice while reviewing the thesis.

Prof.K.Vasudevan, Head, Department of Electronics, Cochin University of Science and Technology for his whole-hearted support and for extending the facilities of the Department during my research work.

Prof.C.S.Sridhar, Prof.P.R.S.Pillai and Prof.K.G.Balakrishnan, former Heads, Department of Electronics, Cochin University of Science and Technology for their encouragement.

Prof.K.T.Mathew, Dr.C.K.Aanandan, and other faculty members, Department of Electronics, Cochin University of Science and Technology for their timely advice and cooperation.

Dr.M.T.Sebastian, Scientist, Regional Research Laboratory, Thiruvananthapuram for his generous support and for providing the Dielectric Resonator Samples.

Dr.H.Sreemoolanadhan, Scientist-E, Advanced materials and Ceramics Division, Vikram Sarabhai Space Centre, Thiruvananthapuram and P.V.Bijumon, Senior Research Fellow, Ceramics Technology Division, Regional Research Laboratory, Thiruvananthapuram for preparing the Dielectric Resonator Samples and for the worthy discussions.

Dr.Babu.T.Jose, former Director, Centre for Engineering Studies and Smt. Shoba Cyrus, former Principal, School of Engineering, Cochin University of Science and Technology for helping me achieve my goal by granting study leave from my parent department.

Dr.R.Gopikumari, Head of Division and all my colleagues at the Division of Electronics and Communication Engineering, School of Engineering, Cochin University of Science and Technology for their encouragement.

Dr. Jacob. George, Senior Research Scientist, Corning Inc., Corning, New York for his fervent support and encouragement in my work. The discussions I had with him regarding the intricacies of MATLAB® and its application to the problem were instrumental in developing the source code for the numerical computation.

Mr.Deepukumar.M.Nair, Systems Engineer-Microwave/Millimeter Packaging, Delphi Autosystems, Indianapolis, U.S., for initiating me to HFSS - the powerful simulation software. The simulations included in this thesis were done with his patient help during my visit to the US.

Prof.T.K.Mani and Prof. Mini.M.G, Model Engineering college, Thrikkakara, Prof.V.P.Devassia, Principal, College of Engineering, Chengannur and Dr.Joe.Jacob, Dept of Physics, Newman College, Thodupuzha for their support.

My dear friend Binu Paul, for being there whenever I needed her.

The research scholars, Centre for Research in Electromagnetics and Antennas, Department of Electronics, Cochin University of Science and Technology for their cooperation.

Mr.K.K.Suresh, Librarian, Department of Electronics, Cochin University of Science and Technology for providing me with the necessary reference materials.

The technical and non-technical staff of the Department of Electronics, Cochin University of Science and Technology especially, Mr. P.M. Ibrahimkutty, Mr.C.B.Muraleedharan and Mr. P.P.Russel for their timely help.

My parents and my mother-in-law for their motivation and encouragement.

Hari, Krishna and Rishi for their love, sacrifice and support.

Mridula.S

PREFACE

The new millennium has begun with a revolution in wireless systems that no one imagined a decade ago. Dielectric Antenna solutions for Mobile Telecommunications offer the possibility of drastic size reduction compared to their conventional counterparts. The Dielectric Resonator Antenna (DRA) is a resonant antenna fabricated from a low-loss Microwave dielectric material, the resonant frequency of which is predominantly a function of its size, shape and material permittivity. DRA's are very versatile elements that can be adapted to numerous applications by the appropriate choice of design parameters. Small size, wide bandwidth and absence of conductor losses make them attractive to antenna designers. The DRA is available in various geometrical shapes; the hemispherical, circular cylinder and the rectangular being popular. The greater dimensional degrees of freedom of the rectangular geometry offer better design flexibility to meet impedance and radiation requirements.

The thesis relates to the investigations carried out on Rectangular Dielectric Resonator Antenna configurations suitable for Mobile Communication applications. The main objectives of the research are to:

- numerically compute the radiation characteristics of a Rectangular DRA
- identify the resonant modes
- validate the numerically predicted data through simulation and experiment
- ascertain the influence of the geometrical and material parameters upon the radiation behaviour of the antenna
- develop compact Rectangular DRA configurations suitable for Mobile Communication applications

Although approximate methods exist to compute the resonant frequency of Rectangular DRA's, no rigorous analysis techniques have been developed so far to evaluate the resonant modes. In this thesis a 3D-FDTD (Finite Difference Time Domain) Modeller is developed using MATLAB® for the numerical computation of

the radiation characteristics of the Rectangular DRA. The FDTD method is a powerful yet simple algorithm that involves the discretization and solution of the derivative form of Maxwell's curl equations in the time domain.

The thesis comprises of six chapters. Chapter one serves as an introductory chapter, sketching the important milestones in the history of antennas and their practical applications. The relevance of Dielectric Antenna technology and an overview of Mobile Communication along with various methods of Computational Electromagnetics are explained.

The significant works in the field of Microwave Antennas are reviewed in the Chapter two, with due emphasis on Dielectric Resonator Antennas and the methods employed for their modelling.

Chapter three describes the characteristic features of the Dielectric Resonator (DR), the Dielectric Resonator Antenna (DRA), design constraints, excitation techniques and important applications. The scheme of work and measurement techniques are also explained in this chapter.

The Numerical Computation of the radiation characteristics of the Rectangular DRA is described in Chapter four. The fundamentals of FDTD method and its adaptation to the present problem are explained.

The results of the theoretical and experimental investigations are presented in Chapter five. Discussions on several DRA configurations suitable for wireless applications are also carried out in this chapter.

Chapter six presents the conclusions drawn from the outcome of the Numerical Computation and Experimental Observations. Suggestions for future work in the field are also provided.

The experimental work done by the author in related fields are incorporated as appendices in the thesis. Appendix A describes a compact very high permittivity eye-shaped Dielectric Resonator Antenna for multi-band wireless applications. A Microstrip Antenna with reduced radiation hazards for Mobile telephone handset applications is outlined in Appendix B.

CONTENTS

Chapter 1

INTRODUCTION	1
1.1 Antennas	3
1.2 Dielectric antennas	4
1.3 Antenna applications	6
1.4 Mobile Communication – a glimpse of history	6
1.5 Computational Electromagnetics	10
1.6 Numerical methods for Electromagnetic modelling	11
References	18

Chapter 2

REVIEW OF LITERATURE	25
2.1 Mobile communication handset antennas	27
2.2 Dielectric Resonators – the early years	37
2.3 Dielectric Resonator Antenna Configurations	38
2.4 Numerical analysis of Dielectric Resonator Antennas	49
References	57

Chapter 3

DIELECTRIC RESONATOR ANTENNA	75
3.1 Dielectric Resonator	77
3.2 Material Properties	77
3.3 The Resonance phenomenon	82
3.4 The Rectangular Dielectric Resonator Antenna	86
3.5 Excitation Techniques	88
3.6 Applications	91
3.7 Scheme of work	92
3.8 Measurement techniques	100
References	104

Chapter 4

NUMERICAL COMPUTATION OF THE RADIATION CHARACTERISTICS OF A RECTANGULAR DIELECTRIC RESONATOR ANTENNA 109

4.1	The FDTD method	111
4.2	Discretization in FDTD	112
4.3	Boundary conditions	118
4.4	FDTD code requirements and architecture	123
4.5	Incident field and source modelling	127
4.6	The 3D FDTD modeller of the Rectangular DRA	131
	References	138

Chapter 5

OUTCOME OF NUMERICAL COMPUTATION AND EXPERIMENTAL OBSERVATIONS 141

5.1	Radiation characteristics of the Microstrip line fed Rectangular Dielectric Resonator Antenna incorporating DR-1	143
5.1.1	The b-a-d orientation	144
5.1.1.1	Return Loss Characteristics	145
5.1.1.2	Radiation Pattern	147
5.1.1.3	Polarization	148
5.1.1.4	Gain	148
5.1.1.5	Resonant mode	149
5.1.1.6	Compactness	154
5.1.1.7	Truncated ground plane configuration	154
5.1.1.8	Resonant behaviour at different positions of the DR with respect to the feed	158
5.1.1.9	Characteristics for varying feed lengths	163
5.1.1.10	Resonant behaviour of the DRA when the DR is placed symmetrically with respect to the feed axis	181
5.1.1.11	Salient features of the b-a-d orientation	183
5.1.2	The a-b-d orientation	184
5.1.2.1	Return Loss Characteristics	184
5.1.2.2	Radiation Pattern	186

5.1.2.3	Polarization	187
5.1.2.4	Gain	187
5.1.2.5	Resonant Mode	188
5.1.2.6	Compactness	189
5.1.2.7	Truncated ground plane configuration	189
5.1.2.8	Resonant behaviour at different positions of the DR with respect to the feed	193
5.1.2.9	Characteristics for varying feed lengths	199
5.1.2.10	Resonant behaviour of the DRA when the DR is placed symmetrically with respect to the feed axis	216
5.1.2.11	Salient features of the a-b-d orientation	218
5.1.3	The d-a-b orientation	219
5.1.3.1	Return Loss Characteristics	219
5.1.3.2	Radiation Pattern	220
5.1.3.3	Polarization	221
5.1.3.4	Gain	222
5.1.3.5	Resonant Mode	222
5.1.3.6	Compactness	223
5.1.3.7	Truncated ground plane configuration	224
5.1.3.8	Resonant behaviour at different positions of the DR with respect to the feed	227
5.1.3.9	Characteristics for varying feed lengths	232
5.1.3.10	Resonant behaviour of the DRA when the DR is placed symmetrically with respect to the feed axis	246
5.1.3.11	Salient features of the d-a-b orientation	248
5.1.4	The d-b-a orientation	249
5.1.4.1	Return Loss Characteristics	249
5.1.4.2	Radiation Pattern	252
5.1.4.3	Gain	255
5.1.4.4	Resonant behaviour at different positions of the DR with respect to the feed	257

5.1.4.5	Resonant behaviour of the DRA when the DR is placed symmetrically with respect to the feed axis	260
5.1.4.6	Salient features of the d-b-a orientation	261
5.1.5	The a-d-b orientation	262
5.1.5.1	Return Loss Characteristics	262
5.1.5.2	Radiation Pattern	266
5.1.5.3	Gain	269
5.1.5.4	Resonant behaviour at different positions of the DR with respect to the feed	271
5.1.5.5	Resonant behaviour of the DRA when the DR is placed symmetrically with respect to the feed axis	275
5.1.5.6	Salient features of the a-d-b orientation	276
5.1.6	Performance of the DRA in various orientations of the DR upon the feed line	277
5.2	Radiation Characteristics of the Microstrip line fed Rectangular Dielectric Resonator Antenna incorporating DR-2 & DR-3	282
5.2.1	Return Loss Characteristics	283
5.2.2	Resonant Mode	284
5.2.3	Compactness	286
5.2.4	Radiation Pattern	287
5.2.5	Gain	287
5.3	Radiation Characteristics of the Microstrip line fed Rectangular Dielectric Resonator incorporating DR-3 & DR-4	289
5.3.1	Return Loss Characteristics	289
5.3.2	Resonant Mode	292
5.3.3	Compactness	292
5.3.4	Radiation Pattern	295
5.3.5	Gain	295
5.4	Concluding remarks	297
5.5	Wideband Rectangular Dielectric Resonator Antenna for W-LAN Applications	298

Chapter 6

CONCLUSIONS	301
6.1 Thesis Highlights	303
6.2 Inferences from Numerical Computation using FDTD method	303
6.3 Inferences from Experimental Observations	304
6.4 Salient features of the Microstrip excited Rectangular Dielectric Resonator Antenna	306
6.5 Suggestions for future work	307

Appendix A

A COMPACT VERY HIGH PERMITTIVITY EYE-SHAPED DIELECTRIC RESONATOR ANTENNA FOR MULTIBAND WIRELESS APPLICATIONS	309
---	-----

Appendix B

MICROSTRIP ANTENNA WITH REDUCED RADIATION HAZARDS FOR MOBILE TELEPHONE HANDSET APPLICATIONS	317
--	-----

LIST OF PUBLICATIONS OF THE AUTHOR	323
RESUME OF THE AUTHOR	326
INDEX	329

Chapter 1

Introduction

This chapter serves to explore the history of Antennas and introduce the Dielectric Antenna technology. The practical applications of antennas are discussed and the important milestones in the evolution of Mobile Communication are presented. Various methods of Computational Electromagnetics for the numerical analysis of antennas are explained.

1.1 Antennas

The historic invention of Heinrich Rudolph Hertz in 1886 remained a laboratory curiosity until Guglielmo Marconi of Bologna, Italy, startled the world in mid-December 1901, with his transatlantic transmission. Rarely has an invention captured the public imagination as Marconi's wireless did at the turn of the 20th century [1]. Marconi drew inspiration for his invention from the works of Hertz and the great Indian scientist J.C. Bose, who experimented with the electromagnetic horn antenna in 1897. The *IEEE Standard Definitions of terms for Antennas* (IEEE Std 145-1983) defines the antenna or aerial as "a means for radiating or receiving radio waves". The antenna serves as a connecting link between a radio system and the outside world, launching energy into space as electromagnetic waves or, in the reverse process, extracting energy from an existing electromagnetic field.

A variety of antennas are designed for specific use in the various regions of the electromagnetic spectrum. For many years since Marconi's experiment, antennas operated at low frequencies up to the UHF region and were primarily wire-type antennas (long wires, dipoles, helices, rhombuses, fans, etc.). The demands for effective communication systems during World War II, made the centimetre wavelengths popular and the entire radio spectrum opened up to wide usage. The new entrants were of the aperture type (open-ended waveguides, slots, horns, reflectors, lenses, etc.) and were capable of producing highly directive beams. However the increasing use of radio, particularly the ever-expanding range of cellular, W-LAN, satellite, and other radio communication systems has led to a recent upsurge of interest in new approaches to antenna design. Microstrip radiators developed in the 70's gained popularity by virtue of their lightweight, low profile and structural conformity [2]. The other novel approaches [3-10] include Planar- inverted antennas, antennas based on fractal principles, as well as the use of dielectric materials to enhance performance or even to act as the radiating element itself (dielectric antennas).

1.2 Dielectric antennas

The use of dielectric materials in antennas adds an additional degree of freedom because both the shape and dielectric permittivity are important parameters in trimming the antenna radiation properties [11-18]. The term ‘dielectric antennas’ encompasses different types of technology [19]. A Venn diagram representation of the Dielectric Antenna technology is shown in Figure 1.1.

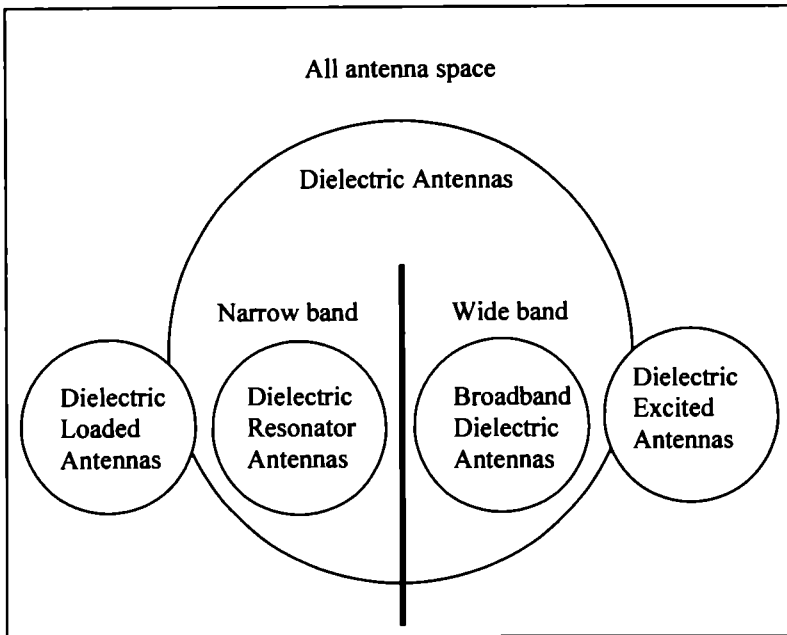


Figure 1.1 Venn diagram representation of dielectric antenna technology

The coupling between closely spaced antennas in an array has components produced by the radiating fields of the element antennas and also by local fields, which only represent the stored energy. In high dielectric antennas, this local field is largely contained within the dielectric, so as their spacing is reduced the coupling between these antennas rises less quickly than for conventional antennas. Therefore, dielectric antennas are often the solution, when there is a need for antennas that do

not easily detune, or when high isolation is required between antennas for radio systems operating at the same frequency but with different protocols [20-25].

◆ **Dielectric loaded antenna**

The primary radiating component in this type of antenna is a conducting element and the dielectric just modifies the medium, imparting important performance advantages [26-30].

◆ **Dielectric Resonator Antenna**

The radiating mechanism in a Dielectric Resonator Antenna (DRA) is a displacement current circulating in a dielectric medium, usually a ceramic pellet. The stored energy inside the dielectric is extremely high and it is difficult for external objects to detune the device [31-33]. Unlike patch antennas they can radiate from all surfaces, rendering high radiation efficiency and low Q factor. Since its birth in the early 1980's, there has been a steady progress of research in this area over the years, as reviewed in Chapter two. The Dielectric Resonator Antenna is described in detail in Chapter three.

◆ **Broadband dielectric antenna**

The bandwidth of a resonant device is a function of its loaded Q, which is controlled by the manner in which energy is coupled into and out of the resonant device and is under the control of the designer. The unloaded Q is a measure of the internal losses in the device. A device with a high unloaded Q may be used to create an antenna structure with low loaded Q and wide impedance bandwidth. Broadband dielectric antennas can be obtained by suitably configuring the feed structure [34-36].

◆ **Dielectric excited antenna**

Dielectric antennas can be used to excite parasitic copper antennas or vice versa. In this class of antennas often the conductor forms the major radiating part of the

antenna. There are bandwidth advantages in this dielectric-copper hybrid approach [37-40].

1.3 Antenna Applications

Antennas enjoy a very large range of applications - both military and commercial. The selection of the type of antenna to be used for a particular application is determined by electrical and mechanical constraints and operating costs, as listed in Table 1.1.

Electrical Parameters	Mechanical Parameters
◆ Frequency of operation	◆ Size
◆ Gain	◆ Feed structure
◆ Polarization	◆ Weight
◆ Radiation pattern	◆ Reliability
◆ Input impedance	◆ Manufacturing Process

Table 1.1 Antenna Design Parameters

The applications in the field of communications and broadcasting are well known to the common man [41]. Today antennas find extensive use in biomedicine, radar, remote sensing, astronomy, collision avoidance, air traffic control, GPS, W-LANs etc., and cover a wide range of frequencies as shown in Table 1.2.

1.4 Mobile Communication – a glimpse of history

Mobile communications are being increasingly integrated into both terrestrial and satellite based radio systems with the impetus being personal voice conversations. The birth of mobile radio generally is accepted to have occurred in 1897, when Marconi was credited with the patent for wireless telegraph [42]. The milestones in the evolution of this ever-growing business [43-44] are listed in Table 1.3.

Band Designation	Frequency Range	Usage
VLF	3 – 30 KHz	Long- distance telegraphy, navigation
LF	30 - 300 KHz	Aeronautical navigation services, long distance communications, radio broadcasting
MF	300 – 3000 KHz	Regional broadcasting, AM radio
HF	3 – 30 MHz	Communications, broadcasting, surveillance, CB radio
VHF	30 – 300 MHz	Surveillance, T V broadcasting, FM radio
UHF	30 – 1000 MHz	Cellular communications
L	1 – 2 GHz	Long range surveillance, remote sensing, Radar
S	2 – 4 GHz	Weather, traffic control, tracking, hyperthermia, Microwave oven, W-LAN, Radar
C	4 – 8 GHz	Weather detection, long-range tracking, Satellite communications
X	8 – 12 GHz	Satellite communications, missile guidance, mapping
Ku	12 – 18 GHz	Satellite communications, altimetry, high resolution mapping
K	18 – 27 GHz	Very high resolution mapping
Ka	27 - 40 GHz	Airport surveillance

Table 1.2 Frequency bands and general usage of Antennas

1921	Radio dispatch service initiated for police cars in Detroit
1934	AM (Amplitude modulation) mobile communications systems used by state and municipal forces in the U.S.
1946	Radiotelephone connections made to PSTN (public-switched telephone network)
1968	Development of the cellular telephony concept at Bell Labs
1980's	<p>1G - First Generation – only mobile voice service – analog technology Ericsson Corporation's NMT (Nordic Mobile Telephone – 450, 900 MHz) in Scandinavian countries becomes the first cellular system fielded</p> <p>Cellular service in the US – AMPS (Advanced Mobile Phone System - 850 MHz) using FM (frequency modulation) – placed in service in Chicago by Ameritech Corporation</p> <p>TACS (Total Access System- 900 MHz band) introduced in Europe & China</p>
1990's	<p>2G - Second Generation digital cellular deployed throughout the world. Mostly for voice service – data delivery possible – digital technology (TDMA, CDMA.– Time/Code Division Multiple Access)</p> <p>The GSM (Global System for Mobile Communications - 900/1800 MHz) becomes the pan-European standard</p> <p>Qualcomm IS-95 (Interim standard-95) CDMA (900 MHz) cellular system gains popularity</p>
2000's	<p>3G - Third Generation (3G) digital systems standardized at the network level to allow world-wide roaming start becoming operational.</p> <p>Mainly for data service, voice service also possible (Wideband-CDMA)</p>

Table 1.3 Mobile Communication – important milestones

Wireless personal communication systems, particularly cellular systems are relatively young applications of communications technology. The frequency bands allotted for the popular wireless communication services are listed in Table 1.4.

WIRELESS COMMUNICATION SERVICE		ALLOTTED FREQUENCY BAND
GPS 1575	Global Positioning System	1565-1585 MHz
GPS 1400		1227-1575 MHz
GSM 900	Global system for mobile communication	890-960 MHz
DCS 1800	Digital communication system	1710-1880 MHz
PCS 1900	Personal Communication System	1850-1990 MHz
UMTS 2000	Universal Mobile Telecommunications Systems	1920-2170 MHz
3G IMT-2000	International Mobile Telecommunications-2000	1885-2200 MHz
ISM 2.4	Industrial, scientific, medical	2400-2484 MHz
ISM 5.2		5150-5350 MHz
ISM 5.8		5725-5825 MHz

Table 1.4 Frequency bands allotted for various wireless communication services

1.5 Computational Electromagnetics

Antenna engineers rely heavily on computer techniques to analyze and help evaluate new designs or design modifications. They have revolutionized the way in which electromagnetic problems are analysed. Computer methods for analysing problems in electromagnetics generally fall into one of the three categories:

i. Analytical techniques

Analytical techniques make simple assumptions about the geometry of a problem in order to apply a closed-form (or table look-up) solution. These techniques can be a useful tool when important electromagnetic (EM) interactions of the configuration can be anticipated. However, most electromagnetic compatibility (EMC) problems of interest are simply too unpredictable to be modelled by this approach.

ii. Expert systems

Expert systems approach a problem in much the same way as a quick-thinking, experienced EM engineer with a calculator would. They do not actually calculate the fields directly, but instead estimate values for the parameters of interest based on a rules database. However, they are no better than their rules database and are seldom used to model the complex EM interactions that cause EMI sources to radiate.

iii. Numerical techniques

Numerical techniques attempt to solve fundamental field equations directly, subject to the boundary constraints posed by the geometry. They are the most powerful EM analysis tools, requiring more computation than the other techniques. They calculate the solution to a problem based on full-wave analysis. A variety of numerical techniques are available. The method used by a particular EM analysis program plays a significant role in determining the nature of problems it can handle and accuracy of results so obtained.

1.6 Numerical methods for Electromagnetic modelling

The main objective of any numerical method for Microwave circuit analysis is to develop an algorithm with minimum effort (in terms of CPU time & memory space), maximum accuracy and flexibility (to model a large variety of structures). Thus the choice of a numerical method is determined by its efficiency, accuracy and flexibility. The choice, however, is also strictly dependent on the problem at hand. No method can be thought of as the best one, but depending on the application, each can have advantages over the others. Referring to Figure 1.2, the EM modelling of Microwave circuits can be viewed as consisting of the following steps:

- * Description of the problem (geometry, electrical parameters, etc.)
- * Excitation of the structure - INPUT
- * Computation of EM field in the structure by solution of Maxwell's equations, applying proper boundary conditions
- * Extraction of terminal parameters – OUTPUT

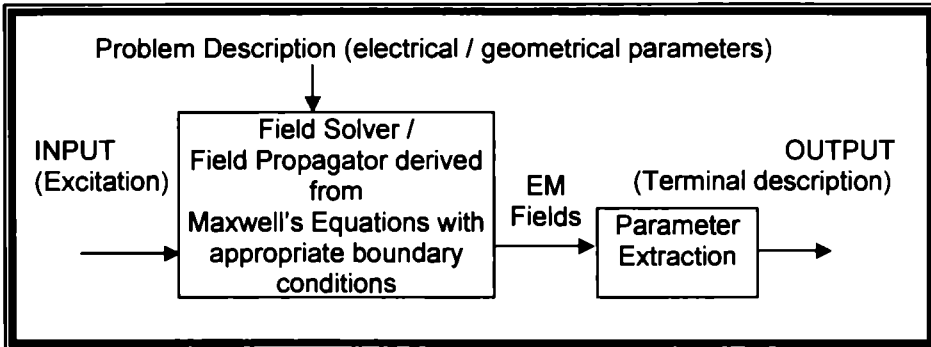


Figure 1.2 Electromagnetic Modelling of Microwave Circuits

The most important stage in EM modelling is the computation of EM fields in the structure by the solution of Maxwell's equations [45]. These equations are linear. But the boundary and interface conditions make it difficult to solve the Maxwell's equations analytically. The numerical methods for the solution of Maxwell's

equations may be classified as shown in Table 1.5. The most commonly used methods in each category are listed in the table.

		Frequency Domain	Time Domain
		Solution of Maxwell's equations	
Integral method	Efficient computational codes. Limited to simple geometries.	MoM (Method of Moments) can be merged to the class of finite element methods	TDIE (Time Domain Integral equation)
Differential method	Highly flexible. Suited for irregular geometry.	FEM (Finite element method) can be used for the solution of integral equations	TLM (Transmission Line Matrix) FDTD (Finite Difference Time Domain)

Table 1.5. Classification of Numerical methods for solving Maxwell's equations

1.6.1 Method of Moments (MoM)

In the mid-1960's, Harrington worked out a systematic, functional-space description of electromagnetic interactions, which he called the '*Method of Moments*'. The MoM is a general method for solving linear operator equations [46]. Here, an integral or integro-differential equation derived from Maxwell's equations for the structure of interest is interpreted as the infinite-dimensional functional equation, $Lf = g$, where L is a linear operator, g is a known function related to the excitation and f is an unknown function such as an induced current distribution that is to be determined. The MoM approach is to set up a numerical solution by representing the unknown function f as a linear combination of a finite set of basis functions f_i in the domain of L . Then, a finite set of weighting functions w_i is defined in the range of L . After taking the inner product (usually integration) of the functional expansion with each weighting function, the linearity of the inner product is used to obtain a finite set of equations for the coefficients of the basis functions. This set of equations is then solved to obtain the approximate or exact solution of f , depending on the choice of the basis and weighting functions. The set of basis functions should have the ability to accurately represent and resemble the anticipated unknown function, while minimizing the computational effort required [47].

In principle, the MoM can be applied to the numerical modelling of arbitrary linear structures. However, this method has limitations primarily governed by the speed and storage capabilities of available digital computers [48]. Using more powerful computers increases the capability of MoM. Another option is to refine the method by choosing proper starting equations, developing flexible basis and weighting functions and using more sophisticated algorithms for the numerical evaluation of integrals encountered in the solution. However, Moment Method techniques based on integral equations are not very effective when applied to arbitrary configurations with complex geometries or inhomogeneous dielectrics. Nevertheless, they do an excellent job of analysing a wide variety of three –

dimensional electromagnetic radiation problem. Historically, the use of basis and testing functions to discretize integral equations of electromagnetics is most often named the '*Method of Moments*'; the same process applied to differential equations is usually known as the '*finite element method*'. However, the term finite element method is reserved for variational methods, explicitly minimising a quadratic functional [49] as explained in the following section.

1.6.2 Finite element method (FEM)

The Finite element method is one of the classic tools of numerical analysis, suitable for the solution of a wide class of partial differential or integral equations. In the mid-1970's Mei, Morgan and Chang introduced the finite-element approach for the Helmholtz equation [46]. Later, in the early 1980's, they shifted their finite element research to direct solutions of Maxwell's curl equations. Finite element techniques require the entire volume of the configuration to be meshed as opposed to surface integral techniques, which require only the surfaces to be meshed. Each mesh element has completely different properties from those of neighbouring elements. In general, finite element techniques excel at modelling complex inhomogeneous configurations. However they do not model unbounded radiation problems as effectively as moment method techniques.

The first step in finite element analysis is to divide the configuration into a number of small homogeneous pieces or *elements*. An example of a finite-element model is shown in Figure 1.3. The model contains information about the device geometry, material constants, excitations and boundary constraints. In each finite element, a simple (often linear) variation of the field quantity is assumed. The corners of the elements are called *nodes*. The goal of the finite-element analysis is to determine the field quantities at the nodes. Generally, finite element analysis techniques solve for the unknown field quantities by minimising an energy functional. The energy functional is an expression describing all the energy associated with the configuration being analysed.

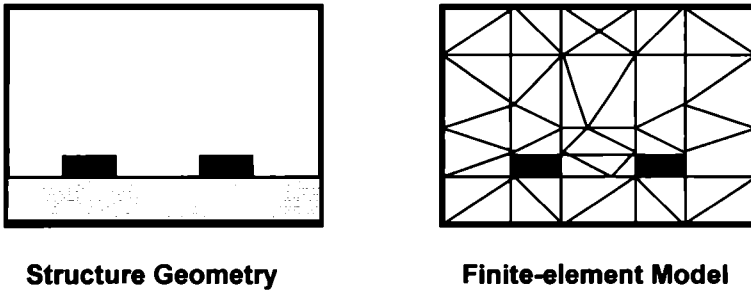


Figure 1.3 Finite-element modelling example

For 3-dimensional time-harmonic problems this functional may be represented as

$$F = \int_v \left(\frac{\mu |H|^2}{2} + \frac{\epsilon |E|^2}{2} - \frac{J \cdot E}{2j\omega} \right) dv \quad (1.1)$$

The first two terms represent the energy stored in the magnetic and electric fields, and the third term is the energy dissipated by the conduction current. Expressing H in terms of E and setting the derivative of this functional with respect to E equal to zero, an equation of the form $f(J, E) = 0$ is obtained. A k^{th} order approximation of the function f is then applied at each node and boundary conditions enforced, resulting in the system of equations,

$$[J] = [Y][E] \quad (1.2)$$

The elements of J are referred to as the source terms, representing the known excitations. The elements of the Y -matrix are functions of the problem geometry and boundary constraints. The elements of the E -matrix represent the unknown electric field at each node, obtained by solving the system of equations. In order to obtain a unique solution, it is necessary to constrain the values of the field at all boundary nodes. For example, the metal box of the model in Figure 1.3 constrains the tangential electric field at all boundary nodes to be zero. Therefore, a major weakness of FEM is that it is relatively difficult to model open configurations. However in finite element methods, the electrical and geometric properties of each element can be defined independently. This permits the problem to be set up with a large number of small

elements in regions of complex geometry and fewer, larger elements in relatively open regions. Thus it is possible to model complicated geometries with many arbitrarily shaped dielectric regions in a relatively efficient manner.

1.6.3 Transmission Line Matrix (TLM) method

In the TLM method, the entire region of the analysis is gridded. A single grid is established and the nodes of this grid are interconnected by virtual transmission lines. Excitations at the source nodes propagate to adjacent nodes through those transmission lines at each time step. Generally, dielectric loading is accomplished by loading nodes with reactive stubs, whose characteristic impedance is appropriate for the amount of loading desired. Lossy media can be modelled by introducing loss into the transmission line equations or by loading the nodes with lossy stubs. Absorbing boundaries are constructed in TLM meshes by terminating each boundary node transmission line with its characteristic impedance. Analysis is performed in the time domain.

TLM method shares the advantages and disadvantages of the FDTD method. Complex, nonlinear materials are readily modelled, impulse responses and time-domain behaviour of the systems are determined explicitly, and the technique is suitable for implementation on massively parallel machines. But, voluminous problems using fine grids require excessive amounts of computation. Nevertheless, both TLM and FDTD techniques are very powerful and widely used. For many types of EM problems, they represent the only practical methods of analysis. Deciding whether to utilize a TLM or FDTD technique is a largely personal decision. Though the TLM method requires significantly more computer memory per node, it generally does a better job of modelling complex boundary geometries. On the other hand, the FDTD method is attractive because of its simple, direct approach to the solution of Maxwell's equations.

1.6.4 Finite Difference Time Domain (FDTD) Method

The Finite Difference Time Domain (FDTD) method introduced by K.S.Yee in 1966 [50] and later developed by Taflove [51] in the 1970's permits in principle, the modelling of electromagnetic wave interactions with a level of detail as high as that of the Method of Moments. Unlike MoM, however, the FDTD does not lead to a system of linear equations defined over the entire problem space. Updating each field component requires knowledge of only the immediately adjacent field components calculated one-half time step earlier. Therefore, overall computer storage and running time requirements for FDTD are linearly proportional to N , the number of field unknowns in the finite volume of space being modelled. The FDTD method has thus emerged as a viable alternative to the conventional Frequency Domain methods because of its dimensionally reduced computational burdens and ability to directly simulate the dynamics of wave propagation [52-58]. The survey paper by Shlager and Schneider illustrates the rapid growth of FDTD [59]. Chapter four describes in detail the FDTD method employed for the numerical computation of the radiation characteristics of the Rectangular Dielectric Resonator Antenna in the present work.

REFERENCES

-
1. John.D.Kraus, "Antennas since Hertz and Marconi," *IEEE Trans. Antennas Propagat.*, vol.33, no.2, pp.131-136, February 1985.
 2. David.M.Pozar, "Microstrip Antennas," *Proc. IEEE*, vol.80, no.1, pp.79-91, January 1992.
 3. A.Ittipiboon, R.K.Mongia, Y.M.M.Antar, P.Bhartia and M.Cuhaci, "Aperture-fed rectangular and triangular dielectric resonators for use as magnetic dipole antennas," *Electron.Lett.*, vol.29, no.23, pp.2001-2002, 11 November 1993.
 4. G.Vermeeren, H.Rogier, F.Olyslager and D.De Zutter, "Low-cost planar rectangular ring antenna for operation in HiperLAN band," *Electron.Lett.*, vol.38, no.5, pp.208-209, 28 February 2002.
 5. Kin-Lu Wong, Saou-Wen Su, Tzung-Wern Chou and Yeh-Chian Lin, "Dual-band plastic chip antenna for GSM/DCS Mobile phones," *Microwave Opt. Technol Lett.*, vol.33, no.5, pp.330-332, 5 June 2002.
 6. Jeemyun Lee, Chanik Jeon, Bomson Lee, "Design of ceramic chip antenna for Bluetooth applications using Meander Lines," *Proc. IEEE Antennas Propagat. Soc. Int. Symp.*, San Antonio, Texas, pp. 68-71, June 2002.
 7. Chi-Fang Huang and Li Chen, "Realisation of printed-on display antenna for mobile terminals," *Electron. Lett.*, vol.38, no.20, pp.1162-1163, 26 September 2002.
 8. Gwo-Yun Lee, Wen-Shyang Chen and Kin-Lu Wong, "A dual-frequency triangular chip antenna for WLAN operation," *Microwave Opt. Technol. Lett.*, vol.38, no.3, pp.244-247, 5 August 2003.
 9. Jung-Ick Moon and Seong-Ook Park, "Small chip dielectric antenna for Bluetooth application," *Microwave Opt. Technol. Lett.*, vol.39, no.5, pp.366-368, 5 December 2003.
 10. Shoichiro Hirai, Naoya Arakawa, Takahiro Ueno, Hiroki Hamada and Koichi Kamei, "A chip antenna for CDMA One Mobile phones," *Furukawa Review*, no.25, pp.28-31, 2004.
 11. J.C.Sethares and S.J.Naumann, "Design of microwave dielectric resonators," *IEEE Trans. Microwave Theory Tech.*, vol.14, no.1, pp.2-7, January 1966.

12. P.Guillon and Yves Garault, "Accurate resonant frequencies of dielectric resonators," *IEEE Trans. Microwave Theory Tech.*, vol. 25, no.11, pp.916-922, November 1977.
13. J.F.Legier, P.Kennis, S.Toutian and J. Citerne, "Resonant frequencies of rectangular dielectric resonators," *IEEE Trans. Microwave Theory Tech.*, vol.28, no.9, pp.1031-1034, September 1980.
14. D. Singh and G. B. Morgan, "Higher mode resonances of high permittivity square cuboid dielectric resonators on integrated circuit substrates," *Proc.IEE.* vol.134, no.6, December 1987.
15. R.K.Mongia, A.Ittipiboon, M.Cuhaci and D.Roscoe, "Radiation Q-Factor of rectangular dielectric resonator antennas : Theory and experiment," *Proc. IEEE Antennas Propagat. Soc. Int. Symp.*, Seattle, WA, pp.764-767, June 1994.
16. M.H.Neshati and Z.Wu, "The determination of the resonant frequency of the TE_{111}^y mode in a rectangular dielectric resonator for antenna application," *11th International conference on Antennas and Propagation (IEE)*, pp.53-56, 17-20 April 2001.
17. M.H.Neshati and Z.Wu, "Rectangular dielectric resonator antennas: theoretical modelling and experiments," *11th International conference on Antennas and Propagation (IEE)*, pp.866-870, 17-20 April 2001.
18. M. W. McAllister, S. A. Long and G. L. Conway, "Rectangular Dielectric Resonator Antenna," *Electron. Lett.*, vol.19, no.6, pp.218-219, 17 March 1983.
19. URL: <http://www.antenova.com/media/news/Technology>
20. G.Drossos, Z.Wu and L.E.Davis, "Two-element end-fire dielectric resonator antenna array," *Electron. Lett.*, vol.32, no.7, pp.618-619, 28 March 1996.
21. M.G.Keller, M.B.Oliver, D.J.Roscoe, R.K.Mongia, Y.M.M.Antar and A.Ittipiboon, "EHF dielectric resonator antenna array," *Microwave Opt. Technol. Lett.*, vol.17, no.6, pp.345-349, 20 April 1998.
22. Jung-Ick Moon and Seong-Ook Park, "Dielectric resonator antenna for dual-band PCS/IMT-2000," *Electron. Lett.*, vol.36, no.12, pp.1002-1003, 8 June 2000.
23. K.K.Pang, H.Y.Lo, K.W.Leung, K.M.Luk and E.K.N.Yung, "Circularly polarized dielectric resonator antenna subarrays," *Microwave Opt. Technol. Lett.*, vol.27, no.6, pp.377-379, 20 December 2000.

24. Guido Biffi Gentili, Marco Morini and Stefano Selleri, "Relevance of coupling effects on DRA array design," *IEEE Trans. Antennas Propagat.*, vol.51, no.3, pp.399-404, March 2003.
25. D.Cormos, A.Laisne, R.Gillard, F.Le. Bolzer and C.Nicolas, "Compact dielectric resonator antenna for WLAN applications," *Electron. Lett.*, vol.39, no.7, pp.588-590, 3 April 2003.
26. Jacob George, C.K.Aanandan, P.Mohanan, K.G.Nair, H.Sreemoolanadhan and M.T.Sebastian, "Dielectric resonator loaded Microstrip antenna for enhanced impedance bandwidth and efficiency," *Microwave Opt. Technol Lett.*, vol.17, no.3, pp.205-207, 20 February 1998.
27. I.Ida, J.Sato, H.Yoshimura and K.Ito, "Improvement in efficiency-bandwidth product in small dielectric loaded antennas," *Electron. Lett.*, vol.36, no.10, pp.861-862, 11 May 2000.
28. P.V.Bijumon, Sreedevi.K.Menon, M.T.Sebastian and P.Mohanan, "Enhanced bandwidth Microstrip patch antennas loaded with high permittivity dielectric resonators," *Microwave Opt. Technol. Lett.*, vol.35, no.4, pp.327-330, 20 November 2002.
29. Vijay Gupta, Sumit Sinha, Shibani.K.Koul and Bharati Bhat, "Wideband dielectric resonator loaded suspended Microstrip patch antennas," *Microwave Opt. Technol. Lett.*, vol.37, no.4, pp.300-302, 20 May 2003.
30. Marc Lapierre, Yahia.M.M.Antar, A.Ittipiboon and A.Petosa, "A wideband monopole antenna using dielectric resonator loading," *Proc. IEEE Antennas Propagat. Soc. Int. Symp.*, Columbus, Ohio, pp.16-19, June 2003.
31. Aldo Petosa, Neil Simons, Riaz Siushansian, Apisal Ittipiboon and Michel Cuhaci, "Design and analysis of multisegment dielectric resonator antennas," *IEEE Trans. Antennas Propagat.*, vol.48, no.5, pp.738-742, May 2000.
32. M.T.Lee, K.M.Luk, K.W.Leung and M.K.Leung, "A small Dielectric Resonator Antenna," *IEEE Trans. Antennas Propagat.*, vol.50, no.10, pp.1485-1487, October 2002.
33. Tayeb A.Denidni, Qinjiang Rao and Abdel R.Sebak, "Multi-eccentric ring slot fed dielectric resonator antenna for multi-frequency operations," *IEEE Antennas Propagat. Soc. Int. Symp.*, Monterrey, CA, June 2004.

34. A.Ittipiboon, A.Petosa, D.Roscoe and M.Cuhaci, "An investigation of a novel broadband dielectric resonator antenna," *IEEE International Symposium on Antennas and Propagation Digest*, pp.2038-2041, Baltimore, MA, July 1996.
35. K.W.Leung, K.M.Luk, K.Y.Chow and E.K.N Yung, "Bandwidth enhancement of dielectric resonator antenna by loading a low profile dielectric disk of very high permittivity," *Electron. Lett.*, vol.33, no.9, pp.725-726, 24 April 1997.
36. R.Chair, A.A.Kishk, K.F,lee and C.E.Smith, "Broadband aperture coupled flipped staired pyramid and conical dielectric resonator antennas," *IEEE Antennas Propagat. Soc. Int. Symp.*, Monterrey, CA, June 2004.
37. Z.Fan, Y.M.M.Antar, A.Ittipiboon and A.Petosa, "Parasitic coplanar three-element dielectric resonator antenna subarray," *Electron. Lett.*, vol.32, no.9, pp.789-790, 25 April 1996.
38. Karu P.Esselle, "A dielectric-resonator-on-patch (DROP) antenna for broadband wireless applications: concept and results," *Proc. IEEE Antennas Propagat. Soc. Int. Symp.* Boston, USA, pp.22-25, June 2001.
39. Karu.P.Esselle and Trevor.S.Bird, "Hybrid resonator antennas for broadband wireless applications," *XXVIIth URSI GA*, Maastricht, Netherlands, 17-24 August 2002.
40. Bin Li, Hoi Kuen Ng and Kwok Wa Leung, "A circularly polarized dielectric resonator antenna with a parasitic patch," *IEEE Antennas Propagat. Soc. Int. Symp.*, Monterrey, CA, June 2004.
41. Christos G.Christodoulou, Parveen F.Wahid, "*Fundamentals of Antennas: Concepts and Applications*," Prentice-Hall of India, 2004.
42. Andy D Kucar, "Mobile Radio: An overview," *IEEE Communications Magazine*, pp.72-85, November 1991.
43. Bernard Sklar, "Digital Communications – Fundamentals and Applications," Pearson Education Asia, 2nd edition 2003.
44. 'Cordless Communications in Europe', Ed.Wally H.W.Tuttlebee, Springer-Verlag London Limited, pp.144-148, 1990.
45. Roberto Sorrentino, "Modelling and Design of Millimetrewave passive circuits: from 2 to 3D," *Proc. 24th European Microwave conference*, September 1994.
46. Korada Umashankar and Allen Taflove, "Computational Electromagnetics," Artech House; Norwood, MA, 1993.

47. Constantine A. Balanis, "Advanced Engineering Electromagnetics," John Wiley and Sons, USA, 1989.
48. Branko M. Kolundzija and Antonije R. Djordjevic, "Electromagnetic modelling of composite metallic and dielectric structures," Artech House, Inc., Norwood, MA, 2002.
49. Andrew.F.Peterson, Scott L Ray and Raj Mittra, "Computational methods for electromagnetics," Universities Press, India, 2001.
50. K.S.Yee, "Numerical solution of initial boundary value problems involving Maxwell's equations in isotropic media," *IEEE Trans. Antennas Propagat.*, vol.14, no.4, pp.302-307, May 1966.
51. Allen.Taflove, "Numerical issues regarding finite-difference time-domain modelling of Microwave structures," *Time-Domain Methods for Microwave structures – Analysis and Design*, Ed.Tatsuo Itoh and Bijan Houshmand, *IEEE Press*.
52. Allen Taflove and Morris E. Brodwin, "Numerical solution of steady –state electromagnetic scattering problems using the time-dependent Maxwell's equations," *IEEE Trans. Microwave Theory Tech.*, vol.23, pp.623-630, August 1975.
53. Ying Shen, Zhiqiang Bi, Keli Wu and John Litva, "FD-TD analysis of open cylindrical dielectric resonators," *Microwave Opt. Technol Lett.*, vol.5, no.6, pp.261-265, 5 June 1992.
54. S.M.Shum and K.M.Luk, "Characteristics of dielectric ring resonator antenna with an air gap" *Electron. Lett.*, vol.30, no.4, pp. 277-278, 17 February 1994.
55. Jaakko Juntunen, Outi Kivekas, Jani Ollikainen and Pertti Vainikainen, "FDTD Simulation of a wide-band half volume DRA," *IEEE Antennas Propagat. Soc. Int. Symp.*, Salt lake city, Ohio pp.223-226, June 2000.
56. Elena Semouchkina, Wenwu Cao, Michael Lanagan, Raj Mittra and Wenhua Yu, "Combining FDTD simulations with measurements of Microstrip ring resonators for characterization of low and high K dielectrics at microwaves," *Microwave Opt. Technol Lett.*, vol.29, no.1, pp.21-24, 5 April 2001.
57. Elena Semouchkina, George Semouchkin, Raj Mittra and Wenwu Cao, "Finite-Difference Time-Domain simulation of resonant modes of rectangular dielectric resonators," *Microwave Opt. Technol.Lett.*, vol.36, no.3, pp.160-164, 5 February 2003.

58. Takashi Ando, Junji Yamauchi and Hisamatsu Nakano, "Numerical analysis of a dielectric rod antenna-demonstration of the discontinuity-radiation concept," *IEEE Trans. Antennas Propagat.*, vol.51, no.8, pp. 2007-2013, August 2003.
59. Kurt L.Shlager and John B.Schneider, "A selective survey of the Finite-Difference Time-Domain literature," *IEEE Antennas Propagat. Mag.*, vol.37, no.4, pp.39-57, August 1995.

Chapter 2

Review of Literature

Recent advances in 3G Mobile Communication systems, wireless LAN, etc. demand broadband capabilities in high mobility environments. High data rate, and spectral efficiencies necessitate stringent requirements like small size, lightweight, large bandwidth, high efficiency, reconfigurability, etc. This has motivated scientists all over the world to develop compact, broadband, high efficiency antennas. Over the last decade, research has fast advanced with the development of novel versatile Dielectric Resonator Antenna elements, which can be adapted to numerous applications by appropriate choice of the design parameters.

The relevant works in the field of Microwave antennas are reviewed in this chapter, with due emphasis on Dielectric Resonator Antennas and the methods employed for their modelling.

2.1 Mobile Communication handset antennas

A major trend in Mobile Communication technology is the dramatic reduction in the size and weight of handsets. Common requirements on the antenna design regardless of the frequency include low cost, low profile, and in most applications, a large operating bandwidth. Antenna designers are therefore encountered with the difficulty of designing compact, multi-band, highly efficient antennas. Some of the typical antenna elements used for small mobile terminals are the monopole, the dipole, the normal mode helix, the planar inverted-F, the Microstrip, the meander line, the ceramic and the chip antenna. Although whip antennas are inexpensive and mechanically simple, they are easily prone to damage. Helical antennas are relatively inexpensive and exhibit wide bandwidth performance, but are not low profile. Mechanical resistance, aesthetic criteria and the need for high performance antennas are the key points that have brought internal antennas into the spot light. In the existing built-in antenna schemes, much attention has been paid to Microstrip antennas. However, they suffer from inherent bandwidth limitations and their physical size becomes large at low frequencies. Dielectric Resonator Antennas present a better alternative because of their relatively large bandwidth and compact size. A chronological review of the work done in the field of Mobile communication handset antennas is presented in the beginning of the chapter. The progress in the DRA research is outlined in the next section.

Fuhl.J *et al.* [1] analysed the performance of a radiation coupled Dual L antenna, placed on the back side of the metallic housing of the handset, resulting in a radiation pattern pointing away from the user's head. The antenna was designed for operation in the GSM 900 frequency band.

Z.D.Liu and P.S.Hall [2] proposed a dual-band Planar Inverted – F Antenna (PIFA) for hand held portable telephones to operate at 0.9 GHz and 1.8 GHz. The compact antenna displayed omni-directional radiation patterns and 7% and 6.25% impedance bandwidths respectively in the two bands.

J.C.Batchelor and R.J.Langley [3] carried out an investigation into narrow annular Microstrip slot antennas excited in a higher order mode, so as to give circularly polarized, conical radiation pattern at 7.1 GHz.

G.T.Pedersen *et al.* [4] discussed the development of a single integrated PIFA and diversity antenna configurations with low absorption. FDTD analysis of the antenna was performed including the head, and measurements of angular information in the environment were made. Their study highlighted the fact that a significant amount of shielding could be achieved by the case of the handset.

Y.J. Guo *et al.* [5] reported a TM_{02} circular patch antenna operating at 5.2 GHz. The antenna exhibited 3.3% bandwidth, 4.2 dB gain and a circularly symmetrical pattern with a notch in the zenith direction, suitable for radio LAN's.

K.Takei *et al.* [6] proposed a 3 layered TEM slot antenna for personal handy - phone terminal. The antenna exhibited one sided radiation pattern, resulting in high antenna gain and low electromagnetic hazard to the user and possessing a conventional surface mounting technology application capability, resulting in reduced fabrication cost.

Corbett R.Rowell *et al.* [7] investigated the feasibility of utilizing a PIFA with a capacitive load to reduce the overall length from $\lambda/4$ to less than $\lambda/8$ for a mobile telephone handset suitable for DCS 1800. They also proposed a design methodology for capacitively loaded PIFA's.

Hiroyuki Arai *et al.* [8] measured the variation in antenna gain of handheld terminals for different terminal boxes and different human carriers. A $\lambda/4$ whip antenna mounted on a conducting box was used for the study.

A compact printed antenna consisting of an annular ring coupled to a shorted circular patch was proposed by R.B.Waterhouse [9]. The antenna provided ~10% bandwidth.

Kathleen.L.Virga and Yahya Rahmat- Samii [10] discussed the development of low profile integrated antennas with enhanced bandwidth performance. The Planar Inverted F Antenna (PIFA), Radiation coupled dual L antenna and the diode tunable

PIFA were considered for use in the 900 MHz band. Up to 9.6%, 16% and 50% bandwidth respectively was obtained for the three antennas.

A.Serrano-Vaello and D.Sanchez-Hernandez [11] demonstrated a dual band bow-tie antenna with impressive size reduction compared to conventional patch antennas. The radiation characteristics of this antenna for dual-band GSM/DCS 1800 mobile handsets were similar to conventional Microstrip patches.

C.L.Mak *et al.* [12] presented the design and experimental results of a proximity-coupled U-slot patch antenna excited by a π shaped feed line connected at the end of the usual microstrip line. The antenna displayed 20% bandwidth at 4.3 GHz, 7.5 dBi average gain and -20 dB cross-polarisation.

Ch.Dalaveaud *et al.* [13] proposed a monopolar wire-patch antenna for portable telephones. The antenna operating at 1.8 GHz was characterized by a monopolar type radiation, a wide frequency band-pass and a small-sized flat plate physical configuration.

Corbett R. Rowell and R. D. Murch [14] described the design of a compact Planar Inverted-F Antenna (PIFA) suitable for cellular and PCS operation. The frequency of the conventional PIFA designed at 2.2 GHz was brought down to 900 MHz by the introduction of a shorting post, capacitor load and a slot cut on the top plate. By removing part of the top plate and inserting another PIFA, a dual fed, dual band antenna resonating at 900 and 1800 MHz was also constructed.

Reflectively coupled dipole configuration with strongly improved radiation efficiency was proposed by Roger Yew-Siow Tay *et al.* [15]. They demonstrated that reduction of the magnetic field strength at the surface of the user's head was the key parameter to improve the efficiency of the transmitter.

H.Iwasaki [16] proposed a Microstrip antenna with back-to-back configuration relative to a slot on a ground plane, for use in base station / portable telephones. The input impedance and radiation pattern were measured as parameters of the slot length. It was observed that an omni-directional or bi-directional radiation

pattern could be obtained by feeding the antenna in phase or out of phase respectively.

O. Leisten *et al.* [17] described a dielectric loaded twisted loop antenna, which projected a magnetic field minimum and a radiated far field minimum towards the head. SAR measurements of the proposed antenna were performed using the DASY3 - the enhanced version of the dosimetric system.

R.B.Waterhouse [18] presented a loaded cavity backed patch antenna for PCS Network operating at 1.9 GHz, which could be easily integrated within a handset terminal. The observed radiation patterns were similar to a conventional shorted patch mounted on a large ground plane.

K.Hettak *et al.* [19] presented the design and experimental results of a coplanar waveguide (CPW) aperture coupled patch antenna for EHF band around 37 GHz. The antenna structure combined the advantages of CPW with those of aperture coupled Microstrip Antennas and also reduced the no: of metallization levels.

N.Chiba *et al.* [20] proposed a compact dual band internal antenna fed by a single feed, designed for the 900/1800 MHz band. The antenna comprised of an outer $\lambda/4$ annular ring antenna with a short circuited plane and an inner $\lambda/4$ rectangular patch antenna, designed for the lower and higher resonant frequency respectively. The radiation patterns of the antenna were shown to be almost similar to that of a conventional $\lambda/4$ microstrip antenna with a short-circuited plane.

J. Ollikainen *et al.* [21] demonstrated a stacked, shorted patch antenna resonating at 900/1800 MHz. The small size, low profile antenna with 9% impedance bandwidth was found to be suitable for directive, internal cellular handset antenna applications.

Jack.T.Rowley and Rod.B.Waterhouse [22] compared the performance of a single shorted patch and a stacked shorted patch antenna at 1800 MHz with that of a $\lambda/4$ monopole. Experimental and simulation results were presented for each of the antennas, in 3 different cases: on a handset in isolation, a handset near the realistic head model, and with the inclusion of a block model of the hand.

C.T.P.Song *et al.* [23] presented a novel method for improving the design of a circular disc monopole by introducing a discontinuity effect resulting in multiple loop monopole. Better control of the radiation pattern beyond a frequency ratio of 1:5.33 was demonstrated.

A compact circularly polarised printed antenna was proposed by H.Kan and R.B.Waterhouse [24]. The antenna consisted of a synchronous subarray of shorted patches with the required feed network etched on a high dielectric constant substrate located below the ground plane of the antenna. The antenna displayed 10 dB return loss bandwidth of 8.5% and 3 dB axial ratio bandwidth of 11.3%.

An antenna configuration incorporating one shorted driven patch and another shorted and coupled coplanar patch using a single probe feed to achieve broadband characteristics (up to 25% bandwidth) was proposed by Ya Jun Wang *et al.* [25] for use in IMT 2000 handsets. The patches were either rectangular or semicircular and 8 different combinations were used.

Marta Martínez-Vazquez, and her team of researchers [26] reported a compact dual-band antenna consisting of a shorted rectangular patch designed for 1.8 GHz. A spur-line filter embedded in its perimeter introduced a new resonance at 925 MHz.

Hassan M.Elkamchouchi and Hossam El-dien M.Hafez [27] presented the detailed investigations using the Moment Method on a single layer multi-probe fed patch antenna. The antenna consisted of a hexagonal plate with unequal arms, suspended parallel to the ground plane. Up to 35% impedance bandwidth and stable radiation patterns throughout the band was observed.

Tsung-Wen Chiu *et al.* [28] proposed a Microstrip line fed circularly polarized ceramic chip antenna for GPS operation at 1575 MHz. The antenna comprised of a square radiating patch printed on the top surface of a grounded square disk ceramic chip having two side feeds printed at the centres of the two adjacent side surfaces of the ceramic chip ($\epsilon_r = 45$) to excite the antenna through capacitive coupling. A connection metal line printed between the two side feeds served to

provide the 90° phase difference. 12 MHz impedance bandwidth, 3.5 MHz 3 dB axial ratio bandwidth and 3.4 dBi gain was obtained.

Zhizhang Chen *et al.* [29] described a novel tuning technique that allows independent tuning of the two frequency bands of an integrated antenna for GPS/PCS dual-band application.

Will Mckinzie *et al.* [30] presented a miniature Bluetooth antenna known as a DC inductive shorted patch antenna (DSPA), fabricated as a single layer flex circuit wrapped around a high temperature foam substrate. A new packaging concept in which the antenna contains an embedded Bluetooth radio MCM (multi chip module) was also introduced. Peak antenna efficiency of 47% was observed.

A compact Planar Inverted – F Patch Antenna with two shorted branch strips, sharing a common shorting pin and fed by the same feed for triple-frequency operation at 900, 1800 and 2450 MHz was presented by Fu-Ren Hsiao and Kin-Lu Wong [31]. Ansoft HFSS (High Frequency Structure Simulator) was used to obtain the design parameters. The three operating bands exhibited an impedance bandwidth of 1.9%, 4.8% and 2.9% respectively. The antenna possessed radiation characteristics acceptable for practical wireless communication applications.

C.W.Chiu and F.L.Lin [32] presented a design for a compact dual band PIFA with multiresonators for use in GSM/DCS band. The nearly omni-directional patterns and the impedance bandwidth obtained indicated the usefulness in mobile phone devices.

Gwo-yun Lee and Kin-Lu Wong [33] proposed a very low profile antenna for GSM / DCS dual-band mobile phone applications, by inserting several slits into a rectangular planar monopole and further bending it into two equal and perpendicular sections. The obtained radiation patterns were stable across the operating bands – (837-994 MHz) and (1705-1936 MHz).

Yongjin Kim and Sangseol Lee [34] designed and fabricated a Planar Inverted F Antenna with the rectangular planar element replaced by an L shaped element to increase the spatial efficiency. IE3D software was employed to obtain the

various optimal design parameters. The antenna exhibited an impedance bandwidth of 580 MHz and good radiation characteristics for wireless LAN applications centered at 5.25 GHz.

Hisashi Morishita, Yongho Kim and Kyohei Fujimoto [35] described in detail the design concept of antennas for small mobile terminals. The future perspective for the antenna structure was also discussed.

Hyun Jun Kim *et al.* [36] presented a small-chip Meander antenna for dual frequency operation. The frequency ratio of the proposed antenna was 1.35 and it offered more than 50% size reduction compared to the rectangular patch.

Han-Cheol Ryu *et al.* [37] described the design, fabrication and testing of a triple-stacked Microstrip patch antenna consisting of three patches for use in cellular phone/GPS/PCS centred at 0.83, 1.575 and 1.7 GHz.

Marc. C. Greenberg *et al.* [38] presented the far field radiation pattern characteristics of the dual exponentially tapered slot antenna (DE TSA) for wireless communications applications. The low profile antenna had slotline conductors tapered along the outer edge. The obtained radiation patterns remained fairly constant over a broad range of frequencies, indicating the suitability for multifunction applications.

Gwo-Yun Lee *et al.* [39] presented a low cost surface-mount monopole antenna for GSM / DCS dual band operation by folding a metallic strip onto a foam base. The antenna was mounted on a FR4 substrate and fed by a 50Ω Microstrip line. The broad impedance bandwidths and radiation patterns confirmed the suitability of the antenna for Mobile Communications applications.

Kin-Lu Wong *et al.* [40] proposed a diversity antenna comprising of two back-to-back PIFA's, with their shorting pins facing each other. The antenna showed 186 MHz bandwidth, less than -22.5 dB isolation and good gain at 2.4 GHz.

Yong-Xin Guo *et al.* [41] proposed a compact internal antenna for quad band operation at the GSM 900, DCS 1800, PCS 1900 and ISM 2450 band. The antenna comprised of a main plate in the top layer, a ground plane in the bottom layer, two folded arms in-between, a short circuited strip and a feed strip, the entire structure

supported by foam. The measured -6 dB return loss was 68 MHz, 260 MHz and 130 MHz respectively in the three bands and the patterns were all omni-directional. The experimental results were compared with the simulation results performed using XFDTD 5.3.

A ceramic chip antenna for 2.4 /5.8 GHz dual ISM band applications was proposed by Jung-Ick Moon and Seong-Ook Park [42]. The antenna comprised of a small ceramic dielectric alumina ($\epsilon_r=7.7$) placed at the corner of the substrate through surface mount process and two metal layers forming meander lines, printed on the top and bottom faces of the substrate. The antenna exhibited $\sim 12\%$ bandwidth and radiation patterns similar to that of a monopole antenna.

Shih-Huang Yeh *et al.* [43] presented a compact, dual band, internal antenna suitable for GSM/DCS applications. The antenna had 3 resonant elements; 2 meandered metallic strips and a nearly rectangular patch leading to 2 resonant modes in the lower band (890-960 MHz) and 3 resonant modes in the upper band (1710-1880 MHz), covering the entire GSM and DCS bands.

Triple-frequency annular-ring slot antennas operating at 1.74, 2.38 and 3.12 GHz for CPW-fed and 1.8, 2.38 and 2.91 GHz for Microstrip line-fed were proposed by Jin-Sen Chen [44]. It was observed that by controlling the circumference of the annular-ring slot of the proposed antenna, proper operating frequency could be obtained.

A compact antenna design for 900/1800-MHz Cellular Systems was proposed by Tzung-Wern Chiou and Kin-Lu Wong [45]. The antenna comprised of a rectangular ring patch (900 MHz) and a notched rectangular patch (1800 MHz) printed on the same layer and aperture coupled by a properly designed feed network. The antenna exhibited 10% impedance bandwidth in both bands and high isolation between the two feeding ports.

Christian Sabatier [46] described the use of T-Dipole arrays for mobile base stations in the different frequency bands for GSM, UMTS, HIPERLAN, etc. Low side

lobes and low coupling between two orthogonal polarizations were the characteristic features.

Qwo-Yun Lee *et al.* [47] proposed a planar folded-dipole antenna for spatial diversity in 5 GHz WLAN operations. The antenna comprised of two back-to-back folded dipoles separated by a central ground plane. Wide impedance bandwidth of about 1 GHz covering the 5.2 and 5.8 GHz bands, and good directional radiation pattern covering the two complementary half spaces was observed.

Chien-Jen Wang and Wen-Tsai Tsai [48] demonstrated a triple band microstrip-fed stair-shaped slot antenna operating at 2.4, 5.2 and 5.8 GHz. 9.45% and 15.5% impedance bandwidths were obtained in the 2.4 GHz and 5 GHz bands respectively.

Yeh-Chian Lin *et al.* [49] proposed a 50Ω grounded coplanar waveguide excited circularly polarized antenna for GPS application at 1575 MHz, mainly consisting of a cross-slot loaded square patch printed on the top surface of a grounded square-disk ceramic chip [$\epsilon_r = 90$], and a single side-feed printed on the side surface of the ceramic chip.

D.S.Yim *et al.* [50] proposed a broadband, small, chip antenna with a branch structure meander line, suitable for Korean PCS (1750-1870 MHz) and IMT-2000 (1930-2170 MHz) dual bands. The conductor strip-line patterns were printed on the top and bottom layers of the substrate chip, and connected with each other through via holes. The antenna configuration was characterized by $\sim 21.4\%$ bandwidth, 2.6 dBi gain and an omnidirectional radiation pattern similar to a monopole antenna.

Hornng-Dean Chen and Hong-Two Chen [51] experimentally studied CPW-fed dual frequency monopole antennas. A frequency tunable ratio of 1.3 to 1.6 was obtained by varying the length of one of the two monopoles of the proposed antennas.

H.C.Go and Y.W.Jang [52] proposed a multi-band modified fork-shaped microstrip monopole antenna with a probe feed line. The antenna exhibited wideband characteristics; 29.8% for the lower band (cellular and GSM) at 860 MHz and 90.2% for the higher band (DCS, PCS, IMT-2000 and ISM) at 2.28 GHz.

Y.S.Shin and S.O.Park [53] performed experiments and numerical simulation on a compact, planar monopole type internal antenna suitable for use in the DCS (1710-1880 MHz), PCS (1750-1870 MHz) and IMT-2000 (1885-2200 MHz) bands. The antenna resonated at 1810 MHz with a bandwidth of 41%, displaying omnidirectional radiation patterns and ~2.9 dBi gain.

B.S.Collins *et al.* [54] described an unconventional antenna comprising of a dual band radiator coupled to a Microstrip line by means of a shaped ceramic pellet, for use in the 2.4-2.5 GHz and 4.9-5.9 GHz band.

A multiple U-shaped slot Microstrip patch antenna for 5 GHz Band WLANs was described by Jeong-Min Ju *et al.* [55]. The U slot width, the position of U-slot sections, the thickness of the foam layer, and the position of the feed point were the optimising parameters. The antenna exhibited 17.04% bandwidth and 3.88-9.28 dBi gain in the 5.02-5.955 GHz band.

H.K.Kan *et al.* [56] presented a compact dual-interleaved printed antenna consisting of two interleaved L shaped shorted patches with the required feed network etched on a high-dielectric constant substrate located below the ground plane of the antenna. The antenna displayed 16.9% impedance bandwidth and 2.3 dBi gain at 2.95 GHz.

Jeong-Min Ju *et al.* [57] designed, fabricated and measured a coaxial probe fed, arrow-shaped Microstrip patch antenna for the 5 GHz band WLAN applications. To achieve sufficient bandwidth a foam layer was inserted between the ground plane and the substrate. The antenna exhibited a gain of 5.02-7.25 dBi and broad radiation pattern.

Saou-Wen Su *et al.* [58] experimentally studied the effects of a finite ground plane on the impedance and radiation characteristics of an ultra-wideband planar monopole antenna with a circular ground plane.

2.2 Dielectric Resonators – the early years

In the early days of microwaves, guided electromagnetic wave propagation in dielectric media received wide spread attention. The term ‘dielectric resonator’ was coined by Richtmyer [59] of Stanford University in 1939, when he showed that unmetallized dielectric objects (toroid) functioned as microwave resonators. However, his theoretical work failed to generate significant interest, and practically nothing happened in this field for more than 25 years. In the early 1960’s, Okaya and Barash of Columbia University, rediscovered dielectric resonators, while working on high dielectric materials (single – crystal TiO_2 rutile). Their paper [60] provided the first analysis of modes and resonator design. However, in spite of the high Q and small size, dielectric resonators were not considered for use in microwave devices, due to their poor temperature stability. The development of the first temperature stable, low loss, barium tetratitanate ceramics, followed by $(\text{Zr-Sn})\text{TiO}_4$ ceramics in the early 1970’s was a real breakthrough in ceramic technology [61-62]. The miniaturization of microwave circuits has aided their popularisation. Together, these technologies permit the realization of small, reliable, lightweight and stable microwave systems, offering new design opportunities for microwave engineers. S. Jerry Fiedziuszko *et al.* [63] have reviewed a sequential evolution of the application of dielectric materials in microwave devices.

Wei Ke Hui and Ingo Wolff [64] calculated the resonant frequencies and unloaded Q factor of quasi- TE_{0pq} modes in a ring gap resonator. The resonator could be directly coupled to a slotline or a coplanar waveguide, resulting in compact MMIC’s.

Edward K.N.Yung *et al.* [65] used a dielectric disk resonator ($\epsilon_r = 37.5$), designed to operate in the $\text{HEM}_{11\delta}$ mode, to widen the bandwidth of a circular Microstrip patch antenna operating at 1.2123 GHz. The $\text{HEM}_{11\delta}$ mode at 990 MHz was preferred to the $\text{TE}_{01\delta}$ mode at 1133 MHz, because the $\text{TE}_{01\delta}$ mode radiates in a direction normal to the patch antenna.

Hoojun Yoo *et al.* [66] modelled a cylindrical dielectric resonator of high permittivity using the variational formula and the 2 dimensional search method. The variational method was found to be more accurate, the resonant frequency and the Q factor being within 1%.

Christopher L.Wagner and John B. Schneider [67] demonstrated that the dispersion relation could accurately predict the resonant mode frequencies of a rectangular resonator modelled with the Yee algorithm. Further it was shown that the degenerate modes in the continuous world could split into distinct modes in FDTD resonators, while separate modes could combine, yielding missing or extra modes.

A MoM formulation using combined entire-domain and sub-domain basis functions was proposed by Yaxun Liu *et al.* [68] and applied to the simulation of the fundamental mode of a rectangular DR in free space. Numerical simulations showed that this formulation is more efficient than formulations using only sub-domain functions.

A dual-mode band-pass filter was designed using the two degenerated modes (TE_{101}^y and TE_{011}^x) of a rectangular DR ($\epsilon_r = 35.5$), with square cross section and the HFSS simulation results were presented by Yaxun Liu *et al.* [69]. Cutting off a corner of the DR could control the coupling between the two modes. When the cross section of the DR was made rectangular, two non-degenerate modes (TE_{111}^x and TE_{111}^y) were excited.

Yaxun Liu *et al.* [70] studied the coupling between two rectangular DR's ($\epsilon_r = 34.19$) in an MIC environment. They applied the MoM with combined sub domain and entire domain basis functions to demonstrate the dependence of the coupling coefficient on the distance between two DR's.

2.3 Dielectric Resonator Antenna Configurations

The radiation Q-factors of isolated spherical DR's were reported by Gastine *et al.* in 1967 [71]. The possibility of constructing very small antennas using DR's

was first considered by Sager and Tisi [72]. The early experimental study of the dielectric resonator antenna (DRA) by Stuart A. Long *et al.* [73], followed by a numerical computation of the radiation characteristics of dielectric resonators by A.A.Kishk *et al.* [74], have shown that the DRA is an efficient radiator at microwave frequencies. A good overview of the early work on DRA's is given by R.K.Mongia and P.Bhartia [75]. Keen research by the antenna engineers in this field has led to the development of several novel DRA elements offering significant enhancements in bandwidth, gain and coupling [76-77]. Dielectric resonator antennas of various geometries, parameters and excitation methods have been studied extensively. This section reviews the work done on various DRA configurations, classified according to the excitation technique employed.

◆ Probe fed DRA

M.W.McAllister *et al.* [78] described a probe fed rectangular Dielectric Resonator Antenna fabricated from four different dielectric materials ($\epsilon_r = 8.9, 12.8, 15.2$ and 17.1) and studied the effects of feed probe length variations. The radiation patterns were calculated by considering the tangential electric fields on the resonator surfaces as equivalent current sources for far-field radiation. It was found that the resonant frequency evaluated using the magnetic wall model (MWM) was adequate for the purely TM modes, but for the lower order TE modes, the resonator had to be treated using the Dielectric waveguide model (DWM).

M.W.McAllister and S. A. Long [79] proposed a probe fed hemispherical dielectric antenna ($\epsilon_r = 8.9$). The resonant frequency of the dominant TE_{111} mode was evaluated theoretically from the tangential field continuity at the surface. The effect of the feed probe positions on the resonant behavior was also observed experimentally.

R.K.Mongia *et al.* [80] reported a probe excited dielectric ring resonator antenna ($\epsilon_r = 36.2$) which radiates like an electric-monopole (TM_{018} mode). It was

observed that the bandwidth of the antenna could be improved by lowering the ϵ_r or by increasing the inner radius/outer radius ratio.

G.P.Junker *et al.* [81] confirmed the effect of an air gap around the coaxial probe exciting a high permittivity cylindrical dielectric resonator antenna ($\epsilon_r = 12$) in the TM_{01} or HEM_{11} mode. It was suggested that the performance of the antenna could be improved by using a coaxial probe coated with a low permittivity material.

R.K.Mongia *et al.* [82] demonstrated that circular polarization could be obtained by exciting two orthogonal HE_{118} modes of a coaxial probe fed cylindrical ring DRA ($\epsilon_r = 36.2$) in phase quadrature. The measured resonant frequency and Q factor were 4.56 GHz and 31 respectively.

Z.Li, C.Wu and J.Litva [83] proposed an easy method of tuning the resonant frequency of cylindrical and ring dielectric resonator antennas ($\epsilon_r = 76, 37, 85$) using different diameters of conducting plates. Up to 300-500 MHz frequency tuning range was observed.

R.K.Mongia [84] presented a first order theory to analyse a probe fed cylindrical ring dielectric resonator antenna ($\epsilon_r = 20$) with a metallic cylinder at its centre. A high frequency separation was observed between the lowest order TM_{018} mode at 2.52 GHz radiating like an electric monopole and the next higher order mode.

A soldered through probe was used by K.W.Leung *et al.* [85] to excite a cylindrical ring DRA ($\epsilon_r = 36$), in the TM_{018} mode. The measured return loss and the radiation pattern of the configuration were presented.

M.T.K.Tam and R.D.Murch [86] demonstrated that additional conducting plate could reduce the volume of a conventional DRA. Experimental and simulation results were provided for a probe fed cylindrical and rectangular DRA ($\epsilon_r = 12$), excited in the fundamental HEM_{118} broadside mode and the TE_{118} mode, exhibiting 5.2 % and 5.4 % bandwidths respectively.

A.Sangiovanni *et al.* [87] experimentally investigated a coaxial probe excited cylindrical DRA ($\epsilon_r = 30.5$) embedded in a cylindrical annular ring ($\epsilon_r = 36.7$). Up to 38% impedance bandwidth was observed when the coaxial probe was in contact with both the DR's.

R.T.Long *et al.* [88] reported the results of the experimental investigations performed on a probe fed cylindrical DRA ($\epsilon_r = 13.2$), with a parasitic strip attached to its surface. The effect of the position and length of the strip on bandwidth and polarisation was also studied.

Ahmed A.Kishk *et al.* [89] investigated the performance of coaxial probe excited conical shaped DRAs ($\epsilon_r = 12$). The split cone was found to support more modes than the other cones, exhibiting 50% impedance bandwidth. Some of the results were verified numerically, using the method of moments.

Young-do Kim *et al.* [90] studied a probe-fed notched typed rectangular DRA ($\epsilon_r = 20.8$) and a rectangular DRA with air gap ($\epsilon_r = 45$) with broadband characteristics (15.2% and 12.3% respectively) for IMT-2000 handset. They also presented a frequency tuning technique using a tuning patch placed on top of the rectangular DRA.

B.J.Fasenfast *et al.* [91] performed experimental investigations on low profile, conformable, cylindrical Dielectric Resonator Antennas ($\epsilon_r = 16.1, 17.2$) placed in a conducting well. The results showed that the input resistance and resonant frequency of the structure generally increased when placed in the well. But the radiation patterns were unaffected.

C.Nannini *et al.* [92] proposed a coaxial probe fed dual frequency DRA, operating at 6 GHz and 8 GHz wherein, a cylindrical resonator ($\epsilon_r = 30$) was inserted into another ($\epsilon_r = 15$). They observed that the gap between the two bands could be matched by adjusting the antenna parameters.

Jian-Juang Chen *et al.* [93] presented an elliptical DRA ($\epsilon_r = 37$), excited by two coaxial cables for dual band operation in the $HEM_{11\delta}$ mode at 2.44 GHz and 3.36

GHz. It was observed that impedance matching could be obtained by extending or shortening the probe at each port.

Stepped Dielectric Resonator Antenna ($\epsilon_r = 37$) with a large effective aperture was introduced by K.Pliakostathis and D.Mirshekar-Syahkal [94]. The antenna was excited through a conductor strip etched on the vertical side, which is compatible to a coaxial feed line. 10% bandwidth and 6.5 dB directivity was observed.

Mohamed Al Sharkawy *et al.* [95] proposed a coaxial probe fed stacked elliptical DRA ($\epsilon_{r1} = 2.5$, $\epsilon_{r2} = 15$) for wideband applications (61.5% bandwidth) at 10 GHz. The characteristics were computed using the software package WIPL-D.

◆ Aperture coupled DRA

A Microstrip line-slot coupled rectangular DRA ($\epsilon_r = 10.8$) excited in its lowest order “magnetic dipole” mode (TE_{118}^z) at 6.9 GHz, was reported by A. Ittipiboon *et al.* [96]. Theoretical analysis was performed by modelling the DR surfaces along x and y-axes by perfect magnetic walls and the surfaces along the z - axis by imperfect magnetic walls. 10% impedance bandwidth and radiation patterns similar to that of a horizontal magnetic dipole were obtained.

R.K.Mongia *et al.* [97] showed that reasonable bandwidth (upto 3.4%) could be obtained using low profile, very high permittivity rectangular DRA's ($\epsilon_r = 100$). Microstrip slot coupling was used to excite the TE_{111}^z mode and the resonant frequency was predicted using the fundamental equation similar to that of a rectangular cavity.

Aperture coupling was used by K.W.Leung *et al.* [98] to investigate the broadside fundamental mode (TE_{111}) of a spherical cap Dielectric Resonator Antenna ($\epsilon_r = 9.5$). The antenna exhibited 3.7 dB gain at 4.74 GHz.

K.W.Leung *et al.* [99] studied the fundamental broadside TM_{110} mode of a low profile aperture coupled circular DRA ($\epsilon_r = 82$) resonating at 4.25 GHz, exhibiting an impedance bandwidth of 3.8% and 3 dB bandwidth of the antenna gain

of 11.8%. The front-to-back ratio was ~ 10 dB, showing that the energy was mainly radiated from the DRA instead of the dielectric substrate.

M.B.Oliver *et al.* [100] presented the results of a single slot fed rectangular DRA ($\epsilon_r = 40$) placed inclined at 45° with respect to the slot using mutually orthogonal nearly degenerate modes - TE_{111}^x and TE_{111}^y (at 5.2 GHz and 5.5 GHz respectively) to produce circular polarisation. The dimensions of the DRA were chosen to satisfy the relation between the two resonant frequencies and the unloaded radiation Q factors of the two modes.

G.P.Junker *et al.* [101] presented the results of the experimental studies performed on a slot coupled cylindrical Dielectric Resonator Antenna ($\epsilon_r = 12$) operating in HEM_{11} mode, illustrating the effect of filling the aperture with a dielectric material.

K.Y.Chow *et al.* [102] studied the characteristics of a cylindrical DRA array ($\epsilon_r = 9.5$) excited by an aperture-coupled source and operated at the fundamental broadside TM_{110} mode.

M.G.Keller *et al.* [103] investigated an active aperture-coupled rectangular Dielectric Resonator Antenna ($\epsilon_r = 20$) operating at 5 GHz, excited in the lowest order TE_{111}^y mode, radiating like a slot directed magnetic dipole. The DRA demonstrated superior tolerance levels with respect to fabrication, post assembly gain optimisation by slight adjustments of the DRA position with respect to the slot and much higher bandwidth in comparison to the Microstrip patch antenna.

K.P.Esselle [104] presented a low profile, circularly polarised, rectangular DRA ($\epsilon_r = 10.8$) fed by a 50Ω Microstrip line through a single aperture. The resonator was rotated by 45° with respect to the aperture in order to excite two frequency bands centered around 13.2 GHz and 14.75 GHz. Numerical analysis of the antenna was also performed using the FDTD method.

A low profile, aperture coupled, rectangular DRA ($\epsilon_r = 10.8$) radiating like a magnetic dipole at 11.6 GHz was proposed by Karu P.Esselle [105]. The theoretical radiation patterns were obtained using the FDTD method and compared with

experimental results. The DRA was also well matched at 13 GHz, but the pattern was more directional due to the influence of higher order modes.

The bandwidth enhancement of an aperture coupled cylindrical Dielectric Resonator Antenna ($\epsilon_r = 9.5$) loaded by a low profile dielectric disk of very high permittivity ($\epsilon_r = 82$) was experimentally investigated by K.W.Leung *et al.* [106]. They observed an increase in bandwidth from 8% to 25%.

Y.Hwang *et al.* [107] experimentally investigated a double layered high permittivity rectangular DRA ($\epsilon_r = 38,80$) operating in the 1.8 GHz band. The measured results showed that the double-layered DRA had a 1.2 dB gain enhancement and 25% height reduction over a single-layered antenna ($\epsilon_r = 38$). The bandwidth was 2.7% and antenna gain was 6.2 dBi.

K.W.Leung and M.W.To [108] discussed the fundamental broadside TM_{110} mode characteristics of a slot-coupled cylindrical Dielectric Resonator Antenna ($\epsilon_r = 9.5$) using a proximity feed on a perpendicular substrate. The usefulness of a tuning stub on the impedance matching was also demonstrated.

K.W.Leung *et al.* [109] described an annular slot-coupled, linearly polarised cylindrical Dielectric Resonator ($\epsilon_r = 10$) Antenna excited in the broadside TM_{110} mode. 18% impedance bandwidth was observed at 5.21 GHz. This was 2.3 times higher than the rectangular slot version.

H.Y.Lo *et al.* [110] performed experimental investigations on an aperture coupled equilateral triangular DRA of very high permittivity ($\epsilon_r = 82$). The antenna was excited in its fundamental broadside TM_{101} mode at 7.61 GHz. The reflection and radiation characteristics of the antenna were also discussed. The antenna exhibited an impedance bandwidth of ~3%.

K.W.Leung and S.K.Mok [111] reported the outcome of the experimental investigations on a circularly polarized cylindrical Dielectric Resonator Antenna ($\epsilon_r = 9.5$) excited by a perturbed annular slot with backing cavity. 18% impedance bandwidth, 4.5 dBi gain and broadside radiation patterns were observed at 1.96 GHz.

A Laisne *et al.* [112] presented the design of a circularly polarised slot fed rectangular DRA ($\epsilon_r = 9.9$). A metallic strip printed diagonally on the surface of the DR excited the two orthogonal modes – TE_{111}^x and TE_{111}^y , with the same amplitude and phase for circular polarisation. Simulations as well as measurements performed on a single antenna and a four DRA sequential rotation array confirmed good results achieved by this design.

Chih-Yu Huang and Jieh-Sen Kuo [113] experimentally investigated a Microstrip line feed- C shaped slot coupled cylindrical DRA ($\epsilon_r = 4.4$) for circular polarisation. Two orthogonal near-degenerate resonant modes were mainly excited.

A.Petosa *et al.* [114] reported a Microstrip-fed rectangular aperture excited DRA formed by perforating a dielectric substrate ($\epsilon_r = 10.2$). The performance of several experimental prototypes was compared to a conventional DRA and the results demonstrated better gain and cross-polarization levels. This fabrication technique could be used as an alternative for the fabrication of large DRA arrays, eliminating the need for positioning and bonding the individual elements.

Yong Xin Guo and Kwai.Man Luk [115] presented a high input isolation (> 35 dB) dual-polarized cylindrical DRA ($\epsilon_r = 9.5$) excited using two narrow slots forming a 'T'. A hybrid feed mechanism with a CPW feed and a slot feed was also studied.

Aldo Petosa *et al.* [116] investigated the performance of a DRA array designed at 25 GHz, formed by perforating a dielectric substrate ($\epsilon_r = 10.2$), with a lattice of holes. The array was excited by a corporate feed network of aperture coupled Microstrip lines.

C.Nannini *et al.* [117] presented the experimental and simulated results on an aperture fed dual-frequency cylindrical DRA configuration comprising of two stacked cylindrical DRA's ($\epsilon_r = 15$) separated by a foam layer. $\sim 80\%$ bandwidth enhancement was observed in comparison to a single DRA.

◆ Coplanar waveguide (CPW) fed DRA

Roger. A. Kranenburg *et al.* [118] suggested the coplanar waveguide to be an effective mechanism for a cylindrical DRA ($\epsilon_r = 8.1$ to 20.8) excited in the TE_{111} mode. The circuit and radiation properties were measured experimentally. Theoretically calculations were based on a simple magnetic wall model.

Richard.Q.Lee and Rainee.N.Simons [119] reported the use of parasitic elements to enhance the bandwidth of a cylindrical DRA ($\epsilon_r = 36$), aperture coupled to a notched CPW feed and excited in the HE_{118} and HE_{138} mode. In the experiment, identical dielectric resonators were placed directly above and on both sides of the driven DRA.

The characteristics of a CPW fed low-profile, square DRA ($\epsilon_r = 79$) were experimentally studied by Jian-Yi Wu *et al.* [120]. The antenna exhibited 2.4% bandwidth when excited in the TE_{111} mode at 2.09 GHz. The calculated resonant frequency of the low profile DRA deviated from the measured frequency by $\sim 8\%$.

Sheng-Ming Deng *et al.* [121] presented a CPW fed Rectangular DRA ($\epsilon_r = 82$). The antenna exhibited an impedance bandwidth of 2.3% at 3.64 GHz. The significance of the alignment between the ceramic body and the CPW in deciding the reflection coefficient was discussed.

M.S.Al Salameh *et al.* [122] proposed and investigated a novel coupling scheme wherein, coupling was achieved through a narrow slot at the end of a coplanar waveguide. The lowest order TE_{111}^y mode was excited in a rectangular DRA ($\epsilon_r = 20$) at 4.635 GHz. The difference between measured and calculated resonant frequencies was 2.5%.

Yong-Xin Guo and Kwai-Man Luk [123] demonstrated that a vertical strip connected at the end of a center strip of the coplanar waveguide improved the input impedance matching of a low permittivity ($\epsilon_r = 9.5$) cylindrical DRA operating in the HEM_{11} mode leading to a wideband (22%) operation.

S.M.Deng *et al.* [124] compared the performance of a CPW fed rectangular DRA ($\epsilon_r = 36$) placed in low and high profile upon the feed. It was observed that the high profile configuration resonated at a lower frequency and exhibited better bandwidth performance (84 MHz).

A comparison of CPW feed configurations was presented by Bratin Ghosh *et al.* [125] to optimise the feed geometry of a rectangular DRA ($\epsilon_r = 20$) with respect to its topology and radiation performance. They observed that the space requirement of the feed and the radiation pattern was dependent on the feed configuration.

◆ Microstrip Line fed DRA

R. A. Kranenburg and S. A. Long [126] performed an investigation of a Microstrip fed cylindrical Dielectric Resonator Antenna of different heights and varying ϵ_r (8.1 to 20.8) and concluded that the critical parameter that determines the amount of coupling and the particular mode excited by the Microstrip Transmission line was the overlap distance.

A.Petosa *et al.* [127] described an experimental procedure for designing a 10 element Microstrip-fed series array of DRA's ($\epsilon_r = 10.8$) with a Taylor amplitude distribution. A gain of 13.2 dBi was measured at 8.2 GHz with maximum side lobe levels of -17.5 dB.

G.Drossos *et al.* [128] reported a simple Microstrip line excited circular polarised cylindrical DRA ($\epsilon_r = 37$). Two orthogonal HE_{118} modes were excited using a $\lambda/4$ semi circle shaped transmission line. A boresight axial ratio of 0.45 dB and 3.9% impedance bandwidth was obtained.

A.Petosa *et al.* [129] showed that the replacement of the individual rectangular DRA elements ($\epsilon_r = 10$) by DRA element pairs in a series-fed array enhanced both the impedance and pattern bandwidth of the array.

Cheng-Shong Hong [130] presented a technique for tuning the resonant frequency of a Microstrip line fed rectangular DRA ($\epsilon_r = 79$) excited in the HEM_{118} using a parasitic disk on top of the DR with an adjustable air gap.

K.M.Luk *et al.* [131] demonstrated that by connecting a vertical strip at the end of the Microstrip line, the input impedance of a cylindrical Dielectric Resonator Antenna ($\epsilon_r = 16, 10$) could be improved substantially. 19% impedance bandwidth and stable radiation pattern across the operating frequency was observed.

K.W.Leung *et al.* [132] performed experimental investigations on a circular polarised cylindrical DRA ($\epsilon_r = 9.5$) excited by dual conformal strips, in phase quadrature and displaced at 90° in space, giving two degenerate modes (TM_{110}) in phase quadrature. A wide axial ratio bandwidth of 20% was obtained.

A conformal-strip excited hemispherical DRA ($\epsilon_r = 9.5$) excited in the single TE_{111} mode was analysed theoretically and experimentally by K.W.Leung [133]. A simple result for the input impedance was presented. A larger resistance was obtained for a longer strip length.

Fu-Ren Hsiao *et al.* [134] proposed two novel designs of very high permittivity ($\epsilon_r = 90.5, 79$) Microstrip line fed DRA. The broadband (4.8%) strip-loaded square DRA excited a dual-resonant mode and in the circularly polarized patch-loaded square DRA, the fundamental resonant mode of the DRA was split into two orthogonal near-degenerate resonant modes.

G.Bit-Babik *et al.* [135] described the design strategy of a wide band, Microstrip line fed rectangular DRA ($\epsilon_r = 80$). Two closely spaced resonant modes at 2.28 GHz and 2.7 GHz were excited to enhance band coverage (25% bandwidth). The use of parasitically coupled conducting strips on the upper side was also reported to excite resonance at a lower frequency of 1.67 GHz.

Y.Sung *et al.* [136] proposed a dual frequency ring DRA ($\epsilon_r = 37$) excited by two orthogonal Microstrip line feeds. The impedance bandwidths observed were 636 MHz and 409 MHz at 7.9 GHz and 9.8 GHz respectively.

2.4 Numerical analysis of Dielectric Resonator Antennas

A review of the numerical analysis of the DRA is presented in this section. The DRA is generally modelled using Perfect Magnetic Walls and the Dielectric Waveguide Model (DWM) using the Surface Integral technique, Mode Matching Method, Greens function, etc. for formulation. The Method of Moments (MoM), Finite Element Method (FEM), Transmission Line Matrix (TLM) method and Finite Difference Time Domain (FDTD) method, etc. are the popular numerical methods employed. Several novel methods also have been suggested by the researchers.

G.P.Junker *et al.* [137] presented a formulation for active and parasitic radiators in the presence of dielectric bodies of revolution. They used the Method of moments and analysed a coaxial probe fed hemispherical DRA ($\epsilon_r = 8.9$). The input impedance computed using this method was compared to that computed using the dyadic Green's function and the results were found to be in close agreement.

The results of the numerical and experimental study pertaining to the effect of an air gap on the input impedance and resonant frequency of a probe fed cylindrical DRA ($\epsilon_r = 8.9, 22$) operating in the TM_{01} mode were presented by G.P.Junker *et al.* [138]. The antenna was analysed as a dielectric body of revolution composed of a dipole antenna surrounded by a dielectric cylinder isolated in free space.

Ahmed A.Kishk *et al.* [139] provided a review of the development of the DRA and demonstrated that the DRA is an efficient radiator. The Dyadic-Green's function with the MoM was used to implement the study of a hemispherical DRA, located above an infinite ground plane and excited by a coaxial dipole or a slot aperture. A parametric analysis of the antenna was presented to show the effect of the antenna parameters on the resonant frequency, input impedance, and radiation pattern for the TE_{111} mode.

R.K.Mongia *et al.* [140] derived a closed form expression for the radiation Q factor of a coaxial probe fed rectangular DRA ($\epsilon_r = 37.84$) excited in the TE_{111}^z mode, by replacing the DR by a polarization current source. Their analytical model was a

combination of the Magnetic wall model (MWM) and the Dielectric Waveguide Model (DWM). Though the mixed model was computationally simpler than the DWM, the predicted resonant frequencies were lower than the true values by about 6-8% for $\epsilon_r \geq 38$.

FDTD analysis of a rectangular DRA ($\epsilon_r = 10$) fed by a Microstrip line through an aperture on the ground plane was performed by S.M.Shum and K.M.Luk [141]. The numerical calculations were compared to the experimental results and ~3% error was observed between the calculated (3.8 GHz) and measured resonant frequency (3.92 GHz).

Kwai-Man Luk *et al.* [142] analytically studied the mutual coupling between two probe fed hemispherical DRA's ($\epsilon_r = 9.5$) operated at the lowest order broad-side TE_{111} mode. The Green's function for a point electric current located vertically inside a dielectric sphere was derived rigorously by the mode matching technique. The mutual impedance was subsequently obtained by employing the reaction theorem.

Y.M.M.Antar and Z.Fan [143] presented the theoretical analysis of an aperture coupled rectangular DRA ($\epsilon_r = 10.8$), operating in the TE_{111} mode at 6.88 GHz, based on the Modal Expansion Method and the Spectral Domain approach. The effect of the slot dimensions, slot displacement and stub length was also studied. The front to back ratio observed was 18 dB.

S.M.Shum and K.M.Luk [144] presented the FDTD analysis of a probe-fed cylindrical Dielectric Resonator Antenna ($\epsilon_r = 12$) operating in the fundamental broadside mode (HEM_{116}). The effects of the probe length, feed position and the dielectric constant on the input impedance were studied.

G.P.Junker *et al.* [145] performed the two port analysis of a linear array of half-split cylindrical Dielectric Resonator Antennas ($\epsilon_r = 12$) excited in TE_{01} mode. The Method of Moments was used for the analysis.

K.W.Leung *et al.* [146] developed a single mode theory for a centre-fed hemispherical Dielectric Resonator Antenna ($\epsilon_r = 9.5, 15, 20$). The MoM was used to

calculate the probe current. From the theory, a simple formula was derived for the efficient computation of the impedance matrix.

R.K.Mongia and A.Ittipiboon [147] reported the theoretical and experimental investigations on rectangular DRAs ($\epsilon_r=10$ to 100). The accuracy of the first-order theory in predicting the resonant frequency and radiation Q factor was determined by the measurements made on different DRA samples. The radiation patterns of probe and Microstrip slot feed schemes were shown.

Shiu-Ming Shum and Kwai-Man Luk [148] employed the FDTD method to analyze a probe-fed cylindrical DRA ($\epsilon_r=9.2$). Numerical results for the input impedance and radiation patterns of the DRA operating in the HEM_{118} mode were presented. The effects of various parameters on the characteristics of the DR antenna were studied.

From the results of a numerical procedure based on the Method of Moments as applied to a system of surface integral equations, Gregory.P.Junker *et al.* [149] presented the criteria for optimising the performance of a linear array of coaxial probe fed half split cylindrical DR elements ($\epsilon_r=12$) operating in the TE_{01} mode.

K.W.Leung *et al.* [150] investigated an aperture-coupled hemispherical Dielectric Resonator Antenna ($\epsilon_r=9.5$) with a thick ground plane excited in the TE_{111} mode. The modal and spectral domain Green's functions were used in calculating the DRA and feed line fields respectively. The unknown magnetic currents in the upper and lower interfaces of the slot were solved using the moment method. It was observed that as the thickness increases, the resonant frequency increases, but the input impedance and the front-to-back ratio decreases.

Yahia.M.M.Antar *et al.* [151] introduced a Modified Waveguide Model (MWGM) based on the concept of effective dimensions, for predicting the resonant frequency of rectangular DRA's. The method was found to yield more accurate results than the Conventional Waveguide Model (CWGM). This method is based on the argument that the portion of the electromagnetic energy confined within the DRA

was closely related to the resonant frequency and therefore a concept of effective dimensions was proposed to improve the accuracy.

A Microstrip-coupled cylindrical DRA ($\epsilon_r = 37$) excited in the $HE_{11\delta}$ mode was investigated theoretically and experimentally by George Drassos *et al.* [152]. Simulation was performed using a software package based on the finite element method. The variation of the resonant frequency, return loss, radiation pattern, directivity, unloaded Q-factor and impedance bandwidth with the position of the DRA on the Microstrip line was also discussed.

B.Henry *et al.* [153] performed numerical TLM simulations (using MicrostripesTM) and experimentation to investigate the mutual coupling between Microstrip line fed rectangular Multi-Segment Dielectric Resonator Antennas (MSDRA) excited in the TE_{111} mode ($\epsilon_r = 10, 40$). The higher permittivity dielectric below provided better impedance match to the Microstrip, while the lower permittivity dielectric on top maintained large bandwidth capabilities.

K.W.Leung *et al.* [154] studied the cross-polarization characteristics of a probe-fed hemispherical DRA excited in the fundamental TE_{111} mode ($\epsilon_r = 9.5$). The mode matching method was employed to obtain the exact Green's functions of the radiation field rigorously.

Supriyo Dey and Raj Mittra [155] presented a generalization of the conformal FDTD technique to model arbitrarily shaped metallic as well as dielectric objects. The accuracy of the method was demonstrated by modelling both open and closed type Dielectric Resonators.

Y.X.Guo *et al.* [156] applied the FDTD method with Berenger's PML ABC to investigate the characteristics of aperture-coupled cylindrical Dielectric Resonator Antennas ($\epsilon_r = 9.2$) on a thick ground plane, operated in the fundamental broadside $HEM_{11\delta}$ mode. Experimental and numerical results showed that the thickness substantially affected the characteristics. It was also demonstrated that a H-shaped slot provided better coupling than a rectangular slot of the same slot length.

A.Sangiovanni *et al.* [157] presented a numerical analysis of various DRA's: simple and complex shape configurations with different excitations (dipole, coaxial probe, slot-coupled Microstrip line) using a time-harmonic Surface Finite Element Method (SFEM).

A conducting conformal strip excitation scheme was proposed by Kwok Wa Leung [158] for a hemispherical DRA whose exact Green Function was found using the Mode Matching method. The input impedance was obtained from the unknown strip current solved by the moment method. Novel recurrence formulas were obtained to evaluate the impedance integrals analytically. The results were validated through experiments ($\epsilon_r=9.5$).

K.W.Leung [159] performed the analysis of an aperture-coupled hemispherical Dielectric Resonator Antenna ($\epsilon_r=9.5$) with a perpendicular feed. Moment method and Galerkin's procedure was employed to calculate the input impedance.

Zhongxiang Shen *et al.* [160] performed the modal expansion analysis of a cylindrical DRA fed by an embedded coaxial probe by introducing a cylindrical magnetic wall to enclose the resonator and then treating the resulting structure as a cascaded waveguide discontinuity. The air gap between the resonator and the ground plane was accurately characterized as a short waveguide section. It was noticed that a small air gap could considerably change both the resonant frequency and the input impedance by 5 %.

Yuehe Ge and Karu P.Esselle [161] demonstrated that volume-integral-equation-based MoM techniques could be used to design and analyze an aperture coupled rectangular DRA. The theoretical radiation patterns of the low profile rectangular DRA ($\epsilon_r=10.8$) resonating at 11.6 GHz compared well with measurements and previously published FDTD results.

S.G.O'Keefe [162] explored the use of symmetry planes to divide the HEM_{118} and TE_{018} modes of resonance in cylindrical and half cylindrical DRA's. The antennas were evaluated using FDTD numerical simulation techniques, applying

Berenger's PML ABC to terminate the simulation space. The resonant frequency and bandwidth of the half DRA was greater than the full DRA, the effect being more significant for the TE_{018} mode. The half DRA also demonstrated a more directional pattern than the full DRA.

It was shown by M.H.Neshati and Z.Wu [163] that the Conventional Dielectric Waveguide model (CDWM) provided a better prediction of the resonance frequency of the TE_{111}^y mode of a rectangular DRA than the Marcatili method and the Effective dielectric constant (EDC) method. They obtained a fitted closed formula for the calculation of the resonance frequency of a RDRA with $\epsilon_r > 30$, with an error ranging from -9.3% to $+2.05\%$.

M.H.Neshati and Z.Wu [164] employed the Conventional Dielectric Waveguide model (CDWM) to calculate the radiation characteristics of a rectangular DRA and compared the results with the experiments performed on a coaxial probe excited Rectangular DRA ($\epsilon_r=38$) and simulations performed using HFSS (employing the Finite element method - FEM). They concluded that CDWM could be used for a first order estimation of antenna parameters, but FEM provided more accurate results for radiation patterns.

N.Farahat *et al.* [165] analysed a circularly polarised cross-shaped Dielectric Resonator Antenna ($\epsilon_r = 10.8$) using the edge-based Conformal Finite Difference Time-Domain method. They showed that the conformal FDTD technique offered a 2:1 advantage over staircasing without compromising accuracy.

A coaxial probe excited triangular DRA ($\epsilon_r=12$) was investigated numerically and experimentally by Ahmed. A. Kishk [166]. The resonance frequency was predicted using a simple waveguide model with magnetic walls, the DR placed inside the waveguide. The selected mode had a broadside radiation pattern.

A.A.Kishk and A.W.Glisson [167] performed the numerical study of the HEM_{11} and HEM_{12} modes of coaxial probe excited split cylindrical DRA's ($\epsilon_r = 10, 22$ and 38) on a conducting plane. The Method of Moments was used for the analysis.

Dual band operation was also observed by inserting a resonator of a different dielectric material ($\epsilon_r = 36$) inside another resonator ($\epsilon_r = 12$).

Zhijun Liu *et al.* [168] developed an MoM based surface integral equation solver for analysing a hemispherical and rectangular shaped aperture coupled DRA's ($\epsilon_r = 2.96, 2.2$). The numerical model included the ability to handle layered medium Green's function, piecewise homogeneous finite dielectric resonators, Microstrip lines, and aperture coupling in Microstrip geometry.

Steven G.O'Keefe *et al.* [169] performed the FDTD simulation of the radiation characteristics of Half-volume cylindrical and rectangle DRA's ($\epsilon_r = 12$) excited in the HEM_{118} , TE_{018} and TE_{118} mode. The DRA's were bisected through an image plane by a conducting sheet. The resultant half DRA's were smaller in volume and had a more directional radiation pattern.

The resonant modes of a rectangular DRA ($\epsilon_r = 38,90$) were analysed using FDTD method by E.Semouchkina *et al.* [170]. It was shown that the resonant fields in DRA's were equivalent to those created by combinations of magnetic or electric dipoles located in the DR's. Their data also proved that the formation of TM modes in rectangular DRA's was possible only if the antenna dimensions provided sufficient 'space' to host each dipole.

Coaxial probe fed truncated tetrahedron and triangular DRA ($\epsilon_r = 12$) with wideband performance was analysed by Ahmed. A. Kishk [171] employing the numerical code WIPL-D. Up to 40% impedance bandwidth was observed.

K.K.So and K.W.Leung [172] employed the Mode Matching method to perform the theoretical analysis of an annular-slot excited hemispherical Dielectric Resonator Antenna ($\epsilon_r = 9.5$) with a backing cavity, excited in the fundamental broadside TE_{111} mode. 1.3% error was observed between experimental and numerical results.

FDTD method using non-uniform orthogonal grids was employed by B.Li *et al.* [173] to perform the theoretical investigations on a circularly polarized cylindrical Dielectric Resonator Antenna ($\epsilon_r = 16$) excited by an asymmetrical U-slot with a

backing cavity. It was found that the arms of the U-slot have dominant effect on the aspect ratio.

Guido Biffi Gentili *et al.* [174] presented an accurate study of the inter element coupling phenomena in a DRA array, based on FDTD approach, exploiting Berenger's Perfectly matched layer (PML) boundary conditions and geometrical symmetries. Rectangular DRA elements ($\epsilon_r=10.8$) were excited in the dominant TE_{118} mode at 7.2 GHz. A new corrective term to the array factor was derived from the computation of the phase of the coupling co-efficients.

A.A.Kishk *et al.* [175] employed the surface integral equation formulation and MoM to perform the numerical analysis of a coaxial probe fed stacked DRA configuration comprising of two cylindrical DRA's of different permittivity ($\epsilon_r=4.5$ and 10.5) and excited in the HEM_{118} mode, displaying 35% bandwidth. The effects of different parameters on the antenna performance were investigated.

Ahmed A.Kishk [176] presented the numerical and experimental analysis of a coaxial probe excited wide-band truncated tetrahedron Dielectric Resonator Antenna ($\epsilon_r = 12$) in three different configurations. The numerical code WIPL-D using the method of moments was used for the analysis.

X.Q.Sheng *et al.* [177] used a hybrid Finite Element Method / Moment Method to analyse a rectangular DR ($\epsilon_r=4,8,10$)-attached waveguide-fed hemispherical DRA ($\epsilon_r = 8$). It was demonstrated that an empty waveguide-fed DRA failed to radiate energy, but placing a DR inside the waveguide significantly improved the radiation.

The excitation of a circular disk DRA ($\epsilon_r = 10.5$) using a probe extending in a rectangular waveguide and excited by the incident dominant mode was analysed by Islam.A.Eshrah *et al.* [178]. The results obtained using the MoM were compared with those obtained using FDTD and good agreement was obtained.

REFERENCES

-
1. J.Fuhl, P.Nowak and E.Bonek, "Improved internal antenna for hand-held terminals," *Electron. Lett.*, vol.30, no.22, pp.1816-1818, 27 October 1994.
 2. Z.D.Liu and P.S.Hall, "Dual-band antenna for hand held portable telephones," *Electron. Lett.*, vol.32, no.7, pp.609-610, 28 March 1996.
 3. J.C.Batchelor and R.J.Langley, "Microstrip annular ring slot antennas for mobile applications," *Electron. Lett.*, vol.32 no.18, pp.1635-1636, 29 August 1996.
 4. G.T. Pedersen, J.B. Andersen and S.Skjaeris, "Integrated Handset Antenna with Low absorption and handset antenna diversity," *IEE Colloquium*, Ref.1997 /022.
 5. Y.J. Guo, A.Paez, R.A. Sadeghzadeh and S.K.Barton, "A circular patch antenna for radio LAN's," *IEEE Trans. Antennas Propagat.*, vol.45, no.1, pp.177-178, January 1997.
 6. K.Takei, H.Okabe, Y.Imakado, "TEM slot antenna for personal handy - phone terminal," *Electron. Lett.*, vol.33, no.9, pp.732-733, 24 April 1997.
 7. Corbett R.Rowell, R.D.Murch, "A capacitively loaded PIFA for compact mobile telephone handsets," *IEEE Trans. Antennas Propagat.*, vol.45, no.5, pp.837-841, May 1997.
 8. Hiroyuki Arai, Nobuhiro Igi and Hirokazu Hanaoka, "Antenna-gain measurement of handheld terminals at 900 MHz," *IEEE Trans. Veh. Technol.*, vol.46, no.3, pp.537-543, August 1997.
 9. R.B.Waterhouse, "Printed antenna suitable for mobile communication handsets," *Electron. Lett.*, vol.33, no.22 pp.1831-1832, 23 October 1997.
 10. Kathleen.L.Virga, Yahya Rahmat- Samii, "Low Profile Enhanced Bandwidth PIFA Antennas for Wireless Communications Packaging," *IEEE Trans. Microwave Theory Tech.*, vol.45, no.10, pp.1879-1889, October 1997.
 11. A.Serrano-Vaello and D.Sanchez-Hernandez, "Printed antennas for dual-band GSM/DCS 1800 mobile handsets," *Electron. Lett.*, vol.34, no.2, pp.140-141, 22 January 1998.

12. C.L.Mak, K.M.Luk and K.F.Lee, "Proximity-coupled U-slot patch antenna," *Electron. Lett.*, vol.34, no.8, pp.715-716, 16 April 1998.
13. Ch.Delaveaud, Ph.Leveque and B.Jecko, 'Small-sized low-profile antenna to replace monopole antennas', *Electron. Lett.*, vol.34, no.8, pp.716-717, 16 April 1998.
14. Corbett R. Rowell and R. D. Murch, "A compact PIFA suitable for Dual-Frequency 900/1800-MHz operation," *IEEE Trans. Antennas Propagat.*, vol.46, no.4, pp.596-598, April 1998.
15. Roger Yew-Siow Tay, Quirino Balzano and Niels Kuster, "Dipole Configurations with strongly improved radiation efficiency for hand-held transceivers," *IEEE Trans. Antennas Propagat.*, vol.46, no.6, pp.798-806, June 1998.
16. H.Iwasaki, "Microstrip antenna with back-to-back configuration relative to a slot on a ground plane," *Electron. Lett.*, vol.34, no.14, pp.1373-1374, 9 July 1998.
17. O. Leisten, Y. Vardaxglou, T. Schmid, B. Rosenberger, E. Agboraw, N. Kuster and G. Nicolaidis, "Miniature dielectric-loaded personal telephone antennas with low user exposure," *Electron. Lett.*, vol.34, no.17, pp.1628 -1629, 20 August 1998.
18. R.B.Waterhouse, "Small printed antenna easily integrated into a mobile handset terminal," *Electron. Lett.*, vol.34, no.17, pp.1629-1631, 20 August 1998.
19. K.Hettak, G.Delisle and M.Boulmalf, "A novel integrated antenna for millimeter-wave personal communications systems," *IEEE Trans. Antennas Propagat.*, vol.46, no.11, pp.1757-1759, November 1998.
20. N.Chiba, T.Amano and H. Iwasaki, "Dual-frequency planar antenna for handsets," *Electron. Lett.*, vol.34, no.25, pp.2362-2363, 10 December 1998.
21. J.Ollikainen, M.Fischer and P.Vainikainen, "Thin dual-resonant stacked shorted patch antenna for mobile communications," *Electron. Lett.*, vol.35, no.6, pp.437-438, 18 March 1999.
22. Jack.T.Rowley and Rod.B.Waterhouse, "Performance of shorted Microstrip Patch Antennas for Mobile Communications Handsets at 1800 MHz," *IEEE Trans. Antennas Propagat.*, vol.47, no.5, pp.815 – 822, May 1999.
23. C.T.P.Song, P.S.Hall, H.Ghafouri-Shiraz and D.Wake, "Multi-circular loop monopole antenna," *Electron. Lett.*, vol.36, no.5, pp. 391-393, 2 March 2000.
24. H.Kan and R.B.Waterhouse, "Small circularly polarised printed antenna," *Electron. Lett.*, vol.36, no.5, pp. 393-394, 2 March 2000.

25. Ya Jun Wang, Ching Kwang Lee, Wee Jin Koh and Yeow Beng Gan, "Design of Small and Broad-band Internal Antennas for IMT-2000 Mobile Handsets," *IEEE Trans. Microwave Theory Tech.*, vol.49, no.8, pp.1398 – 1403, August 2001.
26. Marta Martinez-Vazquez, Matthias Geissier, Dirk Heberling, Antonio Martinez-Gonzalez and David Sanchez-Hernandez, "Compact Dual-band antenna for mobile handsets", *Microwave Opt. Technol. Lett.*, vol.32, no.2, pp. 87-88, 20 January 2002.
27. Hassan M.Elkamchouchi and Hossam El-dien M.Hafez, "Multi-band smart patch antenna for GPS/PCS hand held units," Proc., *IEEE 3rd International Conference on Microwave and Millimeter wave Technology, 2002.*
28. Tsung –Wen Chiu, Cliff Wang, Chih-Ming Su and Kin-Lu Wong, "Surface mountable dual side-feed circularly polarized ceramic chip antenna," Proc. *IEEE International symposium on Electronic Materials and packaging*, pp. 434- 437, 2002.
29. Zhizhang Chen, Acep D. Ganjara and Xiaomin Chen, "Dual-L antenna with a novel tuning technique for dual frequency applications," *IEEE Trans. Antennas Propagat.*, vol.50, no.3, pp.402-404, March 2002.
30. Will Mckinzie, Greg Mendolia and John Dutton, "Novel packaging approaches for miniature antennas", *Proc. IMAPS/SMTA Conference on Telecom Hardware solutions*, Plano, TX, pp. 1-7, May 15-16 2002.
31. Fu-Ren Hsiao and Kin-Lu Wong, "Compact Planar Inverted – F Patch Antenna for triple frequency operation," *Microwave Opt. Technol. Lett.*, vol. 33, no.6, pp.459-462, 20 June 2002.
32. C.W.Chiu and F.L.Lin, "Compact dual-band PIFA with multi-resonators," *Electron. Lett.*, vol.38, no.12, pp.538-540, 6 June 2002.
33. Gwo-yun Lee and Kin-Lu Wong, "Very-low-profile bent planar monopole antenna for GSM/DCS dual-band mobile phone," *Microwave Opt. Technol. Lett.*, vol.34, no.6, pp.406-409, 20 September 2002.
34. Yongjin Kim and Sangseol Lee, "Design and fabrication of a planar inverted-F antenna for the wireless LAN in the 5 GHz band," *Microwave Opt. Technol Lett.*, vol.34, no.6, pp.469-475, 20 September 2002.
35. Hisashi Morishita, Yongho Kim and Kyohei Fujimoto, "Design concept of antennas for small mobile terminals and the future perspective," *IEEE Antennas Propagat. Mag.*, vol.44, no.5, pp.30-43, October 2002.

36. Hyun Jun Kim, Sewoong Kwon, Sung Hun Sim, Young Joong Yoon, Huyn Jai Kim, Seok Ji Yoon and Chong-Yun Kang, "Dual-frequency small-chip Meander Antenna," *Microwave Opt. Technol. Lett.*, vol.35, no.4, pp. 274-277, 20 November 2002.
37. Han-Cheol Ryu, Hee-Ran Ahn, Sang-Hwa Lee and Wee Sang Park, "Triple-stacked microstrip patch antenna for multi-band system," *Electron. Lett.*, vol.38, no.24, pp.1496-1497, 21 November 2002.
38. Marc. C. Greenberg, Kathleen L. Virga and Cynthia. L. Hammond, "Performance characteristics of the dual exponentially tapered slot antenna (DE TSA) for wireless communications applications," *IEEE Trans. Veh. Technol.*, vol.52, no.2, pp.305-312, March 2003.
39. Gwo-Yun Lee, Hong-Twu Chen and Kin-Lu Wong, "A Low cost surface-mount monopole antenna for GSM / DCS operation," *Microwave Opt. Technol. Lett.*, vol.37, no.1, pp.2-4, 5 April 2003.
40. Kin-Lu Wong, An-Chia Chen and Yen-Liang Kuo, "Diversity metal-plate planar inverted F antenna for WLAN operation," *Electron. Lett.*, vol.39, no.7, pp.590-591, 3 April 2003.
41. Yong-Xin Guo, Irene Ang and M.Y.W.Chia, "Compact Internal Multiband Antennas for Mobile Handsets," *IEEE Antennas and wireless Propagation. Lett.*, vol.2, pp.143-146, 2003.
42. Jung-Ick Moon and Seong-Ook Park, "Small Chip Antenna for 2.4/5.8- GHz Dual ISM Band Applications," *IEEE Antennas and wireless Propagation Lett.*, vol.2, pp.313-315, 2003.
43. Shih-Huang Yeh, Kin-Lu Wong, Tzung-Wern Chiou and Shyh-Tirng Fang, "Dual-Band Planar Inverted F Antenna for GSM/DCS Mobile Phones," *IEEE Trans. Antennas Propagat.*, vol.51, no.5, pp.1124 – 1129, May 2003.
44. Jin-Sen Chen, "Triple-frequency annular-ring slot antennas fed by CPW and Microstrip line," *IEEE Antennas Propagat. Soc. Int. Symp.*, Michigan, pp. 557-560, June 2003.
45. Tzung-Wern Chiou, Kin-Lu Wong, "A Compact Dual-Band Dual-Polarized Patch Antenna for 900/1800-MHz Cellular Systems," *IEEE Trans. Antennas Propagat.*, vol.51, no.8, pp.1936-1940, August 2003.

46. Christian Sabatier, "T-Dipole arrays for Mobile applications," *IEEE Antennas Propagat., Mag.*, vol.45, no.6, pp.9-26, December 2003.
47. Qwo-Yun Lee, Wen-Shyang Chen and Kin-Lu Wong, "Planar diversity folded-dipole antenna for 5 GHz WLAN operation," *Microwave Opt. Technol. Lett.*, vol.39, no.5, pp.158-161, 5 December 2003.
48. Chien-Jen Wang and Wen-Tsai Tsai, "A stair-shaped slot antenna for the triple band WLAN applications," *Microwave Opt. Technol. Lett.*, vol.39, no.5, pp.370-373, 5 December 2003.
49. Yeh-Chian Lin, Tsung-Wen Chiu and Kin-Lu Wong. "Small-size surface-mountable circularly polarized ceramic-chip antenna for GPS application," *Microwave Opt. Technol. Lett.*, vol.40, no.4, pp.300-302, 20 February 2004.
50. D.S.Yim. J.Kim and S.O.Park, "Novel wideband internal chip antenna for PCS / IMT-2000 Dual-band applications," *Microwave Opt. Technol Lett.*, vol.40, no.4, pp.324-326, 20 February 2004.
51. Horng-Dean Chen and Hong-Two Chen, "A CPW-fed dual frequency monopole antenna," *IEEE Trans. Antennas Propagat.*, vol.52, no.4, pp.978-982, April 2004.
52. H.C.Go and Y.W.Jang, "Multi-band modified fork-shaped microstrip monopole antenna with ground plane including dual-triangle portion," *Electron. Lett.*, vol.40, no.10, 13 May 2004.
53. Y.S.Shin and S.O.Park, "Broadband internal antenna of planar monopole type for mobile handsets," *IEEE Antennas Propagat. Soc. Int. Symp.*, Monterrey, CA, June 2004.
54. B.S.Collins, V.Nahar, S.P.Kingsley, S.Q.Zhang and S.Krupa, "A dual-band hybrid dielectric antenna for laptop computers," *IEEE Antennas Propagat. Soc. Int. Symp.*, Monterrey, CA, June 2004.
55. Jeong-Min Ju, Gyey-Teak Jeong, Joong-Han Yoon, Sung-Won Ko and Kyung-Sup Kwak "Design of multiple U-shaped slot microstrip patch antenna for 5 GHz Band WLANs," *Microwave Opt. Technol. Lett.*, vol.43, no.6, pp. 486-488, 20 December 2004.
56. H.K.Kan, D.Pavlickovski and R.B.Waterhouse, "A compact dual-interleaved printed antenna," *Microwave Opt. Technol. Lett.*, vol.43, no.6, pp. 501-503, 20 December 2004.

57. Jeong-Min Ju, Joong-Han Yoon, Sung-Won Ko, Moon-Gyu Kang and Kyung-Sup Kwak, "Fabrication and measurement of an arrow-shaped Microstrip patch antenna in the 5 GHz band," *Microwave Opt. Technol. Lett.*, vol.43, no.6, pp.503-505, 20 December 2004.
58. Saou-Wen Su, Kin-Lu Wong, Yuan-Tung Cheng and Wen-Shyang Chen, "Finite ground-plane effects on the ultra-wideband planar monopole antenna," *Microwave Opt. Technol. Lett.*, vol.43, no.6, pp. 535-537, 20 December 2004.
59. R.D.Richtmyer, "Dielectric resonators," *J.Appl. Phys.*, vol.10, pp. 391-398, June 1939.
60. A.Okaya and L.F.Barash, "The dielectric microwave resonator," *Proc. IRE*, vol.50, pp.2081-2092, October 1962.
61. Kikuo Wakino, Hiroshi Tamura and Takuji Sudo, "Dielectric Resonator materials and their applications," *Microwave Journal*, pp.133-148, June 1987.
62. S.Jerry Fiedziuszko and Stephen Holme, "Dielectric Resonators – raise your High-Q," *IEEE Microwave Magazine*, pp.51-60, September 2001.
63. S.Jerry Fiedziuszko, Ian.C.Hunter, Tatsuo Itoh, Yoshio Kobayashi, Toshio Nishikawa, Steven N. Stitzer and Kikuo Wakino, "Dielectric materials, devices and circuits," *IEEE Trans. Microwave Theory Tech.*, vol.50, no.3, pp.706-720, March 2002.
64. Wei Ke Hui and Ingo Wolff, "Dielectric Ring-gap resonator for application in MMIC's," *IEEE Trans. Microwave Theory Tech.*, vol.39, no.12, pp.2061-2068, November 1991.
65. Edward. K. N. Yung, Wilson. W. S. Lee, K. M. Luk, "A Dielectric resonator on a microstrip antenna," *IEEE Antennas Propagat. Soc. Int. Symp.*, Seattle, WA, pp.1504-1507, June 1994.
66. Hojoon Yoo, Chang-Hee Hyoung, Nam -Young Kim and Jong-Heon Kim, "Numerical method for computing the resonant frequencies and Q-factor in Microwave Dielectric Resonator," *Proc.,5th Int. Conf-Properties and Applications of dielectric materials*, Seoul, Korea, pp.1095-1098, May 1997.
67. Christopher L.Wagner and John B. Schneider, "On the analysis of resonators using Finite-Difference Time-Domain techniques," *IEEE Trans. Antennas Propagat.*, vol.51, no.10, pp.2885-2890, October 2003.

68. Yaxun Liu, Safieddin Safavi-Naeini, Sujeet K. Chaudhuri and Ramin Sabry, "Efficient simulation of rectangular dielectric resonators using volume MPIE-MoM formulation with combined entire-domain and sub domain basis functions," *IEEE Trans. Antennas Propagat.*, vol.52, no.1, pp.327-332, January 2004.
69. Yaxun Liu, Safieddin Safavi-Naeini, "Degenerated TE^{xy} modes of rectangular DR in MIC environment and their application to dual-mode bandpass filter," *IEEE Antennas Propagat. Soc. Int. Symp.*, Monterrey, CA, June 2004.
70. Yaxun Liu, Safieddin Safavi-Naeini and Sujeet K. Chaudhuri, "The coupling between two Te₁₁₈² mode rectangular DR's in MIC-environment," *IEEE Antennas Propagat. Soc. Int. Symp.*, Monterrey, CA, June 2004.
71. M.Gastine, L.Courtois and J.J.Dormann, "Electromagnetic Resonances of Free Dielectric Spheres," *IEEE Trans. Microwave Theory Tech.*, vol.15, pp. 694-700, December 1967.
72. O.Sager and F.Tisi, "On Eigen modes and Forced Resonance-Modes of Dielectric Spheres," *Proc. IEEE*, vol.56, pp.1593-1594, September 1968.
73. Stuart. A. Long, Mark W. McAllister, Liang C. Shen, 'The resonant Cylindrical Dielectric Cavity Antenna,' *IEEE Trans. Antennas Propagat.*, vol.31, no.3, pp. 406-412, May 1983.
74. A.A.Kishk, H.A.Auda and B.C.Ahn, "Accurate prediction of radiation patterns of dielectric-resonator antennas," *Electron. Lett.*, vol.23, no.25, pp.1374-1375, 1987.
75. R.K.Mongia and P.Bhartia, "Dielectric resonator antennas – a review and general design relations for resonant frequency and bandwidth," *International Journal of Microwave and Millimeter-Wave Computer-Aided Engineering*, vol.4, no.3, pp.230-247, 1994.
76. A.Petosa, A.Iltipiboon, Y.M.M.Antar, D.Roscoe and M.Cuhaci, "Recent advances in Dielectric resonator antenna technology," *IEEE Antennas Propagat. Mag.*, vol.40, no.3, pp.35-48, June 1998.
77. I.S.Ghosh, A.Hilgers, T.Schlenker and R.Porath, "Ceramic microwave antennas for mobile applications," *Journal of the European Ceramic Society*, vol.21, pp.2621-2628, 2001.
78. M. W. McAllister, S. A. Long and G. L. Conway, "Rectangular Dielectric Resonator Antenna," *Electron. Lett.*, vol.19, no.6, pp.218-219, 17 March 1983.

79. M. W. McAllister and S. A. Long "Resonant Hemispherical Dielectric Antenna," *Electron. Lett.*, vol.20, no.16, pp.657-659, 2 August 1984.
80. R.K.Mongia, A.Ittipiboon, P.Bhartia and M.Cuhaci, "Electric-monopole antenna using a dielectric ring resonator," *Electron. Lett.*, vol.29, no.17, pp.1530-1531, 19 August 1993.
81. G.P.Junker, A.A.Kishk, A.W.Glisson and D.Kajfez, "Effect of an air gap around the coaxial probe exciting a cylindrical dielectric resonator antenna," *Electron. Lett.*, vol.30, no.3, pp.177-178, 3 February 1994.
82. R. K. Mongia, A. Ittipiboon, M. Cuhaci, and D. Roscoe, "Circularly polarized dielectric resonator antenna," *Electron. Lett.*, vol.30, no.17, pp.1361-1362, 18 August 1994.
83. Z.Li, C.Wu and J.Litva, "Adjustable frequency dielectric resonator antenna," *Electron. Lett.*, vol.32, no.7, pp.606 - 607, 28 March 1996.
84. R.K.Mongia, "Small electric monopole mode dielectric resonator antenna," *Electron. Lett.*, vol.32, no.11, pp.947-948, 23 May 1996.
85. K.W.Leung, K.Y.Chow, K.M.Luk and E.K.N.Yung, "Excitation of dielectric resonator antenna using a soldered-through probe," *Electron. Lett.*, vol.33, no.5, pp.349-350, 27 February 1997.
86. M.T.K.Tam and R.D.Murch, "Half volume dielectric resonator antenna designs," *Electron. Lett.*, vol.33, no.23, pp. 1914-1916, 6 November 1997.
87. A.Sangiovanni, J.Y.Dauvignac and C.Pichot, "Embedded dielectric resonator antenna for bandwidth enhancement," *Electron. Lett.*, vol.33, no.25, pp.2090-2091, 4 December 1997.
88. R.T.Long, R.J.Dorris, S.A.Long, M.A. Khayat and J.T.Williams, "Use of parasitic strip to produce circular polarisation and increased bandwidth for cylindrical dielectric resonator antenna," *Electron. Lett.*, vol.37, no.7, pp.406-408, 29 March 2001.
89. Ahmed A.Kishk, Yan Yin and A.W.Glisson, "Conical dielectric resonator antennas for wide-band applications," *IEEE Trans. Antennas Propagat.*, vol.50, no.4, pp.469-474, April 2002.

90. Young-do Kim, Myoung-seok Kim and Hong-min Lee, "Internal rectangular dielectric resonator antenna with broadband characteristic for IMT-2000 handset," *IEEE Antennas Propagat. Soc. Int. Symp.*, San Antonio, Texas, pp.22-25, June 2002.
91. B.J.Fasenfast, A.G.Walsh, C.S. De Young, T.F.Kennedy, S.A.Long and J.T.Williams, "Investigation of low profile, conformable, dielectric resonator antennas," *Electron. Lett.*, vol.39, no.1, pp. 12-13, 9 January 2003.
92. C.Nannini, J.M.Ribero, J.Y.Dauvignac and Ch.Pichot, "A dual frequency dielectric resonator antenna," *Microwave Opt. Technol. Lett.*, vol.38, no.1, pp.9-10, 5 July 2003.
93. Jian-Juang Chen, Yi-Cheng Lin and Ruey-Beei Wu, "A dual band elliptical DRA," *IEEE Antennas Propagat. Soc. Int. Symp.*, Monterrey, CA, June 2004.
94. K.Pliakostathis and D.Mirshekar-Syahkal, "Stepped dielectric resonator antennas for wideband applications," *IEEE Antennas Propagat. Soc. Int. Symp.*, Monterrey, CA, June 2004.
95. Mohamed Al Sharkawy, Atef Z.Elsherbini and Charles E.Smith, "Stacked elliptical dielectric resonator antennas for wideband applications," *IEEE Antennas Propagat. Soc. Int. Symp.*, Monterrey, CA, June 2004.
96. A.Ittipiboon, R.K.Mongia, Y.M.M.Antar, P.Bhartia, M.Cuhaci, "An Integrated rectangular Dielectric Resonator Antenna," *IEEE Antennas Propagat. Soc. Int. Symp.*, Michigan, pp.604-607, June 1993.
97. R.K.Mongia, A.Ittipiboon, M.Cuhaci, "Low profile Dielectric Resonator Antennas using a very high permittivity material," *Electron. Lett.*, vol.30, no.17, pp.1362-1363, 18 August 1994.
98. K.W.Leung, K.M.Luk and E.K.N.Yung, "Spherical cap dielectric resonator antenna using aperture coupling," *Electron. Lett.*, vol.30, no.17, pp.1366-1367, 18 August 1994.
99. K.W.Leung, K.M.Luk, E.K.N Yung, S.Lai, "Characteristics of a low-profile circular disk DR antenna with very high permittivity," *Electron. Lett.*, vol.31, no.6, pp.417-418, 16 March 1995.
100. M.B.Oliver, Y.M.M.Antar, R.K.Mongia A.Ittipiboon, "Circularly polarized rectangular dielectric resonator antenna," *Electron. Lett.*, vol.31, no.6, pp.418-419, 16 March 1995.

101. G.P.Junker, D.Kajfez, A.A.Kishk and A.W.Glisson, "Effect of aperture filling on slot-coupled dielectric resonator antennas operating in HEM_{11} mode," *Electron. Lett.*, vol.31, no.10, pp.774-775, 11 May 1995.
102. K.Y.Chow, K.W.Leung, K.M.Luk and E.K.N.Yung, "Cylindrical dielectric resonator antenna array," *Electron. Lett.*, vol.31, no.18, pp. 1536-1537, 31 August 1995.
103. M.G.Keller, D.J.Roscoe, M.B.Oliver, R.K.Mongia, Y.M.M.Antar and A.Ittipiboon, "Active aperture-coupled rectangular dielectric resonator antenna," *IEEE Microwave and guided wave letters*, vol.5, no.11, pp. 376-378, November 1995.
104. K.P.Esselle, "Circularly polarized higher-order Rectangular dielectric resonator antenna," *Electron. Lett.*, vol.32, no.3, pp.150-151, 1 February 1996.
105. Karu P.Esselle, "A low profile rectangular dielectric resonator antenna," *Electron. Lett.*, vol.44, no.9, pp.1296-1297, September 1996.
106. K.W.Leung, K.Y.Chow, K.M.Luk, and E.K.N Yung, "Offset dual-disk dielectric resonator antenna of very high permittivity," *Electron. Lett.*, vol.32, no.22, pp.2038-2039, 24 October 1996.
107. Y.Hwang, Y.P.Zhang, K.Mluk and E.K.N.Yung, "Gain enhanced miniaturised rectangular dielectric resonator antenna," *Electron. Lett.*, vol.33, no.5, pp.350-352, 27 February 1997.
108. K.W.Leung and M.W.To, "Slot-coupled dielectric resonator antenna using a proximity feed on a perpendicular substrate," *Electron. Lett.*, vol.33, no.20, pp.1665-1666, 25 September 1997.
109. K.W.Leung, W.C.Wong, K.M.Luk and E.K.N Yung, "Annular slot-coupled dielectric resonator antenna," *Electron. Lett.*, vol.34, no.13, pp.1275-1276, 25 June 1998.
110. H.Y.Lo, K.W.Leung, K.M.Luk and E.K.N Yung, "Low profile equilateral – triangular dielectric resonator antenna of very high permittivity," *Electron. Lett.*, vol.35, no.25, pp.2164-2166, 9 December 1999.
111. K.W.Leung and S.K.Mok, "Circularly polarized dielectric resonator antenna excited by perturbed annular slot with backing cavity," *Electron. Lett.*, vol.37, no.15, pp.934-936, 19 July 2001.

112. A.Laisne, R.Gillard and G.Piton, "Robust slot-fed dielectric resonator antenna using an intermediate substrate," *Electron. Lett.*, vol.37, no.25, pp.1497-1498, 6 December 2001.
113. Chih-Yu Huang and Jieh-Sen Kuo, "Frequency-adjustable circularly polarized dielectric resonator antenna," *Microwave Opt. Technol. Lett.*, vol.34, no.3, pp.211-213, 5 August 2002.
114. A.Petosa, A.Ittipiboon and S.Thirakoune, "Perforated dielectric resonator antenna," *Electron. Lett.*, vol.38, no.24, pp.1493-1495, 21 November 2002.
115. Yong Xin Guo and Kwai.Man Luk, "Dual Polarized dielectric resonator antennas," *IEEE Trans. Antennas Propagat.*, vol.51, no.5, pp.1120-1123, May 2003.
116. Aldo Petosa, Soulideth Thirakoune and Apisak Ittipiboon, "Array of perforated dielectric resonator antennas," *IEEE Antennas Propagat. Soc. Int. Symp.*, Monterrey, CA, June 2004.
117. C.Nannini, J.M.Ribero, J.Y. Dauvignac and Ch.Pichot, "Bifrequency behaviour and bandwidth enhancement of a dielectric resonator antenna," *Microwave Opt. Technol. Lett.*, vol.42, no.5, pp.432-434, 5 September 2004.
118. Roger. A. Kranenburg, Stuart.A.Long and Jeffrey.T.Williams, "Coplanar waveguide excitation of Dielectric Resonator Antennas," *IEEE Trans. Antennas Propagat.*, vol.29, no.1, pp.119-122, January 1991.
119. Richard Q. Lee and Rainee N.Simons, "Bandwidth enhancement of Dielectric Resonator Antennas," *IEEE Antennas Propagat. Soc. Int. Symp.*, Seattle, WA, pp.1500-1503, June 1994.
120. Jian-Yi Wu, Chih-Yu Huang, Kin-Lu Wong, "Low Profile very high permittivity DRA excited by a coplanar waveguide," *Microwave Opt. Technol. Lett.*, vol.22, no.2, pp.96-97, 20 July 1999.
121. Sheng-Ming Deng, Tsung-Wen Chen and Hsiao-Hsun Kan, "A CPW-Fed Rectangular Dielectric Resonator Antenna," *Proc. IEEE APMC*, Taipei, pp.954-956, 2001.
122. M.S.Al Salameh, Yahia. M.M.Antar and Guy Seguin, "Coplanar-Waveguide-fed Slot-coupled Rectangular Dielectric Resonator Antenna," *IEEE Trans. Antennas Propagat.*, vol.50, no.10, pp.1415-1419, October 2002.

123. Yong Xin Guo and Kwai-Man Luk, "On improving coupling between a coplanar waveguide feed and a dielectric resonator antenna," *IEEE Trans. Antennas Propagat.*, vol.51, no.8, pp. 2142-2144, August 2003.
124. S.M.Deng, C.L.Tsai, C.W.Chiu and S.F.Chang, "CPW_Fed rectangular ceramic dielectric resonator antennas with high profile," *IEEE Antennas Propagat. Soc. Int. Symp.*, Monterrey, CA, June 2004.
125. Bratin Ghosh, Yahia.M.M.Antar, Aldo Petosa and Apisak Ittipiboon, "Feed configurations of CPW fed DRA," *IEEE Antennas Propagat. Soc. Int. Symp.*, Monterrey, CA, June 2004.
126. R.A.Kranenburg and S. A. Long, "Microstrip Transmission Line Excitation of Dielectric Resonator Antennas," *Electron. Lett.*, vol.24, no.18, pp.1156-1157, 1 September 1988.
127. A.Petosa, R.K.Mongia, A.Ittipiboon and J.S.Wight, "Design of microstrip-fed series array of dielectric resonator antennas," *Electron. Lett.*, vol.31, no.16, pp.1306-1307, 3 August 1995.
128. G.Drossos, Z.Wu and L.E.Davis, "Circular polarised cylindrical dielectric resonator antenna," *Electron. Lett.*, vol.32, no.4, pp.281-283, 15 February 1996.
129. A.Petosa, A.Ittipiboon, M.Cuhaci and R.Larose, "Bandwidth improvement for a microstrip-fed series array of dielectric resonator antennas," *Electron. Lett.*, vol.32, no.7, pp.608-609, 28 March 1996.
130. Cheng-Shong Hong, "Adjustable frequency dielectric resonator antenna," *Proc. Natl. Sci. Counc. ROC (A)*, vol.23, no.6, pp.736-738, 1999.
131. K.M.Luk, M.T.Lee, K.W.Leung and E.K.N.Yung, "Technique for improving coupling between microstripline and dielectric resonator antenna," *Electron. Lett.*, vol.35, no.5, pp.357-358, 4 March 1999.
132. K.W.Leung, W.C.Wong, K.M.Luk and E.K.N.Yung, "Circular-polarised dielectric resonator antenna excited by dual conformal strips," *Electron. Lett.*, vol.36, no.6, pp.484-486, 16 March 2000.
133. K.W.Leung, "Simple result for conformal-strip excited hemispherical dielectric resonator antenna," *Electron. Lett.*, vol.36, no.11, pp.933-935, 25 May 2000.
134. Fu-Ren Hsiao, Jieh-Sen Kuo, Tzung-Wern Chiou and Kin-Lu Wong, "A broadband very-high-permittivity dielectric resonator antenna for WLAN application in the 5.2

- GHz band," *Microwave Opt. Technol. Lett.*, vol.32, no.6, pp.426-427, 20 March 2002.
135. B.Bit-Babik, C. Di Nallo and A. Faraone, "Multimode dielectric resonator antenna of very high permittivity," *IEEE Antennas Propagat. Soc. Int. Symp.*, Monterrey, CA, June 2004.
 136. Y.Sung, C.S.Ahn and Y.S.Kim, "Microstripline fed dual-frequency dielectric resonator antenna," *Microwave Opt. Technol. Lett.*, vol.42, no.5, pp.388-390, 5 September 2004.
 137. G.P.Junker, A.A.Kishk, and A.W.Glisson, "MoM Solution of wire radiators coupled to dielectric bodies of revolution," *IEEE Antennas Propagat. Soc. Int. Symp.*, Michigan, pp. 40-43, June 1993.
 138. G.P.Junker, A.A.Kishk, A.W.Glisson and D.Kajfez, "Effect of air gap on cylindrical dielectric resonator antenna operating in TM_{01} mode," *Electron. Lett.*, vol.30, no.2, pp. 97-98, 20 January 1994.
 139. Ahmed A.Kishk, G.Zhou and Allen W.Glisson, "Analysis of Dielectric Resonator Antennas with emphasis on hemispherical structures," *IEEE Antennas Propagat., Mag.*, vol.36, no.2, pp.20-31, April 1994.
 140. R.K.Mongia, A.Ittipiboon, M.Cuhaci, D.Roscoe, "Radiation Q-Factor of rectangular Dielectric Resonator Antennas: Theory and Experiment," *IEEE Antennas Propagat. Soc. Int. Symp.*, Seattle, WA, pp.764-767, June 1994.
 141. S.M.Shum and K.M.Luk, "Analysis of aperture coupled rectangular dielectric resonator antenna," *Electron. Lett.*, vol.30, no.21, pp. 1726-1727, 13 October 1994.
 142. Kwai.Man. Luk, Wai-Kee Leung and Kwok-Wa Leung, "Mutual impedance of hemispherical dielectric resonator antennas," *IEEE Trans. Antennas Propagat.*, vol.42, no.12, pp.1652-1654, December 1994.
 143. Y.M.M.Antar and Z.Fan, "Characteristics of aperture-coupled rectangular dielectric resonator antenna," *Electron. Lett.*, vol.31, no.15, pp.1209-1210, 20 July 1995.
 144. S.M.Shum and K.M.Luk, "FDTD analysis of probe-fed cylindrical dielectric resonator antenna operating in fundamental broadside mode," *Electron. Lett.*, vol.31, no.15, pp.1210-1212, 20 July 1995.

145. Gregory P.Junker, Ahmed.A.Kishk and Allen.W.Glisson, "Input impedance of aperture-coupled dielectric resonator antenna," *IEEE Trans. Antennas Propagat.*, vol.44, no.5, pp.600-607, May 1996.
146. K.W.Leung, K.W.Ng, K.M.Luk and E.K.N.Yung, "Simple formula for analysing the centre-fed hemispherical dielectric resonator antenna," *Electron. Lett.*, vol.33, no.6, pp.440-441, 13 March 1997.
147. R.K Mongia and A.Ittipiboon, "Theoretical and experimental investigations on rectangular dielectric resonator antennas," *IEEE Trans. Antennas Propagat.*, vol.45, no.9, pp.1348-1356, September 1997.
148. Shiu-Ming Shum and Kwai-Man Luk, "FDTD Analysis of Probe-fed cylindrical dielectric resonator antenna," *IEEE Trans. Antennas Propagat.*, vol.46, no.3, pp.325-333, March 1998.
149. Gregory.P.Junker, Ahmed.A.Kishk and Allen W.Glisson, "Multiport network description and radiation characteristics of coupled dielectric resonator antennas," *IEEE Trans. Antennas Propagat.*, vol. 46, no.3, pp.425-433, March 1998.
150. K.W.Leung, Z.N.Chen, K.M.Luk and Edward.K.N.Yung, "Aperture-coupled dielectric resonator antenna with a thick ground plane," *IEEE Trans. Antennas Propagat.*, vol.46, no.8, pp. 1242-1243, August 1998.
151. Yahia M.M. Antar, Dajun Cheng, Guy Sequin, Bruce Henry and Mike G. Keller, "Modified waveguide model (MWGM) for rectangular dielectric resonator antenna (DRA)," *Microwave Opt. Technol. Lett.*, vol.19, no.2, pp.158-160, 5 October 1998.
152. George Drassos, Zhipeng Wu and Lionel D.Davis, "Theoretical and experimental investigations on a microstrip-coupled cylindrical dielectric resonator antenna," *Microwave Opt. Technol. Lett.*, vol.21, no.1, pp.18-25, 5 April 1999.
153. B.Henry, A.Petosa, Y.M.M.Antar and G.A.Morin, "Mutual coupling between rectangular multisegment dielectric resonator antennas," *Microwave Opt. Technol. Lett.*, vol.21, no.1, pp.46-48, 5 April 1999.
154. K.W.Leung, K.K.Tse, K.M.Luk and Edward K.N.Yung, "Cross-polarisation characteristics of a probe-fed hemispherical dielectric resonator antenna," *IEEE Trans. Antennas Propagat.*, vol.47, no.17 pp.1228-1230, July 1999.

155. Supriyo Dey and Raj Mittra, "A conformal Finite-Difference Time Domain technique for modelling cylindrical dielectric resonators," *IEEE Trans. Microwave Theory Tech.*, vol.47, no.9, pp.1737-1739, September 1999.
156. Y.X.Guo, K.M.Luk and K.W.Leung, "Characteristics of aperture-coupled cylindrical dielectric resonator antennas on a thick ground plane," *Proc. IEE Microwave Antennas. Propag.*, vol.146, no.6, December 1999.
157. A.Sangiiovanni, P.Y.Garel, J.Y.Dauvignac and Ch.Pichot, "Numerical analysis of dielectric resonator antennas," *International Journal of Numerical modelling: Electronic Networks, Devices and fields*, vol.13, pp.199-215, March 2000.
158. Kwok Wa Leung, "Conformal strip excitation of dielectric resonator antenna," *IEEE Trans. Antennas Propagat.*, vol.48, no.6, pp.961-967, June 2000.
159. K.W.Leung, "Analysis of aperture-coupled hemispherical dielectric resonator antenna with a perpendicular feed," *IEEE Trans. Antennas Propagat.*, vol.48, no.6, pp.1005-1007, June 2000.
160. Zhongxiang Shen, John L.Volakis and Robert H.MacPhie, "Modeling of cylindrical dielectric resonator antennas by the modal-expansion analysis," *Microwave Opt. Technol. Lett.*, vol.26, no.1, pp.13-16, 5 July 2000.
161. Yuehe Ge and Karu P.Esselle, "Computation of the radiation patterns of a rectangular dielectric resonator antenna using the Method of Moments," *Microwave Opt. Technol. Lett.*, vol.27, no.6, pp.382-384, 20 December 2000.
162. S.G.O'Keefe, "Use of symmetry planes in two excitation modes of the cylindrical dielectric resonator antenna," *Proc. Microelectronic engineering research conference*, 2001.
163. M.H.Neshati and Z.Wu, "The determination of the resonant frequency of the TE_{111}^y mode in a rectangular dielectric resonator for antenna application," *11th International conference on Antennas and Propagation (IEE)*, pp.53-56, 17-20 April 2001.
164. M.H.Neshati and Z.Wu, "Rectangular dielectric resonator antennas: theoretical modelling and experiments," *11th International conference on Antennas and Propagation (IEE)*, pp.866-870, 17-20 April 2001.
165. N.Farahat, W.Yu, R.Mittra and T.Koleck, "Cross-shaped dielectric resonator antenna analysis using conformal finite difference time-domain method," *Electron. Lett.*, vol.37, no.18, pp.1105-1106, 30 August 2001.

166. Ahmed. A. Kishk, "A triangular dielectric resonator antenna excited by a coaxial probe," *Microwave Opt. Technol. Lett.*, vol.30, no.5, pp. 340-341, 5 September 2001.
167. A.A.Kishk and A.W.Glisson, "Bandwidth enhancement for split cylindrical dielectric resonator antennas," *Progress in Electromagnetics Research*, PIER – 33, pp. 97-118, 2001.
168. Zhijun Liu, Weng Cho Chew and Eric Michielssen. "Numerical modelling of dielectric resonator antennas in a complex environment using the method of moments," *IEEE Trans. Antennas Propagat.*, vol.50, no.1, pp.79-82, January 2002.
169. Steven G.O'Keefe, Simon P.Kingsley and Seppo Saario, "FDTD Simulation of Radiation characteristics of Half-volume HEM- and TE-mode dielectric resonator antennas," *IEEE Trans. Antennas Propagat.*, vol.50, no.2, pp.175-179, February 2002.
170. E. Semouchkina, G. Semouchkin, W. Cao, and Raj Mittra, "FDTD analysis of modal characteristics of dielectric resonator antennas," *IEEE Antennas Propagat. Soc. Int. Symp.*, San Antonio, Texas, pp.466-469, June 2002.
171. Ahmed. A. Kishk, "Tetrahedron and Triangular Dielectric Resonator Antenna with wideband performance," *IEEE Antennas Propagat. Soc. Int. Symp.*, San Antonio, Texas, pp.462-465, June 2002.
172. K.K.So and K.W.Leung, "Annular-slot excited dielectric resonator antenna with a backing cavity," *IEEE Antennas Propagat. Soc. Int. Symp.*, San Antonio, Texas, pp.470-473, June 2002.
173. B.Li, K.K.So and K.W.Leung, "A circularly polarized dielectric resonator antenna excited by an asymmetrical U-slot with a backing cavity," *IEEE Antennas and Wireless Propagation Lett.*, vol.2, pp.133-135, 2003.
174. Guido Biffi Gentili, Marco Morini and Stefano Selleri, "Relevance of coupling effects on DRA array design," *IEEE Trans. Antennas Propagat.*, vol.51, no.3, pp.399-404, March 2003.
175. A.A.Kishk, Xiao Zhang, Allen W.Glisson and Darko Kajfez, "Numerical analysis of stacked dielectric resonator antennas excited by a coaxial probe for wideband applications," *IEEE Trans. Antennas Propagat.*, vol.51, no.8, pp. 1996-2006, August 2003.

176. Ahmed.A.Kishk, "Wide-band truncated tetrahedron dielectric resonator antenna excited by a coaxial probe," *IEEE Trans. Antennas Propagat.*, vol.51, no.10, pp.2913-3006, October 2003.
177. X.Q.Sheng, K.W.Leung and E.K.N.Yung, "Analysis of waveguide-fed dielectric resonator antenna using a hybrid finite element method / moment method," *IEE Proc. Microwave Antennas Propagat.*, vol.151, no.1, pp. 91-95, February 2004.
178. Islam A.Eshrah, A.A.Kishk, Alexander B.Yakovlev and Allen W.Glisson, "Modeling of a waveguide probe excitation for dielectric resonator antennas," *IEEE Antennas Propagat. Soc. Int. Symp.*, Monterrey, CA, June 2004.

Dielectric Resonator Antenna

In the recent past, the frequency range of interest for many applications has gradually progressed upward, reaching beyond the usual microwave band. Most of the antennas commonly used in the microwave band cannot be simply scaled up in frequency. Conduction losses do not remain constant after scaling, and as a result affect the efficiency of the system. In this scenario, Dielectric Resonator Antennas attract the attention of antenna designers.

The chapter describes the important properties of the Dielectric Resonator, the resonance phenomenon and its potential as a radiator. Various resonator shapes, feeding mechanism, and applications are also discussed. The scheme of work and measurement techniques is explained towards the end of the chapter.

3.1 Dielectric Resonator

Dielectric materials are key to the realization of low-loss, temperature stable microwave resonators. High quality resonating elements are fundamental to the operation of filters and oscillators, and the performance of these circuits is primarily limited by the Quality factor (Q) of the resonator used. In as early as 1939, Richtmyer [1] of Stanford University showed that unmetallized dielectric objects (toroid) could function as microwave resonators. In fact, he is credited for coining the term, “Dielectric Resonator (DR)”. Dielectric Resonators are an attractive, low cost alternative to traditional metallic resonant cavities. They have the advantage of size reduction without reduction in performance. They also exhibit a significantly higher Q factor than transmission lines and Microstrips. In addition, temperature variation of the resonant frequency of DR’s can be engineered to a desired value to meet the requirements of the circuit designer. Table 3.1 compares the properties of various resonators.

Resonator	Size	Q factor	τ_f	Integrability with MICs
Metallic Cavity	Large	High	Low	Non-integrable
Microstrip Resonators	Small	Very Low	High	Integrable
DR	Very Small	Very High	Very Low	Integrable

Table 3.1 Properties of resonators

3.2 Material Properties

By virtue of their compactness, the dielectric resonators have replaced waveguide filters in such demanding applications as satellite communications where Microstrip and Stripline resonators cannot perform well because of their inherently

high losses. The important requirements of a dielectric material for use as resonating elements are:

- * High dielectric constant ($10 < \epsilon_r < 100$) for better miniaturization
- * High Quality factor ($Q > 5000$) for better frequency selectivity
- * Nearly zero temperature coefficient of resonant frequency (τ_f) for frequency stability with temperature

◆ Dielectric Constant

The ability of dielectric materials to be polarized under the action of an external electric field is numerically described by the Polarization \mathbf{P} . In the absence of an external electric field, each element in the volume of a dielectric has no electric moment because the algebraic sum of the charges in all molecules of the dielectric in a given volume is equal to zero, and the centres of gravity of the positive and negative charges coincide in space. An external electric field brings the charges of the molecules of the dielectric into a certain ordered arrangement in space. The dielectric polarization \mathbf{P} is equal to the total dipole moment induced in the volume of the material by the electric field. In most cases, the magnitude of polarization is directly proportional to the intensity of the electric field at a given point of a dielectric.

$$\mathbf{P} = \chi_e \epsilon_0 \mathbf{E} \quad (3.1)$$

χ_e is the electric susceptibility and the coefficient $\epsilon = \epsilon_r \epsilon_0$ is the absolute permittivity of the medium, where ϵ_r is the dielectric constant / relative permittivity of the medium and $\epsilon_0 = 8.854 \times 10^{-12}$ F/m. The relative permittivity is related to the dielectric susceptibility by the relation

$$\epsilon_r = 1 + \chi_e \quad (3.2)$$

ϵ_r of a dielectric determines its ability to form a capacitance by virtue of its polarization [2].

$$Q_d = 1 / \tan \delta \quad (3.12)$$

The manufacturers of dielectric resonators usually specify the value of Q_d to be inversely proportional to frequency. i.e, $Q_d = C/f$ or $C = Q_d \times f$. For eg: the material $\text{Ca}_5\text{Nb}_2\text{TiO}_{12}$ has $Q_d \times f = 26000$, when f is expressed in GHz. At 2 GHz, this material has $Q_d = 13000$, and at 3 GHz the same material has $Q_d = 8667$. Q in the microwave region is measured by placing a cylindrical sample in a transmission cavity proposed by Krupka *et al.* [4].

◆ Temperature Coefficient of resonant frequency (τ_f)

The sensitivity of the resonant frequency of a DR with temperature is denoted by the temperature coefficient of the resonant frequency (τ_f).

$$\tau_f = (1 / f) (\Delta f / \Delta T) \quad (3.13)$$

where f is the resonant frequency at room temperature, Δf is the variation of resonant frequency from room temperature for a change in temperature ΔT . τ_f depends on the temperature variation of ϵ_r (τ_ϵ), and the co-efficient of linear expansion α as given by the expression

$$\tau_f = -\alpha - 1/2 \tau_\epsilon \quad (3.14)$$

Since all solid materials expand with rising temperature, the dielectric material must exhibit a negative τ_ϵ for temperature compensation. The value of τ_f ought to be nearly zero for practical applications. However, often the device engineer requires a low positive or negative τ_f to compensate for the temperature variation of the resonant frequency due to the circuit. τ_f in the microwave region is measured by varying the temperature in the range from 25°C to 80°C at $\sim 2^\circ\text{C}/\text{minute}$. The shift in resonant frequency as a result of heating in the reflection mode is noted using the Network analyser [5].

3.3 The Resonance phenomenon

A dielectric resonator is defined as “an unmetallized piece of dielectric which functions as a resonant cavity by means of reflections at the dielectric – air interface”. The discontinuity of the relative permittivity at the resonator surface allows a standing electromagnetic wave to be supported in its interior at a particular resonant frequency, thereby leading to maximum confinement of energy within the resonator. The reflection coefficient of a wave in a high dielectric constant region incident on an air-filled region approaches +1.

$$\Gamma = \left| \frac{\eta_o - \eta}{\eta_o + \eta} \right| = \frac{\sqrt{\epsilon_r} - 1}{\sqrt{\epsilon_r} + 1} \rightarrow 1 \text{ as } \epsilon_r \rightarrow \infty \quad (3.15)$$

Figure 3.1 illustrates the total multiple internal reflections at the dielectric - air interface.

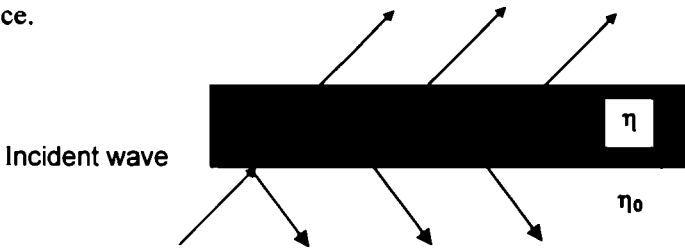


Figure 3.1 Schematic sketch of the total multiple internal reflections at the dielectric-air interface

If the transverse dimensions are comparable to the wavelength of the microwave within the dielectric ($\lambda_g = \lambda_0 / \sqrt{\epsilon_r}$), then certain field distributions or modes will satisfy Maxwell's equations and boundary conditions. Therefore, in the microwave frequency range, the dielectric constant (ϵ_r) of the resonator materials is in the range 10-100 to aid miniaturization.

Dielectric resonators have been modelled numerically, studied analytically, and many aspects of the performance have been confirmed experimentally. An accurate mathematical description of the electromagnetic field in a dielectric

resonator is considerably more complicated than the field description in a hollow waveguide resonator. Among the various shapes of resonators, the cylindrical disc resonators have been investigated in detail. Though the closed cavity model with perfect magnetic conductor walls proposed by Hung Yuet Yee and S.B.Cohn [6] and the Conventional Waveguide Model (CWGM), proposed by Itoh and Rudokas [7] are suitable for CAD applications due to the reduced computation time, the CWGM which yields accurate results for the cylindrical DR, gives rise to larger error when applied to the rectangular DR. More accurate results for a rectangular DRA have been yielded by MWGM - the modified waveguide model proposed by Yahia.M.M.Antar *et al.* [8].

◆ Resonant modes in a DR

Resonant modes are field structures that can exist inside the DR. As in the case of all resonant cavities, there are many possible resonant modes that can be excited in dielectric resonators. These can be divided into three main families.

Transverse Electric mode (TE)

Transverse Magnetic mode (TM)

Hybrid Electromagnetic mode (HEM)

For higher modes, the pure transverse electric or transverse magnetic fields cannot exist, so that both electric and magnetic fields have non-vanishing longitudinal components. These are called hybrid electromagnetic (HEM) modes. According to Van Bladel [9], the modes in an arbitrarily shaped DR can be of the confined or non-confined types, the confined modes being supported only by dielectric bodies of revolution (eg: spherical, cylindrical, etc.). For both confined (TM) and non-confined (TE) modes, the following condition is satisfied at all the surfaces of the resonator.

$$n \cdot \mathbf{E} = 0 \quad (3.16.a)$$

where \mathbf{E} denotes the electric field intensity and n denotes the normal to the surface of the resonator. The above equation is one of the conditions that fields satisfy a magnetic wall. The other condition,

$$n \times \mathbf{H} = 0 \quad (3.16.b)$$

is not necessarily satisfied at all the surfaces of the DR by all the modes. The modes that satisfy both 3.16(a) and 3.16(b) are known as *confined* modes, while those that satisfy only (a) are known as *non-confined* modes. The lowest order *non-confined* and *confined* modes radiate like a magnetic dipole and electric dipole respectively. Theoretically a rectangular DR not being a body of revolution, does not satisfy equation. 3.16(b) and hence does not support confined modes [10].

◆ Radiation from a DR

Low loss ($\tan\delta < 10^{-4}$) and high relative permittivity ($10 \leq \epsilon_r \leq 100$) DR's are widely used in shielded microwave circuits, where they exhibit a very high unloaded Q factor given by:

$$Q_u = \frac{1}{\tan \delta} \quad (3.17)$$

The early studies on DR's laid emphasis on the structure as an energy storage device. However, when the cavity is not enclosed by metallic walls, electromagnetic fields do exist beyond the geometrical boundary of the cavity. Open dielectric resonators thus offer attractive features as antenna elements [11], since the Q-factors of the lowest order modes of the resonator are reduced significantly due to the power lost in the radiated fields. Different resonant modes have distinct electromagnetic field distributions within the DRA, and each mode may provide a different radiation pattern. Use of lower dielectric constant materials and proper choice of the resonator dimensions enhance these radiation fields, lowering the radiation Q factor (Q_r), corresponding to a wider bandwidth and higher radiation efficiency. This is made possible by minimizing the volume to surface ratio. A proper selection of the resonator shape mitigates the effect of increasing the dielectric constant, while keeping the antenna size very compact. For eg: a rectangular resonator with a flat tile shape has a wider bandwidth than a dielectric cube resonating at the same frequency. Ring structures, conical DRA, stepped DRA's, stacking of DRA's, use of parasitic

DR's and metal strips added to the DR surface enhance the bandwidth performance of the DRA. Bandwidth can also be enlarged by designing a resonator supporting different modes with closely spaced resonant frequencies [12-21]. Several attractive features of a DRA are listed below.

- Intrinsic mechanical simplicity
- The liberty of the designer in controlling the size and bandwidth of the DRA by choosing from a wide range of permittivity values
- Use of different resonator shapes, allowing for flexibility of design
- Possibility of several feeding mechanisms, making the DRA's amenable to integration with various existing technologies
- Excitation of various modes, producing broadside or conical shaped radiation patterns for different coverage requirements, by making use of the unique internal and associated external field distribution of each mode
- Absence of conductor losses and surface wave losses leading to high radiation efficiency, especially at higher frequencies

However, it is relatively uneasy to form a DR with configurations precisely suitable for a specific resonant frequency. Also, the native hardness of the material makes it difficult to make slight geometrical modifications to a constructed DRA to compensate for manufacturing tolerances or fabrication errors. While the features of the DRA can be fully exploited when the frequencies of operation are of the order of several Giga Hertz or higher, to obtain a reasonable antenna size in such bands, very high dielectric constant would be required, since the size of a DRA is proportional to $\epsilon_r^{-1/2}$. High permittivity is also a requirement for integration with printed technology - to achieve strong direct coupling from Microstrip lines to DRA's. However the Q of the antenna increases as $\epsilon_r^{3/2}$, thereby causing an unacceptable reduction in bandwidth. Nevertheless, the advantage offered by this phenomenon is the reduction of the interaction between antenna elements in DRA arrays [22] due to the high stored energy. Thus there are conflicting requirements in the design of DRA's.

3.4 The Rectangular Dielectric Resonator Antenna

The dimensional degrees of freedom are considered in comparing various DR geometries. Tunable dimensions for hemispherical, circular cylindrical and rectangular shapes are one, two and three respectively. One-dimensional freedom makes hemispherical DRA's easy to design but difficult to optimise for particular requirements, limiting their use. For example, the radius of a hemispherical DRA with a certain material singularly determines its resonant frequency and bandwidth. The radius-height pair determines the behaviour of circular cylindrical DRA's. Hemispheres and circular cylinders always support degenerate resonant modes because of the existence of certain structural symmetry. These modes may increase the cross-polarisation level that is unwanted in linear polarisations, but may be necessary for dual or circular polarisation designs. The existence of two independent aspect ratios in a rectangular DRA offers better design flexibility [23]. Proper choice of the dimensions can also avoid the mode degeneracy problem, leading to lower cross polarisation.

Figure 3.4 (a) illustrates an isolated rectangular DR and Figure 3.4(b) shows a probe excited DRA. Assuming the ground plane to be infinitely large, image theory is applied to replace the isolated DR by a resonator of half the height. Using the conventional dielectric waveguide model, the isolated resonator may be assumed to be the truncation of an infinite rectangular dielectric waveguide. However, in the analytical method proposed by R.K.Mongia *et al.* [23-24], two of the six surfaces of the resonator are assumed to be imperfect magnetic walls, while the remaining four are assumed to be perfect magnetic walls. The TE modes of a rectangular DR can be transverse to any of the three independent dimensions (TE_{mnp}^x , TE_{mnp}^y , and TE_{mnp}^z). The fields of the TE_{mnp}^z mode may be obtained by solving Maxwell's equations with the magnetic wall model boundary conditions at $x = \pm a/2$ and $y = \pm b/2$ and continuous tangential fields at $z = \pm d/2$. This model is therefore essentially a

combination of the Magnetic wall model (MWM) and the Conventional Dielectric Waveguide Model (CDWM).

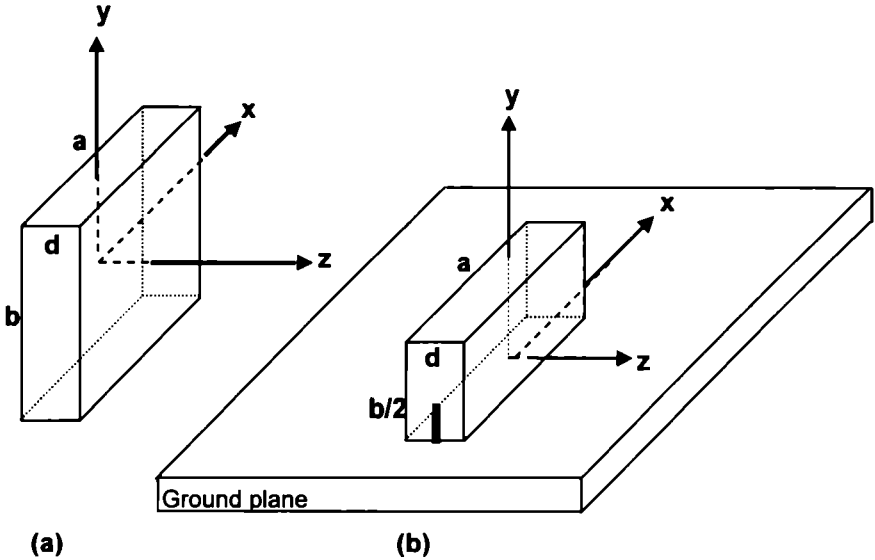


Figure 3.4 (a) Isolated rectangular DRA ($a > b > d$)
(b) Probe fed rectangular DRA on a ground plane

The field components are derived from the z directed magnetic potential ϕ^h :

$$H_z = \frac{(k_x^2 + k_y^2)}{j\omega\mu_0} A \cos(k_x x) \cos(k_y y) \cos(k_z z) \quad 3.18 (a)$$

$$H_x = \frac{k_x k_z}{j\omega\mu_0} A \sin(k_x x) \cos(k_y y) \sin(k_z z) \quad 3.18 (b)$$

$$H_y = \frac{k_y k_z}{j\omega\mu_0} A \cos(k_x x) \sin(k_y y) \sin(k_z z) \quad 3.18 (c)$$

$$E_z = 0 \quad 3.18 (d)$$

$$E_x = A k_y \cos(k_x x) \sin(k_y y) \cos(k_z z) \quad 3.18 (e)$$

$$E_y = -A k_x \sin(k_x x) \cos(k_y y) \cos(k_z z) \quad 3.18 (f)$$

where A is an arbitrary constant and k_x , k_y and k_z denote the wave numbers inside the DR along the x , y and z directions respectively. Enforcing the magnetic wall

boundary condition at the resonator surfaces i.e at $|x| = a/2$ and $|y| = b/2$, the following equations are obtained for the wave number k_z .

$$k_x = m \frac{\pi}{a} \quad k_y = n \frac{\pi}{b} \quad k_z = p \frac{\pi}{d} \quad (3.19)$$

Further, by using the CDWM, the following transcendental equation is obtained for the wave number k_z .

$$k_z \tan(k_z d / 2) = \sqrt{(\epsilon_r - 1)k_0^2 - k_z^2} \quad (3.20)$$

The wave numbers also satisfy the separation equation

$$k_x^2 + k_y^2 + k_z^2 = \epsilon_r k_0^2 \quad (3.21)$$

where k_0 denotes the free space wave number corresponding to the resonant frequency. For given resonator parameters ϵ_r , a , b and d the resonant frequency of the DRA is the one at which the wavenumber k_z , determined using 3.19 and 3.21, also satisfies 3.20. The mixed model described above predicts the TE₁₁₁ mode resonant frequencies which are lower than the true value by about 6-8% for a value of $\epsilon_r > 38$. However, the method is more accurate for lower values of ϵ_r [24].

3.5 Excitation Techniques

Widely adopted excitation schemes of DRA's include conducting probes, Microstrip-slot (aperture), coplanar waveguide and direct Microstrip line coupling as shown in Figure 3.5 (a-d).

◆ Coaxial Probe excitation

The probe excitation requires drilling of a hole into the DR to insert the probe. The probe length, position and depth of penetration are factors controlling the impedance matching. Keeping the conducting probes near the outer surface can also efficiently excite a high permittivity DRA. This greatly simplifies the construction of the antenna since this avoids drilling a hole inside the dielectric.

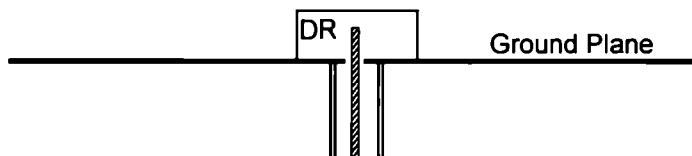


Figure 3.5(a) Probe excitation

Good coupling can be achieved by adjusting the position and length of the probe and aligning the probe along the electric field components. However, the coaxial probe feed is not normally acceptable to high frequencies.

◆ **Microstrip-slot (aperture) excitation**

The aperture-coupling mechanism has been widely studied because it separates the feed line structure from the DRA and thus provides flexibility in the design of the feed line and the DRA. The radiation from the feeding circuit is removed, enhancing the polarisation quality. Unlike aperture coupled Microstrip patch antennas, precise positioning of the DRA over the slot is not required. Furthermore, drilling a hole in a super hard DR to accommodate the probe penetration is no longer necessary.

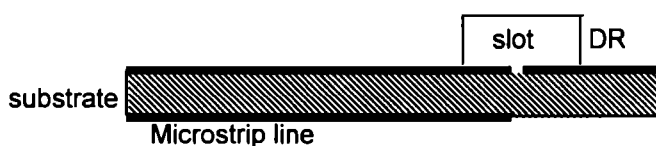


Figure 3.5 (b) Microstrip-slot excitation

This type of excitation scheme avoids large probe self reactances at millimetre wave frequencies and potentially helps the integration of DRA's with MMICs. Much wider impedance bandwidth is exhibited by annular slot fed DRA's instead of rectangular slots. However, the back lobe radiation through the substrate is of concern.

◆ **Coplanar wave guide (CPW) excitation**

The coplanar waveguide excitation is uniplanar and less dispersive in nature. Like other Microstrip feeds, it provides convenience in integration of the DRA with active circuitry since shunt/series components can be connected on the same side of the substrate without via holes [25].

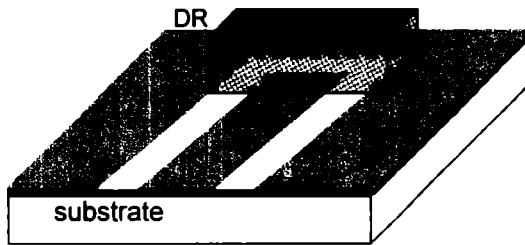


Figure 3.5 (c) Coplanar waveguide excitation

It is characterized by low conductor losses and radiation leakage and is particularly suited for millimetre wave applications because of reduced surface wave excitation in electrically thick substrates, compared to Microstrip feed. Matching the impedance may be difficult with low permittivity DRA's. However, a vertical strip extended from the centre strip of the CPW onto the surface of the DRA is found to improve the coupling.

◆ **Microstrip line excitation**

This is a simple and inexpensive method applicable to frequencies well within the millimetre wave bands. This feeding technique allows the DRA to be integrated with MMIC's without the need of a coupling slot [26]. In the direct Microstrip coupling scheme the far end of a Microstrip line is terminated in an open circuit. The critical parameter that determines the amount of coupling and the particular mode excited by the Microstrip line is the overlap distance of the DR on the Microstrip line.

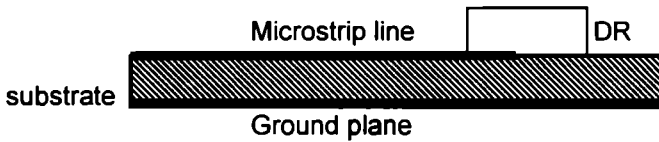


Figure 3.5(d) Microstrip line excitation

The configuration has the merits of low back lobe radiation and structure simplicity for antenna arrays. Moreover it provides a relatively wide bandwidth in comparison with the conventional aperture-coupled DRA. However this method inevitably introduces an undesirable air gap. A Microstrip line fed conformal strip method is also used to excite a DRA [27]. The strip cut from a conducting adhesive tape has the same width of the Microstrip line. This method shares the merits of using a coaxial probe, but avoids the need for drilling a hole to accommodate the probe. Although this feature can be obtained by placing the probe near the outer surface of a DRA, a high dielectric constant ($\epsilon_r \geq 20$) is required. Furthermore, it allows very easy post-manufacturing trimmings, as the conformal strip can be easily cut shorter without leaving an air gap, or extended longer without the need for deepening the hole.

3.6 Applications

Applications of dielectric resonators in microwave circuits are very cost effective and lead to significant miniaturization particularly when used in MMIC structures. Newly developed high Q ceramics have excellent temperature stability and an almost zero temperature coefficient. They extend the commercial applications of dielectric resonators to frequencies as high as 100 GHz. DR's have been employed for the measurement of material properties [28-31]. High resolution, high sensitivity and large dynamic range of test systems are the striking features of such measurements. Small size, low loss, light-weight, mechanical simplicity and ease of integration with Microstrip lines make Dielectric Resonators widely useful in wireless communication systems, satellite TV and broadcasting communication systems,

achieving excellent performance as frequency discriminators, filters and oscillators [32-33]. Open dielectric resonators offer attractive features as antenna elements. The ceramic-based dielectric technology is being developed as a means of building high performance antennas for WLAN and handset applications. Large multielement antenna arrays for millimetre wave bands with excellent radiation characteristics can be realised using Microstrip-fed dielectric resonators. The versatile nature of DRA's makes them adaptable to numerous wireless communication applications by appropriate choice of design parameters [34 - 40].

3.7 Scheme of Work

The DR is excited directly by the 50Ω Microstrip Line fabricated on an FR4 substrate of dielectric constant ϵ_r and thickness h . The feed is fabricated using photolithographic techniques. It comprises of a conducting strip etched on the top side of a dielectric substrate, covered with metal completely on the bottom side to form the ground plane. The width (w) of the conducting strip determines the characteristic impedance (Z_0). An SMA connector soldered to the Microstrip line couples electromagnetic energy from the source to the DR for proper excitation of resonance. Figure 3.6. illustrates the Microstrip excited antenna configuration. The dielectric resonator samples for the study are procured from the Ceramics Technology Division of the Regional Research Laboratory, Thiruvananthapuram and the Advanced Materials and Ceramics Division of the Vikram Sarabhai Space Centre, Thiruvananthapuram.

Five different Rectangular DR samples with moderate permittivity and quality factor are investigated. Their geometrical parameters and electrical characteristics are given in Table 3.2. The samples are prepared using the conventional solid-state ceramic route [41].

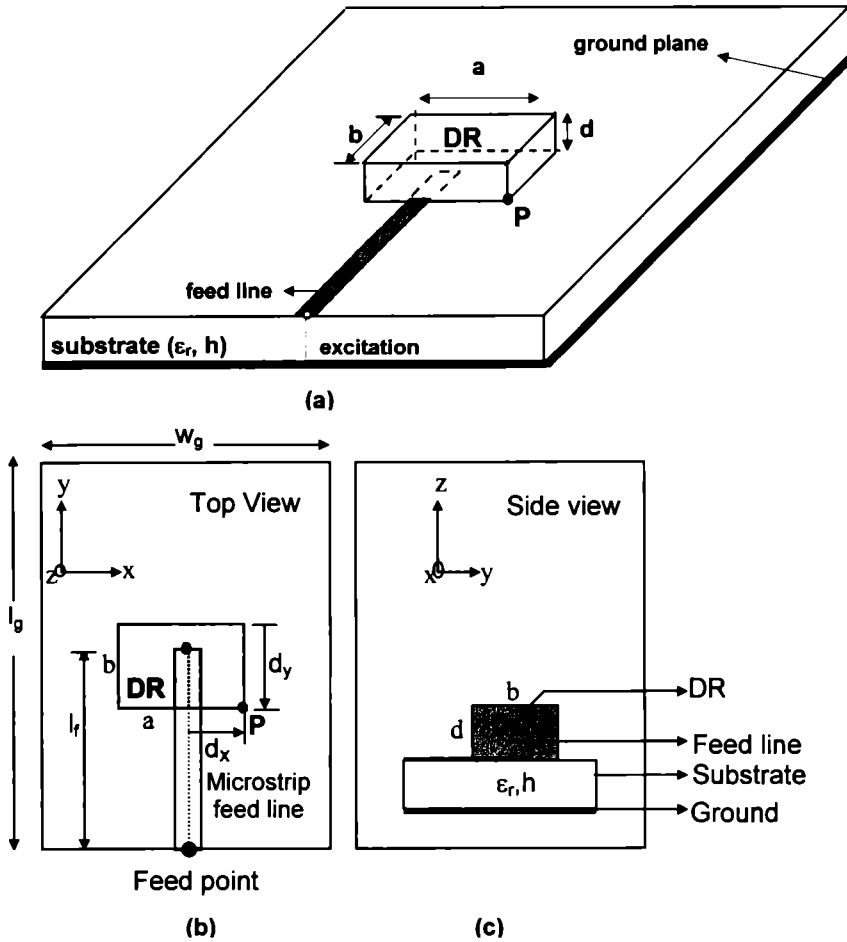


Figure 3.6 The Microstrip Line Excited Rectangular DRA
 Ground plane dimensions $l_g \times w_g$, Substrate $[\epsilon_r, h]$
 Feed Line length l_f DR dimensions : $a \times b \times d$
 (a) 3D view (b) Top view (c) side view

DR sample	Dimensions (cm) a x b x d	Composition	Dielectric Constant (ϵ_r)	$Q_u \times f$ (GHz)	Sintering temperature
DR-1	2.25 x 1.19 x 0.555	Ca ₅ Nb ₂ TiO ₁₂ (Calcium Neobium Titanate)	48	26000	1550 °C
DR-2	3.7 x 1.4 x 0.555				
DR-3	3.7 x 1.4 x 1.1				
DR-4	1.85 x 1.7 x 0.85	(Ba,Sr) ₂ Ti ₉ O ₂₀ (Dibarium nona Titanate)	34	13200	1340 °C
DR-5	2.65 x 1.75 x 0.85				

Table 3.2 Resonator samples used for the study

3.7.1 Design of the Microstrip feed line

The dominant mode of propagation in a microstrip line is quasi-TEM. Therefore, the characteristic impedance of the line is determined by carrying out quasi-static analysis of the transmission structure [42]. The characteristic impedance is determined using the following relations.

$$Z_0 = \frac{\eta_0}{2\pi\sqrt{\epsilon_{re}}} \ln\left\{\frac{F_1}{u} + \sqrt{1 + \frac{4}{u^2}}\right\} \quad (3.22)$$

where, $F_1 = 6 + (2\pi - 6) \times \exp\{- (30.666/u)^{0.7528}\}$ (3.23)

$$\eta_0 = 120\pi\Omega, \quad u = \frac{w}{h} \quad (3.24)$$

ies of the antenna are studied in detail for the different positions of the DR ed in Chapter five.

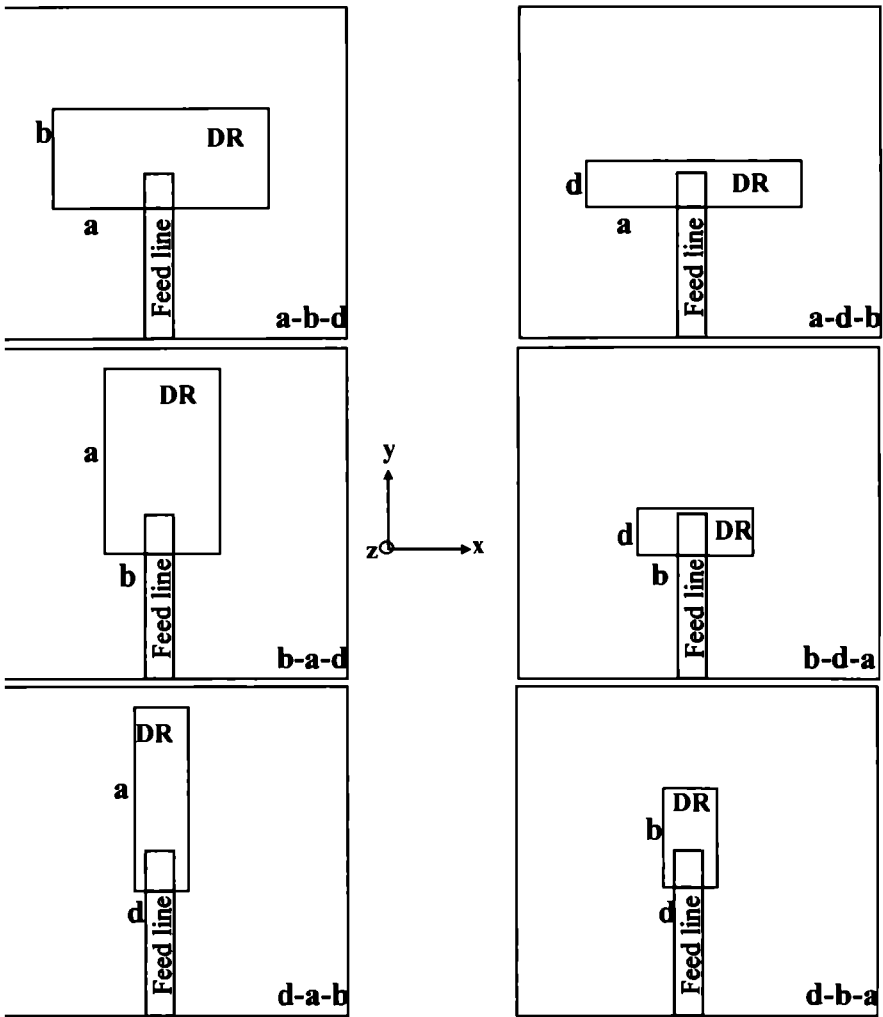


Figure 3.7 Orientations of the DR upon the feed line

Dimensions of the ground plane

For most of the applications it is desirable to have a compact ant
 uration. However, the dimension of the ground plane can also influenc
 on behaviour of an antenna. Therefore, the effect of the ground |

dimensions on the radiation characteristics is studied in detail and the dimensions are experimentally optimized. The geometry of the large ground plane and the truncated ground plane employed for the study are shown in Figure 3.9.

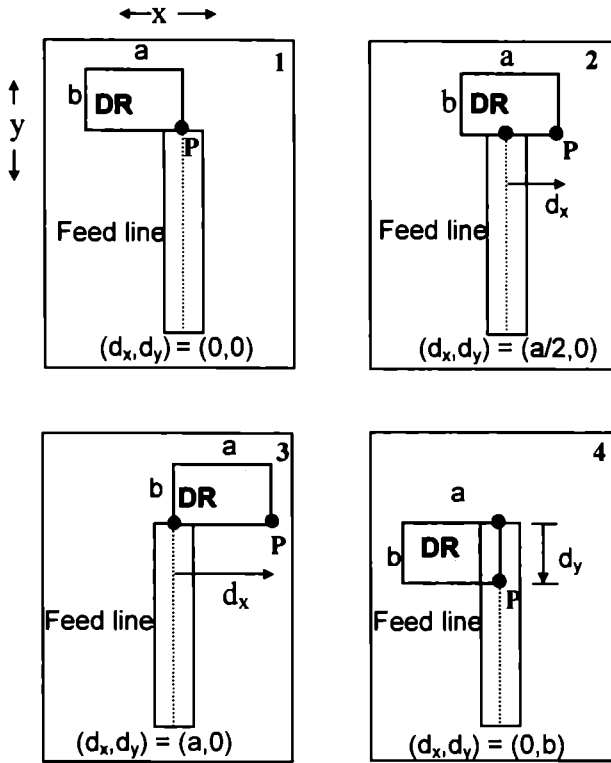


Figure 3.8 Position of the DR with respect to the feed line.
 d_x - displacement of the DR vertex 'P' along the x direction
 d_y - displacement of the DR vertex 'P' along the y direction

3.7.5 Length of the feed line

The overall length of the transmission line required to excite the DR (l_f) is also an important parameter as far as the compactness of the antenna configuration and its electrical performance is concerned. Feed lines of lengths ranging from 2 cm to 9 cm are used for the study. Proper excitation of resonance within the DR and

compactness of the antenna configuration are the criteria considered while choosing the dimensions of the feed line and the ground plane.

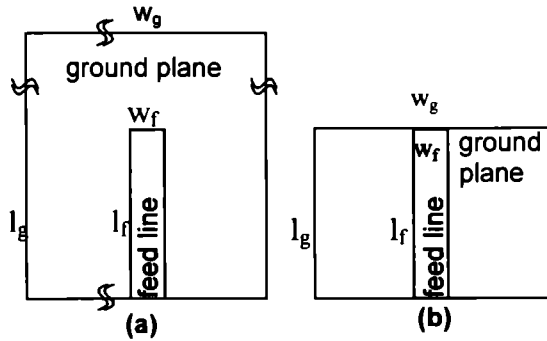


Figure 3.9 Ground plane configurations
 (a) large ground plane
 (b) truncated ground plane

In order to ascertain the influence of the above factors on the performance of the antenna, the return loss characteristics, radiation pattern, gain and resonant modes are computed numerically using FDTD method and validated through experiments and simulation. The following parameters are studied in detail.

Return loss Characteristics	Radiation Pattern
Resonant frequency	Half Power Beam Width
Return Loss	Front-to-Back ratio
Input impedance	Cross-Polarisation
Impedance Bandwidth	

The measurement techniques are explained in the following section. Chapter four explains the methodology employed in the numerical computation of antenna characteristics.

3.8 Measurement techniques

The measurement of the antenna radiation characteristics is performed using HP 8510C Vector Network analyser, which is a versatile equipment capable of making rapid and accurate measurements [44].

3.8.1 Measurement of antenna resonant frequency, return loss and 2:1 VSWR bandwidth

The block diagram of the experimental set up for the measurement of the return loss characteristics using a Network Analyzer interfaced to a PC is shown in Figure.3.10.

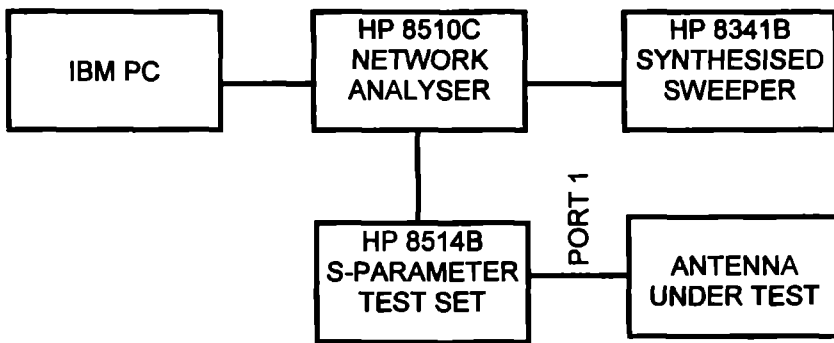


Figure 3.10 Experimental Set up for measurement of resonant frequency and return loss

The Network Analyser is calibrated for one full port (PORT 1) using a 3.5 mm CAL kit to remove the inherent errors in the port cables and connectors. The test antenna is connected to PORT 1 of the S-parameter test set. The measured S_{11} data in the Network Analyzer is retrieved and stored in ASCII format in the computer interfaced with the Analyser using *MERL Soft* - the software indigenously developed by the Research group of the Centre for Research in Electromagnetics and Antennas (CREMA), Department of Electronics, CUSAT. All the precautions to reduce the

reflection from the ground and nearby objects are followed to ensure the repeatability and reliability of the experiment. The dip in the resonant curve determines the resonant frequency (f_r). The 2:1 VSWR bandwidth is directly obtained from the return loss data by noting the range of frequencies (Δf_r) over which the return loss (S_{11}) \leq 10 dB. The percentage bandwidth (% BW) is calculated as $\frac{\Delta f_r}{f_r} \times 100\%$. The

impedance curve of the test antenna can be plotted on the Smith Chart from the magnitude and phase of the return loss data.

3.8.2 Measurement of antenna radiation pattern

The experimental set up for measurement of the antenna radiation pattern is shown in Figure 3.11. The co-polar and cross-polar radiation patterns in the two principal planes of the test antenna (E-plane and H-plane) are measured by mounting the test antenna in the receiving mode on the azimuth positioner and a standard wideband horn antenna in the transmitting mode. The antennas are aligned and a THRU calibration is performed. Gating is applied in the time domain to minimise reflections and measurements are performed in the frequency domain. The entire measured data stored in ASCII format by *MERL Soft* is further processed to yield the different radiation characteristics viz. half power beam width, cross-polar level, etc.

3.8.3 Measurement of antenna gain

The gain-transfer method utilizing a standard antenna of known gain is employed to determine the absolute gain of the test antenna [45]. The experimental set up for the measurement of gain is similar to that of the radiation pattern measurement.

A standard antenna is used as the reference antenna. The measurement is done in two phases. Initially the standard antenna kept within the chamber is connected to PORT 2 of the Network Analyzer. The transmitting antenna (Wide-band

Horn Antenna) is connected to PORT 1. The antenna is bore-sighted and the power received is recorded (P_s). A THRU RESPONSE calibration is performed in the Network Analyser and stored in the CAL SET. This acts as the reference gain response.

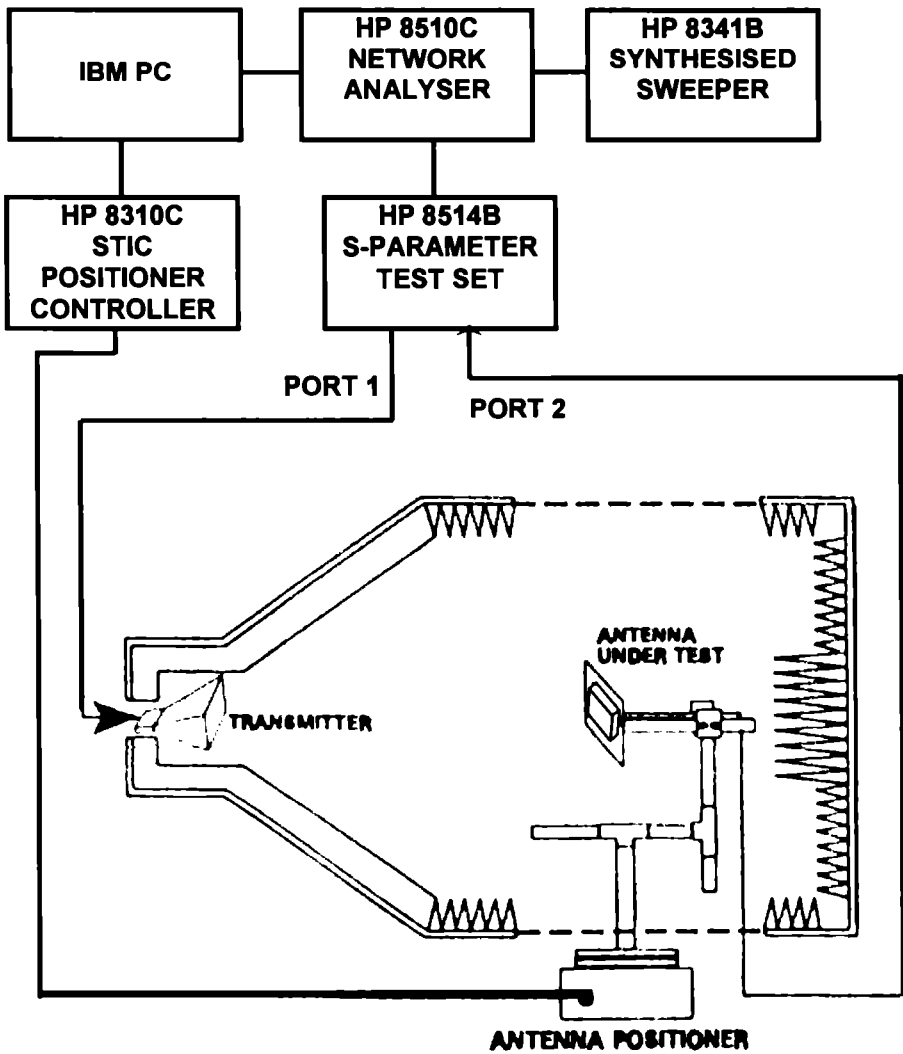


Figure 3.11 Experimental Set up for measurement of radiation pattern / gain

The test antenna then replaces the standard antenna maintaining the geometrical arrangement intact. The power received (P_T) is recorded. The plot displayed on the Network Analyzer indicates the relative gain of the test antenna with respect to the standard antenna ($10 \log_{10} (P_T/P_S)$). The absolute gain of the test antenna (dBi) is determined from the Friis transmission formula using the following equation:

$$(G_T) \text{ dB} = (G_S) \text{ dB} + 10 \log_{10} (P_T/P_S) \quad (3.29)$$

The results of the experimental investigations performed on different rectangular DRA configurations are discussed in chapter five.

REFERENCES

-
1. R.D.Richtmyer, "Dielectric Resonators," *J. Appl. Phys.*, vol.10, pp.391-398 June 1939.
 2. B.Tareev, "Physics of Dielectric Materials," MIR Publishers, Moscow, 1979.
 3. B.W.Hakki and P. D. Coleman, " A dielectric resonator method of measuring inductive capacities in the millimetre range," *IRE Trans. Microwave Theory Tech.*, vol.8, pp.402-410, July 1960.
 4. J.Krupka, K.Derzakowski, B.Riddle and J.B.Jarvis, "A dielectric resonator for measurements of complex permittivity of low loss dielectric materials as a function of temperature," *Meas.Sci.tech.*, vol.9, pp.1751-1756, 1998.
 5. H.Sreemoolanadhan, Ph.D Thesis, "Preparation, Characterisation and properties of some Titanate and Niobate based ceramic microwave dielectric resonators," University of Kerala, July 1996.
 6. D.Kajfez and P.Guillon, Eds., "Dielectric Resonator", Norwood. MA: Artech House, 1986.
 7. Tatsuo Itoh and Ronald S. Rudokas, "New method for computing the resonant frequencies of dielectric resonators," *IEEE Trans. Microwave Theory Tech.*, vol.25, pp.52-54, January 1977.
 8. Yahia M.M. Antar, Dajun Cheng, Guy Sequin, Bruce Henry and Mike G. Keller, "Modified waveguide model (MWGM) for rectangular dielectric resonator antenna (DRA)," *Microwave Opt. Technol.Lett.*, vol.19, no.2, pp.158-160, 5 October 1998.
 9. J.Van Bladel, "On the resonances of a dielectric resonator of very high permittivity," *IEEE Trans. Microwave Theory Tech.*, vol.23; pp.199-208, February 1975.
 10. R.K.Mongia and P.Bhartia, "Dielectric Resonator Antennas-A review and general design relations for resonant frequency and bandwidth," *International journal for Microwave and Millimeter-wave Computer-Aided Engineering*, vol.4, no.3, pp.230-247, 1994.
 11. S.A.Long, M.W.McAllister and C.Sheen, "The resonant cylindrical dielectric cavity antenna," *IEEE Trans. Antennas Propagat.*, vol.31, no.3, pp.406-412, May 1983.

12. M.Verplanken and J.Van Bladel, "The electric-dipole resonances of ring resonators of very high permittivity," *IEEE Trans. Microwave Theory Tech.*, pp.108-112, February 1976.
13. Richard Q.Lee and Rainee N.Simons, "Bandwidth enhancement of dielectric resonator Antennas," *IEEE Antennas Propagat. Soc. Int. Symp.*, Michigan, pp.1500-151503, June 1993.
14. S.M.Shum and K.M.Luk, "Stacked annular ring dielectric resonator antennas for wideband applications," *IEEE Trans. Antennas Propagat.*, vol.43, no.8, pp.889-892, August 1995.
15. Z.Fan, Y.M.M.Antar, A.Ittipiboon and A.Petosa, "Parasitic coplanar three-element dielectric resonator antenna subarray," *Electron. Lett.*, vol.32, no.9, pp.789-790, 25 April 1996.
16. Fu-Ren Hsiao, Jieh-Sen Kuo, Tzung-Wern Chiou and Kin-Lu Wong, "A broadband very-high-permittivity dielectric resonator antenna for WLAN application in the 5.2 GHz band," *Microwave Opt. Technol. Lett.*, vol.32, no.6, pp.426-427, 20 March 2002.
17. A.A.Kishk, Y.Tin and A.W.Glisson, "Conical dielectric resonator antennas for wideband applications," *IEEE Trans. Antennas Propagat.*, vol.50, no.4, pp.469-474, April 2002.
18. B.Bit-Babik, C. Di Nallo and A. Faraone, "Multimode dielectric resonator antenna of very high permittivity," *IEEE Antennas Propagat. Soc. Int. Symp.*, Monterrey, CA, June 2004.
19. K.Pliakostathis and D.Mirshekar – Syahkal, "Stepped dielectric resonator antennas," *IEEE Antennas Propagat. Soc. Int. Symp.*, Monterrey, CA, June 2004.
20. R.Chair, A.A.Kishk, K.F.Lee and C.E.Smith, "Broadband aperture coupled flipped staired pyramid and conical dielectric resonator antennas," *IEEE Antennas Propagat. Soc. Int. Symp.*, Monterrey, CA, June 2004.
21. Mohamed Al Sharkawy, Atef Z. Elsherbeni and Charles E.Smith, "Stacked elliptical dielectric resonator antennas for wideband applications," *IEEE Antennas Propagat. Soc. Int. Symp.*, Monterrey, CA, June 2004.
22. G.B.Gentili, M.Morini, S.Selleri, "Relevance of coupling effects on DRA array design," *IEEE Trans. Antennas Propagat.*, vol.51, no.3, pp.399-404, March 2003.

23. R.K.Mongia, A.Ittipiboon, M.Cuhaci, "Low profile Dielectric Resonator Antennas using a very high permittivity material," *Electron. Lett.*, vol.30, no.17, pp.1362-1363, 18 August 1994.
24. Rajesh Kumar Mongia and Apisak Ittipiboon, "Theoretical and experimental investigations on rectangular dielectric resonator antennas," *IEEE Trans. Antennas Propagat.*, vol.45, no.9, pp.1348-1356, September 1997.
25. Yong Xin Guo and Kwai-Man Luk, "On improving coupling between a coplanar waveguide feed and a dielectric resonator antenna," *IEEE Trans. Antennas Propagat.*, vol.51, no.8, pp.2142-2144, August 2003.
26. K.M.Luk, M.T.Lee, K.W.Leung and E.K.N.Yung, "Technique for improving coupling between microstripline and dielectric resonator antenna," *Electron. Lett.*, vol.35, no.5, pp.357-358, 4 March 1999.
27. K.W.Leung, W.C.Wong, K.M.Luk and E.K.N.Yung, "Circular-polarised dielectric resonator antenna excited by dual conformal strips," *Electron. Lett.*, vol.36, no.6, pp.484-486, 16 March 2000.
28. Y.Shu and T.Y.Wong, "Perturbation of dielectric resonator for material measurement," *Electron. Lett.*, vol.31, no.9, pp.704-705, 27 April 1995.
29. S.Fargeot, A. Veronjanne, M.Auborg and P.Guillon, "Cylindrical dielectric resonator antenna for material characterization," *Microwave Opt. Technol. Lett.*, vol.17, no.4, pp.273-275, March 1998.
30. Elena Semouchkina, Wenwu Cao, Michael Lanagan, Raj Mittra and Wenhua Yu, "Combining FDTD simulations with measurements of Microstrip ring resonators for characterization of low and high K dielectrics at microwaves," *Microwave Opt. Technol Lett.*, vol.29, no.1, pp.21-24, 5 April 2001.
31. Mohan.V.Jacob, Janina Mazierska, Kenneth Leong and Jerzy Krupka, "Novel method for calculation and measurement of unloaded Q-factor of superconducting dielectric resonators," *IEEE Antennas Propagat. Soc. Int. Symp.*, Boston, USA, June 2001.
32. Emine Yesim Yuksel and Thomas T.Y.Wong, "A phase-shifting frequency discriminator employing dielectric resonator," *Microwave Opt. Technol Lett.*, vol.36, no.2, pp.87-89, 20 January 2003.

33. Ji-Chyun Liu, Chin-Shen Cheng and Leo Yao, "Dual-mode double ring resonator for Microstrip band-pass filter design," *Microwave Opt. Technol Lett.*, vol.36, no.4, pp.310-314, 20 February 2003.
34. M.G.Keller, D.J.Roscoe, M.B.Oliver, R.K.Mongia, Y.M.M.Antar and A.Ittipiboon, "Active aperture-coupled rectangular dielectric resonator antenna," *IEEE Microwave and guided wave letters*, vol.5, no.11, pp. 376-378, November 1995.
35. G.Drossos, Z.Wu and L.E.Davis, "Two-element endfire dielectric resonator antenna array," *Electron. Lett.*, vol.32, no.7, pp.618-619, 28 March 1996.
36. G.Drossos, Z.Wu, D.Lacey and L.E.Davis, "Experimental investigation of a cylindrical dielectric resonator antenna at 77 K," *Microwave Opt. Technol. Lett.*, vol.14, no.1, pp.62-64, 5 January 1997.
37. R.Aleksiejunas and V.Ivaska, "Leaky mode cylindrical dielectric resonator antenna," *Electron. Lett.*, vol.33, no.7, pp.547-548, 27 March 1997.
38. K.K.Pang, H.Y.Lo, K.W.Leung, K.M.Luk and E.K.N.Yung, "Circularly polarized dielectric resonator antenna subarrays," *Microwave Opt. Technol.Lett.*, vol.27, no.6, pp.377-379, 20 December 2000.
39. Kin-Lu Wong, Saou-Wen Su, Tzung-Wern Chou and Yeh-Chian Lin, "Dual-band plastic chip antenna for GSM/DCS Mobile phones," *Microwave Opt. Technol Lett.*, vol.33, no.5, pp.330-332, 5 June 2002.
40. Tsung-Shan Yung, Tze-Hsuan Chang, Wen-Zhou Wu and Jean-Fu Kiang, "Dual-band Dielectric Resonator Antenna," *IEEE Antennas Propagat. Soc. Int. Symp.*, Monterrey, CA, June 2004.
41. P.V.Bijumon, P.Mohanan and M.T.Sebastian, 'Synthesis, Characterization and properties of $\text{Ca}_5\text{Nb}_2\text{TiO}_{12}$ [A=Nb, Ta]: Ceramic dielectric materials for applications in Microwave telecommunication systems,' *Japan. J. Appl. Phys.* vol.41, part 1, no.6A, pp.3834-3835, June 2002.
42. Fred Gardiol, "Microstrip Circuits," John Wiley & sons, Inc. 1994.
43. Ramesh Garg, Prakasah Bhartia, Inder Bahl and Apisak Ittipiboon, "Microstrip Antenna Design Handbook," Artech House, Norwood, MA, 2001.
44. Jacob George, Ph.D Thesis, "Development and analysis of a drum shaped compact Microstrip antenna," Cochin University of Science and Technology, June 1998.
45. C.A.Balanis, "Antenna Theory: analysis and design," John Wiley & Sons, Inc. 2004.

Numerical Computation of the Radiation Characteristics of a Rectangular Dielectric Resonator Antenna

The methodology adopted for the numerical computation of the radiation characteristics of a Rectangular DRA is described in this chapter. The fundamentals of the FDTD method and its adaptation to the present problem are explained in detail.

4.1 The FDTD method

The electromagnetic force is the most technologically pervasive force in nature. Of the different methods for predicting electromagnetic effects – experiment, analysis and computation – the newest and fastest growing approach is computation. Electromagnetic computational engineering encompasses the modelling, simulation and analysis of the responses of complex systems to various electromagnetic stimuli, allowing for better design or modification of the system. The key attributes listed below combine to make the FDTD method a useful and powerful tool [1].

- The simplicity of the method is noteworthy. Maxwell's equations in a differential form are discretized in space and time in a straightforward manner.
- The method tracks the time-varying fields throughout a volume of space. Thus FDTD results lend themselves well to scientific visualization methods, providing the user with excellent physical insight into the behaviour of electromagnetic fields.
- The method provides broadband response predictions about the system resonances. Far fields are derived from near fields.
- The geometric flexibility of the method permits the solution of a wide variety of radiation, scattering and coupling problems.
- Desired accuracy can be achieved by selecting suitable discretization parameters and boundary conditions.
- The method is extremely well suited for implementation on parallel computers.
- Personal computer capabilities have caught up with the requirements of FDTD for a wide range of modelling problems. Thus, even without any improvement in the fundamental algorithm, continuation of present trends will aid the generation of highly detailed electromagnetic wave models of volumetric complex structures of great engineering and scientific importance.

4.2 Discretization in FDTD

The FDTD method originally proposed by K.S. Yee [2], is an explicit finite difference scheme using central differences on a Cartesian grid staggered in both space and time. A full three – dimensional FDTD cell (Yee lattice) is shown in Figure 4.1 wherein, the Electric fields lie along the midpoint of the cell edges and the Magnetic fields lie along the centre of the cell faces. Yee defines the grid coordinates (i, j, k) as

$$(i, j, k) = (i\Delta x, j\Delta y, k\Delta z) \quad (4.1)$$

where Δx , Δy and Δz are the actual grid separations.

Any function of space and time is written as

$$F^n(i, j, k) = F(i\Delta x, j\Delta y, k\Delta z, n\Delta t) \quad (4.2)$$

where Δt is the time increment, n is the time index and Δx , Δy , Δz is the space increment along the three coordinate axes.

The spatial and temporal derivatives of F are written using central finite difference approximations as follows.

$$\frac{\partial F^n(i, j, k)}{\partial x} = \frac{F^n(i+1/2, j, k) - F^n(i-1/2, j, k)}{\Delta x} \quad (4.3.a)$$

$$\frac{\partial F^n(i, j, k)}{\partial t} = \frac{F^{n+1/2}(i, j, k) - F^{n-1/2}(i, j, k)}{\Delta t} \quad (4.3.b)$$

The starting point of the FDTD algorithm is the differential form of Maxwell's curl equations for an isotropic medium [Eqn 4.4 (a-b)].

$$\nabla \times \vec{E} = -\mu \frac{\partial \vec{H}}{\partial t} \quad (4.4.a)$$

$$\nabla \times \vec{H} = \sigma \vec{E} + \varepsilon \frac{\partial \vec{E}}{\partial t} \quad (4.4.b)$$

These can be written as six scalar equations in Cartesian coordinates [Eqn. 4.5 (a-f)].

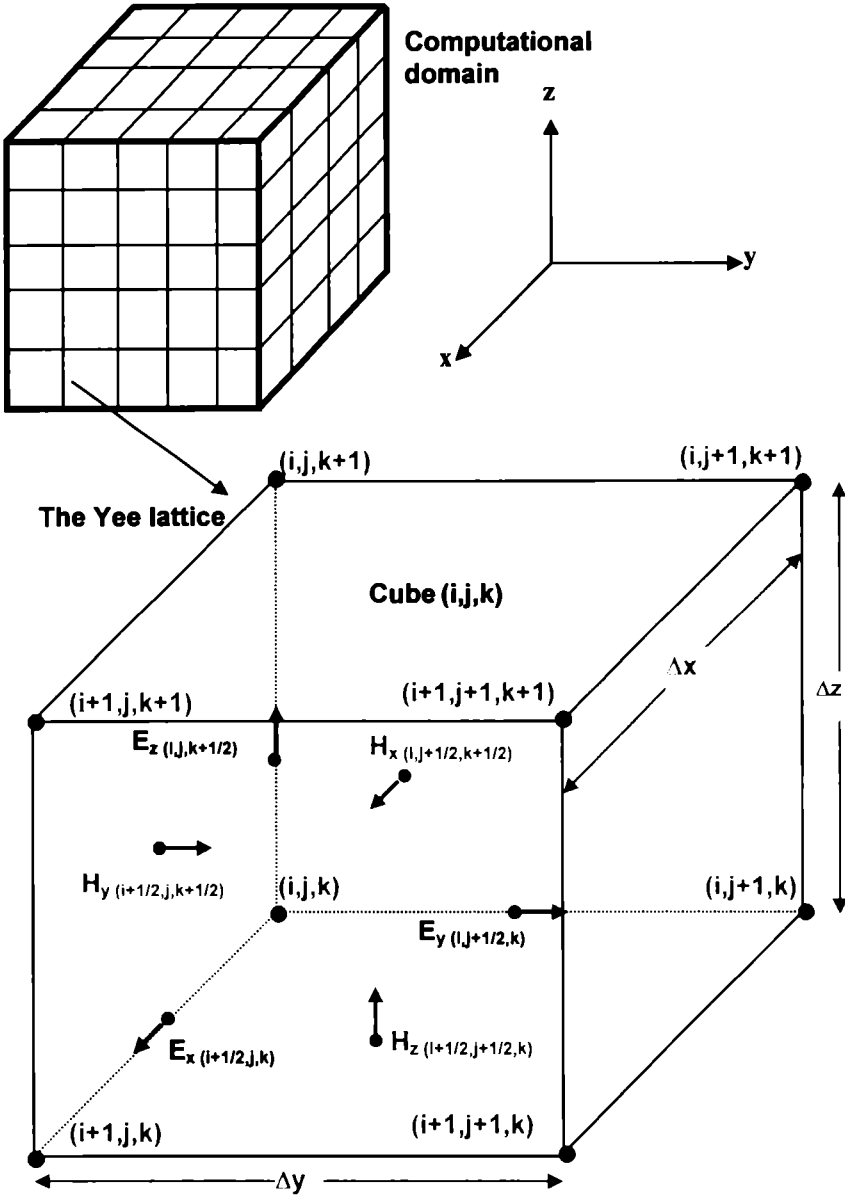


Figure 4.1 The three – dimensional staggered mesh FDTD cell (Yee lattice) in the computational domain

$$\frac{\partial H_x}{\partial t} = \frac{1}{\mu} \left(\frac{\partial E_y}{\partial z} - \frac{\partial E_z}{\partial y} \right) \quad (4.5.a)$$

$$\frac{\partial H_y}{\partial t} = \frac{1}{\mu} \left(\frac{\partial E_z}{\partial x} - \frac{\partial E_x}{\partial z} \right) \quad (4.5.b)$$

$$\frac{\partial H_z}{\partial t} = \frac{1}{\mu} \left(\frac{\partial E_x}{\partial y} - \frac{\partial E_y}{\partial x} \right) \quad (4.5.c)$$

$$\frac{\partial E_x}{\partial t} = \frac{1}{\varepsilon} \left(\frac{\partial H_z}{\partial y} - \frac{\partial H_y}{\partial z} - \sigma E_x \right) \quad (4.5.d)$$

$$\quad (4.5.e)$$

$$\frac{\partial E_y}{\partial t} = \frac{1}{\varepsilon} \left(\frac{\partial H_x}{\partial z} - \frac{\partial H_z}{\partial x} - \sigma E_y \right) \quad (4.5.f)$$

$$\frac{\partial E_z}{\partial t} = \frac{1}{\varepsilon} \left(\frac{\partial H_y}{\partial x} - \frac{\partial H_x}{\partial y} - \sigma E_z \right) \quad (4.5.f)$$

Equations 4.3.a and 4.3.b are applied to the six scalar equations (4.5.a to 4.5.f), resulting in six coupled explicit finite difference equations (4.6.a to 4.6.f).

$$\begin{aligned} H_x^{n+1/2}(i, j+1/2, k+1/2) &= H_x^{n-1/2}(i, j+1/2, k+1/2) \\ &+ \left[\frac{\Delta t}{\mu \Delta z} \right] (E_y^n(i, j+1/2, k+1) - E_y^n(i, j+1/2, k)) \\ &- \left[\frac{\Delta t}{\mu \Delta y} \right] (E_z^n(i, j+1, k+1/2) - E_z^n(i, j, k+1/2)) \end{aligned} \quad (4.6.a)$$

$$\begin{aligned} H_y^{n+1/2}(i+1/2, j, k+1/2) &= H_y^{n-1/2}(i+1/2, j, k+1/2) \\ &+ \left[\frac{\Delta t}{\mu \Delta x} \right] (E_z^n(i+1, j, k+1/2) - E_z^n(i, j, k+1/2)) \\ &- \left[\frac{\Delta t}{\mu \Delta z} \right] (E_x^n(i+1/2, j, k+1) - E_x^n(i+1/2, j, k)) \end{aligned} \quad (4.6.b)$$

$$\begin{aligned}
H_z^{n+1/2}(i+1/2, j+1/2, k) &= H_z^{n-1/2}(i+1/2, j+1/2, k) \\
&+ \left[\frac{\Delta t}{\mu \cdot \Delta y} \right] (E_x^n(i+1/2, j+1, k) - E_x^n(i+1/2, j, k)) \\
&- \left[\frac{\Delta t}{\mu \cdot \Delta x} \right] (E_y^n(i+1, j+1/2, k) - E_y^n(i, j+1/2, k))
\end{aligned}
\tag{4.6.c}$$

$$\begin{aligned}
E_x^{n+1}(i+1/2, j, k) &= E_x^n(i+1/2, j, k) \\
&+ \left[\frac{\Delta t}{\varepsilon \cdot \Delta y} \right] (H_z^{n+1/2}(i+1/2, j+1/2, k) - H_z^{n+1/2}(i+1/2, j-1/2, k)) \\
&- \left[\frac{\Delta t}{\varepsilon \cdot \Delta z} \right] (H_y^{n+1/2}(i+1/2, j, k+1/2) - H_y^{n+1/2}(i+1/2, j, k-1/2))
\end{aligned}
\tag{4.6.d}$$

$$\begin{aligned}
E_y^{n+1}(i, j+1/2, k) &= E_y^n(i, j+1/2, k) \\
&+ \left[\frac{\Delta t}{\varepsilon \cdot \Delta z} \right] (H_x^{n+1/2}(i, j+1/2, k+1/2) - H_x^{n+1/2}(i, j+1/2, k-1/2)) \\
&- \left[\frac{\Delta t}{\varepsilon \cdot \Delta x} \right] (H_z^{n+1/2}(i+1/2, j+1/2, k) - H_z^{n+1/2}(i-1/2, j+1/2, k))
\end{aligned}
\tag{4.6.e}$$

$$\begin{aligned}
E_z^{n+1}(i, j, k+1/2) &= E_z^n(i, j, k+1/2) \\
&+ \left[\frac{\Delta t}{\varepsilon \cdot \Delta x} \right] (H_y^{n+1/2}(i+1/2, j, k+1/2) - H_y^{n+1/2}(i-1/2, j, k+1/2)) \\
&- \left[\frac{\Delta t}{\varepsilon \cdot \Delta y} \right] (H_x^{n+1/2}(i, j+1/2, k+1/2) - H_x^{n+1/2}(i, j-1/2, k+1/2))
\end{aligned}
\tag{4.6.f}$$

\vec{E} and \vec{H} are evaluated at alternate half time steps using equations (4.6.a–f), such that all field components are calculated in each time step Δt . The updated new value of a field component at any layer thus depends upon its value in the previous step and the previous value of the components of the other field at the adjacent spatial points. Table 4.1 indicates the spatial and temporal relation of the E and H nodes in

the Yee lattice. The discretization in space and time and the leap-frog time integration employed in the FDTD method proposed by Yee is illustrated in Figure 4.2.

		x	y	z	t
E node	E_x	$i+1/2$	j	k	n
	E_y	i	$j+1/2$	k	n
	E_z	i	j	$k+1/2$	n
H node	H_x	i	$j+1/2$	$k+1/2$	$n\pm 1/2$
	H_y	$i+1/2$	j	$k+1/2$	$n\pm 1/2$
	H_z	$i+1/2$	$j+1/2$	k	$n\pm 1/2$

Table 4.1 Spatial and temporal relation of the E and H nodes

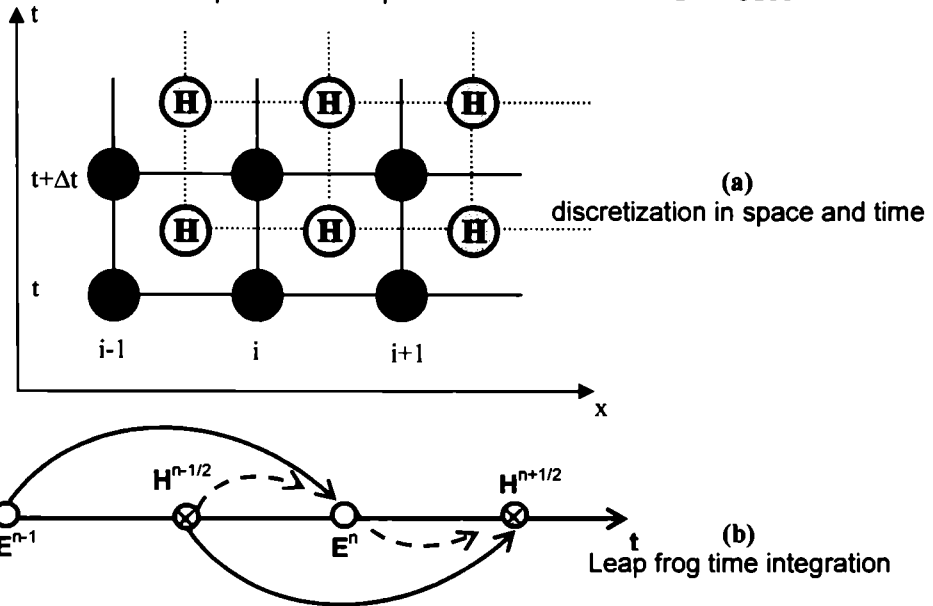


Figure 4.2 The FDTD method proposed by Yee

To facilitate the implementation of the algorithm in a digital computer, the indices of the field components are renamed, eliminating the $1/2$ index notation as suggested by Sheen *et al.* [3]. This allows the value of each field component to be stored in a three-dimensional array, with the array indices corresponding to the spatial indices. Figure

4.3 differentiates the notations proposed by Yee and Sheen, in deriving the H_z component according to equation (4.6.c). Equations (4.6.a-f) may be therefore re-written as (4.7.a-f), forming the basis of the computer implementation of the FDTD scheme in this thesis.

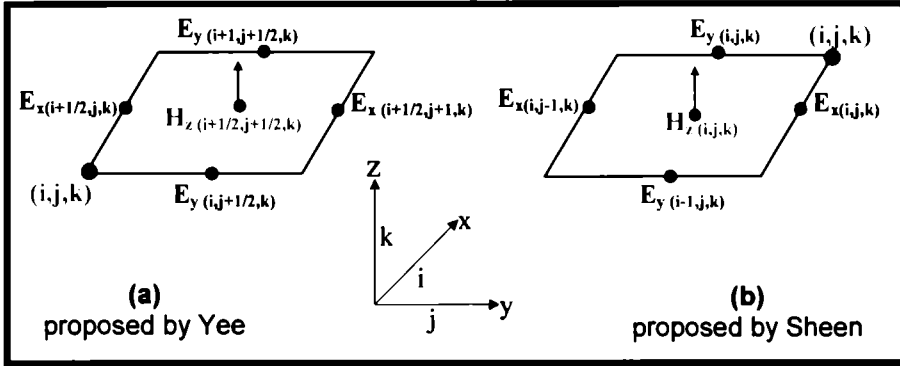


Figure 4.3 The cell indexing

$$\begin{aligned}
 H_x^{n+1/2}(i, j, k) &= H_x^{n-1/2}(i, j, k) \\
 &+ \left[\frac{\Delta t}{\mu \Delta z} \right] \left(E_y^n(i, j, k) - E_y^n(i, j, k-1) \right) \\
 &- \left[\frac{\Delta t}{\mu \Delta y} \right] \left(E_z^n(i, j, k) - E_z^n(i, j-1, k) \right) \\
 H_y^{n+1/2}(i, j, k) &= H_y^{n-1/2}(i, j, k)
 \end{aligned} \tag{4.7.a}$$

$$\begin{aligned}
 &+ \left[\frac{\Delta t}{\mu \Delta x} \right] \left(E_z^n(i, j, k) - E_z^n(i-1, j, k) \right) \\
 &- \left[\frac{\Delta t}{\mu \Delta z} \right] \left(E_x^n(i, j, k) - E_x^n(i, j, k-1) \right) \\
 H_z^{n+1/2}(i, j, k) &= H_z^{n-1/2}(i, j, k)
 \end{aligned} \tag{4.7.b}$$

$$\begin{aligned}
 &+ \left[\frac{\Delta t}{\mu \Delta y} \right] \left(E_x^n(i, j, k) - E_x^n(i, j-1, k) \right) \\
 &- \left[\frac{\Delta t}{\mu \Delta x} \right] \left(E_y^n(i, j, k) - E_y^n(i-1, j, k) \right) \\
 & \tag{4.7.c}
 \end{aligned}$$

$$\begin{aligned}
E_x^{n+1}(i, j, k) &= E_x^n(i, j, k) \\
&+ \left[\frac{\Delta t}{\epsilon \cdot \Delta y} \right] \left(H_z^{n+1/2}(i, j+1, k) - H_z^{n+1/2}(i, j, k) \right) \\
&- \left[\frac{\Delta t}{\epsilon \cdot \Delta z} \right] \left(H_y^{n+1/2}(i, j, k+1) - H_y^{n+1/2}(i, j, k) \right) \\
E_y^{n+1}(i, j, k) &= E_y^n(i, j, k) \tag{4.7.d}
\end{aligned}$$

$$\begin{aligned}
&+ \left[\frac{\Delta t}{\epsilon \cdot \Delta z} \right] \left(H_x^{n+1/2}(i, j, k+1) - H_x^{n+1/2}(i, j, k) \right) \\
&- \left[\frac{\Delta t}{\epsilon \cdot \Delta x} \right] \left(H_z^{n+1/2}(i+1, j, k) - H_z^{n+1/2}(i, j, k) \right)
\end{aligned}$$

$$E_z^{n+1}(i, j, k) = E_z^n(i, j, k) \tag{4.7.e}$$

$$\begin{aligned}
&+ \left[\frac{\Delta t}{\epsilon \cdot \Delta x} \right] \left(H_y^{n+1/2}(i+1, j, k) - H_y^{n+1/2}(i, j, k) \right) \\
&- \left[\frac{\Delta t}{\epsilon \cdot \Delta y} \right] \left(H_x^{n+1/2}(i, j+1, k) - H_x^{n+1/2}(i, j, k) \right)
\end{aligned}$$

(4.7.f)

4.3 Boundary conditions

The large amount of data generated during the implementation of FDTD approach on a computer calls for the truncation of the computational domain with artificial boundaries to simulate its extension to infinity, since modelling of an infinite space is numerically impossible. Nevertheless, the computational domain must be large enough to enclose the structure of interest. The commonly applied boundary conditions are:

- The Perfect Electric Conductor (PEC) or the electric wall
- The Perfect Magnetic Conductor (PMC) or the magnetic wall
- The absorbing boundary condition (ABC)
- Dielectric interface

4.3.1 Perfect Electric Conductor (PEC) boundary

The PEC boundary is used to represent ideal conductors. This type of boundary condition deliberately reflects all incident wave energy back into the computational domain, thus limiting its size. The boundary conditions at a perfect electric conductor are such that the electric field components tangential to the surface must be zero, stated mathematically where \vec{n} is a surface normal vector,

$$\vec{n} \times \vec{E} = 0 \quad (4.8)$$

In the Yee cell [Figure 4.1], the electric fields calculated at points on the surface of a PEC are always tangential to the surface. Thus by using the Yee cell in the FDTD scheme, the boundary condition at the surface of a PEC can be satisfied by simply setting these electric field components to zero at every time step. Nevertheless, if the E components tangential to a PEC boundary are initialized to zero ($E_{\text{tan}} = 0$), they will remain *nearly* zero throughout the iterations since the update equation for the E field component in a material with finite conductivity, derived from Maxwell's Curl equation (4.4.b) using the finite difference approximation for $\partial/\partial t$ as per equation (4.3.b) is:

$$E^n = E^{n-1} \left[\frac{1 - \sigma\Delta t/2\varepsilon}{1 + \sigma\Delta t/2\varepsilon} \right] + \left[\frac{1}{1 + \sigma\Delta t/2\varepsilon} \right] \left[\frac{\Delta t}{\varepsilon} \right] (\nabla \times H^{n-1/2}) \quad (4.9)$$

When $\sigma \gg 1$ in the above equation, $E^n \cong E^{n-1}$. In the FDTD iteration procedure, once the boundary conditions on the tangential fields are satisfied, the boundary conditions on the normal fields will be automatically valid.

'Boundary conditions' refer to the outer boundaries in FDTD terminology. However, in addition to being used on the boundaries of the FDTD mesh, PEC type conditions can be assigned to material interfaces within the computational domain. This allows us to model perfectly conductive surfaces of minute thickness. Eg: The conducting ground plane acting as the lower boundary of a Microstrip geometry, the conducting Microstrip line acting as the feed line, etc.

4.3.2 Perfect Magnetic Conductor (PMC) boundary

The PMC boundary is used to represent perfect magnetic conductors. The boundary conditions at a perfect magnetic conductor are such that the magnetic field components tangential to the surface must be zero, stated mathematically where \vec{n} is a surface normal vector,

$$\vec{n} \times \vec{H} = 0 \tag{4.10}$$

However, on the surface of a Yee cell there are no tangential magnetic fields specified. To estimate the magnetic field tangential to the boundary, the adjacent magnetic field values on either side are to be averaged. Resorting to the image method as illustrated in Figure 4.4, these magnetic field components are made equal and opposite, thus satisfying Eqn.4.10.

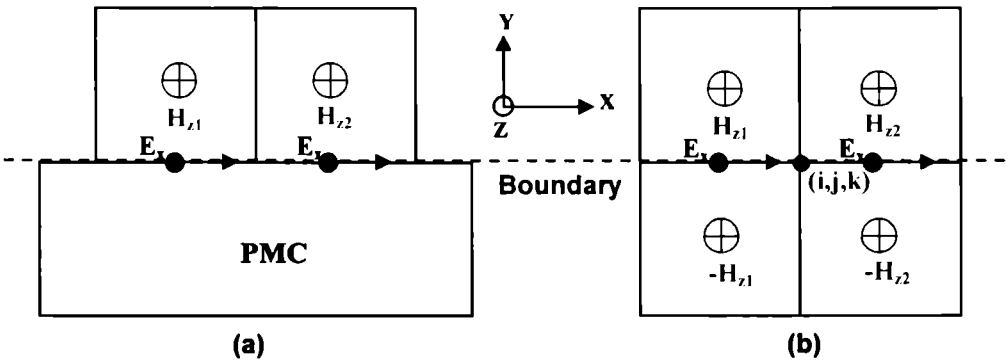


Figure 4.4 PMC Boundary conditions
 (a) Interface between PMC and media
 (b) Image Problem

PMC surfaces are often used in the modelling of a symmetric region to reduce the size of the computational volume by half. Thus by exploiting the symmetry, significant saving in computer resources (time, memory and data storage) is realized and models that would otherwise not fit into the computer memory can be simulated.

4.3.3 Dielectric interface boundary

The tangential electric field components at the interface between two media cannot be updated using the discretized Maxwell's equations. This is because the material constants (ϵ and μ) are assigned a single value, though these are different on either side of the interface due to the two media considered. The equivalent parameter approach employed in this thesis averages the relative permittivity on each side to derive the condition at the dielectric-air interface.

$$\epsilon_{\text{eff}} = \frac{\epsilon_1 + \epsilon_2}{2} \quad (4.11)$$

4.3.4 Absorbing boundary

In order to model open-region problems, an absorbing boundary condition (ABC) is often used to truncate the computational domain since the tangential components of the electric field along the outer boundary of the computational domain cannot be updated using the basic Yee algorithm for want of the unavailable field components lying outside the boundary space. The ABC is sometimes called the outer radiation boundary condition (ORBC) because it is used to absorb the outgoing waves. If the computational domain is extended sufficiently far beyond all sources and scatterers, all waves will be outgoing at the boundary. A rule of thumb is 'to provide a minimum of ten cells between the antenna object and the boundary in order to allow the outgoing waves to become almost planar'.

A multitude of ABC's for FDTD algorithm is available. They can be grouped into two categories – those that are derived from differential equations, and those that employ a material absorber. Differential based ABC's are generally obtained by factoring the wave equation, and by allowing a solution that permits only outgoing waves (Eg: MUR's ABC [4]). Mur's ABC was proposed after the theoretical work by Enquist and Majda [5]. It provides satisfactory absorption for a great variety of problems and is extremely simple to implement. Mur's first order ABC looks back one step in time and one cell into the space location. A second order condition looks

back two steps in time and two cells inward etc. According to Mur's first order ABC, the tangential electric field components on the outer boundaries will obey the one-dimensional wave equation in the direction normal to the mesh wall. For the \hat{y} normal wall the one-dimensional wave equation may be written as:

$$\left(\frac{\partial}{\partial y} - \frac{1}{v} \frac{\partial}{\partial t}\right) E_{\tan} = 0 \quad (4.12)$$

This equation may be discretized using only field components on or just inside the mesh wall, yielding an explicit finite difference equation,

$$E_0^{n+1} = E_1^n + \frac{v\Delta t - \Delta y}{v\Delta t + \Delta y} (E_1^{n+1} - E_0^n) \quad (4.13)$$

where E_0 represents the tangential electric field components on the mesh wall and E_1 represents the tangential electric field components one node inside of the mesh wall. Similar expressions are obtained for the other absorbing boundaries by using the corresponding normal directions for each wall. It may be noted that Mur's first order ABC is applicable only to normal incidence. Mur's second order ABC [6] accounts for oblique incidence of waves at the mesh wall. However, the present study employs Mur's first order ABC for the following reasons.

Mur's first order ABC can be applied to boundary with dielectric discontinuities. But the application of Mur's second order ABC to a boundary with dielectric discontinuity will cause large spurious wave components to be generated in the computational domain, which defeats the purpose of having an ABC with better absorbing property. The reason for this behaviour is the different velocity of the electromagnetic wave in media with different permittivity. Mur's second order ABC assumes all associated E field components to have similar permittivity and velocity, which is not true when the boundary is sandwiched between two dielectrics. This results in substantial error during the interpolation process, which then propagates back to the computational domain. Material ABC's on the other hand, are constructed so that fields are dampened as they propagate into the absorbing medium (Berenger's Perfectly Matched Layer (PML) [7]). Other techniques occasionally used are exact

formulations [8] and superabsorption [9]. Berenger's PML requires considerable enlargement of the computational volume, but is essentially frequency independent, superior to most ABC's and rather easy to implement. More often, when computer memory and ease of programming is determinative, one uses Mur's ABC, otherwise the choice is PML.

4.4 FDTD code requirements and architecture

The FDTD flow chart is shown in Figure 4.5. A main computer routine stepping through time and acting as a driver of the remaining subroutines is a prime requirement. Before time stepping begins a problem space including geometry parameters (cell size, time step and incident field) and material parameters is defined. Constant multipliers that need not be computed at each time step may also be evaluated and stored before hand. Monitor points or test locations at which responses are examined must be specified along with the response type: voltage, current, field, power, etc. After these specifications the fields are advanced one step at a time. This is the core of the code. Though it represents a small fraction of the lines of code, most of the running time will be spent in this section. Outer radiation boundary conditions that absorb the scattered field at the outermost portion of the problem space is an additional mandatory requirement. A data saving routine can store the response data at every time step and then at the end of the run "dump" it out as a listing or as a file for post processing. This output process may involve transformation of the near zone FDTD fields to the far zone for radiation calculations. The code requirements are listed in Table 4.2.

4.4.1 Determining the cell size

The choice of cell size is critical in applying FDTD. The fundamental constraint is that the cell size must be small enough to permit accurate results at the

highest frequency of interest, and yet be large enough to keep resource requirements manageable.

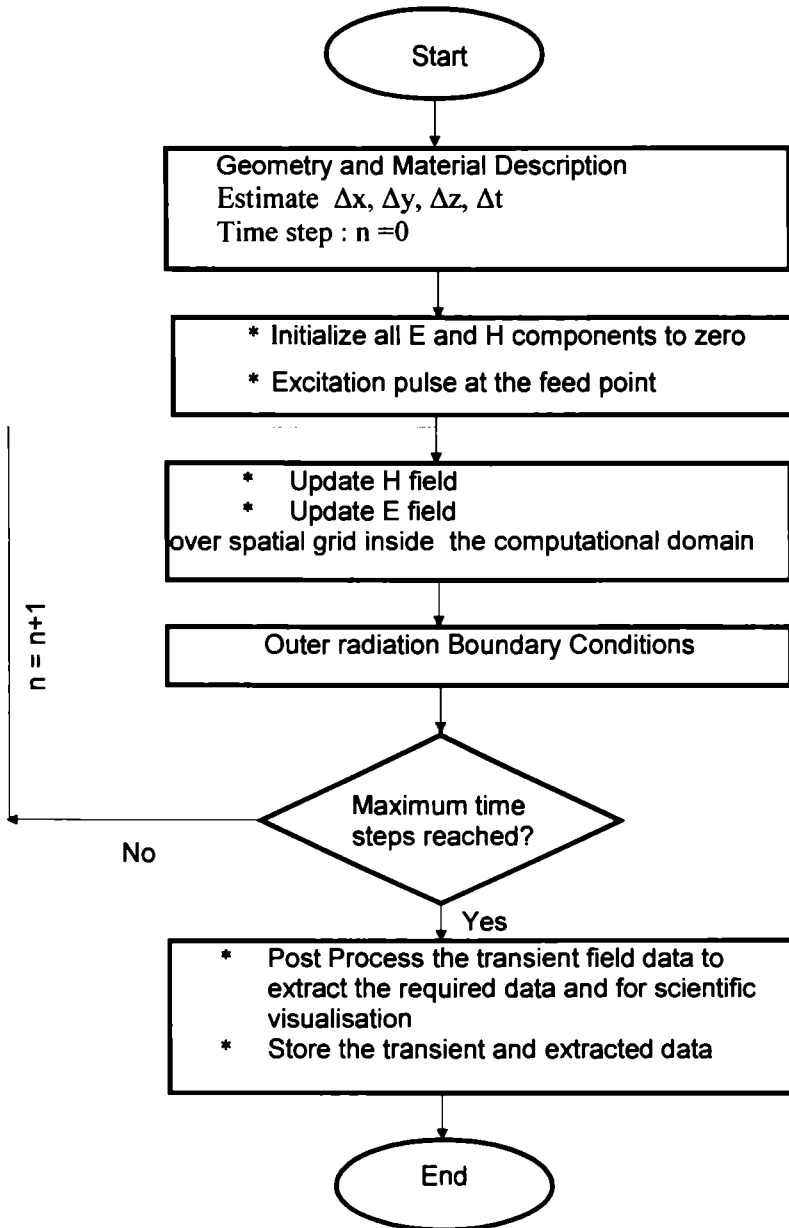


Figure 4.5 The FDTD flow chart

* Driver
* Problem space setup
* Test object definition
* E,H field algorithms
* Outer radiation boundary condition
* Data saver
* Far zone transformation

Table 4.2 FDTD code requirements

An often quoted constraint is “10 cells per wavelength”, meaning that the side of each cell should be $1/10\lambda$ or less at the highest frequency (shortest wavelength) of interest. However for situations demanding high accuracy, $1/20\lambda$ or smaller cells may be necessary. The materials present directly affect the cell size. The FDTD being a volumetric computational method, if some portion of the computational space is filled with a high permittivity material, the shorter wavelength at a given frequency leads to smaller required cell size. A uniform cell size if used throughout the computational space, forces the cells in the entire problem space to be relatively small, thus increasing the total number of cells required. Non- uniform cell size is a possible remedial measure. The following are the reasons substantiating the requirement of a cell size much smaller than one wavelength.

(i) The Nyquist criterion

At any particular time step the FDTD grid is a discrete spatial sample of the field distribution. According to the Nyquist sampling theorem, there must be atleast two samples per spatial period (wavelength) for adequate sampling. Since the sampling is not exact and the smallest wavelength is not precisely determined, more than two samples per wavelength are preferred.

(ii) Grid dispersion error

For a fixed cell size different frequency components of a wave propagate at slightly different velocities. This phenomenon is referred to as numerical dispersion and is inherently present in the FDTD algorithm. Furthermore, velocity depends also on the angle of propagation with respect to the coordinate axis. This is called numerical anisotropy. For accurate and stable results, the grid dispersion error must be reduced to an acceptable level, which can be readily accomplished by reducing the cell size.

(iii) Accurate modelling of the problem geometry

Choosing a cell size smaller than $1/10\lambda$ helps in accurate modelling of the problem geometry, unless some special geometry features smaller than this are factors crucial in determining the response of interest. For example, in thin wire antennas, a change in wire thickness from $1/10\lambda$ to $1/20\lambda$ will affect the antenna impedance. Another example is the staircase effects of modelling a smooth surface with rectangular cells causing significant errors. Good results in these and similar situations may require extremely small cells, or alternative measures such as sub-grid modelling [10] or conformal FDTD techniques [11]. The number of cells needed to model the object and a reasonable amount of free space between the object and the outer boundary in each dimension together determine the total size of the FDTD space.

4.4.2 Time step size for stability

The choice of the spatial grid (Δx , Δy , Δz) and time step (Δt) is motivated by the reasons of accuracy and stability respectively. Though the original FDTD algorithm proposed by Yee is second order accurate in both space and time, the correct stability criteria was first presented by Taflove *et al.* [12]. As time marching continues according to the Yee algorithm, precautions are necessary to ensure that the electric and magnetic fields do not grow beyond bounds. Hence at any point within the computational grid, the propagating wave must not pass through more than one

spatial grid in one time step. Thus, stability is defined as a set of conditions under which the error generated by the finite difference approximations is finite and does not grow in an unbounded fashion as time stepping progresses. In an unstable model, the computed result for E and H field components will increase without limit as the iteration progresses. To ensure the stability of the time-stepping algorithm, Δt is chosen to satisfy the *Courant-Friedrichs –Lewy (CFL) Stability criterion*:

$$v_{\max} \Delta t \leq \frac{1}{\sqrt{\frac{1}{(\Delta x)^2} + \frac{1}{(\Delta y)^2} + \frac{1}{(\Delta z)^2}}} \quad (4.14)$$

where v_{\max} is the maximum wave phase velocity expected within the model. Thus the field cannot change significantly over one space increment. The model will not be stable if the above condition is not obeyed. For actual computations the Δt value specified by the equality in (4.14) provides accurate results, and in most situations a smaller value of Δt does not improve the accuracy [1]. In fact, when the equality holds, the discretized wave most closely approximates the actual wave propagation, and grid dispersion errors are minimized.

4.5 Incident field and Source modelling

Proper excitation of the computational domain excites a field distribution closely resembling that of the physical structure. On the other hand, improper excitation leads to spurious solutions. In time-domain analysis a broadband pulse may be used as the excitation and the frequency-domain parameters may be calculated over the entire frequency range of interest by Fourier transform of the transient results. The frequency band of interest decides the width of the pulse. A wide time domain pulse results in narrow frequency band response. To avoid the unnecessary noise appearing in the FDTD generated response, the excitation pulse and its spectrum must have a smooth roll off and low side lobes.

A sine wave or a Gaussian pulse can be used as the input signal for the 3D FDTD method. However, a Gaussian pulse plane wave is the most widely specified incident field as it provides a smooth roll off in frequency content and is simple to implement. In addition, the frequency spectrum of a Gaussian pulse is also Gaussian and will therefore provide frequency domain information from dc to the desired cut off frequency by adjusting the pulse width. The Gaussian input is of the form

$$g(t) = e^{-\left(\frac{(t-t_0)^2}{T^2}\right)} \quad (4.15.a)$$

where t_0 is the pulse delay and T relates to the Gaussian half width, which sets the required cut off frequency . Writing in the discrete form,

$$g(n\Delta t) = e^{-\left(\frac{(n\Delta t-t_0)^2}{T^2}\right)} \quad (4.15.b)$$

where $T = N \Delta t$ and $t_0 = 3T$. Thus the pulse is sampled N times in a pulse half width T . The Gaussian pulse and its spectrum are shown in Figure 4.6. It is evident from the figure that the pulse provides relatively high signal levels up to the desired frequency. The parameter N can be changed to achieve sharper frequency roll off. In the FDTD method, all functions are assumed to be causal. Therefore, to satisfy the initial condition of zero excitation at the zeroth time step, the time of origin of the Gaussian pulse must be shifted by t_0 ($t_0 \gg 1$). A time delayed Gaussian pulse ($t_0 = 3T$) is used in this thesis.

In order to simulate a voltage source excitation in a Microstrip fed structure, a vertical electric field E_z can be imposed in a rectangular region underneath port 1 in the xz plane as shown in Figure 4.7. The electric field is defined everywhere within the computational region at a time prior to $t = 0$. The launched wave has nearly unit amplitude and is Gaussian in time and propagates in the \hat{y} direction as

$$E_z = g(t) = e^{-\left(\frac{(t-t_0)^2}{T^2}\right)} \quad (4.16)$$

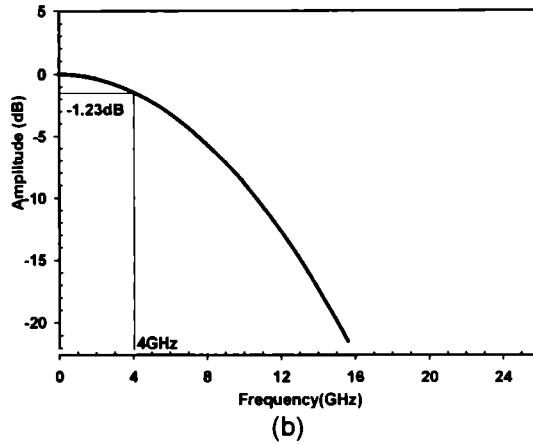
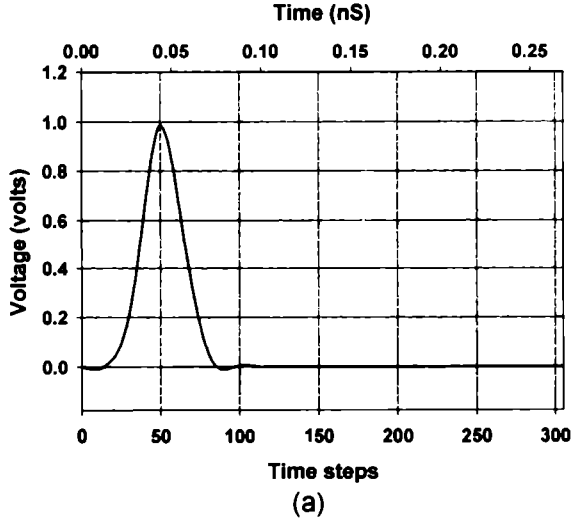


Figure 4.6 (a) Gaussian pulse (b) Gaussian spectrum

Once the time marching begins, this field propagates through the space and interacts with the object. It is assumed that the excitation specified in this way will result in only the fundamental mode propagating down the Microstrip in the frequency range of interest. In order to minimize the effects of numerical dispersion and truncation errors, the Gaussian pulse width is chosen for at least 20 points per wavelength at the highest frequency represented significantly in the pulse.

FDTD calculations are often excited by a “hard” voltage source with zero internal resistance because of the ease of implementation. The Gaussian pulse has

amplitude significantly greater than zero for only a very short fraction of the total computation time, especially for resonant geometries. Once the pulse amplitude drops to zero, the source voltage becomes effectively short-circuited. Thus any reflections from the antenna or Microstrip circuit, which return to the source are totally reflected. The only way to dissipate this energy is through radiation or absorption by lossy media. However certain frequencies of resonant structures require a relatively long time to dissipate the excitation energy. An additional loss mechanism may therefore be provided by modelling the Gaussian voltage source with a series source resistance as proposed by Leubbers *et al.*, thus reducing the number of time steps required for the FDTD calculations to converge [13].

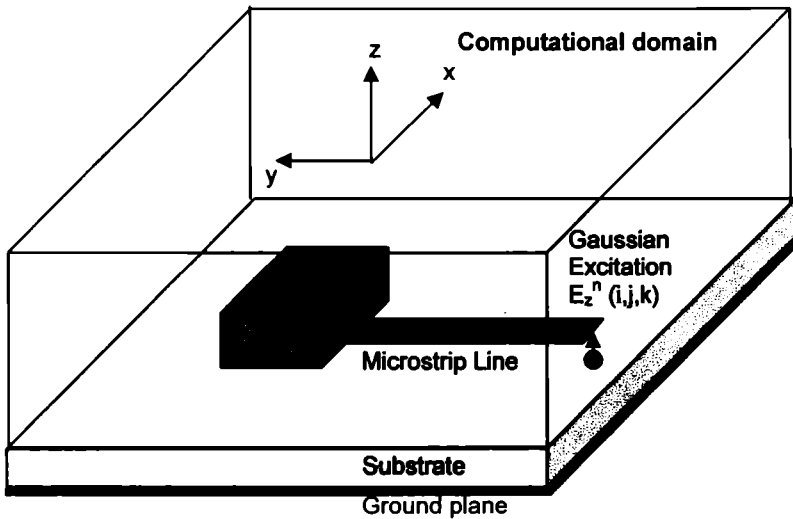


Figure 4.7 The voltage source excitation

Consider the Electric field in the z direction (E_z) corresponding to a Gaussian voltage source (V_s) at a mesh location ($i_s\Delta_x, j_s\Delta_y, k_s\Delta_z$). The equivalent circuit for a voltage source with an internal source resistance (R_s) is illustrated in Figure 4.8. If the source resistance R_s is set to zero, then the FDTD electric field at the source location is simply given by:

$$E_s^n(i_s, j_s, k_s) = \frac{V_s(n\Delta t)}{\Delta z} \quad (4.17)$$

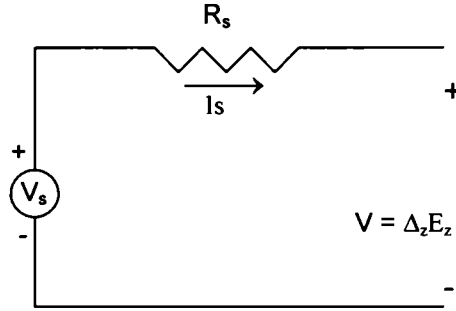


Figure 4.8 FDTD source with internal source resistance R_s

However with the source resistance included, the calculation of the source field necessitates the determination of the current through the source by applying Ampere's circuital law [14] taking the line integral of magnetic field around the electric field source location.

$$\begin{aligned} I_z^{n-1}(i_s, j_s, k_s) = & \left(H_x^{n-1}(i_s, j_{s-1}, k_s) - H_x^{n-1}(i_s, j_s, k_s) \right) \Delta_x \\ & + \left(H_y^{n-1}(i_s, j_s, k_s) - H_y^{n-1}(i_{s-1}, j_s, k_s) \right) \Delta_y \end{aligned} \quad (4.18)$$

By applying Ohm's law to the circuit in Figure 4.8 the electric source field is given by

$$E_z^n(i_s, j_s, k_s) = \left(\frac{V_s(n\Delta t)}{\Delta z} \right) + \left(\frac{I_z^{n-1}(i_s, j_s, k_s) R_s}{\Delta z} \right) \quad (4.19)$$

The value of the internal source resistance is not critical. A reasonable choice is to use the value of the characteristic impedance of the transmission line, coaxial cable, or Microstrip depending on the particular antenna geometry. The internal resistance is fixed as 50Ω in the thesis.

4.6 The 3D FDTD modeller of the Rectangular DRA

The FDTD source code for the numerical computation of the radiation characteristics of a Microstrip line fed Rectangular DRA is developed using MATLAB®. The powerful mathematical computational and graphic visualisation

capabilities of this software tool is very useful in solving three-dimensional electromagnetic problems. The grid lay out and other parameters of the antenna configuration is illustrated in Figure 4.9.

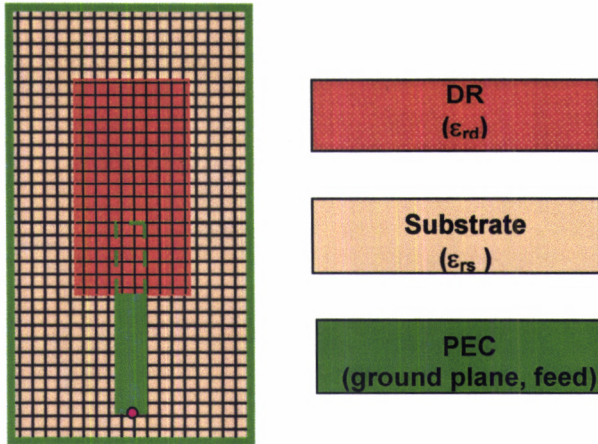


Figure 4.9 The layout of the computational domain

The cell size in each direction is so chosen that there is a minimum of 20 cells per wavelength i.e,

$$\Delta x, \Delta y, \Delta z \leq \frac{\lambda_{\min}}{20} \quad (4.20)$$

where λ_{\min} is the wavelength of the expected highest significant harmonic in the model. Also an integral number of cells must fit within the DR and the substrate as far as possible. To avoid late time instability Δt in the present work is chosen as 0.995 times the minimum value specified by the *CFL* inequality (Equation 4.14). The absorbing boundary is always placed 10 cells away from the antenna object. The different objects constituting the computational domain of the FDTD code for a typical case are listed in Table 4.3.

object		material	dimensions		
			x axis cm	y axis cm	z axis cm
1.	ground plane	PEC	4	4	-
2.	substrate	$\epsilon_{rs} = 4.28$ $h = 0.16$ cm	4	4	0.16
3.	DR	$\epsilon_{rd} = 48$	1.19	2.25	0.555
4.	feed	PEC	0.3	2	-

Table 4.3 Objects in the computational domain

4.6.1 Reflection characteristics

A Gaussian pulse is impressed into the computational domain at the feed point corresponding to the port under study in order to analyze the antenna reflection characteristics. Time is then advanced until the pulse propagates through the workspace and the fields die down to zero. The optimised FDTD code parameters for the present problem are listed in Table 4.4. The direct output of FDTD run is the time domain information, which is then converted appropriately to frequency domain characteristics by applying Fourier transformation.

Excitation	Gaussian Pulse Half width $T = 15$ ps Time delay $t_0 = 3T$
Cell Dimensions (mm)	$\Delta x = 0.5$ $\Delta y = 0.5$ $\Delta z = 0.4$
Time step	$\Delta t = 0.88$ ps
Number of time steps	5000
Simulation interval	4400 ps

Table 4.4 Optimised FDTD code parameters for the present problem

The input impedance of the antenna is computed as ratio of the FFT of voltage derived from E field values at the feed point over the entire time steps, to the FFT of current at the same point, derived from the H field values. Return Loss S_{11} (in dB) is then computed. The voltage and current waveforms at the feed point are shown in Figure 4.10. In FDTD calculations involving $R_s = 50 \Omega$, the voltage waveform is no longer purely Gaussian, since the voltage across the resistance is also included. It is observed during simulation that the system converges in ~ 5000 time steps for the present problem.

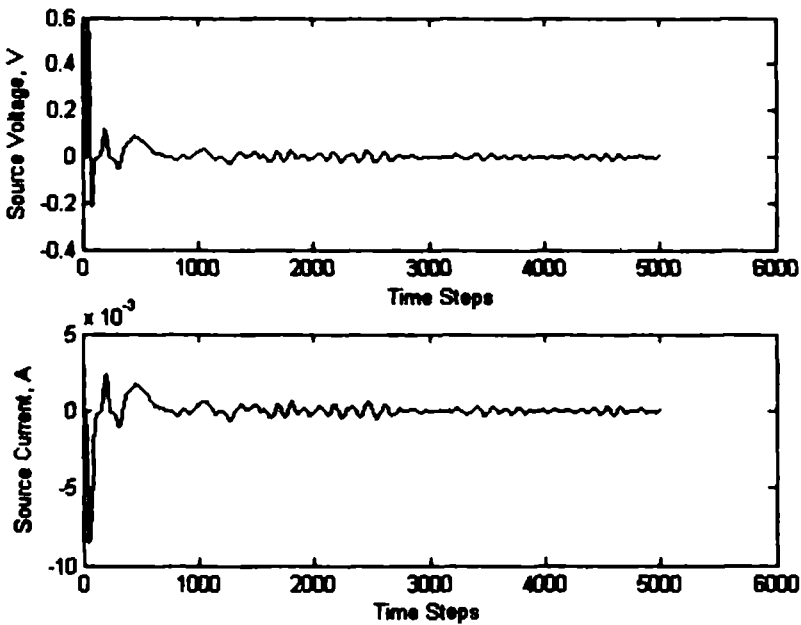


Figure 4.10 Voltage and current waveforms at the feed point due to the matched delayed Gaussian pulse source in the domain

4.6.2 Far field computation

The FDTD approach of predicting the far fields of a radiating structure is simple and straightforward and is adaptable to complex geometries. It serves as a viable alternative to the conventional theoretical techniques involving the formulation of an approximate theoretical model leading to discrepancies between the predicted

and measured results [15]. Accurate models and accurate theoretical analysis have been used with simple radiators, but with increased complexity. In FDTD method the far fields may be computed from the transient near field values using the near field-to-far field transformation techniques in the time/frequency domain. This approach does not require the extension of the computational domain to the far field. However, the frequency domain transformations used in conjunction with a sinusoidal time variation excitation are valid only at one frequency. To obtain wide band results, it would be more efficient to use a pulsed excitation, transform the time domain near field results to far field at each observation point and then transform the far field time domain results to frequency domain. Thus one FDTD computation along with a Fast Fourier Transform (FFT) results in a wideband result [16]. In applications requiring transient or broadband frequency domain far field results at different observation angles, the fully transient approach involving FFT is desirable. For small geometries this can be implemented by storing the transient tangential field components on a closed surface in the computational domain and then computing the transient far field vector potentials at each observation point by a running summation at each time step.

In this thesis, a sinusoidal excitation is used to address the far field computation problem at the operating frequency of the antenna. The return loss characteristics from the previous analysis decide the resonant frequency (f_0) of the antenna. Iterations are carried out with a sinusoidal excitation of the form $V(n\Delta t) = \sin(2\pi f_0 n\Delta t)$, until the system achieves sinusoidal steady state. An aperture is defined in a layer above the DR surface, as shown in Figure 4.11 (a). At each spatial point Q in this plane as shown in Figure 4.11(b), the time independent first harmonic coefficient $E_{(x',y',z'=0)}$ is computed by sampling the tangential field components over N time steps corresponding to one period of the excitation [17].

$$E_{(x',y',z'=0)} = (1/N) \sum_{n=1}^N E(n) \bullet \exp(j2\pi.n/N) \quad (4.21)$$

where $E(n)$ corresponds to the instantaneous tangential E field component E_{xn} or E_{yn} at $Q(x',y',0)$.

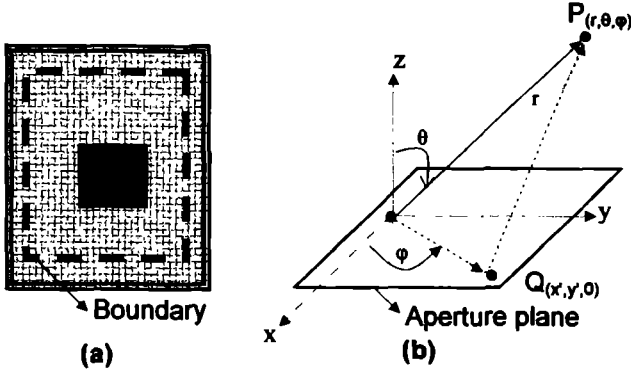


Figure 4.11 Pattern computation using FDTD.
 (a) Aperture boundary in a layer above the DR surface.
 (b) Spatial point Q in the aperture layer and far field point P

From the aperture field so computed, the Magnetic surface current density is given by

$$\mathbf{M} = -2\vec{a}_n \times \mathbf{E} \quad (4.22)$$

Magnetic surface current density so derived is then used to compute the electric vector potential \mathbf{F} over the aperture [18]. Assuming $e^{j\omega t}$ time variation, Electric field at a far field point P (r, θ, ϕ) in free space with characteristic impedance η_0 is computed as

$$\mathbf{E} = j\omega\eta_0.(F_\theta\vec{a}_\phi - F_\phi\vec{a}_\theta) \quad (4.23)$$

The far field components E_θ and E_ϕ are derived by the rectangular to spherical transformation as

$$E_\theta = j\omega\eta_0.(F_x\sin(\phi) - F_y\cos(\phi)) \quad (4.24.a)$$

$$E_\phi = j\omega\eta_0.\cos(\theta)(F_x\cos(\phi) + F_y\sin(\phi)) \quad (4.24.b)$$

with the following assumptions,

- ★ the antenna radiates into the $z > 0$ region from the aperture in the $z = 0$ plane
- ★ r is in the far field i.e ($r \gg (x^2 + y^2)^{1/2}$) &
- ★ aperture defined is such that the tangential electric fields are negligible outside its boundary,

Equation 4.23 now becomes

$$E = j \cdot \exp(-jkz) / (\lambda \cdot r) \cdot \left(\begin{array}{l} \left(\cos(\theta) (f_x \cos(\phi) + f_y \sin(\phi)) \vec{a}_\phi \right) \\ \left(- (f_x \sin(\phi) - f_y \cos(\phi)) \vec{a}_\theta \right) \end{array} \right) \quad (4.25)$$

where

$$f \cdot = \iint_S E \cdot (x', y', 0) \cdot \exp \left(jk \begin{pmatrix} x' \sin(\theta) \cos(\phi) \\ y' \sin(\theta) \sin(\phi) \end{pmatrix} \right) \cdot dx' dy' \quad (4.26)$$

and S is the planar aperture selected. In this thesis, the planar aperture is defined in a plane one cell above the x-y plane containing the top surface of the DR in the computational grid. To plot the principal plane patterns corresponding to $\phi = 0^\circ$ and $\phi = 90^\circ$, E_θ and E_ϕ are computed using Equation 4.25, at discrete θ values.

4.6.3 Resonant modes

The time independent H field components over the surface (H_x and H_y) are computed using a procedure similar to that of the E field computation explained in the previous section. The modes of resonance are identified from the H field distribution in the aperture defined within the DR as illustrated in Chapter five.

The numerical method described above is employed for the analysis of different Rectangular Dielectric Resonator Antenna configurations. The results of the numerical analysis are validated through experiments and commercially available software and presented in chapter five. These results are not presented here in order to avoid repetition.

-
1. Karl.S.Kunz and Raymond J.Luebbers, "The finite difference Time Domain Method for electromagnetics," CRC Press, New York 1993.
 2. K.S.Yee, "Numerical solution of initial boundary value problems involving Maxwell's equations in isotropic media," *IEEE Trans. Antennas Propagat.*, vol.14, no.4, pp. 302-307, May 1966.
 3. David.M.Sheen, Sami.M.Ali, Mohamed D.Abouzahra and Jin Au Kong, "Application of the Three-Dimensional Finite- Difference Time-Domain method to the analysis of planar Microstrip circuits," *IEEE Trans. Microwave Theory Tech.*, vol.38, no.7, pp.849-857, July 1990.
 4. Mur.G, "Absorbing boundary conditions for the finite-difference approximation of the time-domain electromagnetic field equations," *IEEE Trans. Electromagnetic compatibility*, vol.23, no.4, pp.377-382, November 1981.
 5. B.Enquist and A.Majda, "Absorbing boundary conditions for the numerical simulation of waves," *Math of Comput.*, vol.31, pp.629-651, 1977.
 6. Zhang.X, Mei.K.K, "Time domain finite difference approach to the calculation of the frequency dependent characteristics of Microstrip discontinuities," *IEEE Trans. Microwave Theory Tech.*, vol.36, no.12, pp.1775-1787, 1988.
 7. Berenger J.P, "A perfectly matched layer for the absorption of electromagnetic waves," *J. computational physics*, vol.114, pp.185-200, May 1994.
 8. Zhenhai Shao, Wei Hong and Jianyi Zhou, "Generalized Z-Domain absorbing boundary conditions for the analysis of electromagnetic problems with finite – difference time-domain method," *IEEE Trans. Microwave Theory Tech.*, vol.51, no.1, pp.82-90, January 2003.
 9. Kenneth K.Mei and Jiayuan Fang, " Superabsorption – A method to improve absorbing boundary conditions," *IEEE Trans. Antennas Propagat.*, vol.40, no.9, pp. 1001-1010, September 1992.
 10. Michal Okoniewski, Ewa Okoniewska and Maria A.Stuchly, "Three-dimensional subgridding algorithm for FDTD," *IEEE Trans. Antennas Propagat.*, vol.45, no.3, pp. 422-429, March 1997.

11. Supriyo Dey and Raj Mittra, "A conformal Finite-Difference Time Domain technique for modelling cylindrical dielectric resonators," *IEEE Trans. Microwave Theory Tech.*, vol.47, no.9, pp.1737-1739, September 1999.
12. Allen Taflov and Morris E. Brodwin, "Numerical solution of steady state electromagnetic scattering problems using the time-dependent Maxwell's equations," *IEEE Trans. Microwave Theory Tech.*, vol.23, no.8, pp.623-630, August 1975.
13. R.J. Leubbers and H.S. Langdon, "A simple feed model that reduces time steps needed for FDTD antenna and Microstrip calculations," *IEEE Trans. Antennas Propagat.*, vol.44, no.7, pp. 1000-1005, July 1996.
14. Jordan and Balmain "Electromagnetic fields and radiating systems," Prentice Hall of India Pvt Ltd, New Delhi 1986.
15. James G. Maloney, Glenn S. Smith and Waymond R. Scott, Jr, "Accurate computation of the radiation from simple antennas using the Finite-Difference Time-Domain method," *IEEE Trans. Antennas Propagat.*, vol.38, no.7, pp. 1059-1068, July 1990.
16. "A Finite-Difference Time-Domain near zone to far zone transformation," *IEEE Trans. Antennas and Propagat.*, vol.39, no.4, pp. 429-433, April 1991.
17. Martin L Zimmerman and Richard Q. Lee, "Use of the FDTD method in the design of Microstrip antenna arrays," *Int. Journal of Microwave and Millimeter wave Comp. aided Engg.*, vol.4, no.1, pp.58-66, 1994.
18. Ramesh Garg, Prakasah Bhartia, Inder Bahl and Apisak Ittipiboon, "Microstrip Antenna Design Handbook," Artech House, Norwood, MA, 2001.

Outcome of Numerical Computation and Experimental Observations

The primary objective of the research work is the development of a compact Dielectric Resonator Antenna (DRA) suitable for Mobile Communication handset applications. Towards achieving this goal, investigations are carried out on different rectangular DRA configurations. The chapter presents the results of numerical computations employing the Finite Difference Time Domain (FDTD) method performed to predict the radiation characteristics of a Rectangular Dielectric Resonator Antenna. The outcome of the exhaustive experimental investigations detailed in the chapter validate the numerical predictions with reasonably good accuracy. DRA configurations suitable for wireless applications are developed based on the inference derived from this study.

5.1 Radiation characteristics of the Microstrip line fed Rectangular Dielectric Resonator Antenna incorporating DR-1

The chapter presents the outcome of the exhaustive investigations performed on various Dielectric Resonator Antenna (DRA) configurations to study their radiation characteristics and perform their mode identification. The Rectangular Dielectric Resonator sample [DR-1; $\text{Ca}_5\text{Nb}_2\text{TiO}_{12}$; $\epsilon_r = 48$] of dimensions $[a \times b \times d] = [2.25 \times 1.19 \times 0.555] \text{ cm}^3$, excited by a 50Ω Microstrip feed line of length $l_f = 2 \text{ cm}$ is initially chosen for the study. The resonator is placed in different orientations upon the feed line. Measurements are recorded for all orientations of the DR and for varying dimensions of the feed line and ground plane. The overall size of the antenna configuration is decided by the aspect ratio of the DR, the dimensions of the feed line and the ground plane. Table 5.1 lists the aspect ratio of the resonator sample (DR-1) in various orientations. The orientations are described in detail in Chapter 4.

		orientation					
dimensions along							
x-y-z axes \Rightarrow	b-a-d	a-b-d	d-a-b	d-b-a	a-d-b	b-d-a	
aspect ratio							
$(\frac{\text{height}}{\text{width}}) \Rightarrow$	0.25	0.47	0.53	1.9	2.14	4.05	

Table 5.1 Aspect ratio of the DR in different orientations
DR-1 [$\text{Ca}_5\text{Nb}_2\text{TiO}_{12}$, $\epsilon_r = 48$]
 $[a \times b \times d] = [2.25 \times 1.19 \times 0.555] \text{ cm}^3$

The aim of the study is to optimise the DRA parameters for various radiation characteristics. The parameters studied are detailed in Table 5.2.

<ul style="list-style-type: none"> • Orientation of the DR with respect to the feed line • Position of the DR upon the feed line • Dimensions of the DR • Material properties of the DR • Dimensions of the feed line • Truncation effect of the ground plane

Table 5.2 Parameters under investigation

5.1.1 The b-a-d orientation

The b-a-d orientation illustrated in Figure 5.1(a) is a low profile orientation, corresponding to the least value of aspect ratio of the DR [0.25]. A schematic representation of this orientation is shown in Figure 5.1(b).

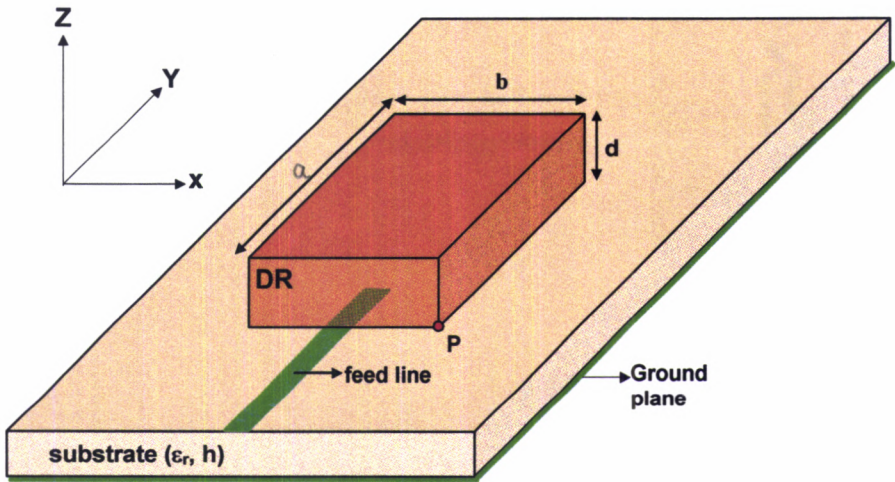


Figure 5.1(a) The b-a-d orientation of the Dielectric Resonator 3-D view

The distance of the reference vertex [P] from the feed axis and the open feed end (d_x, d_y) indicate the position of the DR along the x and y axes respectively. In order to

arrive at a compact antenna configuration, the dimensions of the ground plane are reduced and a truncated ground plane is also employed for all the feed lines under study. The radiation characteristics of the 2 cm line excited DRA in the b-a-d orientation of the resonator is discussed in this section.

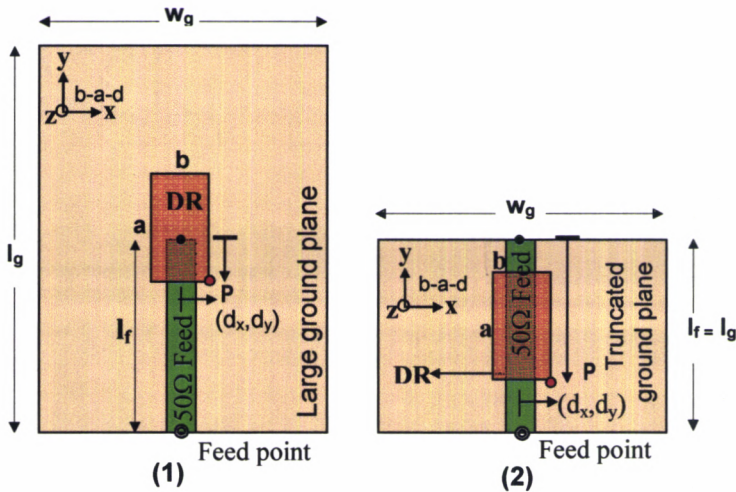


Figure 5.1.b The b-a-d orientation of the DR – schematic lay out
 (1) large ground plane (2) truncated ground plane
 substrate: $\epsilon_{rs} = 4.28$, $h = 0.16$ cm
 DR-1 $[a \times b \times d] = [2.25 \times 1.19 \times 0.555]$ cm³

5.1.1.1 Return Loss Characteristics

Based on the numerical computation as described in Chapter 4, the Dielectric Resonator Antenna (DRA) is analyzed for a feed line of length $l_f = 2$ cm with a ground plane of size $(l_g \times w_g) = (4 \times 4)$ sq cm. From the exhaustive numerical computations it is found that when the DRA is placed at $(d_x, d_y) = (0.5, 1.5)$ cm, the system resonates at 3.202 GHz from 3.098 GHz to 3.2931 GHz with a bandwidth of 6.1%. The numerically computed return loss characteristics are plotted in Figure 5.2 along with the experimentally observed results. The resonant frequency, return loss, input impedance and 2:1 VSWR bandwidth can be determined from the return loss curve.

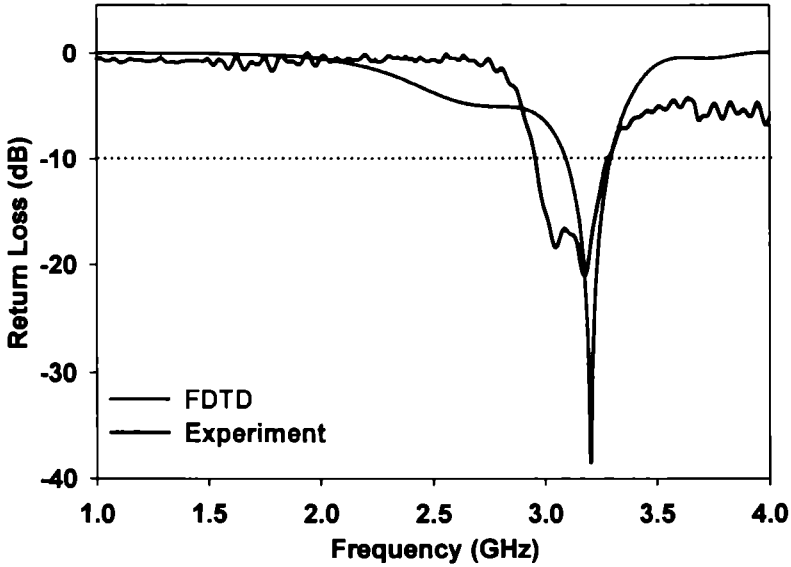


Figure 5.2 Return loss characteristics of the DRA at the optimum bandwidth position
 feed line length = 2 cm large ground plane: 4 x 4 sq cm
 DR-1 orientation : b-a-d (d_x, d_y) = (0.5, 1.5) cm

The experimentally measured resonance is at 3.175 GHz in a band operating from 2.956 GHz to 3.281 GHz. A lower resonant mode at 3.04 GHz is also observed in the operating band. The bandwidth offered is 325 MHz (10.2%). From the figure it is evident that FDTD analysis predicts the resonant frequency and bandwidth of the antenna with reasonable accuracy. The fractional difference between the experimentally measured and numerically computed resonant frequency is -0.85% . The disparity may be due to the following factors.

In the numerical computation, the dimension of the DRA is $[2.25 \times 1.19 \times 0.555]$ cm³. However the surface irregularities if any, are not accounted for in the simulation. The thin air layer between the feed line and the DRA due to these surface irregularities alters the effective dielectric constant of the DRA slightly, shifting the resonant frequency. The grid size in the computational domain also plays a crucial role in deciding the accuracy of prediction.

5.1.1.2 Radiation Pattern

Antennas for Mobile Communication applications ought to radiate equally in all directions. However in many wireless applications the pattern shape plays a secondary role with respect to bandwidth. The co-polar and cross-polar radiation characteristics in the principal planes of the DRA in different orientations of the DR have been studied in detail for varying dimensions of the feed line and ground plane. The predicted and experimentally measured radiation patterns in the b-a-d orientation of the resonator are shown in Figure 5.3. The patterns are broad in both the planes. Table 5.3 summarises the radiation characteristics of the DRA in the b-a-d orientation. The antenna radiates with a maxima along the broad side direction. The slight tilt in the E-plane pattern is perhaps due to the asymmetry of the excitation of the DRA at this position.

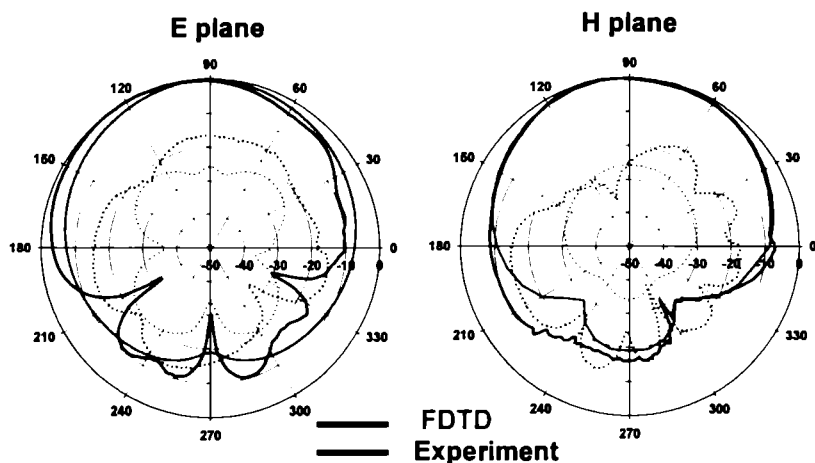


Figure 5.3 Radiation Pattern of the DRA at the optimum bandwidth position ($f = 3.175$ GHz) --- co-polar cross-polar
 feed line length = 2 cm large ground plane: 4 x 4 sq cm
 DR-1 orientation: b-a-d $(d_x, d_y) = (0.5, 1.5)$ cm

The front to back ratio measured along the maxima is better than 15 dB in both the principal planes. The cross polarization along the maxima is better than -20 dB in both the planes. As shown in Figure 5.3, the theoretical radiation patterns agree reasonably well with the experimental curves. It is therefore evident that the FDTD

method can model the DRA and also predict its radiation pattern with fairly good accuracy.

	Half power beam width (degree)		On axis Front-to-Back Ratio (dB)		On axis Cross-Polarisation (dB)	
	E plane	H plane	E plane	H plane	E plane	H plane
Theory	100	98	19	19	-26	-26
Experiment	108	90	15	17	-21	-35

Table 5.3 Radiation characteristics of the DRA at the optimum bandwidth position ($f = 3.175$ GHz)
 feed line length = 2 cm large ground plane: 4 x 4 sq cm
 DR-1 orientation: b-a-d (d_x, d_y) = (0.5, 1.5) cm

5.1.1.3 Polarization

The DRA in the b-a-d orientation is found to exhibit linear polarization in the optimum resonant band. The polarization of the resonant modes at 3.04 GHz and 3.175 GHz is along the longer dimension 'a' of the DR, parallel to the feed axis. The analysis also confirms this result.

5.1.1.4 Gain

The gain is an important figure of merit of the antenna, indicating its radiation efficiency. The Gain Transfer method explained in Chapter 3 is employed to measure the relative gain of the DRA (test antenna) at the optimum bandwidth position. Standard pyramidal horn antenna of known gain is used as the reference antenna. The absolute gain (in dBi) of the test antenna is then calculated. Measurements are repeated for varying dimensions of the feed line and ground plane. The measured gain characteristics of the DRA at the optimum bandwidth position, in the b-a-d orientation of the resonator is shown in Figure 5.4.

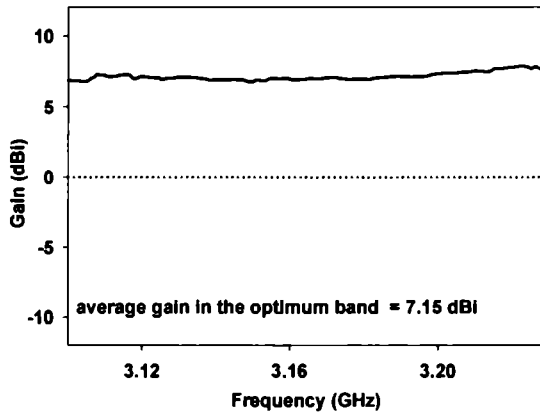


Figure 5.4 Gain of the DRA measured in the optimum band
 feed line length = 2 cm large ground plane: 4 x 4 sq cm
 DR-1 orientation : b-a-d $(d_x, d_y) = (0.5, 1.5)$ cm

The DRA exhibits 7.15 dBi gain in the optimum resonant band. The gain of the antenna is almost constant in the entire operating band. This again confirms that the antenna is linearly polarised in the entire band of operation. The low profile nature, good bandwidth (10.2%) exhibited at a low resonant frequency (3.175 GHz) and excellent gain characteristics (7.15 dBi) of the b-a-d orientation are noteworthy. It is thus inferred that bandwidth enhancement is achieved without sacrificing the antenna gain.

5.1.1.5 Resonant Mode

The modes of the rectangular DRA are identified from the field distributions within the DR at the resonant frequency (3.202 GHz) predicted numerically in different plane cuts (x-y, y-z and x-z planes) as illustrated in Figure 5.5 (a-c). The TE_{mnp}^z mode is identified, where the indices denote the no: of half wave intensity variations along the dimensions 'a', 'b' and 'd' of the DR respectively ($a > b > d$).

The first, second and third row in Figure 5.5(a) illustrate the variation of the H_x , H_y and H_z components respectively in the x-y plane. The first, second and third column of figures correspond to the H field variation in the x-y plane at the bottom,

middle and top layer of the DR. The one half-wave variation of all the three field components along the dimensions 'a' and 'b' is evident from the field distribution at the top layer (column 3: $z_3 = 18$).

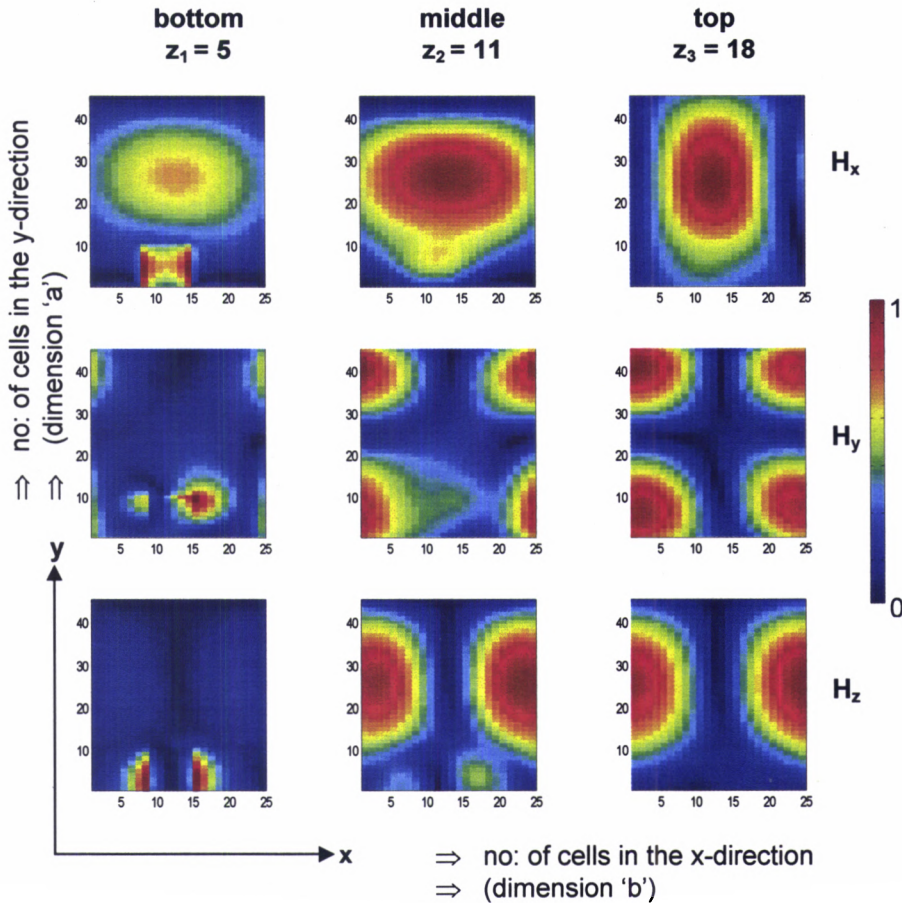


Figure 5.5(a) Field distribution within the DRA predicted using FDTD in the x-y plane at three different z-layers ($f = 3.202$ GHz) feed line length = 2 cm large ground plane: 4 x 4 sq cm DR-1 orientation : b-a-d (d_x, d_y) = (0.5, 1.5) cm

- ◆ In the FDTD computational domain, the cells numbered from $z = 5$ to $z = 18$ define the DR along the z direction.
- ◆ In the b-a-d orientation, the DR occupies 24 cells in the x direction and 45 cells in the y direction

In Figure 5.5(b) the first, second and third column of figures correspond to the H field variation in the y-z plane at the left, middle and right layer of the DR. The one half-

wave variation of all the three field components along the dimension 'a' and less than one half-wave variation along the dimension 'd' is evident from the field distribution at the rightmost layer (column 3: $x_3 = 42$).

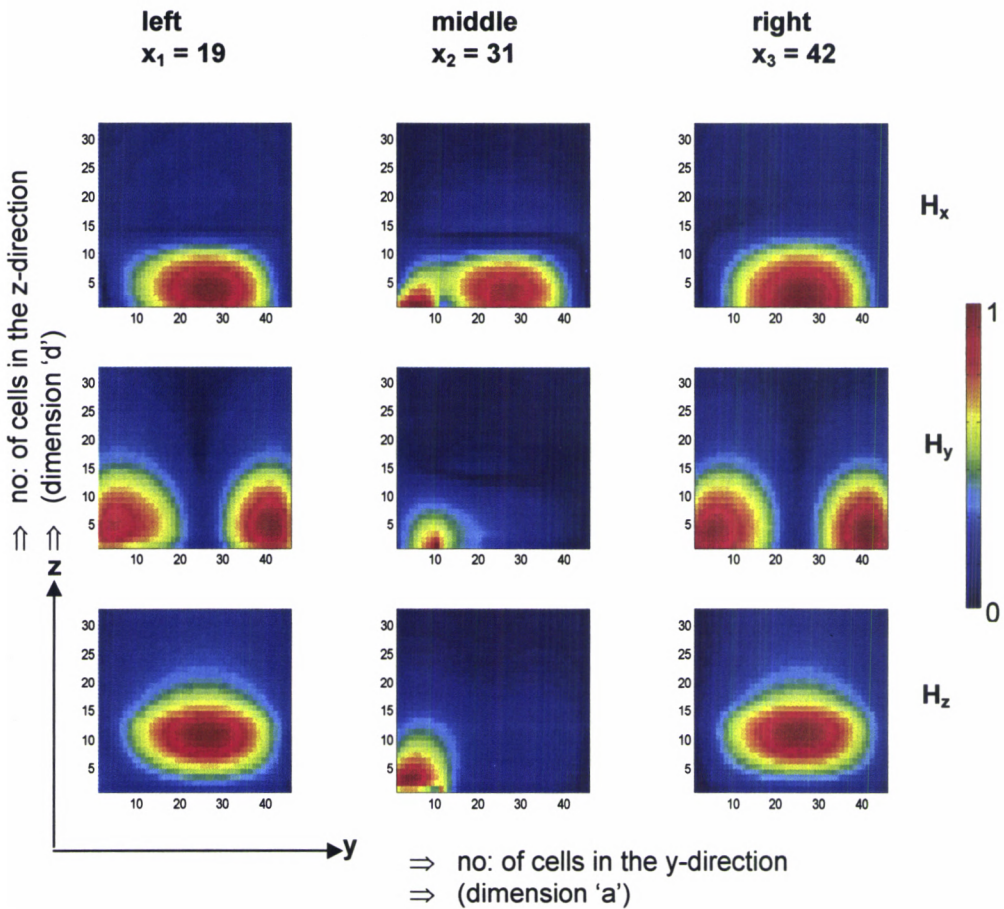


Figure 5.5 (b) Field distribution within the DRA predicted using FDTD in the y-z plane at different x layers
 $(f = 3.202 \text{ GHz})$
 feed line length = 2 cm large ground plane: 4 x 4 sq cm
 DR-1 orientation : b-a-d $(d_x, d_y) = (0.5, 1.5) \text{ cm}$

- ◆ In the FDTD computational domain the cells numbered from $x = 19$ to $x = 42$ define the DR along the x direction.
- ◆ In the b-a-d orientation the DR occupies 45 cells in the y direction and 14 cells in the z direction.

In Figure 5.5(c) the first, second and third column of figures correspond to the H field variation in the x-z plane at the front (source end), middle and back (feed end) layer of the DR. The one half-wave variation of all the three field components along the dimension 'b' and less than one half-wave variation along the dimension 'd' is evident from the field distribution at the back layer (column 3: $y_3 = 85$).

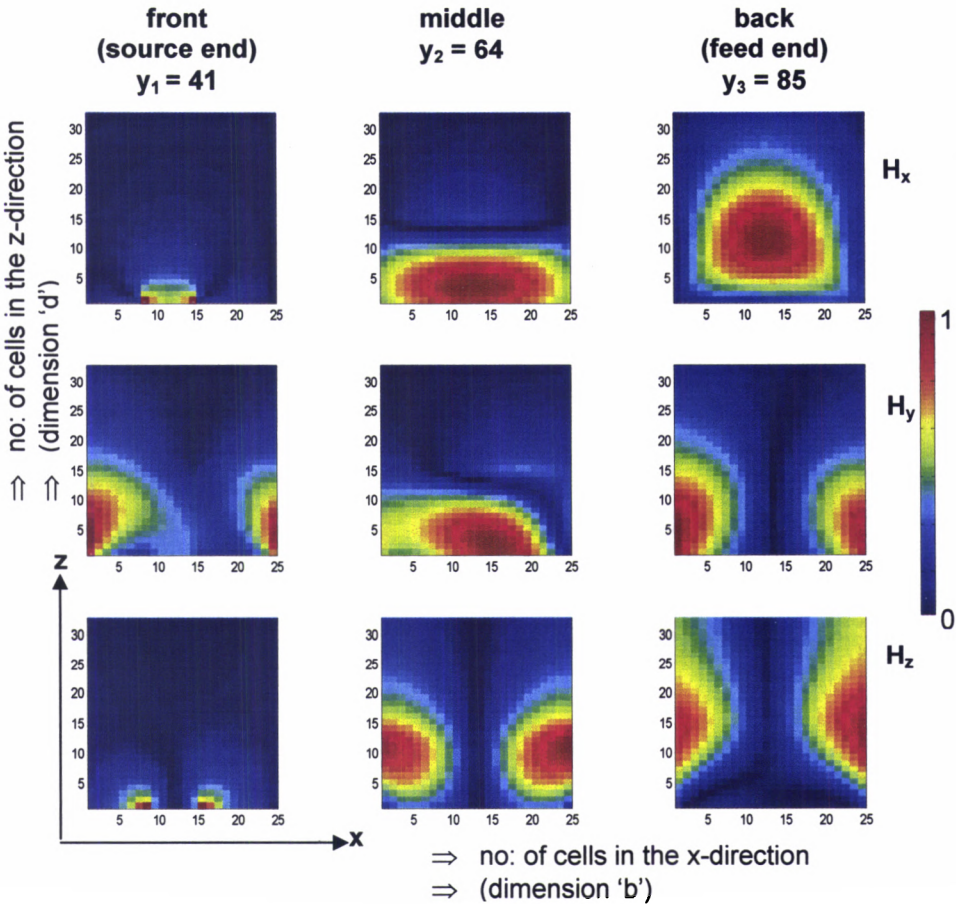


Figure 5.5 (c) Field distribution within the DRA predicted using FDTD in the x-z plane at different y layers ($f = 3.202$ GHz)
 feed line length = 2 cm large ground plane: 4 x 4 sq cm
 DR-1 orientation : b-a-d $(d_x, d_y) = (0.5, 1.5)$ cm

- ◆ In the FDTD computational domain the cells numbered from $y = 41$ to $y = 85$ define the DR along the y direction.
- ◆ In the b-a-d orientation the DR occupies 24 cells in the x direction and 14 cells in the z direction

The one half-wave variation along the dimensions 'a' and 'b' and less than a half-wave variation (δ) along the dimension 'd' as illustrated in Figures 5.5(a-c) confirm the presence of TE_{118}^z mode. Simulation using commercially available software-HFSS™, also gives similar results as shown in Figure 5.6 (a).

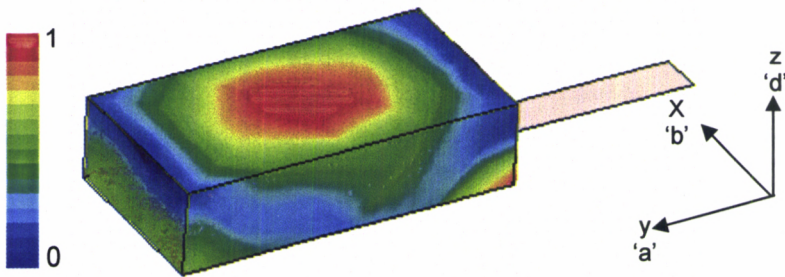


Figure 5.6 (a) Simulated H field distribution within the DR at the optimum bandwidth position
 $f = 3.202$ GHz
 feed line length = 2 cm large ground plane: 4 x 4 sq cm
 DR-1 orientation : b-a-d $(d_x, d_y) = (0.5, 1.5)$ cm

The variation of the normalized Magnetic field monitored experimentally using a loop probe along the three dimensions is shown in Figure 5.6 (b). The experimental and simulation studies confirm that the resonant mode of the DR in the b-a-d orientation at the optimum bandwidth position is TE_{118}^z . The validity of the numerical computation of the DRA characteristics using the FDTD code developed in MATLAB® is thus established.

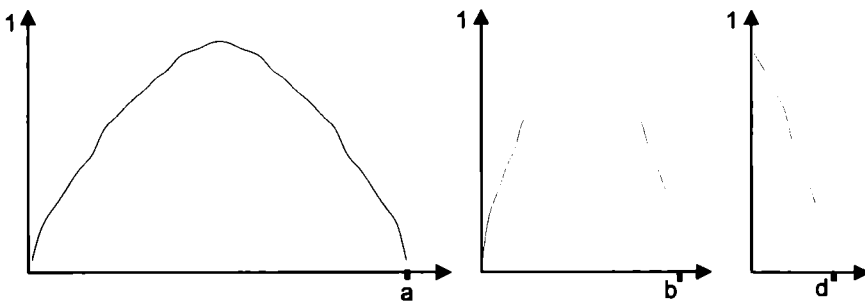


Figure 5.6 (b) Variation of the normalized Magnetic field distribution along the dimensions 'a', 'b' and 'd' of the DR monitored experimentally
 TE_{118}^z mode
 feed line length = 2 cm large ground plane: 4 x 4 sq cm
 DR-1 orientation : b-a-d $(d_x, d_y) = (0.5, 1.5)$ cm

5.1.1.6 Compactness

The overall size of the antenna is determined by the orientation of the DR, the feed line and ground plane dimension. In order to ascertain the compactness of the DRA in the b-a-d orientation at the measured resonant frequency of 3.175 GHz, the antenna is compared with a circular and rectangular Microstrip antenna resonating at the same frequency. Table 5.4 provides a comparison of the dimensions of different antennas operating at 3.175 GHz. The DRA incorporating the resonator in the b-a-d orientation is found to possess 58.6% and 48.4% reduction in the cross-section area with respect to a rectangular and circular Microstrip antenna designed to operate at the same frequency.

Antenna	Dimensions (cm)	Cross sectional area (sq cm)
DRA in the b-a-d orientation	Length (b) = 1.19 Width (a) = 2.25	(b x a) 2.7
Rectangular Microstrip antenna	Length = 2.24 Width = 2.91	6.52
Circular Microstrip antenna	Radius = 1.29	5.23

Table 5.4 Dimensions of different antennas operating at 3.175 GHz

5.1.1.7 Truncated ground plane configuration

In the previous section the experimental observations on the Rectangular DRA on a large ground plane was presented. The system offers comparatively good bandwidth. However for practical applications like Mobile Communication, this leads to an increase in the overall size of the antenna. The effect of the truncated ground plane is presented in this section. Numerical computation predicts a maximum 2:1 VSWR bandwidth of 287 MHz (9.3%) at 3.094 GHz in a band operating from 2.9384 GHz to 3.225 GHz at the position $(d_x, d_y) = (0.6, 1.2)$ cm. A resonant mode centred at

3.115 GHz is experimentally observed in a band from 3.01 GHz to 3.32 GHz, offering 310 MHz bandwidth (9.95%). The fractional difference between the measured and predicted frequency is 0.67%.

Figure 5.7 shows the return loss and gain characteristics of the DRA at the optimum bandwidth position. The resonant behaviour is comparable to that displayed by the large ground plane. However, the truncation of the ground plane results in deterioration of the antenna gain. The DRA is found to exhibit an average gain of 2.1 dBi in the optimum resonant band.

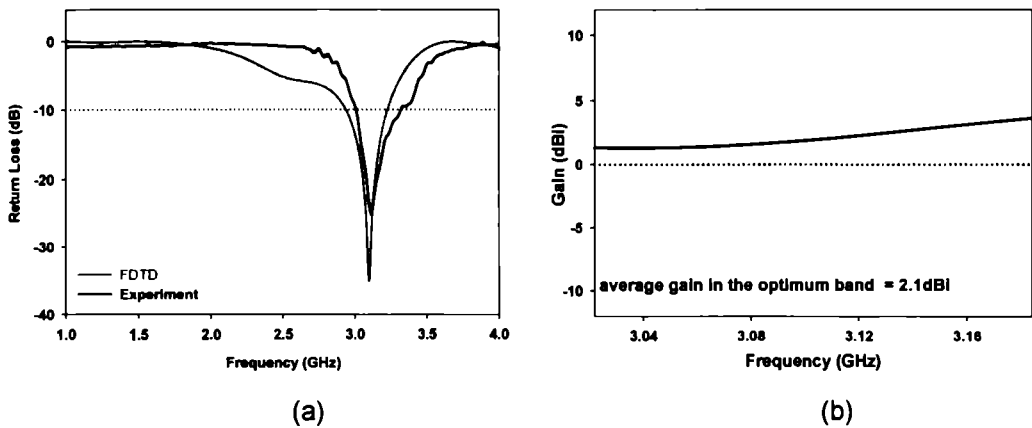


Figure 5.7 Characteristics of the DRA measured at the optimum bandwidth position
 (a) Return loss (b) Gain
 feed line length = 2 cm truncated ground plane: 2 x 4 sq cm
 DR-1 orientation : b-a-d (d_x, d_y) = (0.6, 1.2) cm

The radiation patterns in the principal planes are shown in Figure 5.8. The patterns are broad in both the planes, with a maxima along the broad side direction. The front to back ratio is 8 dB in both the planes. The cross polarization along the maxima is better than -14 dB in both the planes. The measured patterns agree reasonably well with the predicted patterns. Table 5.5 summarises the radiation characteristics of the DRA in the b-a-d orientation at 3.115 GHz.

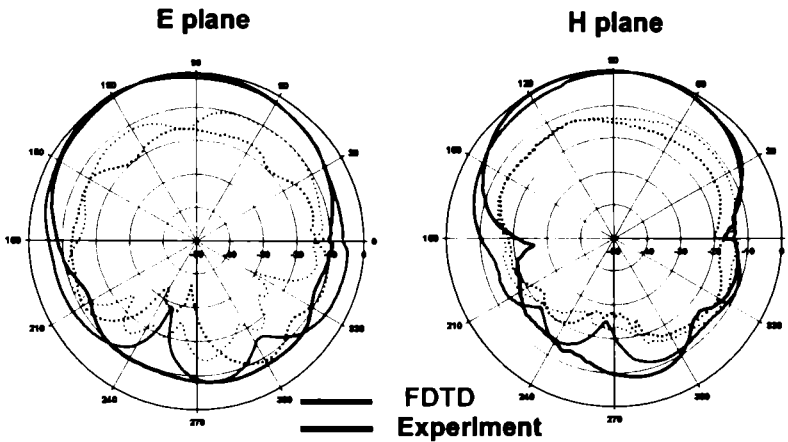


Figure 5.8 Radiation Pattern of the DRA at the optimum bandwidth position ($f = 3.115$ GHz) feed line length = 2 cm DR-1 orientation : b-a-d truncated ground plane: 2×4 sq cm (d_x, d_y) = (0.6, 1.2) cm

Even though the truncation of the ground plane results in reduction in gain of the antenna, the radiation pattern is broad and the configuration is therefore highly desirable for Mobile Communication applications where active circuitry can be incorporated for compensating the reduction in gain. Table 5.6 compares the radiation performance of the 2 cm fed DRA in the b-a-d orientation of the resonator for different ground plane dimensions.

	Half power beam width		On axis Front-to-Back Ratio		On axis Cross-Polarisation	
	(degree)		(dB)		(dB)	
	E plane	H plane	E plane	H plane	E plane	H plane
Theory	102	84	14	18	-12	-14
Experiment	96	94	8	8	-17	-14

Table 5.5 Radiation characteristics of the DRA at the optimum bandwidth position ($f = 3.115$ GHz) feed line length = 2 cm DR-1 orientation : b-a-d truncated ground plane: 2×4 sq cm (d_x, d_y) = (0.6, 1.2) cm

	Large ground plane	Truncated ground plane
Optimum bandwidth position (dx,dy) cm	(0.5,1.5)	(0.6,1.2)
Operating frequency band (GHz)	2.956 – 3.281	3.01 – 3.32
% bandwidth	10.2	9.95
Mode of operation	TE ^z ₁₁₈	TE ^z ₁₁₈
Polarisation	Linear	Linear
3 dB beamwidth		
E plane	108°	96°
H plane	90°	94°
Cross Polarisation (dB)		
E plane	-21	-17
H plane	-35	-14
Front to back ratio (dB)		
E plane	15	8
H plane	17	8
Maximum gain in the operating band (dBi)	7.9	3.6
Size of the antenna with feeding structure	4 x 4 sq cm	2 x 4 sq cm

Table 5.6 Radiation performance of the DRA for different ground plane dimensions measured at the optimum bandwidth position
DR-1 feed line length = 2 cm orientation : b-a-d

5.1.1.8 Resonant behaviour at different positions of the DR with respect to the feed

The radiation characteristics of the DRA at the optimum bandwidth position of the DR on the feed line were discussed in depth in the preceding sections. This section discusses the resonant behaviour of the antenna when the DR is placed at discrete intervals of 0.25 cm along the x and y directions on a 2 cm feed [$0 \leq d_x \leq 0.75$, $0 \leq d_y \leq 1.5$]. The experiment is repeated for all orientations of the DR. Figures 5.9 (1-2) illustrate the return loss characteristics for the b-a-d orientation on a large ground plane.

Multi-mode behaviour is observed as the DR is moved with respect to the feed line. The impedance matching of the dominant mode improves as the DR is moved from the feed end to the source end (increasing d_y). However, the resonant behaviour changes drastically from $d_y=1.25$ cm onwards, where higher frequency resonant modes gain dominance. The DRA exhibits similar behaviour at all the lateral positions of the DR. When the DR is positioned at $(d_x, d_y)=(0.5, 1.5)$, merging of two modes at 3.04 GHz and 3.175 GHz leads to wide band characteristics (10.2% bandwidth) as shown in Figure 5.9.2(a). This is the optimum bandwidth position as explained in section 5.1.1.1 [Figure 5.2]. The numerically evaluated results are presented in Figure 5.9 beside the experimental results. It is found that for all the feed point locations, the experimental and FDTD results are in close agreement. The slight discrepancies may be due to the reasons outlined in Section 5.1.1.1.

An overall frequency variation of the dominant mode from 3.01 GHz to 3.235 GHz and bandwidth variation from 1.6 % to 10.2 % is observed experimentally as the DR is displaced with respect to the feed line as indicated in Figure 5.10. The corresponding variation of resonant frequency and % bandwidth computed numerically is also presented in Figure 5.10. An overall frequency variation of the dominant mode from 2.96 GHz to 3.202 GHz and bandwidth variation from 1.7 % to 6.1 % is observed. This shows that the FDTD method with First order Mur's

Absorbing boundary condition can predict the radiation characteristics of the Rectangular DRA with reasonable accuracy.

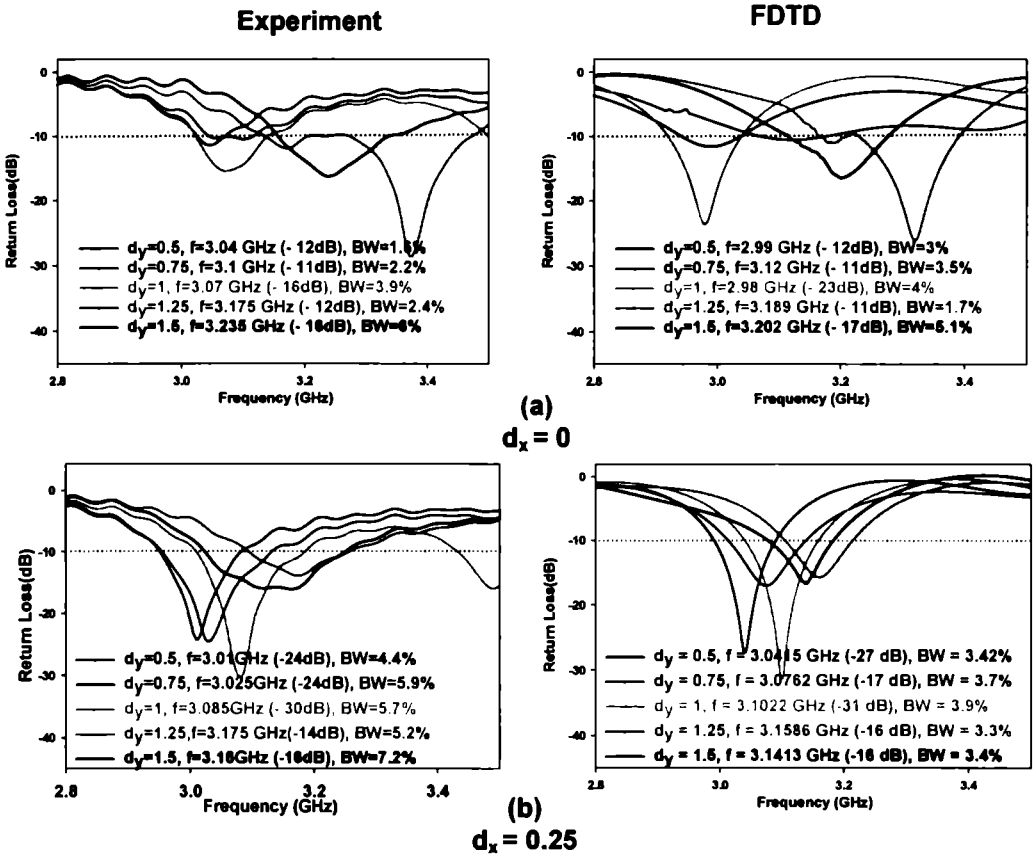


Figure 5.9.1 Return loss characteristics of the DRA at different d_y locations of the DR
 (a) $d_x = 0$ (b) $d_x = 0.25$ cm
 feed line length = 2 cm large ground plane: 4 x 4 sq cm
 DR-1 orientation: b-a-d

The resonant behaviour of the rectangular DRA at different positions in the b-a-orientation is summed up in Table 5.7.

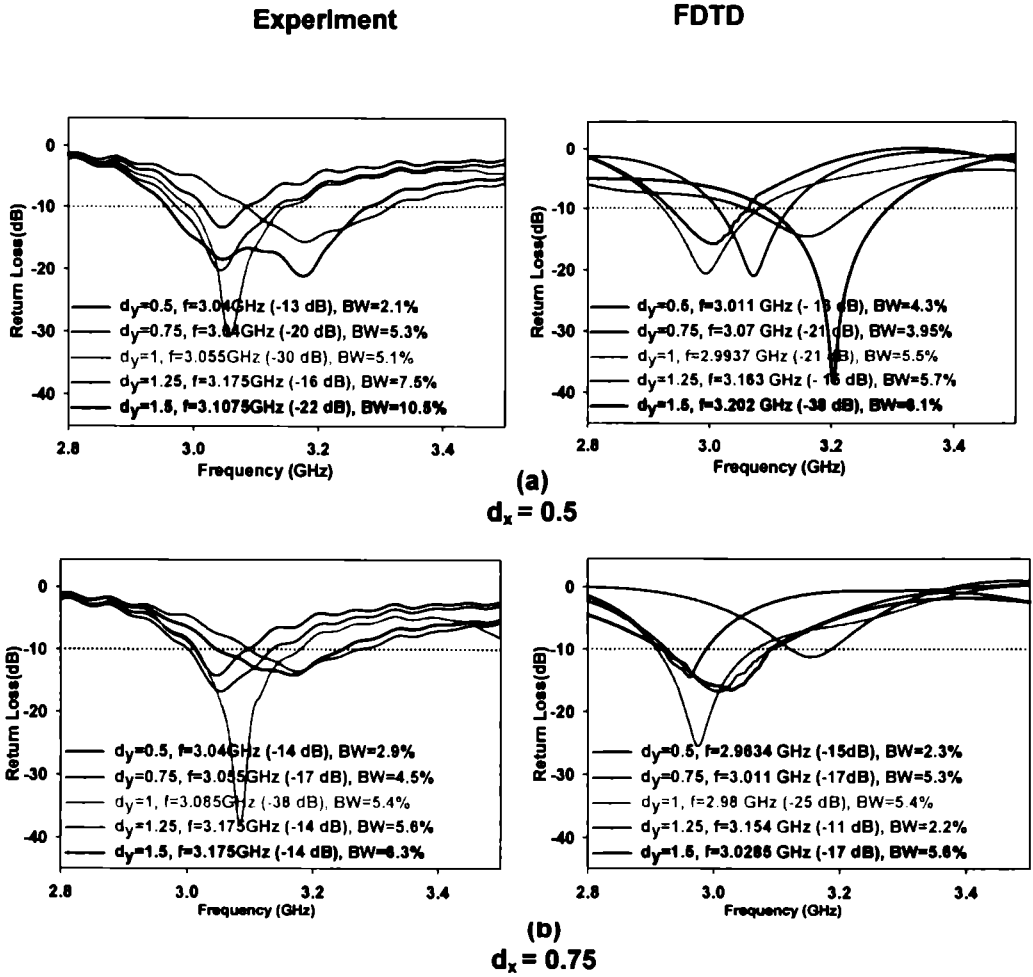
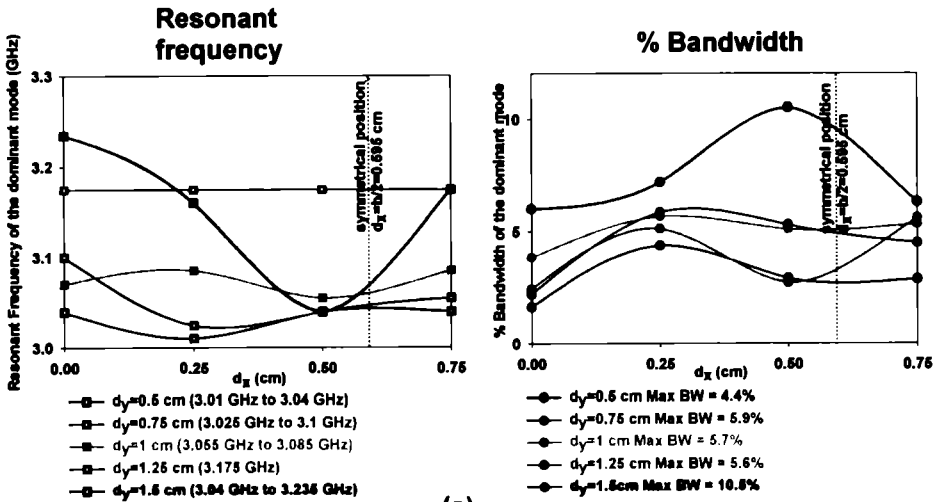
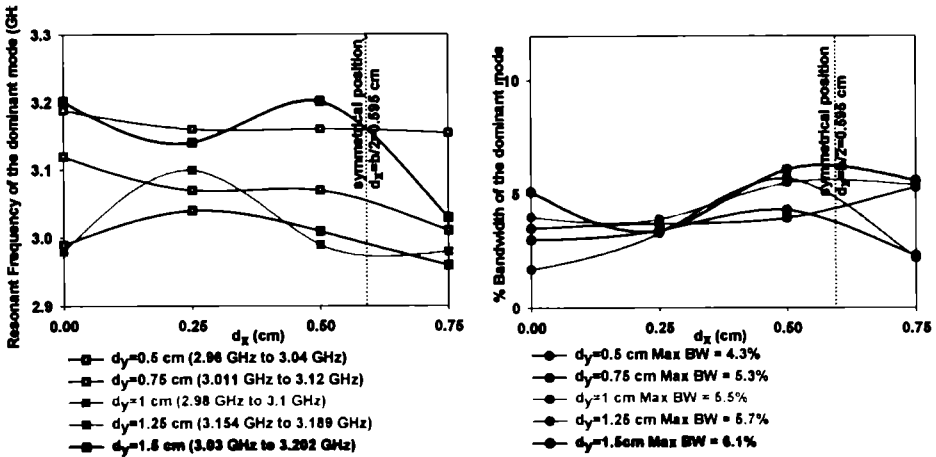


Figure 5.9.2 Return loss characteristics of the DRA at different d_y locations of the DR
 (a) $d_x = 0.5$ cm (b) $d_x = 0.75$ cm
 feed line length = 2 cm large ground plane: 4 x 4 sq cm
 DR-1 orientation: b-a-d



(a)

Experiment



(b)

FDTD

Figure 5.10 Variation in the resonant behaviour of the DRA with the position of the DR on the feed
 (a) Experiment (b) FDTD
 feed line length : 2 cm large ground plane: 4 x 4 sq cm
 DR-1 orientation: b-a-d

Resonant frequency (GHz)				
d_y (cm)	d_x (cm)			
	0	0.25	0.5	0.75
0.5	3.04	3.01	3.04	3.04
0.75	3.1	3.025	3.04	3.055
1	3.07	3.085	3.055	3.085
1.25	3.175	3.175	3.175	3.175
1.5	3.235	3.16	3.04	3.175

% Bandwidth				
d_y (cm)	d_x (cm)			
	0	0.25	0.5	0.75
0.5	3	3.42	4.3	2.3
0.75	3.5	3.7	3.95	5.3
1	4	3.9	5.5	5.4
1.25	1.7	3.3	5.7	2.2
1.5	5.1	3.4	6.1	5.6

(a)
Experiment

Resonant frequency (GHz)				
d_y (cm)	d_x (cm)			
	0	0.25	0.5	0.75
0.5	2.99	3.04	3.01	2.96
0.75	3.12	3.07	3.07	3.011
1	2.98	3.1	2.99	2.98
1.25	3.189	3.16	3.16	3.154
1.5	3.202	3.14	3.202	3.03

% Bandwidth				
d_y (cm)	d_x (cm)			
	0	0.25	0.5	0.75
0.5	1.6	4.4	2.1	2.9
0.75	2.2	5.9	5.3	4.5
1	3.9	5.7	5.1	5.4
1.25	2.4	5.2	2.7	5.6
1.5	6	7.2	10.2	6.3

(b)
FDTD

Table 5.7 Resonant behaviour of the DRA at various positions of the DR on the feed line

(a) Experiment

(b) FDTD

feed line length : 2 cm

large ground plane: 4 x 4 sq cm

DR-1

orientation: b-a-d

5.1.1.9 Characteristics for varying feed lengths

The characteristics of the DRA in the b-a-d orientation excited by a 50Ω Microstrip Line feed of length 2 cm were described in the preceding sections. This section describes the characteristics for varying feed lengths. Figure 5.11 shows the theoretically predicted and experimentally measured return loss characteristics of the DRA at the optimum bandwidth position when the feed length is increased to 3 cm. The FDTD method predicts 147 MHz bandwidth (4.5%) at 3.2063 GHz in a band operating from 3.123 GHz to 3.27 GHz at the position $(d_x, d_y) = (0, 0.5)$ cm. A resonant mode at 3.265 GHz operating from 3.145 GHz to 3.37 GHz, exhibiting 225 MHz bandwidth (6.9%) is observed experimentally. The fractional difference between the experimentally measured and numerically computed resonant frequency is +1.8%.

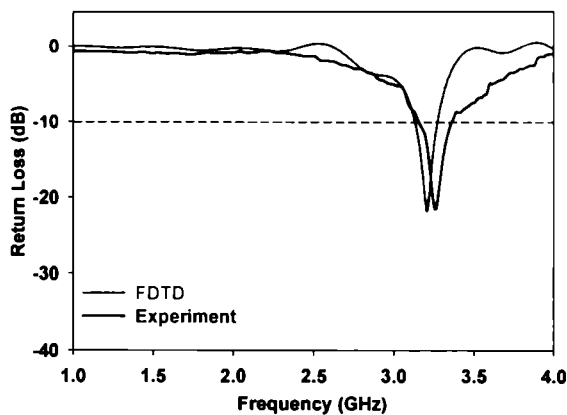


Figure 5.11 Return loss characteristics of the DRA at the optimum bandwidth position.

feed line length = 3 cm large ground plane: 5×4 sq cm
 DR-1 orientation: b-a-d $(d_x, d_y) = (0, 0.5)$ cm

The radiation patterns are broad in both the planes as shown in Figure 5.12. The front to back ratio along the maxima is 16 dB and 28 dB in the E and H planes respectively. The cross polarization along the maxima is better than -11 dB in both the planes. The experimentally measured radiation patterns agree well with the

numerically computed patterns as evident from the figure. The radiation characteristics of the DRA are summarised in Table 5.8.

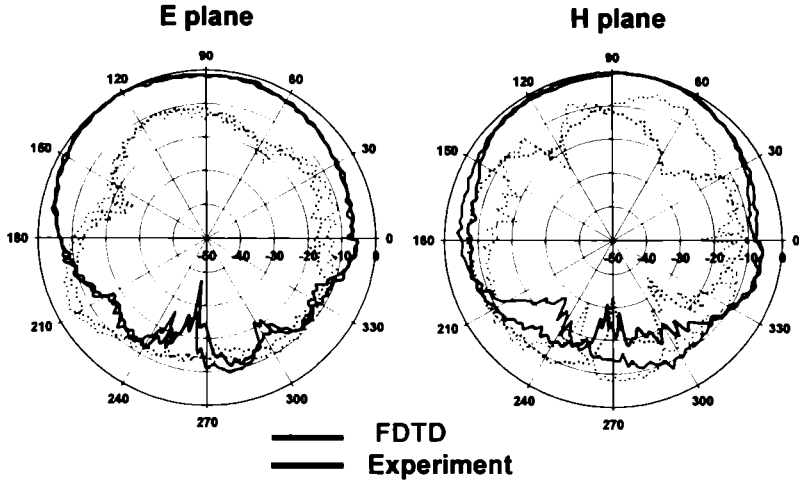


Figure 5.12 Radiation Pattern of the DRA at the optimum bandwidth position ($f = 3.265$ GHz) — co-polar cross-polar
 feed line length = 3 cm large ground plane: 5x4 sq cm
 DR-1 orientation : b-a-d (d_x, d_y) = (0,0.5) cm

	Half power beam width		On axis Front-to-Back Ratio		On axis Cross-Polarisation	
	(degree)		(dB)		(dB)	
	E plane	H plane	E plane	H plane	E plane	H plane
Theory	103	100	15	16	-14	-6
Experiment	100	98	16	28	-12	-11

Table 5.8 Radiation characteristics of the DRA at the optimum bandwidth position ($f = 3.265$ GHz)
 feed line length = 3 cm large ground plane: 5x4 sq cm
 DR-1 orientation : b-a-d (d_x, d_y) = (0,0.5) cm

In the optimum resonant band centred at 3.265 GHz, the 3 cm fed DRA in the b-a-d orientation exhibits linear polarization along the longer dimension ‘a’ of the DR, parallel to the feed axis. However the radiation coverage is better than that of the 2 cm fed DRA. The DRA exhibits an average gain of 8.7 dBi in the optimum resonant

band as shown in Figure 5.13. It is observed that this configuration offers more gain compared to the 2 cm feed, though the bandwidth displayed is less.

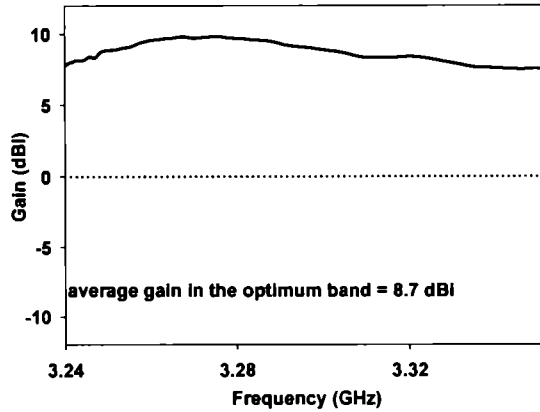


Figure 5.13 Gain of the DRA measured in the optimum band
 feed line length = 3 cm large ground plane: 5 x 4 sq cm
 DR-1 orientation : b-a-d $(d_x, d_y) = (0, 0.5)$ cm

Figure 5.14 shows the return loss and gain characteristics of the DRA measured at the optimum bandwidth position $[(d_x, d_y) = (0.6, 2.5)$ cm] when the ground plane is truncated at the end of the 3 cm feed. A low frequency resonant mode at 3.085 GHz operating from 2.996 GHz to 3.183 GHz with 187 MHz bandwidth (5.93%), offering 6.2 dBi gain is observed.

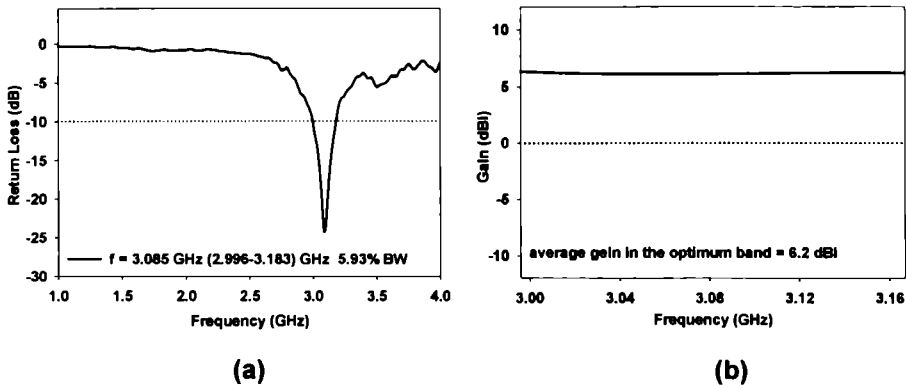


Figure 5.14 Characteristics of the DRA measured at the optimum bandwidth position
 (a) Return loss (b) Gain
 feed line length = 3 cm truncated ground plane: 3 x 4 sq cm
 DR-1 orientation : b-a-d $(d_x, d_y) = (0.6, 2.5)$ cm

The experimentally measured radiation patterns of the 3 cm line fed DRA in the truncated ground plane configuration is shown in Figure 5.15. The front to back ratio along the maxima is 16 dB and 25 dB in the E and H planes respectively. The cross polarization along the maxima is better than -19 dB in both the planes. The H plane pattern is broader than the E plane pattern. The radiation characteristics are summarised in Table 5.9.

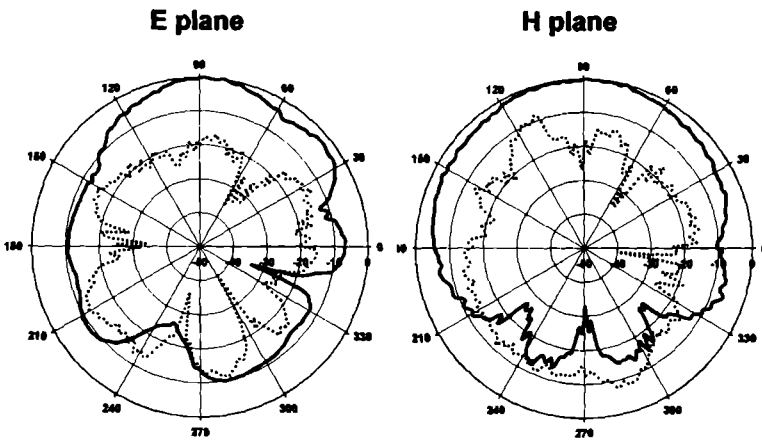


Figure 5.15 Radiation Pattern of the DRA measured at the optimum bandwidth position ($f = 3.085$ GHz)
 — co-polar cross-polar
 feed line length = 3 cm truncated ground plane: 3×4 sq cm
 DR-1 orientation : b-a-d $(d_x, d_y) = (0.6, 2.5)$ cm

When the DRA is excited by the 3 cm feed on a truncated ground plane, the half power beam width is reduced very much at the optimum bandwidth position and hence this antenna configuration is not suited for Mobile communication / W-LAN applications. However it may find applications where directional beam is a requirement.

Figure 5.16 shows the return loss characteristics of the DRA in the b-a-d orientation at the optimum bandwidth position of the resonator, when the length of the Microstrip Line feed is increased to 4 cm. The FDTD method predicts 174 MHz bandwidth (5.2%) at 3.3322 GHz in a band operating from 3.249 GHz to 3.423 GHz at the position $(d_x, d_y) = (0.5, 1)$ cm.

Half power beam width (degree)		Front-to-Back Ratio along the maxima (dB)		Cross-Polarisation along the maxima (dB)	
E plane	H Plane	E plane	H plane	E plane	H plane
44	86	16	25	-20	-19

Table 5.9 Radiation characteristics of the DRA measured at the optimum bandwidth position ($f = 3.085$ GHz)
 feed line length = 3 cm truncated ground plane: 3×4 sq cm
 DR-1 orientation : b-a-d (d_x, d_y) = (0.6, 2.5) cm

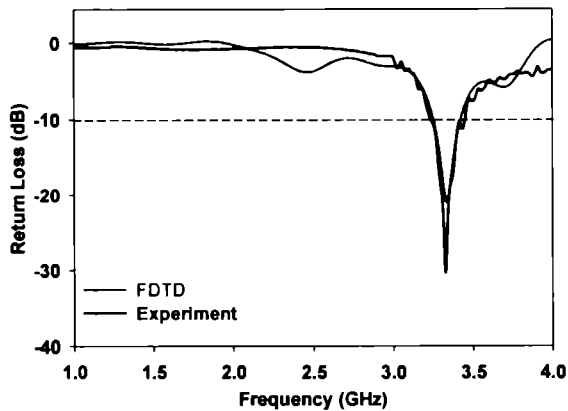


Figure 5.16 Return loss characteristics of the DRA at the optimum bandwidth position.
 feed line length = 4 cm large ground plane: 6×4 sq cm
 DR-1 orientation: b-a-d (d_x, d_y) = (0.5, 1) cm

A resonant mode at 3.325 GHz operating from 3.237 GHz to 3.45 GHz exhibiting 213 MHz bandwidth (6.4%) is observed experimentally. The fractional difference between the experimentally measured and numerically computed resonant frequency is -0.22% . Figure 5.17 shows the radiation patterns of the 4 cm line fed DRA in the b-a-d orientation of the resonator. The front to back ratio along the maxima is 8 dB and 19 dB in the E and H planes respectively. The cross polarization along the maxima is better than -16 dB in both the planes. The H plane pattern is broader than the E plane pattern. The radiation characteristics are summarised in Table 5.10.

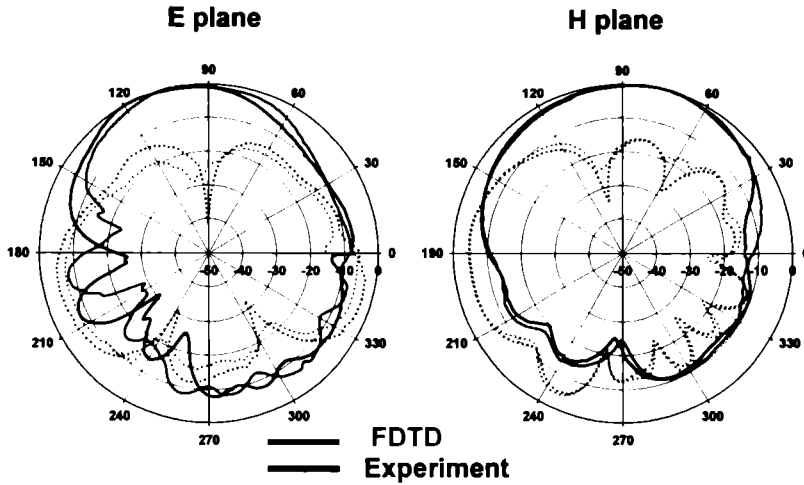


Figure 5.17 Radiation Pattern of the DRA at the optimum bandwidth position ($f = 3.325$ GHz) — co-polar cross-polar
 feed line length = 4 cm large ground plane: 6 x 4 sq cm
 DR-1 orientation : b-a-d (d_x, d_y) = (0.5, 1) cm

In the optimum resonant band centred at 3.325 GHz, the antenna exhibits linear polarization along the longer dimension ‘a’ of the DR, parallel to the feed axis. The DRA exhibits an average gain of 6.1 dBi in the optimum resonant band as shown in Figure 5.18.

	Half power beam width (degree)		On axis Front-to-Back Ratio (dB)		On axis Cross-Polarisation (dB)	
	E plane	H plane	E plane	H plane	E plane	H plane
Theory	60	92	8	17	-28	-16
Experiment	58	84	8	19	-16	-17

Table 5.10 Radiation characteristics of the DRA at the optimum bandwidth position ($f = 3.325$ GHz)
 feed line length = 4 cm large ground plane: 6x4 sq cm
 DR-1 orientation : b-a-d (d_x, d_y) = (0.5, 1) cm

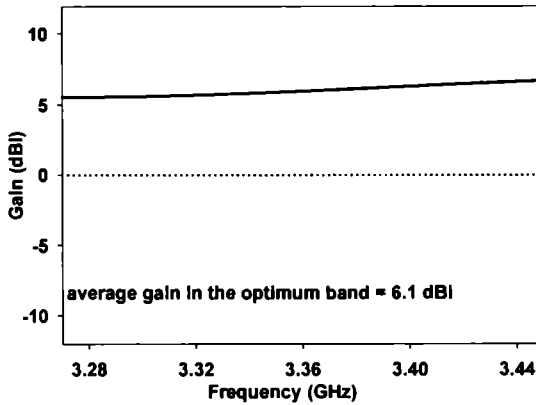


Figure 5.18 Gain of the DRA measured in the optimum band
 feed line length = 4 cm large ground plane: 6 x 4 sq cm
 DR-1 orientation : b-a-d $(d_x, d_y) = (0.5, 1)$ cm

Figure 5.19 shows the return loss and gain characteristics of the DRA at the optimum bandwidth position $[(d_x, d_y) = (0.6, 2.8)$ cm] when the ground plane is truncated at the end of the 4 cm feed. A low frequency resonant mode at 3.085 GHz operating from 2.707 GHz to 3.172 GHz exhibits 465 MHz bandwidth (15.1%), offering an average gain of 5.74 dBi in the operating band.

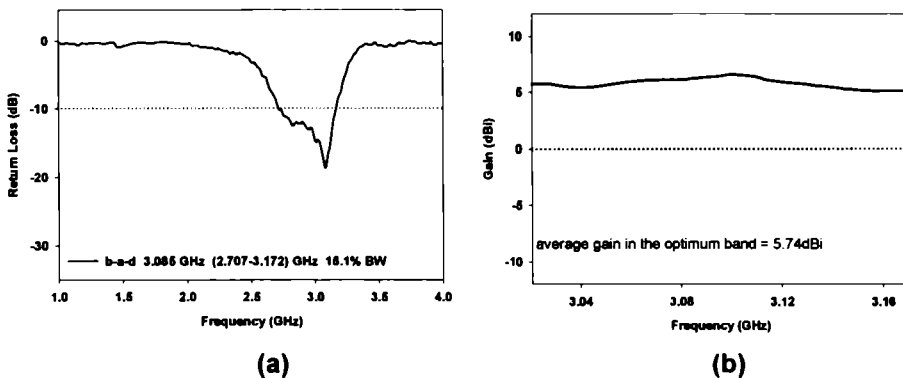


Figure 5.19 Characteristics of the DRA measured at the optimum bandwidth position
 (a) Return loss (b) Gain
 feed line length = 4 cm truncated ground plane: 4 x 4 sq cm
 DR-1 orientation : b-a-d $(d_x, d_y) = (0.6, 2.8)$ cm

The experimentally measured radiation patterns of the 4 cm line fed DRA in the truncated ground plane configuration are shown in Figure 5.20. The front to back ratio along the maxima is 7 dB and 15 dB in the E and H planes respectively. The cross polarization along the maxima is better than -13 dB in both the planes. The H plane pattern is broader than the E plane pattern. The radiation characteristics are summarised in Table 5.11. This antenna configuration also offers broadband coverage and moderate gain and can find use in Mobile Communication applications.

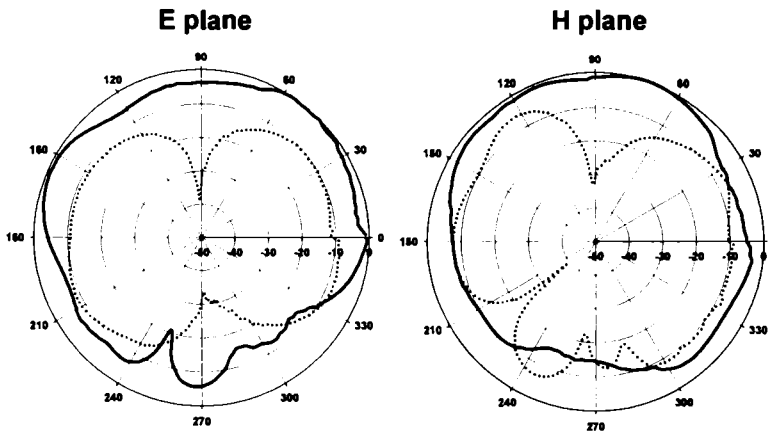


Figure 5.20 Radiation Pattern of the DRA measured at the optimum bandwidth position ($f = 3.085$ GHz)

_____ co-polar
 cross-polar
 feed line length = 4 cm truncated ground plane: 4x4 sq cm
 DR-1 orientation : b-a-d $(d_x, d_y) = (0.6, 2.8)$ cm

Half power beam width (degree)		Front-to-Back Ratio along the maxima (dB)		Cross-Polarisation along the maxima (dB)	
E plane	H plane	E plane	H plane	E plane	H plane
60	110	7	15	-13	-20

Table 5.11 Radiation characteristics of the DRA measured at the optimum bandwidth position ($f = 3.085$ GHz)

feed line length = 4 cm truncated ground plane: 4x4 sq cm
 DR-1 orientation: b-a-d $(d_x, d_y) = (0.6, 2.8)$ cm

The investigations described above suggest that the length of the feed line as well as the dimensions of the ground plane are important parameters determining the resonant behaviour of the DRA. Figure 5.21 illustrates the return loss characteristics at the optimum bandwidth position of the DRA in the b-a-d orientation, when excited by feed lines of lengths ranging from 2 cm to 9 cm on large and truncated ground plane configurations. The variation in resonant frequency and bandwidth of the dominant mode for varying feed lengths and ground plane dimensions is illustrated in Figure 5.22. As the feed length is increased from 2 cm to 9 cm, the resonant frequency at the optimum bandwidth position of the resonator upon a large ground plane exhibits a variation from 2.95 GHz to 3.34 GHz. The 2:1 VSWR bandwidth varies from 5.02% to 13.4%. In the truncated ground plane configuration, the frequency varies from 2.875 GHz to 3.2275 GHz, and the bandwidth varies from 4.6% to 15.1%.

The experimental results described above suggest that in comparison with the larger ground plane, the truncated ground plane excites lower resonant frequencies with relatively good bandwidth performance. The overall size of the antenna configuration is also reduced. However, a decision on a configuration suitable for a particular application can be made only after the gain and radiation patterns are compared.

The experimentally measured gain in the optimum band of the DRA in the b-a-d orientation, when excited by feed lines and ground planes of varying dimensions are shown in Figure 5.23 (1-2). The variation in the average gain is summarised in Figure 5.24. The superior gain performance of the large ground plane configuration is evident from the figure. The truncated ground plane configuration exhibits moderate gain. The overall compactness of truncated ground plane may be exploited where the reduction in gain is compensated by integrating suitable amplifier circuits. Table 5.12 summarises the variation in radiation characteristics of the DRA with feed length and ground plane dimensions.

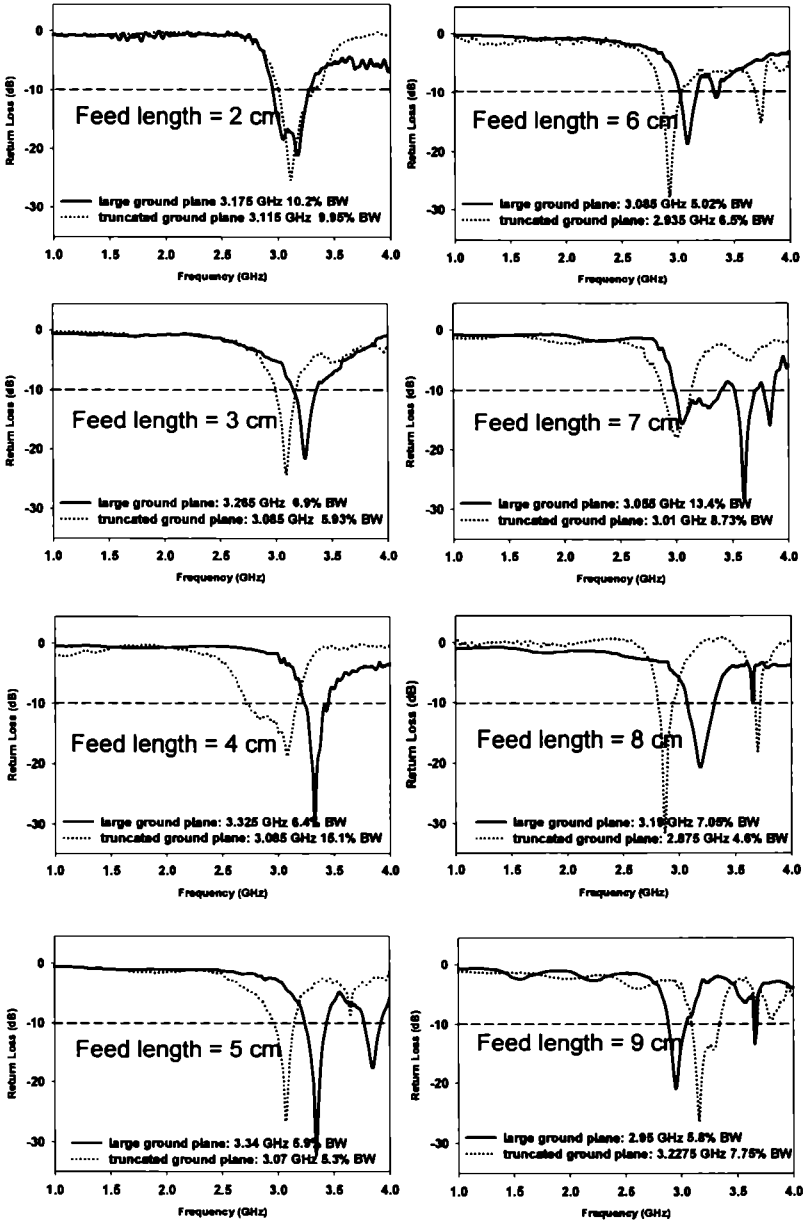
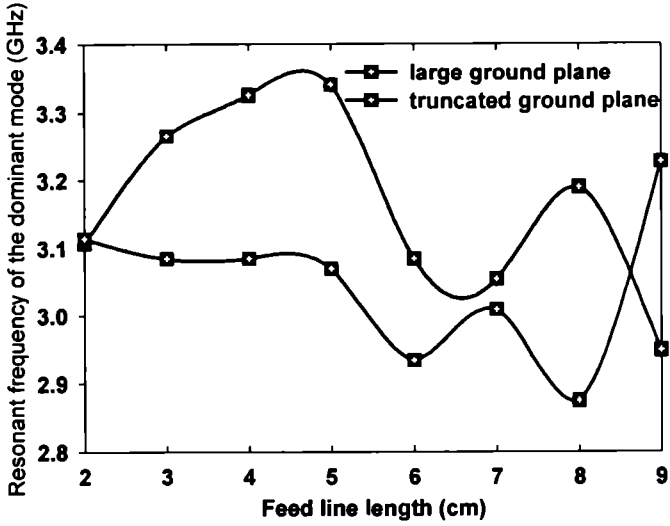
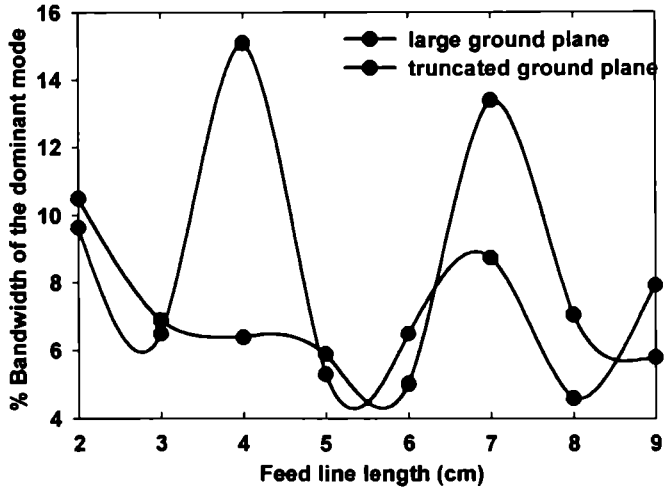


Figure 5.21 Return loss characteristics of the DRA for varying feed lengths and ground plane dimensions measured at the optimum bandwidth position DR-1 orientation : b-a-d



(a)



(b)

Figure 5.22 Variation in resonant behaviour of the DRA with feed length and ground plane dimensions measured at the optimum bandwidth position
 (a) Resonant frequency
 (b) % Bandwidth
 DR-1 orientation : b-a-d

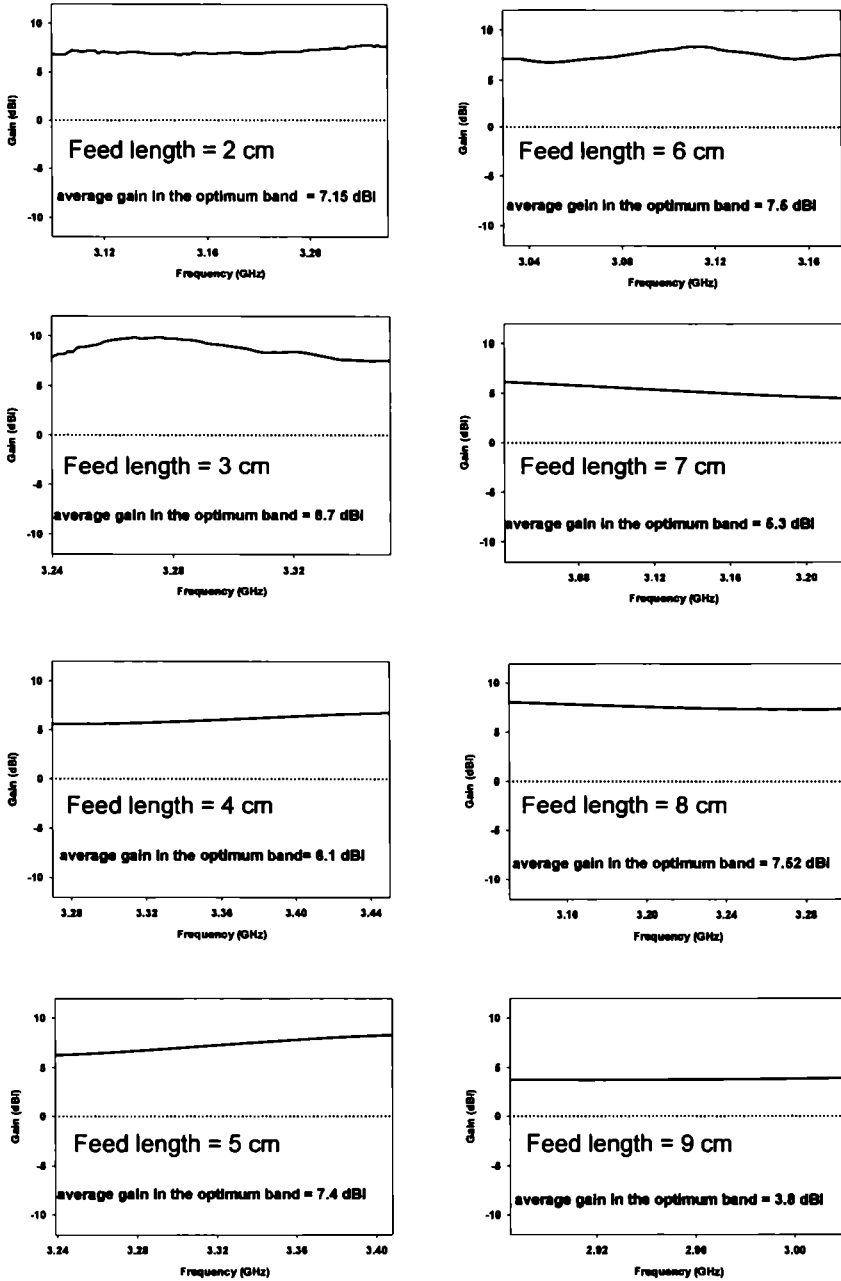


Figure 5.23.1 Gain of the DRA measured in the optimum band for varying feed lengths on a large ground plane DR-1 orientation : b-a-d

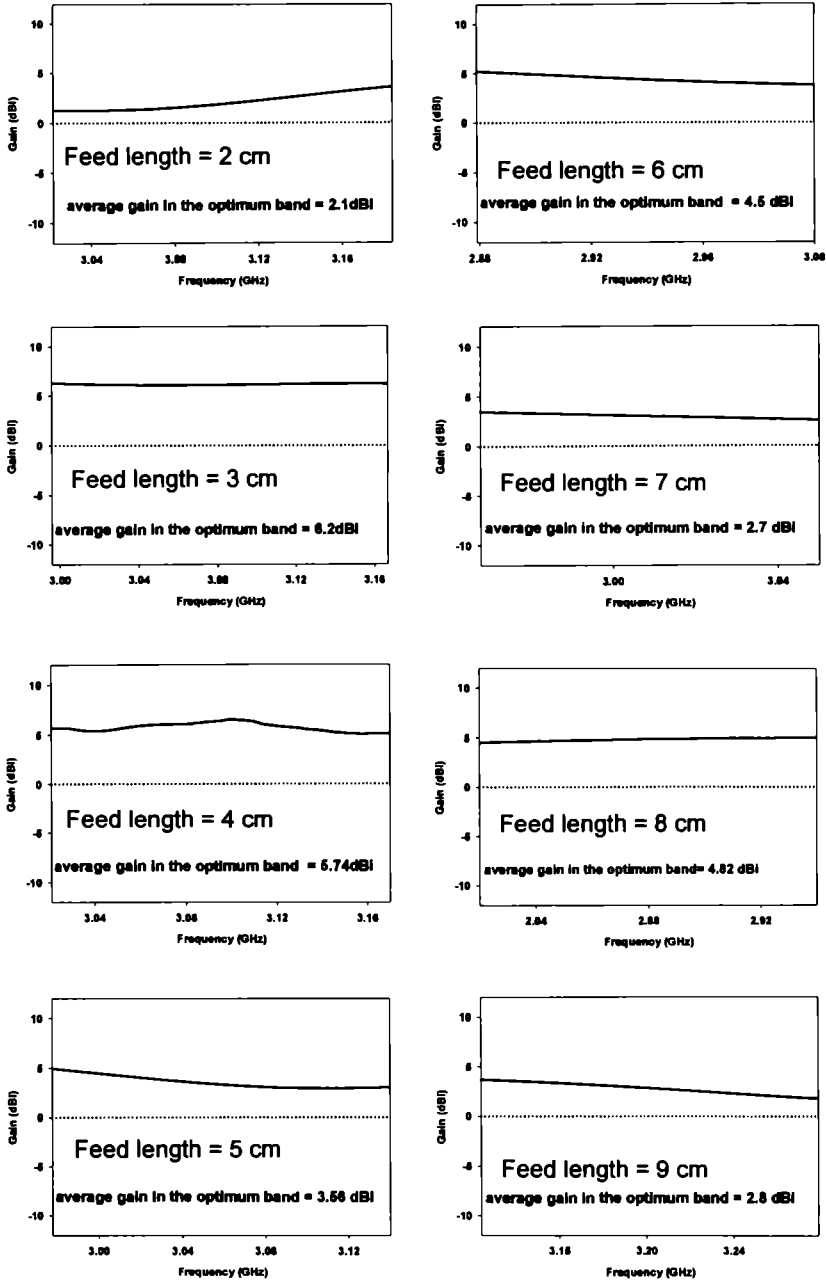


Figure 5.23.2 Gain of the DRA measured in the optimum band for varying feed lengths on a truncated ground plane DR-1 orientation : b-a-d

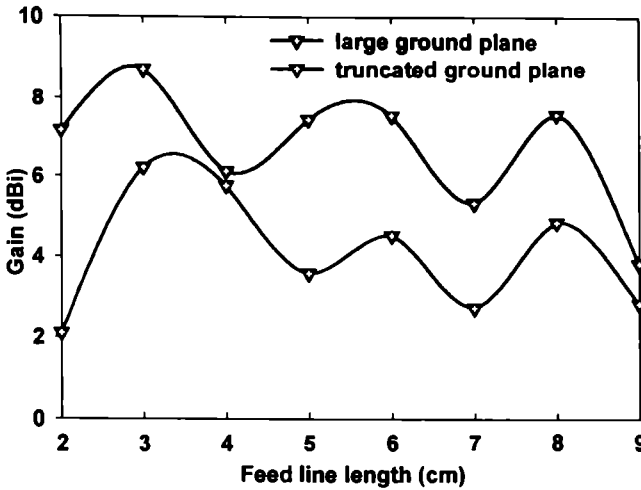


Figure 5.24 Variation in gain of the DRA with feed length and ground plane dimensions measured in the optimum band
DR-1 orientation : b-a-d

Feed Line length (cm)	Large Ground plane			Truncated Ground plane		
	Resonant Freq (GHz)	%BW	Avg gain (dBi)	Resonant Freq (GHz)	%BW	Avg gain (dBi)
2	3.175	10.2	7.15	3.115	9.95	2.1
3	3.265	6.9	8.7	3.085	5.93	6.2
4	3.325	6.4	6.1	3.085	15.1	5.74
5	3.34	5.9	7.4	3.07	5.3	3.56
6	3.085	5.02	7.5	2.935	6.5	4.5
7	3.055	13.4	5.3	3.01	8.73	2.7
8	3.19	7.05	7.52	2.875	4.6	4.82
9	2.95	5.8	3.8	3.2275	7.75	2.8

Table 5.12 Variation in radiation characteristics of the DRA with feed length and ground plane dimensions measured at the optimum bandwidth position
DR-1 orientation : b-a-d

The principal plane radiation patterns are measured in the b-a-d orientation of the resonator for feed lengths varying from 2 cm to 9 cm. The gain performance of the DRA excited by varying feed lengths described in the previous section indicate that in the b-a-d orientation good gain is exhibited by all the feed lines except the 9 cm feed in the large ground plane configuration. The characteristics obtained from the radiation pattern measurements are summed up in Table 5.13. The patterns of the DRA excited by the 2 cm, 3 cm and 4 cm feeds were described in the previous sections. Figure 5.25 shows the principal plane patterns of the DRA excited by the 5 cm, 6 cm and 8 cm feeds.

Feed Length (cm)	Avg Gain (dBi)	Half power beam width (degree)		Front-to-Back Ratio along the maxima (dB)		Cross-Polarisation along the maxima (dB)	
		E plane	H plane	E plane	H plane	E plane	H plane
		2	7.15	108	90	15	17
3	8.7	100	86	16	25	-12	-19
4	6.1	58	84	8	19	-16	-17
5	7.4	64	89	8	14	-11	-11
6	7.5	102	65	11	16	-18	-24
7	5.3	64	72	15	13	-9	-25
8	7.52	144	116	8	7	-18	-11
9	3.8	34	110	6	7	-0.3	-20

Table 5.13 Radiation pattern characteristics of the DRA for varying feed lengths measured at the optimum bandwidth position
DR-1 large ground plane orientation : b-a-d

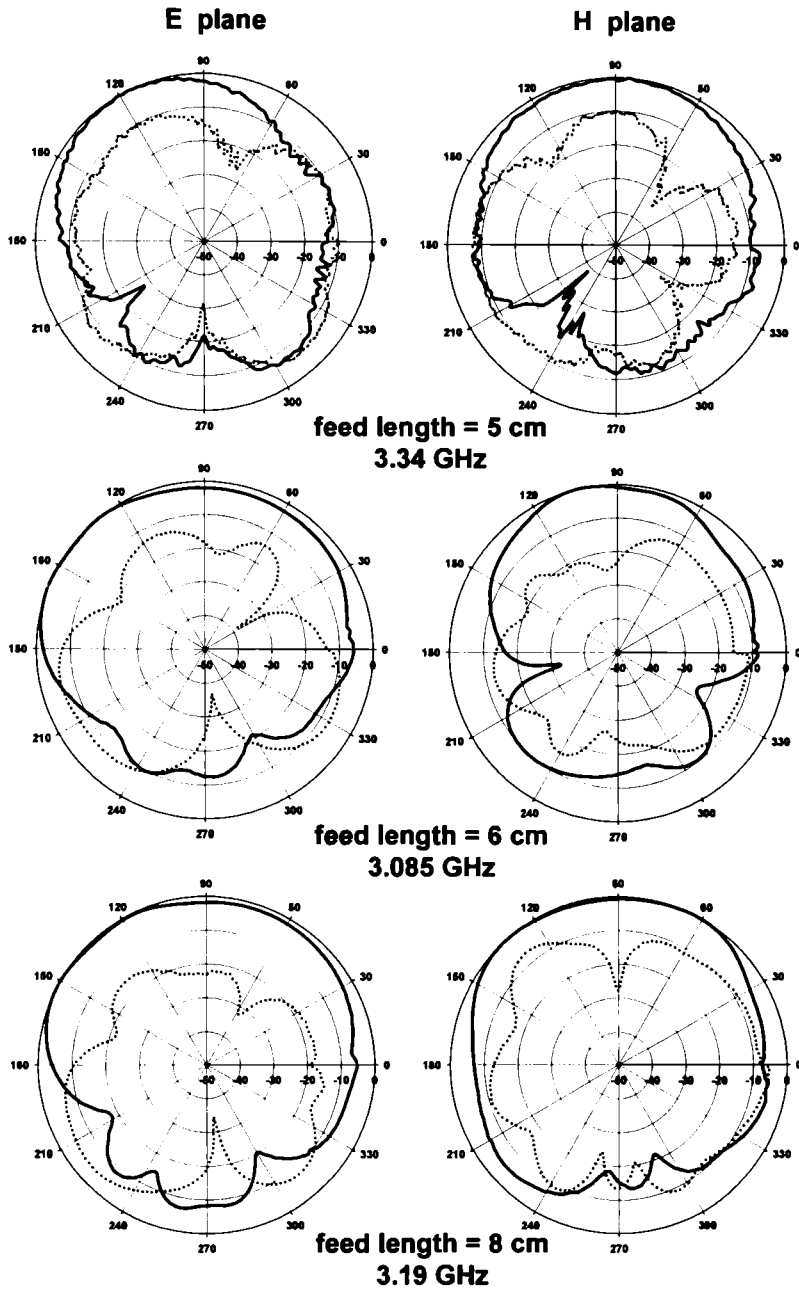


Figure 5.25 Radiation Pattern of the DRA for varying feed lengths measured at the optimum bandwidth position
 — co-polar cross-polar
 DR-1 large ground plane orientation : b-a-d

The results discussed in the previous sections are based on the observations at the optimum bandwidth position of the DR. It is seen that the optimum bandwidth positions are not always symmetric with respect to the feed axis. It also varies with feed length and orientation. Figure 5.26 clearly illustrates two positions of the DR in the b-a-d orientation at $d_x=0.5b$ (the symmetrical position) and $d_x=0$ (DR edge lying along the feed axis). $d_x < 0.5b$ indicates a displacement to the left from the symmetrical position, and $d_x > 0.5b$ indicates a displacement to the right from the symmetrical position.

Similarly $0 < d_y < a$ indicates that the feed line ends within the DR. In the remaining positions ($d_y \geq a$), the configuration behaves like a DR loaded Microstrip line. The experimental observations suggest that this situation prevails at a majority of the optimum bandwidth conditions. Table 5.14 summarises the experimentally observed optimum bandwidth positions of the DR in the b-a-d orientation, when excited by feeds of varying lengths

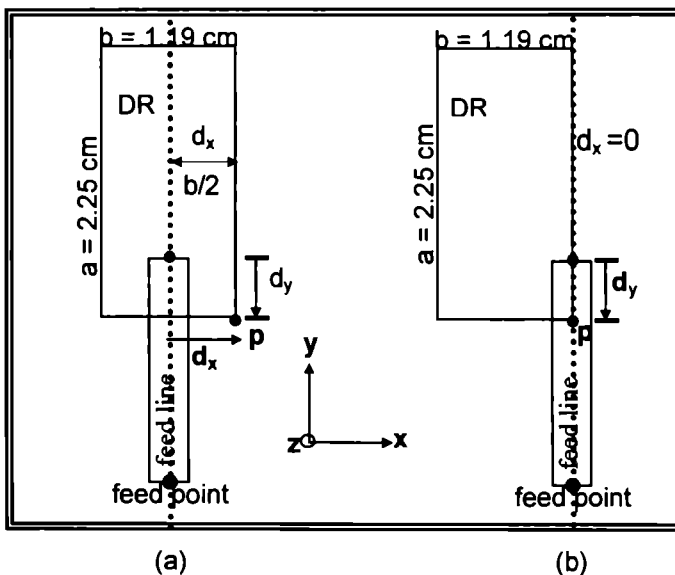


Figure 5.26 Lateral positions of the DR with respect to the feed axis (d_x, d_y) - distance of the DR vertex 'P' from the reference point along the x and y direction respectively
 DR-1 orientation: b-a-d
 (a) symmetrical (b) asymmetrical

Feed length (cm)	Ground plane ($l_g \times w_g$) sq cm	(d_x, d_y) cm
2	large (4 x 4)	0.5,1.5
	truncated (2 x 4)	0.6,1.2
3	large (5 x 4)	0,0.5
	truncated (3 x 4)	0.6,2.5
4	large (6 x 4)	0.5,1
	truncated (4 x 4)	0.6,2.8
5	large (7 x 4)	0.15,1
	truncated (5 x 4)	0.6,2.6
6	large (8 x 4)	0.6,2.5
	truncated (6 x 4)	0,4.5
7	large (9 x 4)	0,2
	truncated (7 x 4)	0.6,2.6
8	large (10 x 4)	0,2.5
	truncated (8 x 4)	0.6,3.7
9	large (11 x 4)	0.5,3
	truncated (9 x 4)	0.6,2.5

Table 5.14 The optimum bandwidth positions of the DR
DR-1 orientation: b-a-d

5.1.1.10 Resonant behaviour of the DRA when the DR is placed symmetrically with respect to the feed axis

The dependence of the characteristics of the DRA on the dimensions of the feed line and ground plane at the optimum bandwidth position of the DR has been discussed in the preceding sections. The performance at varying positions of the DR with respect to the feed axis was also analysed. This section discusses the resonant behaviour of the DRA experimentally measured for varying feed lengths when the DR in the b-a-d orientation is placed at a symmetrical position with respect to the feed axis ($d_x = b/2$) at $d_y = 0.5$ cm. The influence of the feed line length at positions other than the optimum bandwidth position is therefore investigated. Figure 5.27 illustrates the variation in resonant frequency and % bandwidth of the DRA with feed length on a large ground plane.

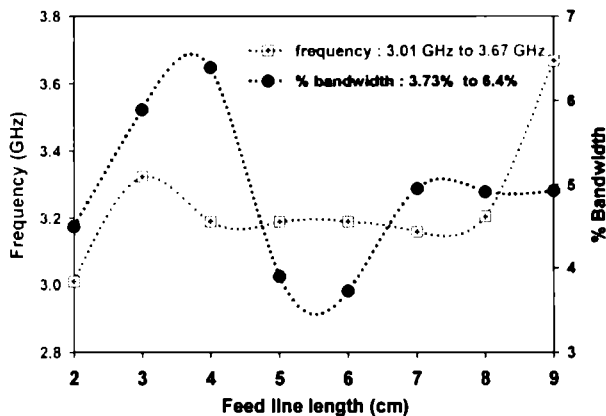


Figure 5.27 Variation in resonant frequency and % bandwidth of the DRA with feed length measured at a symmetrical position of the DR (d_x, d_y) = (b/2, 0.5) cm large ground plane orientation : b-a-d DR-1

The varying feed lengths excite frequencies ranging from 3.01 GHz to 3.67 GHz, with an average bandwidth of 4.9%. Low frequency resonant bands (3.01-3.205 GHz) are excited by all the feeds except the 9 cm feed, which excites 3.67 GHz. The

2 cm feed excites the lowest frequency, with a bandwidth of 4.5%. Maximum bandwidth of 6.4% is exhibited by the 4 cm fed DRA at 3.19 GHz and the minimum bandwidth of 3.73% at 3.19 GHz by the 6 cm fed DRA. The resonant characteristics are summarised in Table 5.15.

	Feed Length (cm)							
	2	3	4	5	6	7	8	9
Freq (GHz)	3.01	3.325	3.19	3.19	3.19	3.16	3.205	3.67
%BW	4.5	5.9	6.4	3.9	3.73	4.96	4.92	4.93

Table 5.15 Resonant behaviour of the DRA for varying feed lengths measured at a symmetrical position of the DR $(d_x, d_y) = (b/2, 0.5)$ cm large ground plane orientation : b-a-d
DR-1

The return loss characteristics measured at the symmetrical position of the DR for varying feed lengths are shown in Figure 5.28. It is observed that the feed length has a profound effect on the input impedance, thereby influencing the reflection characteristics.

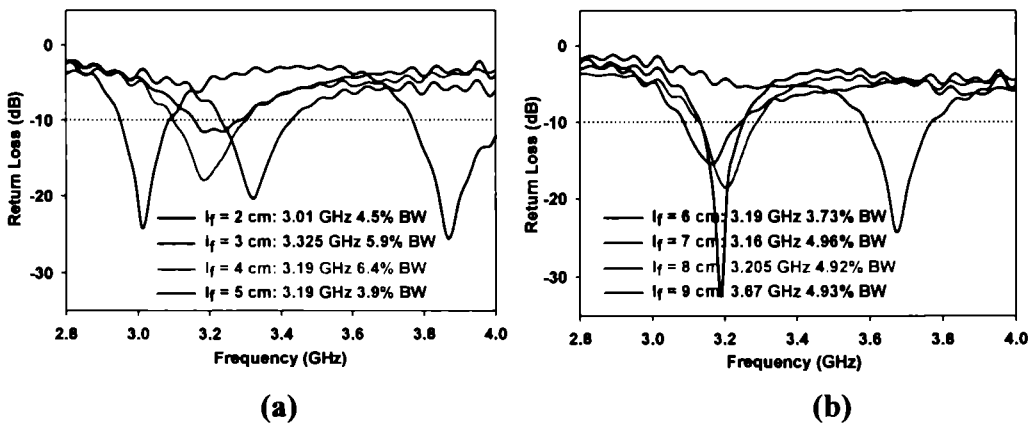


Figure 5.28 Return loss characteristics of the DRA for varying feed lengths measured at a symmetrical position of the DR
(a) feed length = 2 cm to 5 cm (b) feed length = 6 cm to 9 cm large ground plane $(d_x, d_y) = (b/2, 0.5)$ cm orientation: b-a-d
DR-1

5.1.1.11 Salient features of the b-a-d orientation

The b-a-d orientation is the most compact among the various orientations of the rectangular DR upon the feed line. At 3.175 GHz the 2 cm line fed DRA offers ~59% size reduction with respect to a rectangular Microstrip antenna resonating at the same frequency. Tables 5.12 and 5.13 sum up the characteristics of this orientation. The varying feed line lengths on a large ground plane excite frequencies in the S-band, providing an average gain of 6.7 dBi and average 2:1 VSWR bandwidth of 7.6%. The 3 cm feed offers the maximum gain (8.7 dBi). The lowest resonant frequency (2.95 GHz) is excited by the 9 cm feed and maximum bandwidth (13.4%) is provided by the 7 cm feed. The radiation patterns are generally broad - the average half-power beam width along the E plane and H plane being 85° and 89° respectively. The 8 cm line fed DRA offers the broadest radiation pattern with 144° and 116° half-power beam width respectively in the E and H planes [Figure 5.25]. The 2 cm line fed DRA is the most attractive among all the configurations; offering 10.2% bandwidth, 7.15 dBi average gain and broad radiation patterns in an operating band centred at 3.175 GHz. In addition, this compact antenna configuration exhibits good cross-polarisation characteristics.

The truncated ground plane configuration exhibits an average gain of 4.1 dBi and average bandwidth of 10.6% for varying feed lengths. The performance is therefore relatively inferior to that of the large ground plane configuration. Nevertheless, it acquires significance where the size of the antenna is of priority. The 4 cm line fed DRA in the truncated ground plane configuration is strikingly different from the rest [Figure 5.22(b)], offering 15.1% bandwidth and 5.74 dBi average gain in an operating band centred at 3.085 GHz [Figure 5.23.2].

The investigations performed on the Dielectric Resonator Antenna incorporating the rectangular resonator sample DR-1 in the b-a-d orientation confirm the dependence of the antenna characteristics upon the feed length, ground plane dimensions and position of the DR.

5.1.2 The a-b-d orientation

The a-b-d orientation is also a low profile configuration [aspect ratio=0.47]. A schematic representation and 3D view of this orientation is shown in Figure 5.29. The distance of the reference vertex 'P' from the feed axis and the feed end indicate the position of the DR along the x and y axes (d_x, d_y) respectively. The radiation characteristics of the 2 cm line excited DRA in the a-b-d orientation of the resonator for varying feed line lengths and ground plane dimensions are discussed in this section.

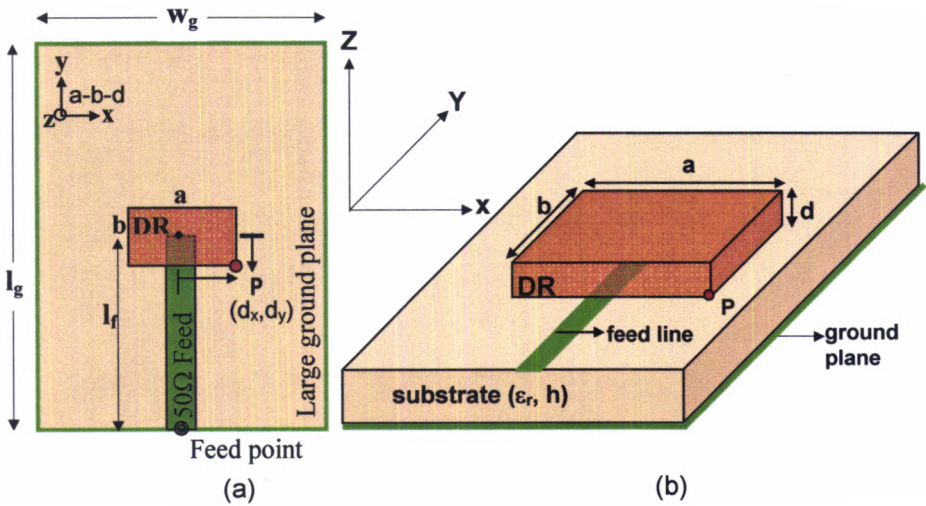


Figure 5.29 The a-b-d orientation of the DR
 substrate: $\epsilon_r = 4.28$, $h = 0.16$ cm
 DR-1 $a \times b \times d = [2.25 \times 1.19 \times 0.555]$ cm³
 (a) schematic lay out (b) 3D view

5.1.2.1 Return Loss Characteristics

The return loss characteristics of the DRA are computed numerically employing the FDTD method and the position of the DR with respect to the feed line (d_x, d_y) is optimised for maximum 2:1 VSWR bandwidth. The numerical results are validated experimentally as shown in Figure 5.30. Theoretically the antenna is found to resonate at 3.3669 GHz in a band operating from 3.2888 GHz to 3.445 GHz with

156.2 MHz bandwidth (4.82%) when placed at $(d_x, d_y) = (1.25, 1)$ cm. Maximum 2:1 VSWR bandwidth is experimentally observed in a band centred at 3.4675 GHz and operating from 3.2435 GHz to 3.69 GHz when two resonant modes at 3.325 GHz and 3.61 GHz combine to display a bandwidth of 446.5 MHz (12.9%). The fractional difference between the experimentally measured and numerically computed resonant frequency is +2.9%.

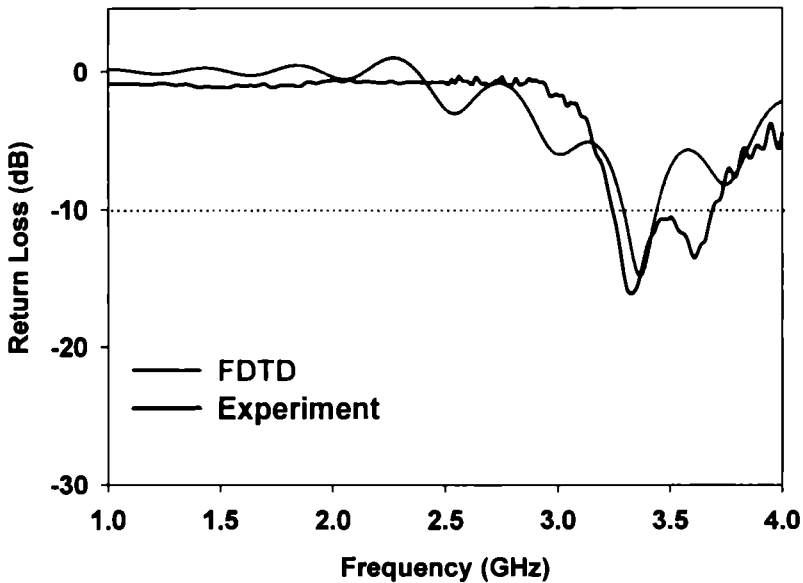


Figure 5.30 Return loss characteristics of the DRA at the optimum bandwidth position.
 feed line length = 2 cm large ground plane: 4 x 4 sq cm
 DR-1 orientation: a-b-d $(d_x, d_y) = (1.25, 1)$ cm

The accuracy of the FDTD analysis in predicting the resonant frequency of the antenna is evident from the figure. However, the bandwidth measured experimentally is considerably larger due to the merging of the two closely spaced modes. The resonant frequency at the optimum position of the a-b-d orientation is slightly greater than that of the b-a-d orientation.

5.1.2.2 Radiation Pattern

The co-polar and cross-polar radiation patterns in the a-b-d orientation of the resonator at the centre frequency of the operating band are shown in Figure 5.31. The experimental radiation patterns agree reasonably well with the theoretical curves. The patterns are broad in both the planes. Table 5.16 summarises the radiation characteristics of the DRA in the a-b-d orientation.

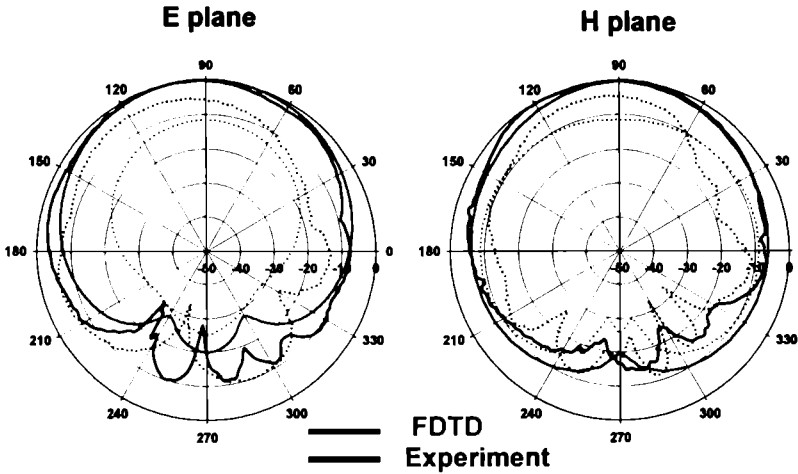


Figure 5.31 Radiation Pattern of the DRA at the optimum bandwidth position ($f = 3.4675$ GHz) co-polar cross-polar
 feed line length = 2 cm large ground plane: 4 x 4 sq cm
 DR-1 orientation: a-b-d $(d_x, d_y) = (1.25, 1)$ cm

	Half power beam width (degree)		On axis Front-to-Back Ratio (dB)		On axis Cross-Polarisation (dB)	
	E plane	H plane	E plane	H plane	E plane	H plane
Theory	100	75	20	19	-12	-11
Experiment	130	94	15	18	-5	-5

Table 5.16 Radiation characteristics of the DRA at the optimum bandwidth position ($f = 3.4675$ GHz)
 feed line length = 2 cm large ground plane: 4 x 4 sq cm
 DR-1 orientation: a-b-d $(d_x, d_y) = (1.25, 1)$ cm

The half-power beam width measured in the E plane measured is considerably large and hence well suited for Mobile Communication applications. However, the cross-polarization is only -5 dB. A pattern of this kind is desirable in mobile handset antenna applications.

5.1.2.3 Polarization

The DRA in the a-b-d orientation exhibits linear polarization in the optimum resonant band centred at 3.4675 GHz. The polarization of both the resonant modes within the operating band is along the dimension 'b' of the DR, parallel to the feed axis. The analysis confirms this result.

5.1.2.4 Gain

The DRA exhibits 7.8 dBi gain in the optimum resonant band as shown in Figure 5.32. The gain is comparable to that exhibited by the antenna in the b-a-d orientation of the resonator as discussed in Section 5.1.1.4.

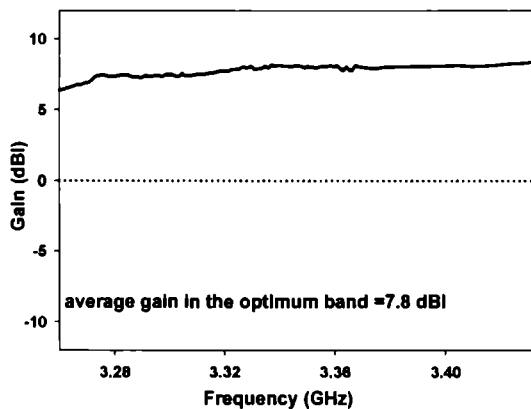


Figure 5.32 Gain of the DRA measured in the optimum band
 feed line length = 2 cm large ground plane: 4 x 4 sq cm
 DR-1 orientation : a-b-d $(d_x, d_y) = (1.25, 1)$ cm

5.1.2.5 Resonant Mode

The field distribution within the DR simulated using the commercially available software - HFSS™, at the numerically predicted frequency (3.3669 GHz) is shown in Figure 5.33 (a). The variation of the normalized Magnetic field monitored experimentally by a loop probe along the three dimensions is shown in Figure 5.33(b).

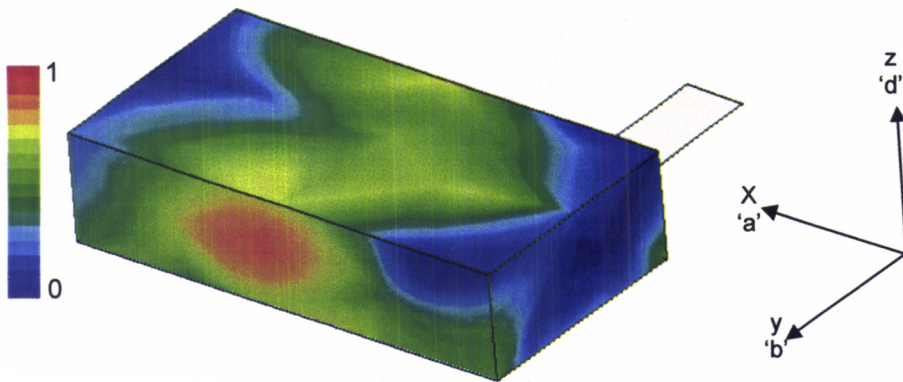


Figure 5.33 (a) Simulated H field distribution within the DR at the optimum bandwidth position
 $f = 3.3669$ GHz
 feed line length = 2 cm large ground plane: 4×4 sq cm
 DR-1 orientation : a-b-d $(d_x, d_y) = (1.25, 1)$ cm

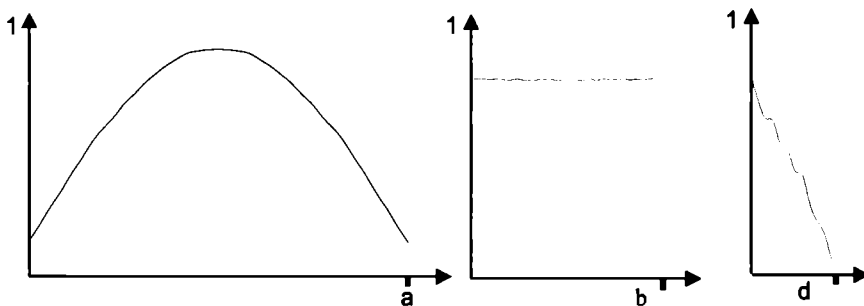


Figure 5.33 (b) Variation of the normalized Magnetic field distribution along the dimensions 'a', 'b' and 'd' of the DR monitored experimentally
 TE_{106}^z mode
 feed line length = 2 cm large ground plane: 4×4 sq cm
 DR-1 orientation : a-b-d $(d_x, d_y) = (1.25, 1)$ cm

The fields undergo one half-wave variation along the dimension 'a' and remains constant along dimension 'b'. They undergo less than a half-wave variation along dimension 'd'. The resonant mode is therefore identified as TE_{10}^z . FDTD theory also predicts similar results.

5.1.2.6 Compactness

In order to ascertain the compactness of the DRA in the a-b-d orientation at 3.4675 GHz, the antenna is compared with a circular and rectangular Microstrip antenna resonating at the same frequency. Table 5.17 provides a comparison of the dimensions of different antennas operating at 3.4675 GHz. The DRA incorporating the resonator in the a-b-d orientation is found to exhibit 50.5% and 37.2% reduction in the cross-section area with respect to a rectangular and circular Microstrip antenna designed to operate at the same frequency.

Antenna	Dimensions (cm)	Cross-sectional area (sq cm)
DRA in the a-b-d orientation	Length(a) = 2.25 Width (b) = 1.19	(b x a) 2.7
Rectangular microstrip antenna	Length = 2.05 Width = 2.66	5.45
Circular microstrip antenna	Radius = 1.17	4.3

Table 5.17 Dimensions of different antennas operating at 3.4675 GHz

5.1.2.7 Truncated ground plane configuration

In the previous section the experimental observations of the rectangular DRA on a large ground plane was presented. The effect of the truncated ground plane is presented in this section. Figure 5.34 shows the return loss characteristics and gain of the DRA at the optimum bandwidth position $[(d_x, d_y) = (1.1, 0.9) \text{ cm}]$ in the a-b-d

orientation of the resonator. Numerical computation predicts a dominant resonant mode at 3.5631 GHz and a higher order mode at 3.753 GHz in a band centred at 3.645 GHz, operating from 3.428 GHz to 3.83 GHz and displaying maximum 2:1 VSWR bandwidth of 402 MHz (11.03%). Two resonant modes are experimentally observed at 3.535 GHz and 3.895 GHz, which combine to display 519 MHz bandwidth (13.9%) from 3.415 GHz to 3.934 GHz in a band centred at 3.715 GHz. The fractional difference between the measured and predicted frequency is 1.9 %.

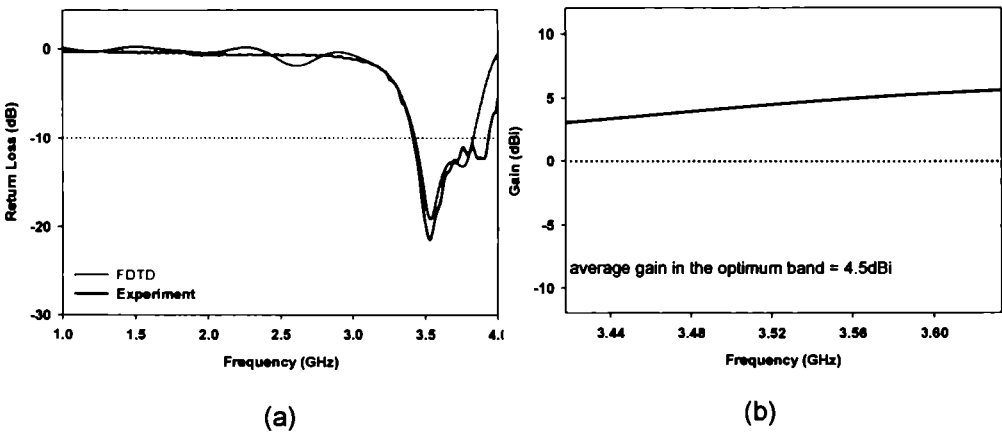


Figure 5.34 Characteristics of the DRA measured at the optimum bandwidth position
 (a) Return loss (b) Gain
 feed line length = 2 cm truncated ground plane: 2 x 4 sq cm
 DR-1 orientation : a-b-d (d_x, d_y) = (1.1, 0.9) cm

The truncation of the ground plane is found to increase the resonant frequency and also enhance the bandwidth. The DRA exhibits 4.5 dBi gain in the optimum resonant band. Therefore, in comparison with the resonant behaviour of the DRA on a large ground plane, the truncated ground plane configuration exhibits maximum bandwidth in a higher frequency band, with slightly reduced gain, thus leading to deterioration of the antenna characteristics in the a-b-d orientation.

The radiation patterns in the principal planes are shown in Figure 5.35. The patterns indicate broad radiation coverage along the E plane and H plane. Table 5.18 summarises the radiation characteristics of the DRA in the truncated ground plane configuration.

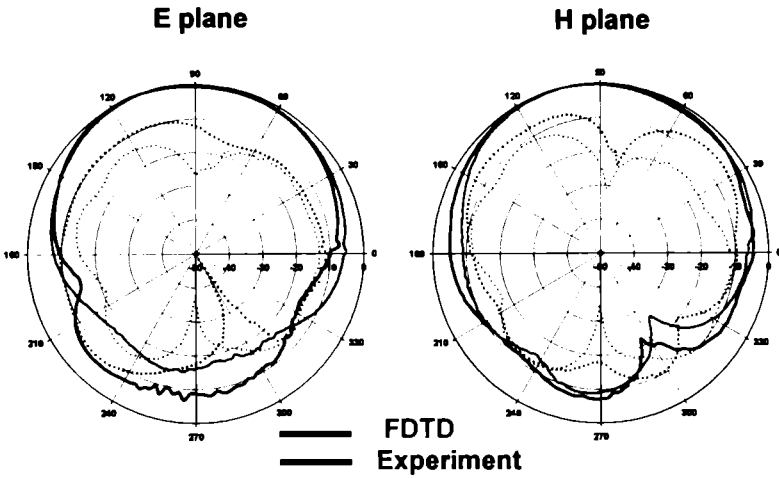


Figure 5.35 Radiation Pattern of the DRA at the optimum bandwidth position ($f = 3.715$ GHz)
 _____ co-polar cross-polar
 feed line length = 2 cm truncated ground plane: 2x4 sq cm
 DR-1 orientation: a-b-d (d_x, d_y) = (1.1, 0.9) cm

	Half power beam width (degree)		On axis Front-to-Back Ratio (dB)		On axis Cross-Polarisation (dB)	
	E plane	H plane	E plane	H plane	E plane	H plane
Theory	116	110	12	13	-16	-15
Experiment	120	106	7	10	-15	-10

Table 5.18 Radiation characteristics of the DRA at the optimum bandwidth position ($f = 3.715$ GHz)
 feed line length = 2 cm truncated ground plane: 2x4 sq cm
 DR-1 orientation : a-b-d (d_x, d_y) = (1.1, 0.9) cm

Table 5.19 compares the radiation performance of the 2 cm fed DRA in the a-b-d orientation of the resonator for different ground plane dimensions. It is observed that the overall radiation performance of the antenna is superior for the large ground plane configuration.

	Large ground plane	Truncated ground plane
Optimum bandwidth position (dx,dy) cm	(1.25,1)	(1.1,0.9)
Operating frequency band (GHz)	3.2435-3.69	3.415-3.934
% bandwidth	12.9	13.9
Mode of operation	TE_{108}^z	TE_{108}^z
Polarisation	Linear	Linear
3 dB beamwidth		
E plane	130°	120°
H plane	94°	106°
Cross Polarisation (dB)		
E plane	-5	-15
H plane	-5	-10
Front to back ratio (dB)		
E plane	15	7
H plane	18	10
Maximum gain in the operating band (dBi)	8.4	5.6
Size of the antenna with feeding structure	4 x 4 sq cm	2 x 4 sq cm

Table 5.19 Radiation performance of the DRA for different ground plane dimensions measured at the optimum bandwidth position
DR-1 feed line length = 2 cm orientation : a-b-d

5.1.2.8 Resonant behaviour at different positions of the DR with respect to the feed

The radiation characteristics of the DRA at the optimum bandwidth position of the DR on the feed line were discussed in the preceding sections. This section discusses the resonant behaviour of the antenna when the DR is placed at discrete intervals of 0.25 cm along the x and y directions on a 2 cm feed [$0.25 \leq d_x \leq 2$, $0.5 \leq d_y \leq 1$]. The experiment is repeated for all orientations of the DR. Figures 5.36 (1-3) illustrate the return loss characteristics for the a-b-d orientation on a large ground plane.

Multi-mode behaviour is observed as the DR is moved with respect to the feed line. Two resonant modes are observed along all d_y positions at $d_x = 0.25$ cm, as illustrated in Figure 5.36.1(a). When the DR is shifted laterally to $d_x = 0.75$ cm as shown in Figure 5.36.1(b), the impedance matching of the lower mode deteriorates, while that of the higher mode improves considerably. Resonant modes at an intermediate frequency (~ 3.4 GHz) display moderate bandwidth ($\sim 8\%$) when the DR is positioned laterally at $d_x = 1.25$ cm as shown in Figure 5.36.2 (a). Two modes at 3.325 GHz and 3.61 GHz combine to exhibit wide band characteristics (12.9% bandwidth in a band centred at 3.4675 GHz) as the DR is moved along the feed axis to $d_y = 1$. This is the optimum bandwidth position [$(d_x, d_y) = (1.25, 1)$] as explained in Section 5.1.2.1 [Figure 5.30]. The two modes separate and the impedance matching of the lower order mode exhibits considerable improvement at $d_x = 1.75$ cm as seen from the sharp resonance curves in Figure 5.36.2(b).

Almost similar behaviour is numerically predicted using FDTD at all the feed point locations. The numerically evaluated results are presented in Figure 5.36 beside the experimental results. An overall frequency variation of the dominant mode from 3.085 GHz to 3.46 GHz and bandwidth variation from 1% to 14.5% is observed experimentally as the DR is displaced with respect to the feed line as indicated in Figure 5.37 (a). The corresponding variation of resonant frequency and % bandwidth

computed numerically is also presented. An overall frequency variation of the dominant mode from 3.04 GHz to 3.47 GHz and bandwidth variation from 1.1% to 8.2% is observed. This shows that the FDTD method can predict the radiation characteristics of the Rectangular DRA with reasonable accuracy.

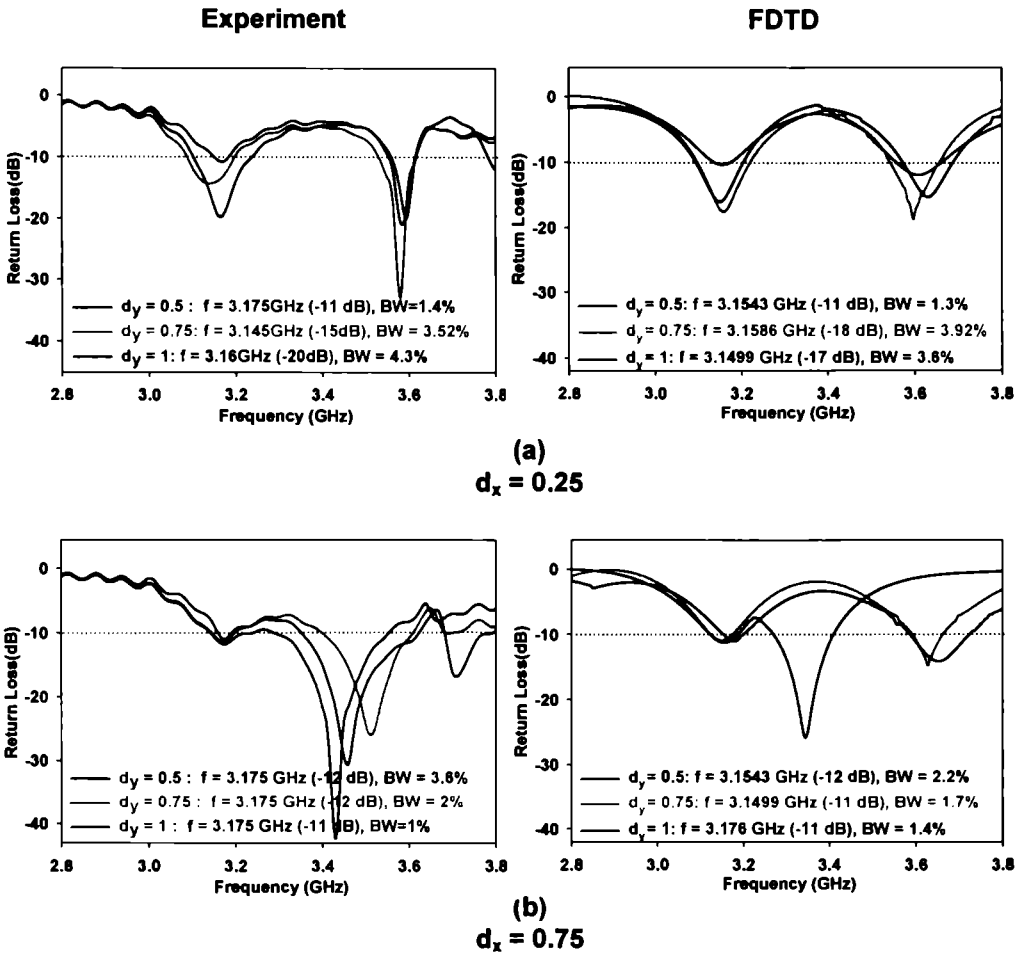


Figure 5.36.1 Return loss characteristics of the DRA at different d_y locations of the DR
 (a) $d_x = 0.25$ cm (b) $d_x = 0.75$ cm
 feed line length = 2 cm large ground plane: 4 x 4 sq cm
 DR-1 orientation : a-b-d

Wide band characteristics are displayed due to mode merging at $(d_x, d_y) = (1.25, 1)$ and $(1.5, 0.5)$ [Figure 5.37 (a)]. However, the two resonant modes excited at the position $(d_x, d_y) = (1.5, 0.5)$ are orthogonally polarized. Therefore, the wide bandwidth (14.5%) exhibited by the antenna can be exploited for dual polarization applications.

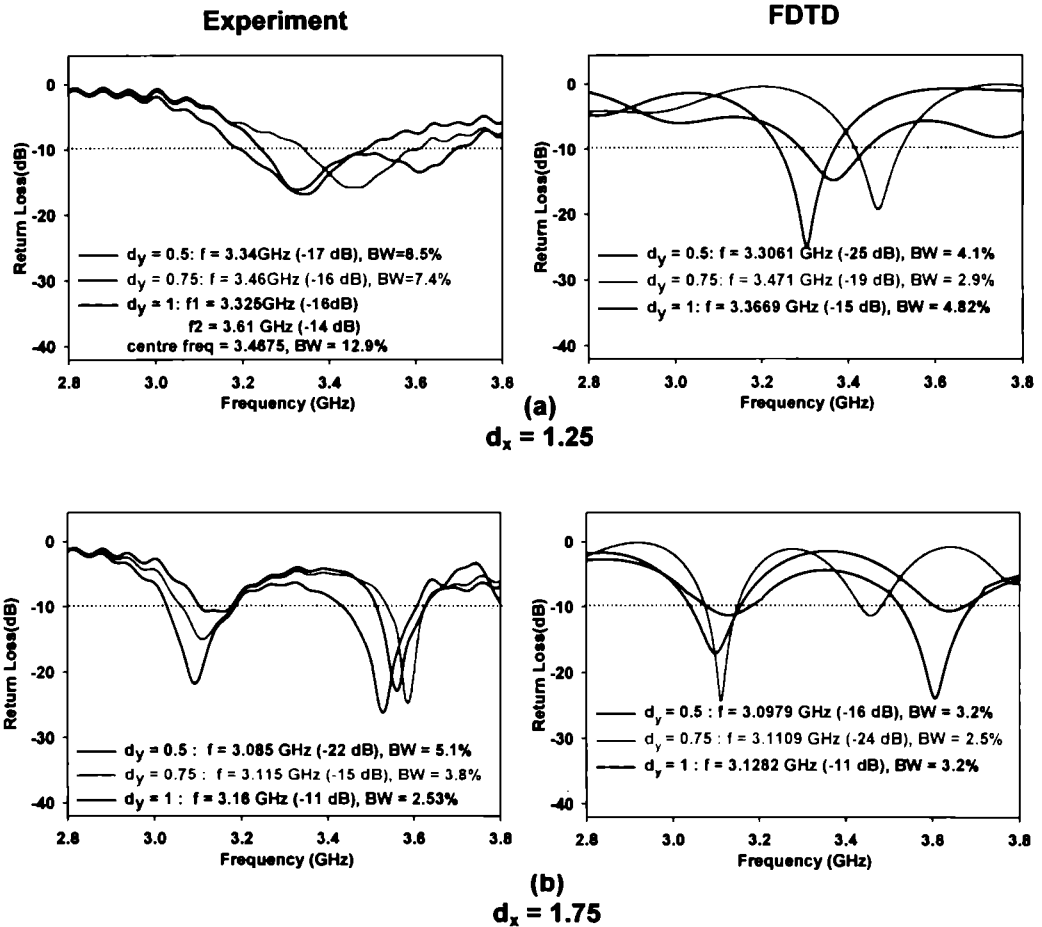


Figure 5.36.2 Return loss characteristics of the DRA at different d_y locations of the DR
 (a) $d_x = 1.25$ cm
 feed line length = 2 cm
 DR-1
 (b) $d_x = 1.75$ cm
 large ground plane: 4 x 4 sq cm
 orientation : a-b-d

The resonant behaviour of the rectangular DRA in the a-b-d orientation is summed up in Table 5.20 (1-2).

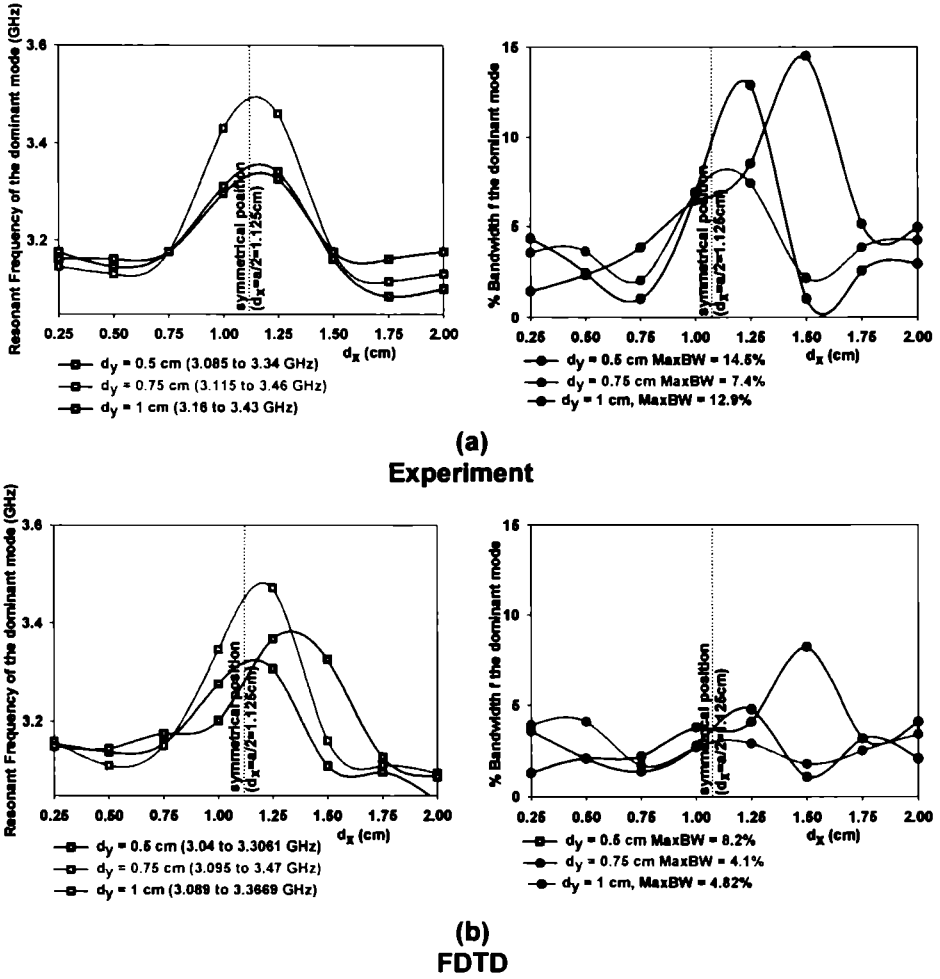


Figure 5.37 Variation in the resonant behaviour of the DRA with the position of the DR on the feed
 (a) Experiment (b) FDTD
 feed line length : 2 cm large ground plane: 4 x 4 sq cm
 DR-1 orientation: a-b-d

Resonant frequency (GHz)								
d_y (cm)	d_x (cm)							
	0.25	0.5	0.75	1	1.25	1.5	1.75	2
0.5	3.175	3.145	3.175	3.31	3.34	3.16	3.085	3.1
0.75	3.145	3.13	3.175	3.43	3.46	3.175	3.115	3.13
1	3.16	3.16	3.175	3.295	3.325	3.43	3.16	3.175

(a)

% Bandwidth								
d_y (cm)	d_x (cm)							
	0.25	0.5	0.75	1	1.25	1.5	1.75	2
0.5	1.4	2.3	3.8	6.4	8.5	14.5	5.1	4.9
0.75	3.52	3.6	2	6.9	7.4	2.14	3.8	4.2
1	4.3	2.4	1	6.8	12.9	1	2.53	2.9

(b)

Table 5.20.1 Experiment ally observed resonant behaviour of the DRA at various positions of the DR on the feed line
(a) Resonant frequency (GHz)
(b) % Bandwidth
 feed line length : 2 cm ground plane: 4 x 4 sq cm
 DR-1 orientation: a-b-d

Resonant frequency (GHz)								
d_y (cm)	d_x (cm)							
	0.25	0.5	0.75	1	1.25	1.5	1.75	2
0.5	3.1543	3.1378	3.1543	3.275	3.3061	3.11	3.0979	3.04
0.75	3.1586	3.1104	3.1499	3.345	3.2471	3.16	3.1109	3.095
1	3.1499	3.145	3.176	3.202	3.3669	3.325	3.1282	3.089

(a)

% Bandwidth								
d_y (cm)	d_x (cm)							
	0.25	0.5	0.75	1	1.25	1.5	1.75	2
0.5	1.3	2.1	2.2	3.8	4.1	8.2	3.2	4.1
0.75	3.92	4.1	1.7	2.7	2.9	1.8	2.5	3.4
1	3.6	2.1	1.4	2.78	4.82	1.1	3.2	2.1

(b)

Table 5.20.2 Numerically predicted resonant behaviour of the DRA at various positions of the DR on the feed line
 (a) Resonant frequency (GHz)
 (b) % Bandwidth
 feed line length : 2 cm ground plane: 4 x 4 sq cm
 DR-1 orientation: a-b-d

5.1.2.9 Characteristics for varying feed lengths

The characteristics of the DRA in the a-b-d orientation excited by a 50Ω Microstrip Line feed of length 2 cm were discussed in the preceding sections. This section describes the characteristics for varying feed lengths. Figure 5.38 shows the theoretically predicted and experimentally measured return loss characteristics of the DRA at the optimum bandwidth position when the resonator is excited by a feed of length 3 cm.

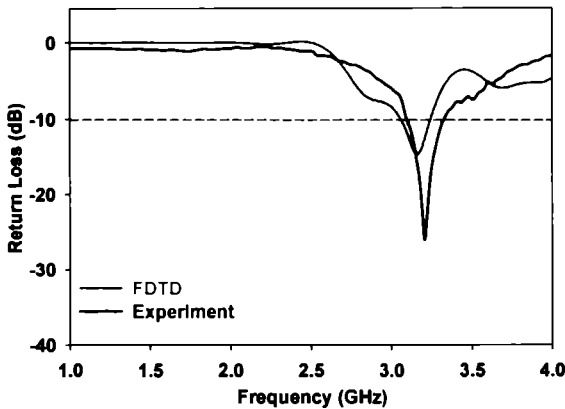


Figure 5.38 Return loss characteristics of the DRA at the optimum bandwidth position.
 feed line length = 3 cm large ground plane: 5×4 sq cm
 DR-1 orientation: a-b-d $(d_x, d_y) = (2.4, 0.8)$ cm

The FDTD method predicts 191 MHz bandwidth (6%) at 3.163 GHz in a band operating from 3.059 GHz to 3.25 GHz at the position $(d_x, d_y) = (2.4, 0.8)$. A resonant mode at 3.205 GHz operating from 3.085 GHz to 3.34 GHz exhibiting 255 MHz bandwidth (7.96%) is observed experimentally at this position. The fractional difference between the experimentally measured and numerically computed resonant frequency is +1.3%. The measured radiation patterns are broad in both the planes as shown in Figure 5.39. The front to back ratio measured along the maxima is 16 dB in both the E and H planes. The cross polarization along the maxima is better than -12 dB in both the planes. The experimentally measured radiation patterns agree well

with the numerically computed patterns as is evident from the figure. The radiation characteristics of the DRA are summarised in Table 5.21.

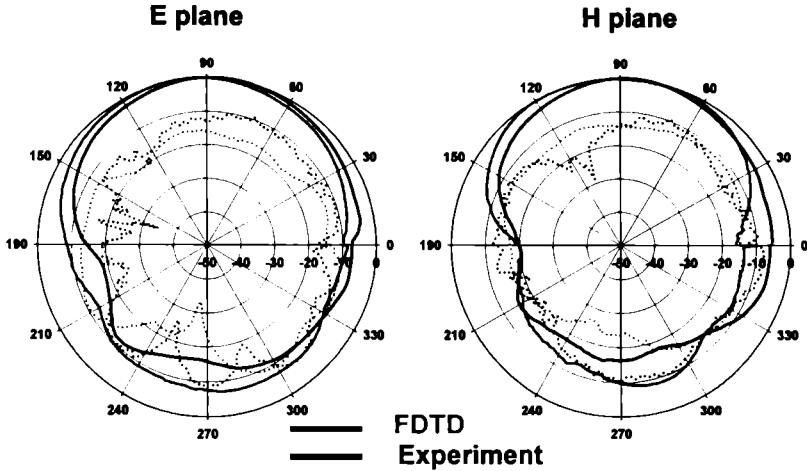


Figure 5.39 Radiation Pattern of the DRA at the optimum bandwidth position ($f= 3.205$ GHz) — co-polar cross-polar
 feed line length = 3 cm large ground plane: 5 x 4 sq cm
 DR-1 orientation : a-b-d (d_x, d_y)= (2.4, 0.8) cm

	Half power beam width		On axis Front-to-Back Ratio		On axis Cross-Polarisation	
	(degree)		(dB)		(dB)	
	E plane	H plane	E plane	H plane	E plane	H plane
Theory	98	98	7	9	-16	-14
Experiment	95	70	16	16	-12	-14

Table 5.21 Radiation characteristics of the DRA at the optimum bandwidth position ($f= 3.205$ GHz)
 feed line length = 3 cm large ground plane: 5 x 4 sq cm
 DR-1 orientation : a-b-d (d_x, d_y)= (2.4, 0.8) cm

In the optimum resonant band centred at 3.205 GHz, the 3 cm fed DRA in the a-b-d orientation exhibits linear polarization along the longer dimension ‘a’ of the DR,

perpendicular to the feed axis. The DRA offers an average gain of 7.05 dBi in the optimum resonant band as shown in Figure 5.40.

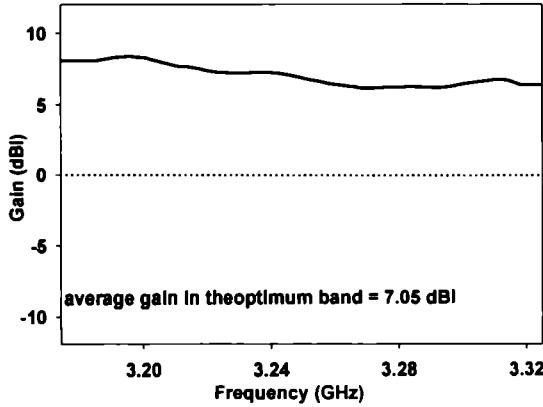


Figure 5.40 Gain of the DRA measured in the optimum band
 feed line length = 3 cm large ground plane: 5 x 4 sq cm
 DR-1 orientation : a-b-d $(d_x, d_y) = (2.4, 0.8)$ cm

The measured return loss and gain characteristics of the DRA at the optimum bandwidth position [$(d_x, d_y) = (1.1, 1.9)$ cm] when the ground plane is truncated at the end of the 3 cm feed is illustrated in Figure 5.41. A high frequency resonant mode at 3.49 GHz operating from 3.34 GHz to 3.58 GHz exhibits 240 MHz bandwidth (6.9%) and offers 7.75 dBi average gain.

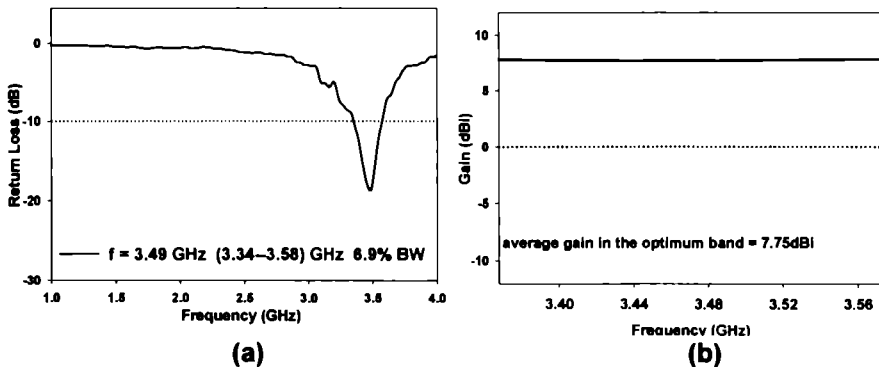


Figure 5.41 Characteristics of the DRA measured at the optimum bandwidth position
 (a) Return loss (b) Gain
 feed line length = 3 cm truncated ground plane: 3x 4 sq cm
 DR-1 orientation : a-b-d $(d_x, d_y) = (1.1, 1.9)$ cm

The truncation of the ground plane results in a compact antenna configuration displaying good radiation characteristics. The experimentally measured radiation patterns of the 3 cm line fed DRA in the truncated ground plane configuration are shown in Figure 5.42. The radiation characteristics are summarised in Table 5.22. The front to back ratio along the maxima is 20 dB and 22 dB in the E and H planes respectively. The cross polarization along the maxima is better than -11 dB in both the planes.

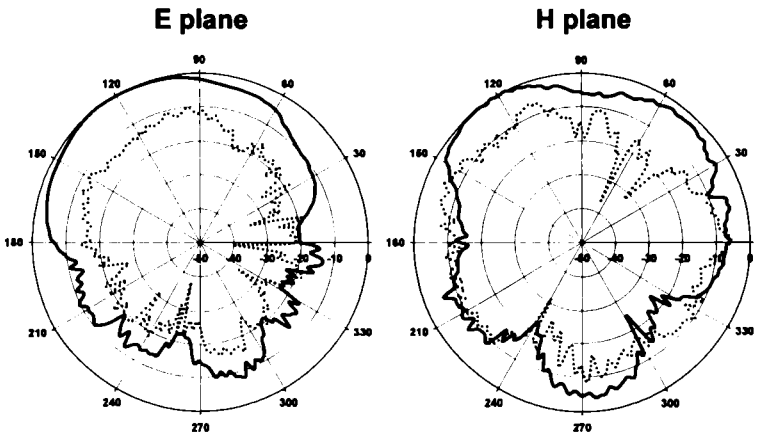


Figure 5.42 Radiation Pattern of the DRA measured at the optimum bandwidth position ($f = 3.49$ GHz)
 — co-polar cross-polar
 feed line length = 3 cm truncated ground plane: 3 x 4 sq cm
 DR-1 orientation : a-b-d $(d_x, d_y) = (1.1, 1.9)$ cm

Half power beam width (degree)		Front-to-Back Ratio along the Maxima (dB)		Cross-Polarisation along the Maxima (dB)	
E plane	H Plane	E plane	H plane	E plane	H plane
84	46	20	22	-14	-11

Table 5.22 Radiation characteristics of the DRA measured at the optimum bandwidth position ($f = 3.49$ GHz)
 feed line length = 3 cm truncated ground plane: 3x4 sq cm
 DR-1 orientation : a-b-d $(d_x, d_y) = (1.1, 1.9)$ cm

Figure 5.43 shows the return loss and gain characteristics of the DRA in the a-b-d orientation at the optimum bandwidth position $[(d_x, d_y) = (1.5, 2.4) \text{ cm}]$ of the resonator, when the length of the Microstrip Line feed is increased to 4 cm.

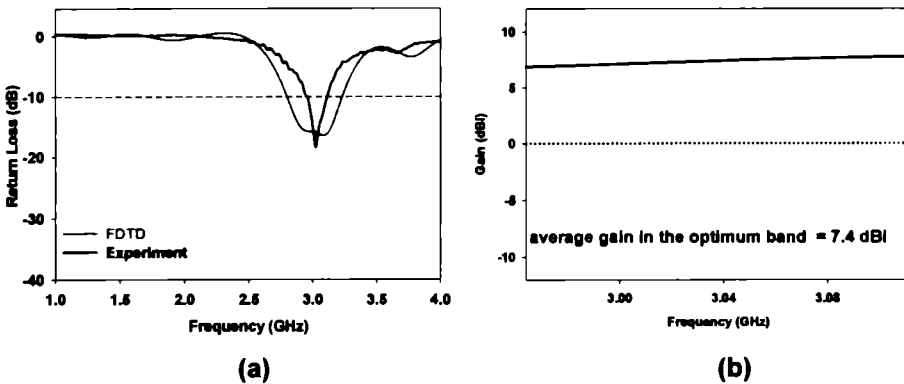


Figure 5.43 Characteristics of the DRA at the optimum bandwidth position
 (a) Return loss (b) Gain
 feed line length = 4 cm large ground plane: 6 x 4 sq cm
 DR-1 orientation : a-b-d $(d_x, d_y) = (1.5, 2.4) \text{ cm}$

The FDTD method predicts 442.5 MHz bandwidth (14.3%) at 3.0849 GHz in a band operating from 2.7942 GHz to 3.2367 GHz at the position $(d_x, d_y) = (1.5, 2.4)$. A resonant mode at 3.025 GHz operating from 2.94 GHz to 3.112 GHz exhibiting 172 MHz bandwidth (5.7%) is observed experimentally at this position. The fractional difference between the experimentally measured and numerically computed resonant frequency is -1.9% . The DRA exhibits an average gain of 7.4 dBi in the optimum resonant band.

Figure 5.44 shows the radiation patterns of the 4 cm line fed DRA in the a-b-d orientation. The front to back ratio measured along the maxima is 6 dB and 20 dB in the E and H planes respectively. The cross polarization along the maxima is -31 dB and -18 dB in the E and H planes respectively. The radiation characteristics are summarised in Table 5.23. The theoretically computed patterns agree well with the measured patterns. In the optimum resonant band centred at 3.025 GHz, the antenna

exhibits linear polarization along the longer dimension ‘a’ of the DR, perpendicular to the feed axis.

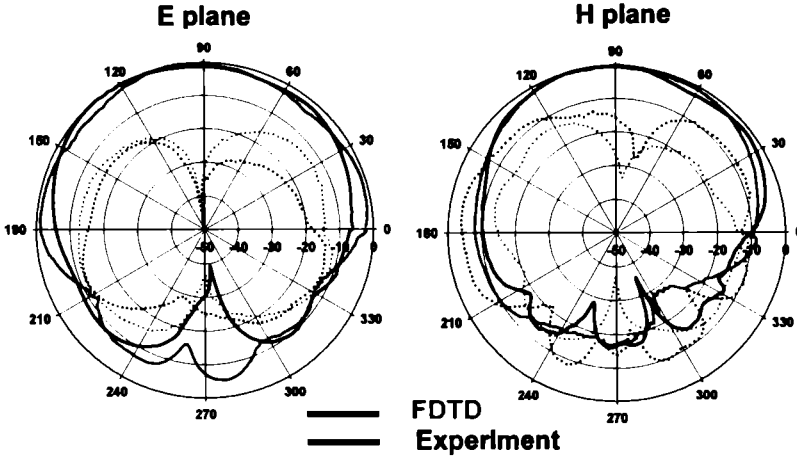


Figure 5.44 Radiation Pattern of the DRA at the optimum bandwidth position ($f = 3.025$ GHz) — co-polar cross-polar feed line length = 4 cm large ground plane: 6 x 4 sq cm DR-1 orientation : a-b-d $(d_x, d_y) = (1.5, 2.4)$ cm

	Half power beam width (degree)		On axis Front-to-Back Ratio (dB)		On axis Cross-Polarisation (dB)	
	E plane	H plane	E plane	H plane	E plane	H plane
Theory	124	72	10	16	-19	-17
Experiment	87	92	6	20	-31	-18

Table 5.23 Radiation characteristics of the DRA at the optimum bandwidth position ($f = 3.025$ GHz) feed line length = 4 cm large ground plane: 6 x 4 sq cm DR-1 orientation : a-b-d $(d_x, d_y) = (1.5, 2.4)$ cm

Figure 5.45 shows the return loss and gain characteristics of the DRA at the optimum bandwidth position [$(d_x, d_y) = (1.2, 3)$] when the ground plane is truncated at the end of the 4 cm feed. A high frequency resonant mode at 3.385 GHz operating from 3.315 GHz to 3.497 GHz exhibits 182 MHz bandwidth (5.4%). A lower resonant mode is

also observed at 2.89 GHz. But it fails to achieve sufficient impedance matching. The DRA exhibits an average gain of 7.8 dBi in the lower band and 3.7 dBi in the optimum resonant band. The radiation patterns of the 4 cm line fed DRA in the truncated ground plane configuration is shown in Figure 5.46.

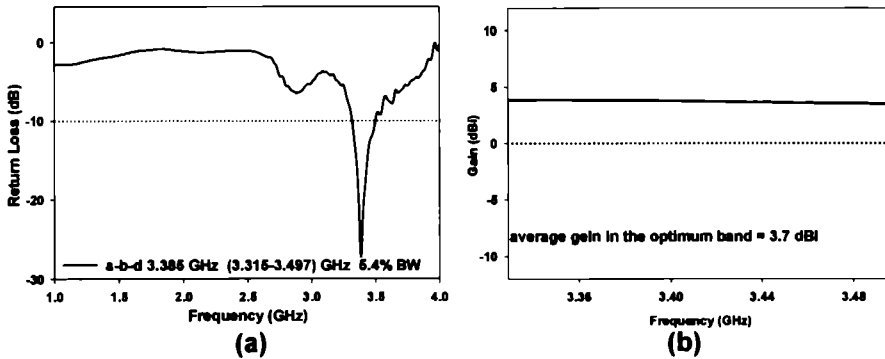


Figure 5.45 Characteristics of the DRA measured at the optimum bandwidth position (a) Return loss (b) Gain
 feed line length = 4 cm truncated ground plane: 4 x 4 sq cm
 DR-1 orientation : a-b-d (d_x, d_y) = (1.2, 3) cm

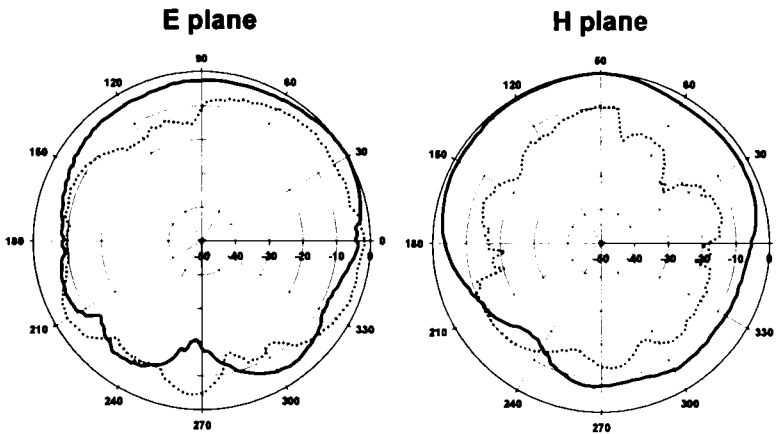


Figure 5.46 Radiation Pattern of the DRA measured at the optimum bandwidth position ($f = 3.385$ GHz)
 — co-polar cross-polar
 feed line length = 4 cm truncated ground plane: 4 x 4 sq cm
 DR-1 orientation : a-b-d (d_x, d_y) = (1.2, 3) cm

In both the planes the front to back ratio is 8 dB and the cross polarization along the maxima is better than -5 dB. The H plane pattern is broader than the E plane pattern. The radiation characteristics are summarised in Table 5.24. The broadband coverage

and moderate gain of the antenna make it suitable for Mobile Communication applications. It is thus observed that the length of the feed line is an important parameter deciding the resonant behaviour of feed line. The return loss characteristics of the DRA in the a-b-d orientation, when excited by feed lengths ranging from 2 cm to 9 cm on varying ground plane dimensions are summarised in Figure 5.47.

Half power beam width (degree)		Front-to-Back Ratio along the maxima (dB)		Cross-Polarisation along the maxima (dB)	
E plane	H Plane	E plane	H plane	E plane	H plane
93	162	8	8	-5	-10

Table 5.24 Radiation characteristics of the DRA measured at the optimum bandwidth position ($f = 3.385$ GHz)
 feed line length = 4 cm truncated ground plane: 4 x 4 sq cm
 DR-1 orientation : a-b-d (d_x, d_y) = (1.2, 3) cm

Figure 5.48 illustrates the variation in resonant frequency and bandwidth of the dominant mode at the optimum bandwidth position of the resonator for increasing feed lengths in different ground plane configurations. As the feed length is increased from 2 cm to 9 cm in the large ground plane configuration of the a-b-d orientation, the resonant frequency of the dominant mode exhibits a variation from 3.01 GHz to 3.61 GHz. The 2:1 VSWR bandwidth varies from 5.7% to 14.1%. In the truncated ground plane configuration, the frequency varies from 3.04 GHz to 3.715 GHz, and the bandwidth varies from 5.3 % to 13.9 %. The experimental results described above suggest that, in comparison with the truncated ground plane the performance of the large ground plane is superior, exciting lower resonant frequencies for all feeds except the 5 cm and 7 cm feed. The overall bandwidth is also better. However, a decision on the suitable configuration can be made only after the gain and radiation patterns are compared The gain of the DRA in the a-b-d orientation, when excited by varying feed and ground plane dimensions are shown in Figures 5.49 [1-2].

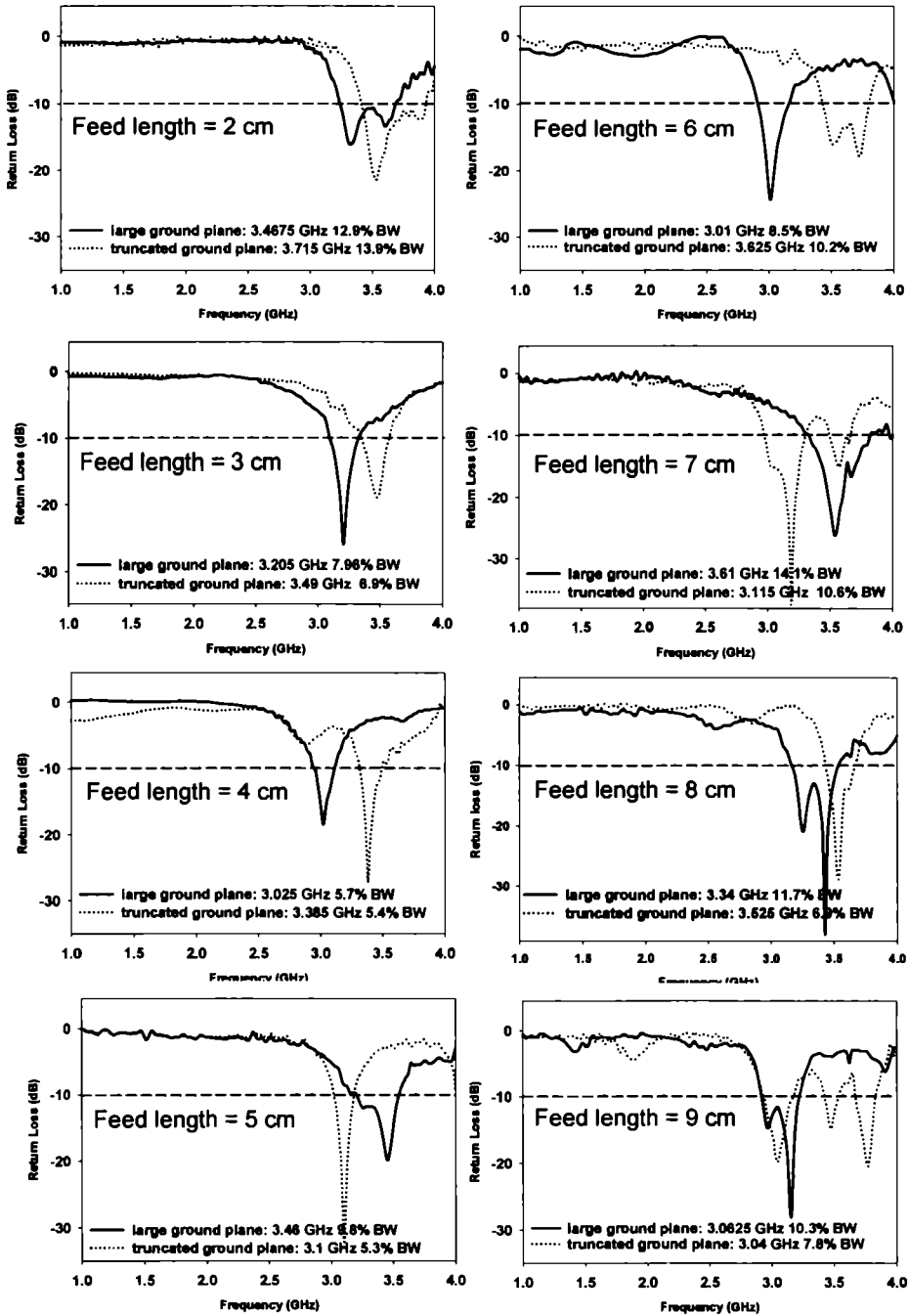


Figure 5.47 Return loss characteristics for varying feed lengths and ground plane dimensions measured at the optimum bandwidth position of the DRA DR-1 orientation : a-b-d

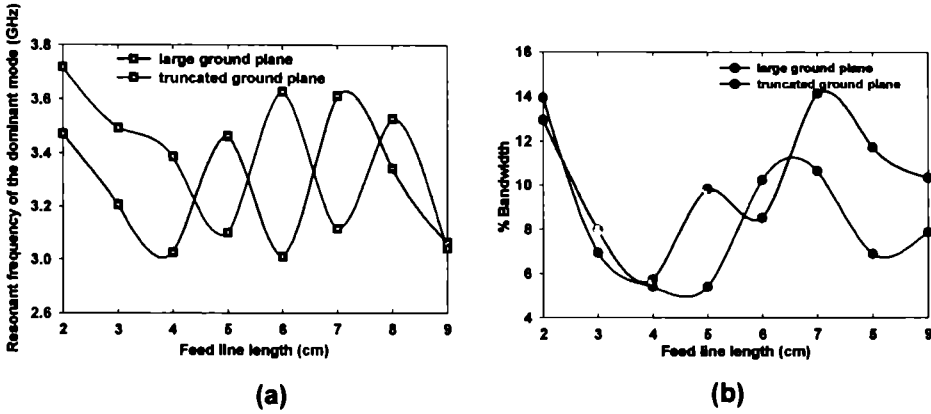


Figure 5.48 Variation in resonant behaviour of the DRA with feed length and ground plane dimensions measured at the optimum bandwidth position
 (a) Resonant frequency
 DR-1
 (b) % Bandwidth
 orientation : a-b-d

The variation in average gain of the DRA in the optimum resonant band for varying feed lengths and ground plane dimensions is summarised in Figure 5.50. The overall compactness of the truncated ground plane may be exploited by integrating suitable amplifier circuits to compensate for the reduced gain. The radiation characteristics in the a-b-d orientation of the DRA for varying feed lengths is summarised in Table 5.25. The gain performance described above indicate that the DRA excited by all the feed lines except the 8 cm feed exhibit good gain in the large ground plane configuration. Feed lines of length 3 cm, 6 cm, 7 cm and 9 cm excite resonant modes exhibiting good gain in the truncated ground plane configuration.

The principal plane radiation patterns are measured in the a-b-d orientation of the resonator for feeds varying in length from 2 cm to 9 cm. The patterns of the DRA excited by the 2 cm, 3 cm and 4 cm feeds in the large ground plane configuration were described in the previous sections. Figure 5.51 shows the principal plane patterns of the DRA excited by the 5 cm, 6 cm and 7 cm feeds in the large ground plane configuration.

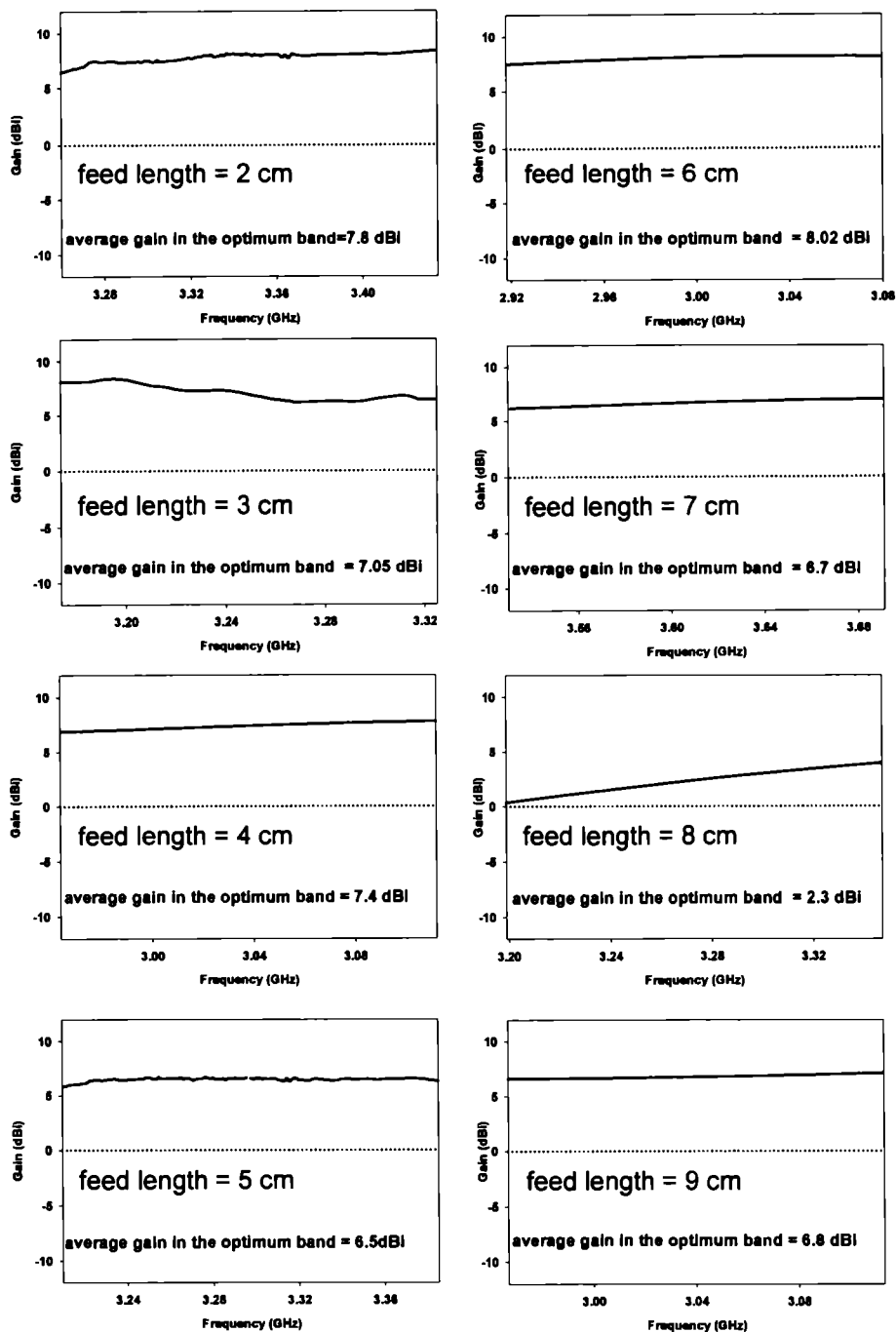


Figure 5.49.1 Gain of the DRA measured in the optimum band for varying feed lengths on a large ground plane orientation : a-b-d

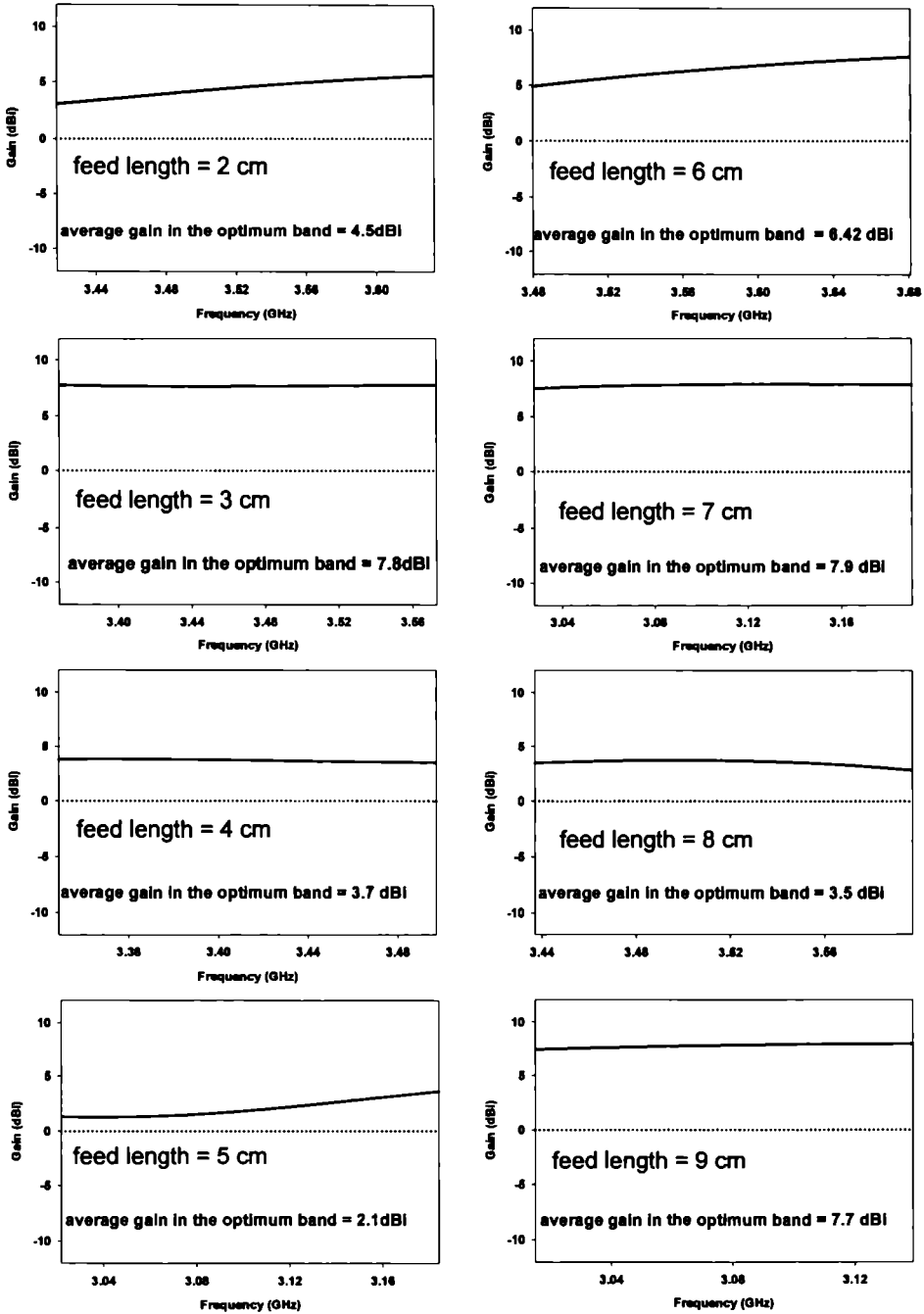


Figure 5.49.2 Gain of the DRA measured in the optimum band for varying feed lengths on a truncated ground plane DR-1 orientation : a-b-d

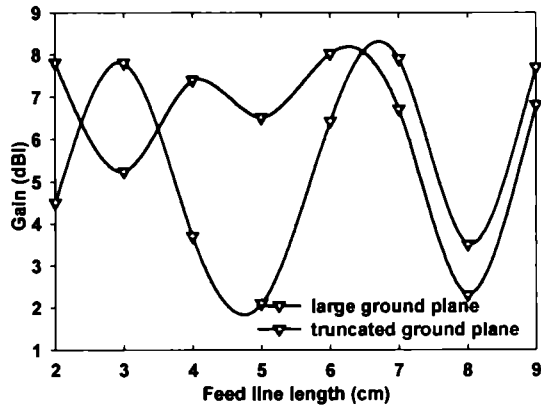


Figure 5.50 Variation in gain of the DRA with feed length and ground plane dimensions measured in the optimum band
DR-1 orientation : a-b-d

Feed Line length (cm)	Large Ground plane			Truncated Ground plane		
	Freq (GHz)	%BW	Avg gain (dBi)	Freq (GHz)	%BW	Avg gain (dBi)
2	3.4675	12.9	7.8	3.715	13.9	4.5
3	3.205	7.96	7.05	3.49	6.9	7.75
4	3.025	5.7	7.4	3.385	5.4	3.7
5	3.46	9.8	6.5	3.1	5.3	2.1
6	3.01	8.5	8.02	3.625	10.2	6.42
7	3.61	14.1	6.7	3.115	10.6	7.9
8	3.34	11.7	2.3	3.525	6.9	3.5
9	3.0625	10.3	6.8	3.04	7.8	7.7

Table 5.25. Variation in radiation characteristics of the DRA with feed length and ground plane dimensions measured at the optimum bandwidth position
DR-1 orientation: a-b-d

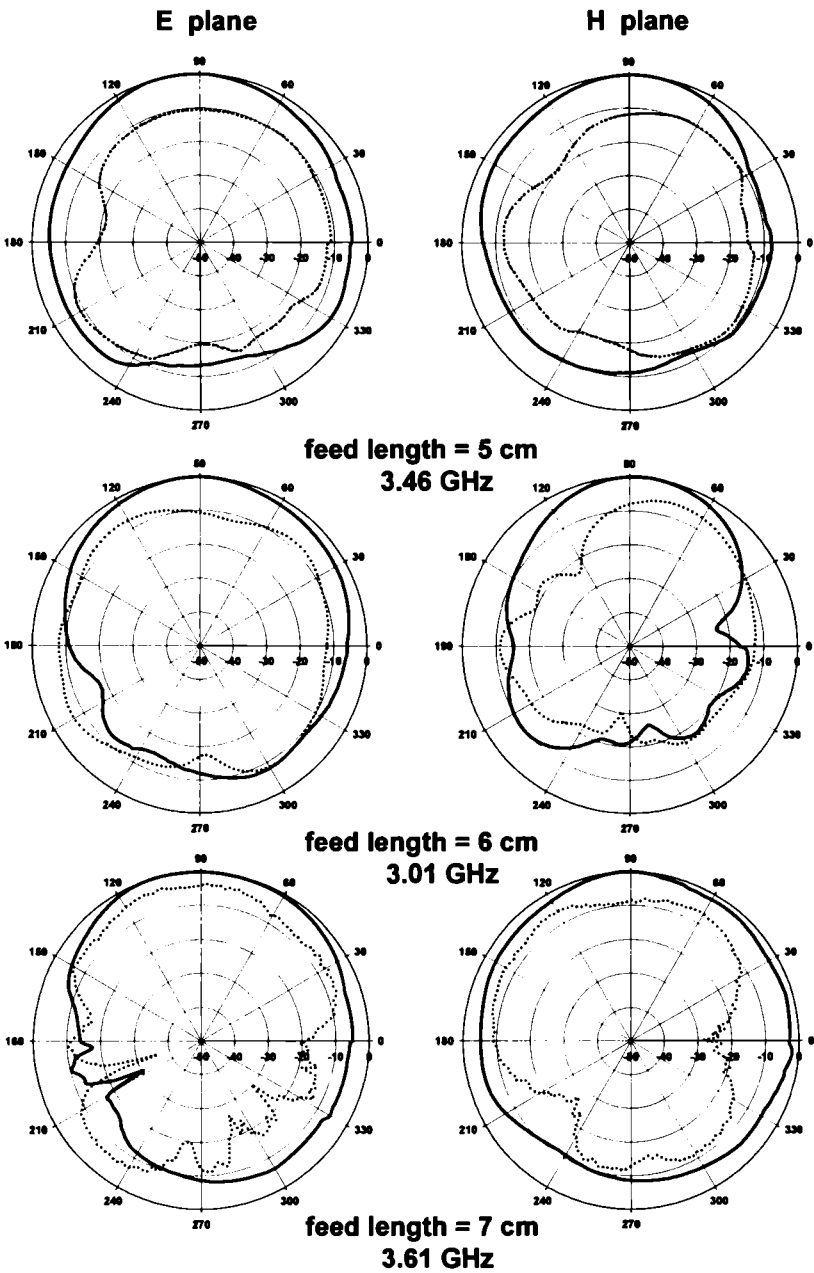


Figure 5.51 Radiation Pattern of the DRA for varying feed lengths measured at the optimum bandwidth position
 — co-polar cross-polar
 DR-1 large ground plane orientation : a-b-d

The characteristics obtained from the radiation pattern measurements are summed up in Table 5.26.

Feed Length (cm)	Half power beam width (degree)		Front-to-Back Ratio along the maxima (dB)		Cross-Polarisation along the maxima (dB)	
	E plane	H plane	E plane	H plane	E plane	H plane
2	130	94	15	18	-5	-5
3	74	52	14	16	-13	-13
4	124	60	10	16	-19	-40
5	86	74	14	11	-11	-12
6	100	58	12	21	-11	-7
7	102	156	8	9	-5	-9
8	100	80	11	7	-18	-12
9	107	82	8	12	-29	-22

Table 5.26 Radiation pattern characteristics of the DRA for varying feed lengths measured at the optimum bandwidth position
DR-1 large ground plane orientation : a-b-d

It is seen that at the optimum bandwidth positions, the DR is not always placed symmetric with respect to the feed axis. The optimum position also varies with feed length and orientation. Figure 5.52 clearly illustrates the two positions of the DR in the a-b-d orientation at $d_x = a/2$ (the symmetrical position) and $d_x = 0$ (DR edge lying

along the feed axis). $d_x < a/2$ indicates a displacement to the left from the symmetrical position, and $d_x > a/2$ indicates a displacement to the right from the symmetrical position. Similarly, $0 < d_y < b$ indicates that the feed end lies within the DR. In the remaining positions ($d_y \geq b$), the configuration behaves like a DR loaded Microstrip line. The experimental observations suggest that this situation prevails at a majority of the optimum bandwidth conditions. Table 5.27 summarises the optimum bandwidth positions of the DR in the a-b-d orientation, when excited by feeds of varying lengths.

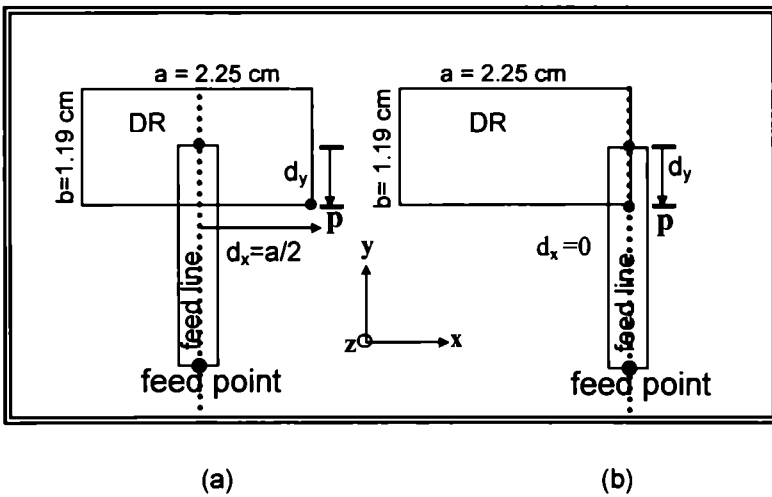


Figure 5.26 Lateral positions of the DR with respect to the feed axis (d_x, d_y) - distance of the DR vertex 'P' from the reference point along the x and y direction respectively
 DR-1 orientation: a-b-d
 (a) symmetrical (b) asymmetrical

Feed length (cm)	Ground plane ($l_g \times w_g$) sq cm	(d_x, d_y) cm
2	large (4 x 4)	1.25, 1
	truncated (2 x 4)	1.1, 0.9
3	large (5 x 4)	2.4, 0.8
	truncated (3 x 4)	1.1, 1.9
4	large (6 x 4)	1.5, 2.4
	truncated (4 x 4)	1.2, 3
5	large (7 x 4)	0.5, 3
	truncated (5 x 4)	0.8, 2.3
6	large (8 x 4)	0.6, 5
	truncated (6 x 4)	0.7, 3.8
7	large (9 x 4)	1.1, 4
	truncated (7 x 4)	2, 1.9
8	large (10 x 4)	1.8, 5.5
	truncated (8 x 4)	1.1, 2
9	large (11 x 4)	1.6, 5
	truncated (9 x 4)	0.5, 7.8

Table 5.27 The optimum bandwidth positions of the DR DR-1 orientation: a-b-d

5.1.2.10 Resonant behaviour of the DRA when the DR is placed symmetrically with respect to the feed axis

This section discusses the resonant behaviour of the DRA for varying feed lengths when the DR in the a-b-d orientation is placed symmetrically with respect to the feed axis at $(d_x, d_y) = (a/2, 0.5)$. Figure 5.53 illustrates the variation in resonant frequency and % bandwidth of the DRA with feed length.

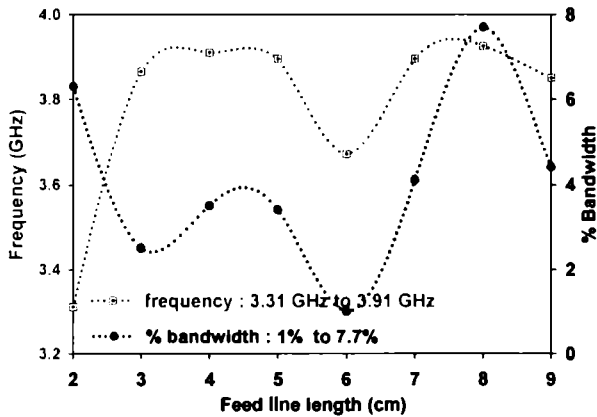


Figure 5.53 Variation in resonant frequency and % bandwidth of the DRA with feed length measured at a symmetrical position of the DR $(d_x, d_y) = (a/2, 0.5)$ cm large ground plane orientation : a-b-d DR-1

The varying feed lengths excite frequencies ranging from 3.31 GHz to 3.925 GHz, with an average bandwidth of 4.1%. The 2 cm feed excites the lowest frequency, with a good bandwidth of 6.3% resulting in a highly compact design. Maximum bandwidth of 7.7% is exhibited by the 8 cm fed DRA at 3.925 GHz and the minimum bandwidth of 1% at 3.67 GHz by the 6 cm fed DRA. The resonant characteristics are summarised in Table 5.28. Figure 5.54 shows the return loss characteristics at the symmetrical position of the DR for varying feed lengths.

	Feed Length (cm)							
	2	3	4	5	6	7	8	9
Freq (GHz)	3.31	3.865	3.91	3.895	3.67	3.895	3.925	3.85
%BW	6.3	2.5	3.5	3.4	-1-	4.1	7.7	4.4

Table 5.28 Resonant behaviour of the DRA for varying feed lengths measured at a symmetrical position of the DR
 $(d_x, d_y) = (a/2, 0.5)$ cm large ground plane orientation : a-b-d
 DR-1

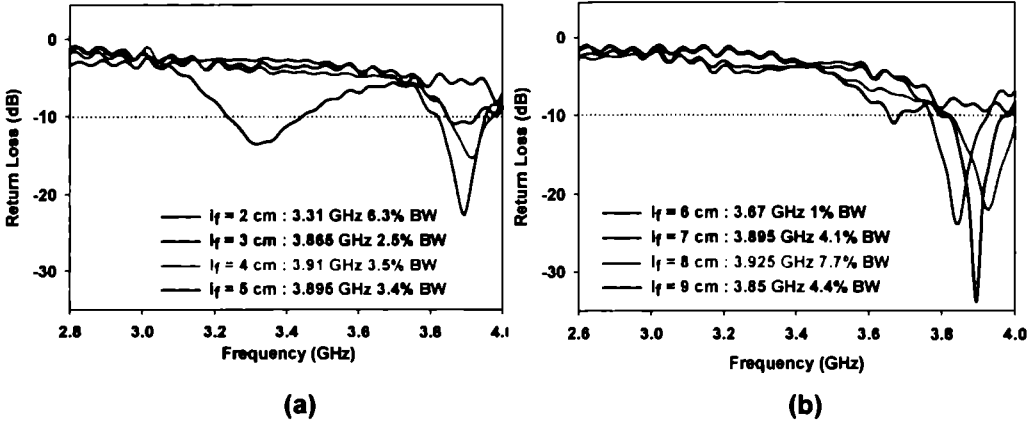


Figure 5.54 Return loss characteristics of the DRA for varying feed lengths measured at a symmetrical position of the DR
 (a) feed length = 2 cm to 5 cm (b) feed length = 6 cm to 9 cm
 large ground plane orientation: a-b-d
 $(d_x, d_y) = (a/2, 0.5)$ cm
 DR-1

5.1.2.11 Salient features of the a-b-d orientation

The a-b-d orientation is the second most compact among the various orientations of the Rectangular DR upon the feed line, possessing a low aspect ratio (height/width = 0.47). At 3.4675 GHz the 2 cm line fed DRA offers ~50% size reduction with respect to a Rectangular Microstrip Antenna resonating at the same frequency. Table 5.25 and 5.26 sum up the characteristics of this orientation. The varying feed line lengths excite frequencies in the S-band, providing an average gain of 6.6 dBi, and average 2:1 VSWR bandwidth of 10.1%. The 6 cm feed offers the maximum gain (8.02 dBi). The lowest resonant frequency (3.01 GHz) is excited by the 6 cm feed and the maximum 2:1 VSWR bandwidth (14.1%) is provided by the 7 cm feed. The radiation patterns are generally broad - the average half-power beam width along the E plane and H plane being 98° and 67° respectively. The 2 cm line fed DRA offers broad radiation coverage with 130° and 94° half-power beam width respectively in the E and H planes [Figure 5.31] and is highly suitable for mobile communications.

The truncated ground plane configuration exhibits an average gain of 5.5 dBi and average 2:1 VSWR bandwidth of 8.4%. The performance is therefore relatively inferior to that of the large ground plane configuration, similar to the b-a-d orientation. Nevertheless, it acquires significance where the size of the antenna is of priority.

The investigations performed on the Dielectric Resonator Antenna incorporating the Rectangular resonator sample DR-1 in the a-b-d orientation confirm the dependence of the antenna characteristics upon the feed length, ground plane dimensions and position of the DR. The performance of the DRA excited by Microstrip line feed of length 2 cm is noteworthy in lieu of its overall compactness, bandwidth, gain and broad radiation pattern, though at a relatively high resonant frequency.

5.1.3 The d-a-b orientation

The d-a-b orientation is also a low profile orientation [aspect ratio = 0.53]. A schematic representation and 3D view of this orientation is shown in Figure 5.55. The distance of the reference vertex 'P' from the feed axis and the feed end (d_x, d_y) indicate the position of the DR along the x and y axes respectively. The radiation characteristics of the 2 cm line excited DRA in the d-a-b orientation of the resonator for varying feed line and ground plane dimensions are discussed in this section.

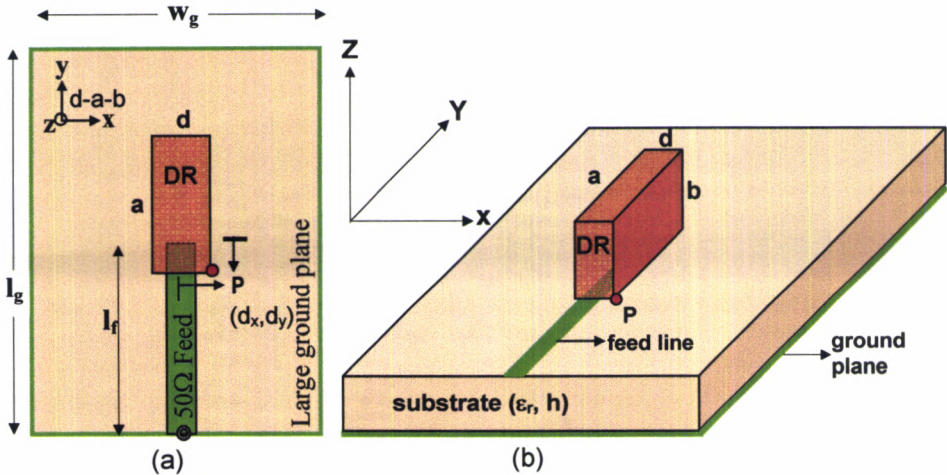


Figure 5.55 The d-a-b orientation of the DR
 substrate: $\epsilon_r = 4.28$, $h = 0.16$ cm
 DR-1 $a \times b \times d = [2.25 \times 1.19 \times 0.555]$ cm³
 (a) schematic lay out (b) 3D view

5.1.3.1 Return Loss Characteristics

The return loss characteristics are computed numerically employing the FDTD method. The offset distance of the DR from the feed (d_x, d_y) is optimised for maximum 2:1 VSWR bandwidth and measurements are recorded for varying dimensions of the feed line and ground plane. The numerically predicted results are validated experimentally as shown in Figure 5.56. Theoretically the antenna is found to resonate at 3.1413 GHz in a band operating from 2.6423 GHz to 3.2497 GHz with 607 MHz bandwidth (19%) when placed at $(d_x, d_y) = (0.25, 1.5)$ cm. A resonant mode

at 3.175 GHz, operating from 3.074 GHz to 3.311 GHz and exhibiting 237 MHz bandwidth (7.5%) is experimentally observed at this position.

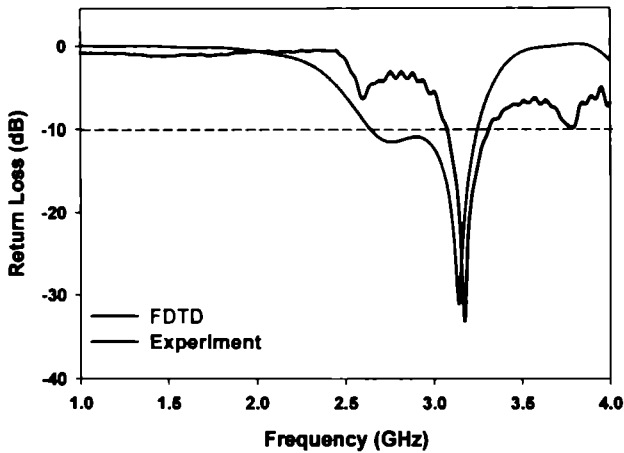


Figure 5.56 Return loss characteristics of the DRA at the optimum bandwidth position
 feed line length = 2 cm large ground plane: 4 x 4 sq cm
 DR-1 orientation: d-a-b $(d_x, d_y) = (0.25, 1.5)$ cm

Though a low frequency resonant mode is observed at 2.6 GHz in the optimum bandwidth position, it fails to achieve sufficient impedance matching. The fractional difference between the experimentally measured and numerically computed resonant frequency is +1.1%. The accuracy of the FDTD analysis in predicting the resonant frequency of the antenna is evident from the figure. However the predicted bandwidth is considerably larger due to the merging of the two closely spaced modes. This may be due to the different tolerance level of the experimental configuration as mentioned in Section 5.1.1.1.

5.1.3.2 Radiation Pattern

The radiation patterns in the d-a-b orientation of the resonator at the centre frequency of the optimum resonant band are shown in Figure 5.57. The theoretical radiation patterns agree reasonably well with the experimental curves. The patterns are broad in both the planes, unlike in the b-a-d and a-b-d orientation. This mode is

thus highly suitable for Mobile phone applications. The radiation characteristics are summarised in Table 5.29.

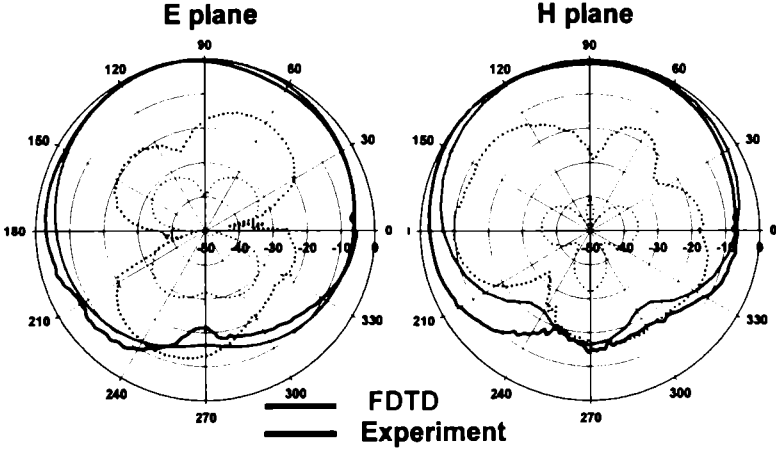


Figure 5.57 Radiation Pattern of the DRA at the optimum bandwidth position ($f = 3.175$ GHz) — co-polar cross-polar
 feed line length = 2 cm large ground plane: 4 x 4 sq cm
 DR-1 orientation: d-a-b (d_x, d_y) = (0.25, 1.5) cm

	Half power beam width (degree)		On axis Front-to-Back Ratio (dB)		On axis Cross-Polarisation (dB)	
	E plane	H plane	E plane	H plane	E plane	H plane
Theory	115	130	16	17	-40	-40
Experiment	138	139	18	16	-25	-12

Table 5.29 Radiation characteristics of the DRA at the optimum bandwidth position ($f = 3.175$ GHz)
 feed line length = 2 cm large ground plane: 4 x 4 sq cm
 DR-1 orientation: d-a-b (d_x, d_y) = (0.25, 1.5) cm

5.1.3.3 Polarization

The DRA in the d-a-b orientation exhibits linear polarization in the optimum resonant band centred at 3.175 GHz. The antenna is polarized along the longer dimension ‘a’ of the DR, parallel to the feed axis.

5.1.3.4 Gain

The DRA exhibits 5.8 dBi gain in the lower resonant band and 1.4 dBi gain in the higher resonant band as shown in Figure 5.58.

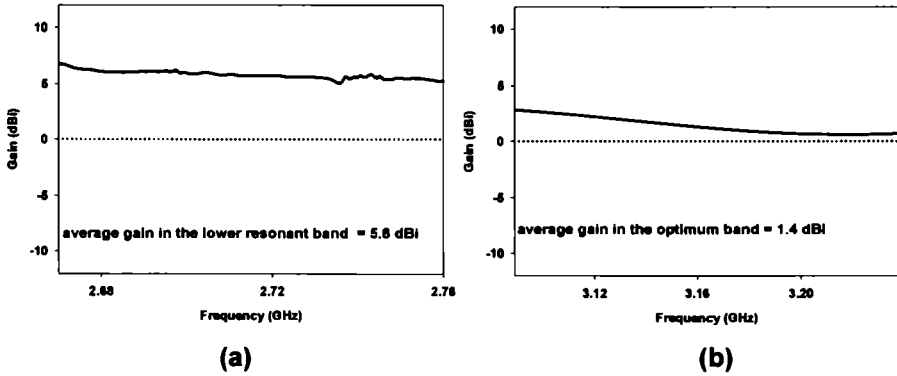


Figure 5.58 Gain of the DRA measured at the optimum bandwidth position
 (a) lower resonant band (b) higher resonant band
 feed line length = 2 cm large ground plane: 4 x 4 sq cm
 DR-1 orientation: d-a-b $(d_x, d_y) = (0.25, 1.5)$ cm

5.1.3.5 Resonant Mode

The field distribution within the DR simulated using the commercially available software - HFSS™, at the numerically predicted frequency 3.175 GHz is shown in Figure 5.59 (a). The variation of the normalized Magnetic field monitored experimentally by a loop probe along the three dimensions is shown in Figure 5.59 (b). It is found that the field exhibits one half-wave variation along the dimension 'a', less than a half-wave variation (δ) along the dimension 'b' and is constant along the dimension 'd'. The resonant mode is therefore identified as TE_{180}^z . This is also verified using FDTD theory.

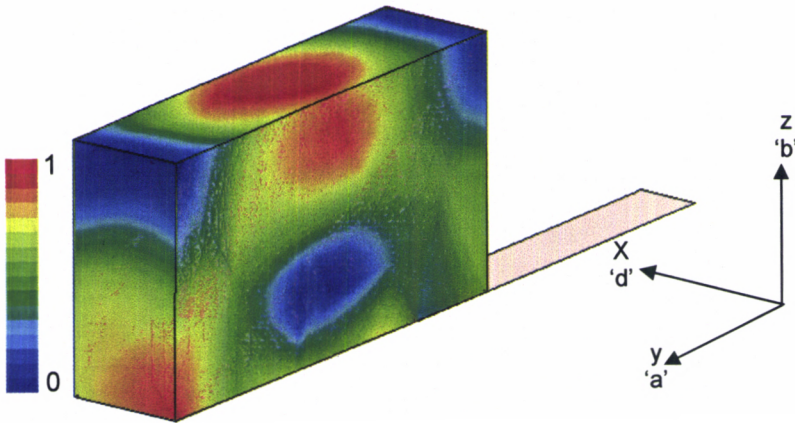


Figure 5.59(a) Simulated H field distribution within the DR at the optimum bandwidth position $f = 3.175$ GHz
 feed line length = 2 cm large ground plane: 4x4 sq cm
 DR-1 orientation : d-a-b $(d_x, d_y) = (0.25, 1.5)$ cm

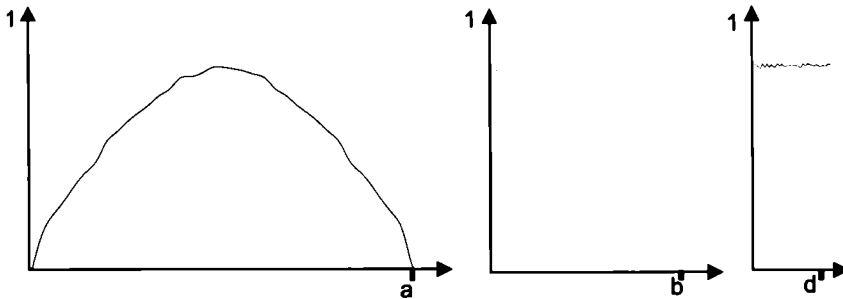


Figure 5.59 (b) Variation of the normalized Magnetic field distribution along the dimensions 'a', 'b' and 'd' of the DR monitored experimentally TE_{180}^z mode
 feed line length = 2 cm large ground plane: 4 x 4 sq cm
 DR-1 orientation : d-a-b $(d_x, d_y) = (0.25, 1.5)$ cm

5.1.3.6 Compactness

In order to ascertain the compactness of the DRA in the d-a-b orientation at 3.175 GHz, the antenna is compared with a circular and rectangular Microstrip antenna resonating at the same frequency. Table 5.30 provides a comparison of the dimensions of the different antennas at 3.175 GHz. The 2 cm line fed DRA

incorporating the resonator in the d-a-b orientation is found to possess 80.8 % and 76% reduction in the cross-section area with respect to a rectangular and circular Microstrip antenna designed to operate at the same frequency. Though the DRA in the b-a-d orientation resonates at the same frequency in the optimum band [Table 5.4], the size reduction with respect to conventional patch antennas is greater in the d-a-b orientation because of the lower cross-sectional area.

Antenna	Dimensions (cm)	Cross-sectional area (sq cm)
DRA in the d-a-b orientation	Length (d)= 0.555 Width (a) = 2.25	(d x a) 1.25
Rectangular microstrip antenna	Length = 2.24 Width = 2.91	6.52
Circular microstrip antenna	Radius = 1.29	5.23

Table 5.30 Dimensions of different antennas operating at 3.175 GHz

5.1.3.7 Truncated ground plane configuration

In the previous section the experimental observations on a rectangular DRA on a large ground plane was presented. The effect of the truncated ground plane is presented in this section. Figure 5.60 shows the return loss characteristics and gain of the DRA in the d-a-b orientation at the optimum bandwidth position $[(d_x, d_y) = (0.28, 1) \text{ cm}]$. Numerical computation predicts a resonant mode at 2.7511 GHz in a band operating from 2.6597 GHz to 2.8115 GHz, displaying 5.5% bandwidth. A low frequency resonant mode is experimentally observed at 2.725 GHz displaying 77 MHz bandwidth from 2.686 GHz to 2.763 GHz (2.8%). The fractional difference between the experimentally observed and numerically computed frequency is -0.96%. An obvious difference from the behaviour of the large ground plane is the lower resonant frequency. The DRA exhibits 1.9 dBi gain in the optimum resonant band. The radiation patterns in the principal planes are shown in Figure 5.61.

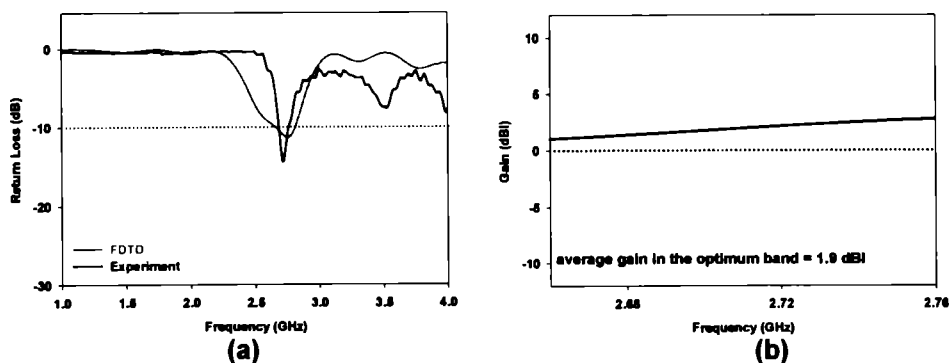


Figure 5.60 Characteristics of the DRA measured at the optimum bandwidth position (a) Return loss (b) Gain
 feed line length = 2 cm truncated ground plane: 2 x 4 sq cm
 DR-1 orientation : d-a-b (d_x, d_y) = (0.28, 1) cm

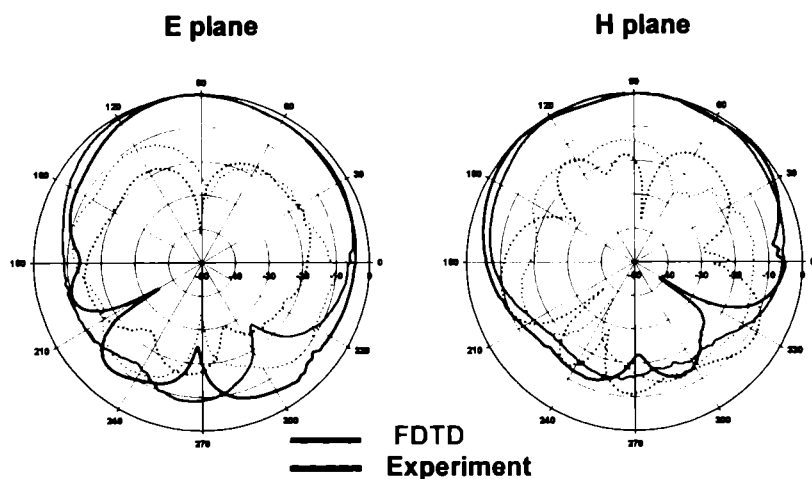


Figure 5.61 Radiation Pattern of the DRA at the optimum bandwidth position ($f = 2.725$ GHz) — co-polar cross-polar
 feed line length = 2 cm truncated ground plane: 2x4 sq cm
 DR-1 orientation: d-a-b (d_x, d_y) = (0.28, 1) cm

The patterns are broad in both the planes, with a maxima along the broad side direction and good cross-polarisation characteristics. Table 5.31 summarises the radiation characteristics of the DRA in the d-a-b orientation at 2.725 GHz. The radiation performance of the 2 cm fed DRA in the d-a-b orientation of the resonator for different ground plane dimensions are compared in Table 5.32.

	Half power beam width (degree)		On axis Front-to-Back Ratio (dB)		On axis Cross-Polarisation (dB)	
	E plane	H plane	E plane	H plane	E plane	H plane
Theory	119	108	12	17	-16	-14
Experiment	95	136	14	12	-33	-38

Table 5.31 Radiation characteristics of the DRA at the optimum bandwidth position ($f = 2.725$ GHz)
 feed line length = 2 cm truncated ground plane: 2x4 sq cm
 DR-1 orientation : d-a-b (d_x, d_y) = (0.28,1) cm

	Large ground plane	Truncated ground plane
Optimum bandwidth position (dx,dy) cm	(0.25,1.5)	(0.28,1)
Operating frequency band (GHz)	3.074 - 3.311	2.686-2.763
% bandwidth	7.5	2.8
Mode of operation	TE ^z _{18,0}	TE ^z _{18,0}
Polarisation	Linear	Linear
3 dB beamwidth		
E plane	138°	95°
H plane	139°	136°
Cross Polarisation (dB)		
E plane	-25	-33
H plane	-12	-38
Front to back ratio (dB)		
E plane	18	14
H plane	16	12
Maximum gain in the operating band (dBi)	2.81	2.76
Size of the antenna with feeding structure	4 x 4 sq cm	2 x 4 sq cm

Table 5.32 Radiation performance of the DRA for different ground plane dimensions measured at the optimum bandwidth position
 DR-1 feed line length = 2 cm orientation : d-a-b

5.1.3.8 Resonant behaviour at different positions of the DR with respect to the feed

This section discusses the influence of the position of the DR upon the antenna characteristics. The resonant behaviour is studied by positioning the DR at discrete intervals of 0.25 cm along the x and y directions on a large ground plane. The return loss characteristics at the lateral positions $d_x = 0.25$ cm and 0.5 cm are illustrated in Figure 5.62.

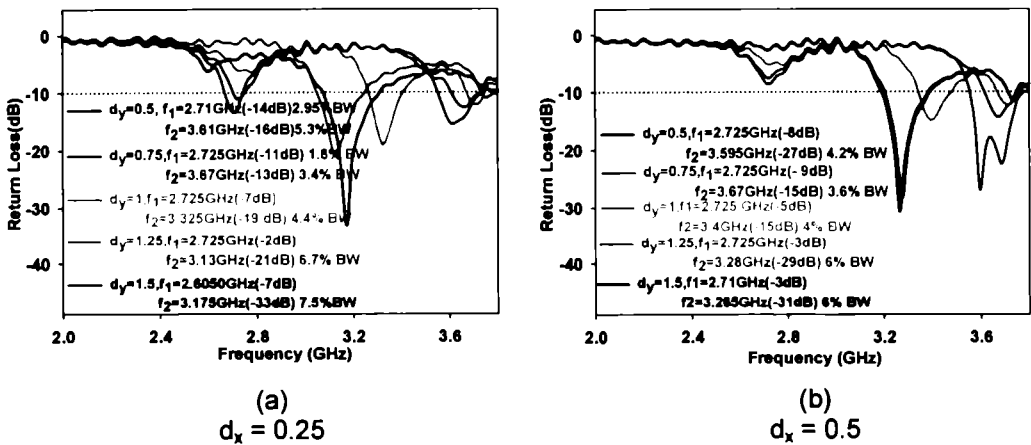


Figure 5.62 Return loss characteristics of the DRA measured at different d_y locations of the DR
 (a) $d_x = 0.25$ cm (b) $d_x = 0.5$ cm
 feed line length = 2 cm large ground plane: 4 x 4 sq cm
 DR-1 orientation: d-a-b

Multi-mode behaviour is observed as the DR is moved with respect to the feed line. A unique feature observed in the d-a-b orientation is the presence of a lower order mode centred at ~ 2.725 GHz, though it fails to obtain sufficient impedance matching at all the positions. On the other hand, the higher frequency modes exhibit excellent impedance matching and wide band characteristics (1.73% to 7.5% bandwidth variation). As the DR is moved along the feed line from the open end to the source end (increasing d_y), the impedance matching of the lower resonant mode

deteriorates and the higher mode dominates. A resonant mode at 3.175 GHz operating from 3.074 GHz to 3.311 GHz exhibits the highest bandwidth (7.5%) at $(d_x, d_y) = (0.25, 1.5)$ as shown in Figure 5.62(a). Figure 5.63 indicates the experimentally observed variation in the resonant frequency and 2:1 VSWR bandwidth of the dominant mode as the DR is located at different positions with respect to the feed. The frequency shows an overall variation from 2.71 GHz to 3.76 GHz and the bandwidth shows a variation from 1% to 7.5%. The resonant behaviour of the Rectangular DRA in the d-a-b orientation is summed up in Table 5.33.

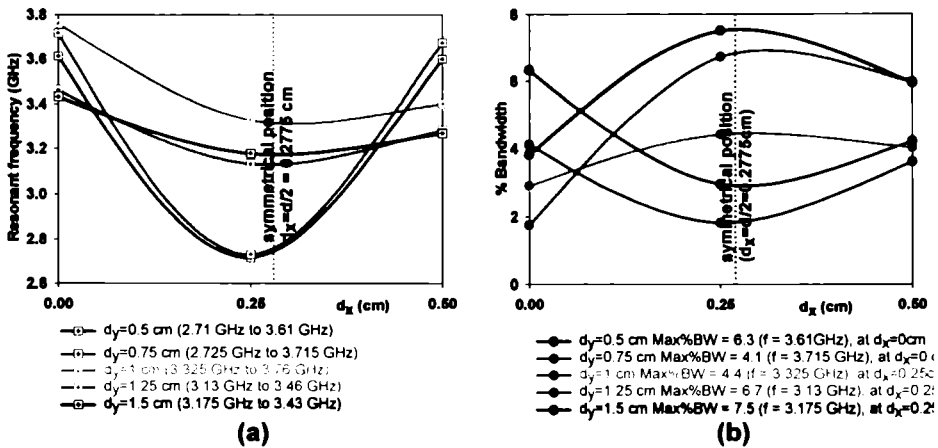


Figure 5.63 Resonant behaviour of the DRA measured with varying position of the DR on the feed line
 (a) Resonant frequency (b) % Bandwidth
 feed line length : 2 cm large ground plane: 4 x 4 sq cm
 DR-1 orientation: d-a-b

The impedance matching at the lower resonant frequency in the d-a-b orientation of the DR can be improved by introducing a stub near the source end as shown in Figure 5.64. The dimensions of the stub chosen for the study are $l_s = 2.8$ cm and $w_s = 0.3$ cm. The length of the stub is designed to be $\sim \lambda_d/2$ at a lower resonant frequency of 2.7 GHz. (λ_d is the wavelength within the substrate). The excitation of different resonant frequencies at various positions of the stub-matched DRA is illustrated in Figure 5.65.

Resonant frequency (GHz)			
d_y (cm)	d_x (cm)		
	0	0.25	0.5
0.25	3.58	2.71	3.58
0.5	3.61	2.71	3.595
0.75	3.715	2.725	3.67
1	3.76	3.325	3.4
1.25	3.46	3.13	3.28
1.5	3.43	3.175	3.265

% Bandwidth			
d_y (cm)	d_x (cm)		
	0	0.25	0.5
0.25	6.6	1	7
0.5	6.3	2.95	4.2
0.75	4.1	1.8	3.6
1	2.9	4.4	4
1.25	1.74	6.7	5.95
1.5	3.8	7.5	5.94

(a)

(b)

Table 5.33 Resonant behaviour of the DRA measured at various positions of the DR on the feed line

(a) Resonant frequency (GHz)

(b) % Bandwidth

feed line length : 2 cm

large ground plane: 4 x 4 sq cm

DR-1

orientation: d-a-b

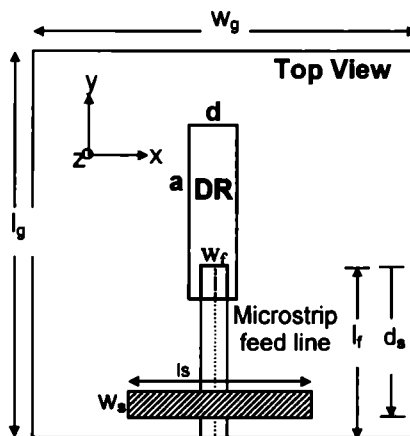


Figure 5.64 Stub matching to improve the impedance matching of the low frequency resonant mode

feed line: $l_f=2$ cm, $w_f=0.3$ cmstub: $l_s=2.8$ cm, $w_s=0.3$ cm, $d_s=1.8$ cmlarge ground plane: ($l_g \times w_g$) = 4 x 4 sq cm

DR-1

orientation : d-a-b

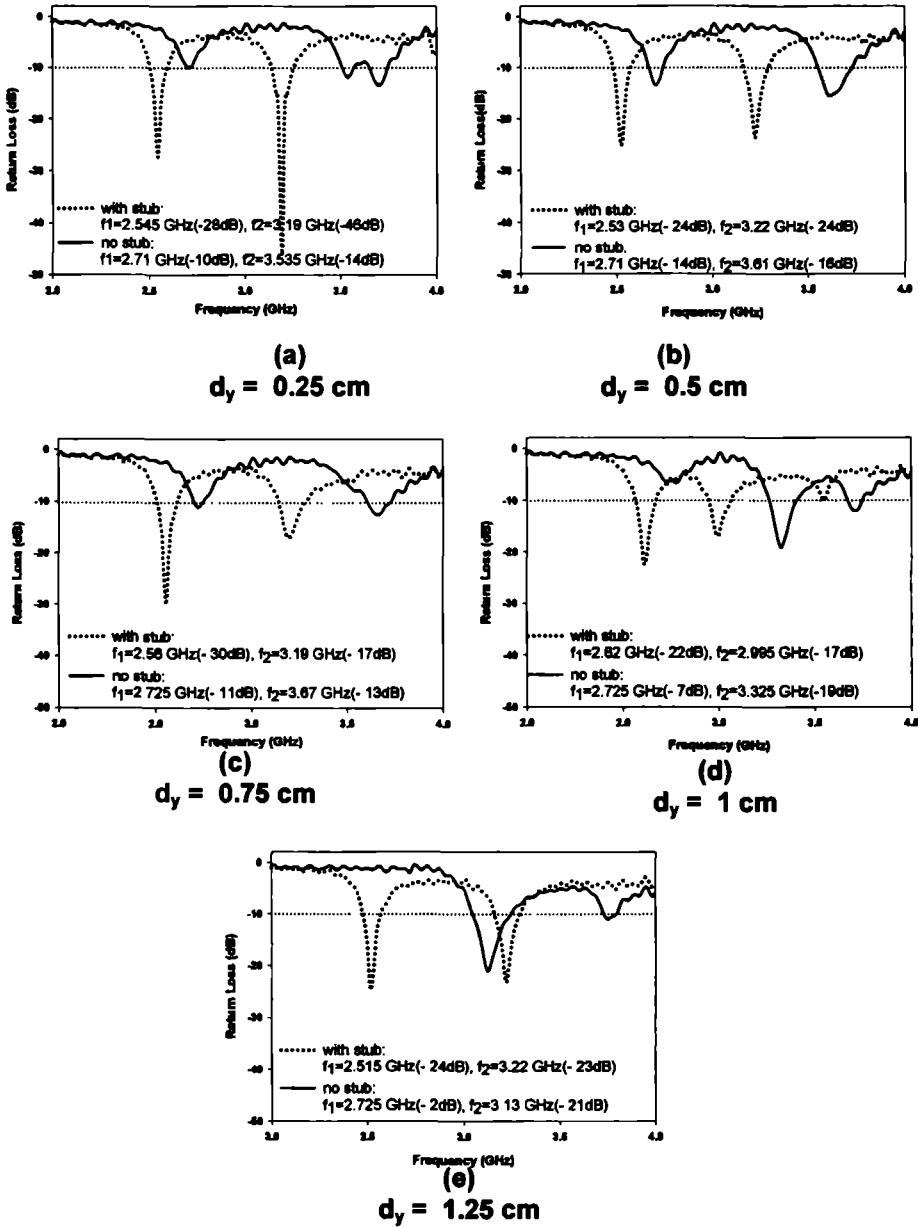


Figure 5.65 Resonant behaviour of the stub matched DRA measured at $d_x = 0.25 \text{ cm}$
 feed line length = 2 cm large ground plane: 4 x 4 sq cm
 DR-1 orientation : d-a-b
 (a) $d_y = 0.25 \text{ cm}$ (b) $d_y = 0.5 \text{ cm}$ (c) $d_y = 0.75 \text{ cm}$ (d) $d_y = 1 \text{ cm}$ (e) $d_y = 1.25 \text{ cm}$

It is observed that the stub improves the impedance matching of the lower resonant frequency. The variation in resonant frequency and % bandwidth of the dominant mode with position of the DR is illustrated in Figure 5.66.

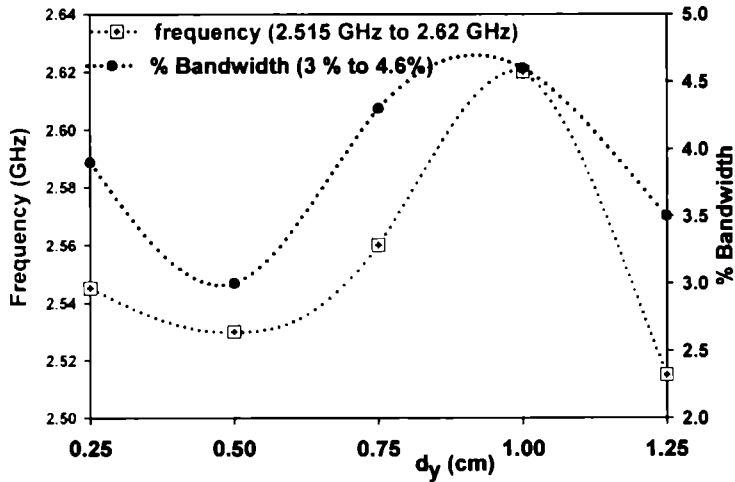


Figure 5.66 Resonant behaviour of the stub matched DRA measured with varying position [d_y] of the DR along the feed axis [$d_x=0.25$ cm]
 feed line length = 2 cm large ground plane: 4 x 4 sq cm
 DR-1 orientation: d-a-b

The resonant frequency of the dominant mode exhibits a variation from 2.515 GHz to 2.62 GHz when the DR is placed laterally at $d_x = 0.25$ cm and moved along the feed line from the open end of the feed to the source end. The bandwidth exhibits an overall variation from 3 % to 4.6 %. Maximum bandwidth (4.6%) is observed at 2.62 GHz when the DR is placed at $(d_x, d_y) = (0.25, 1)$. Tuning the stub length (l_s) and the distance (d_s) has a significant effect on the resonant frequency.

The d-a-b orientation of the DR is thus significant by virtue of its relatively low profile nature and the low frequency resonant mode with moderate bandwidth.

5.1.3.9 Characteristics for varying feed lengths

This section describes the characteristics of the DRA in the d-a-b orientation for varying feed lengths. Figure 5.67 shows the theoretically predicted and experimentally measured return loss characteristics of the DRA at the optimum bandwidth position when the resonator in the d-a-b orientation is excited by a feed of length 3 cm.

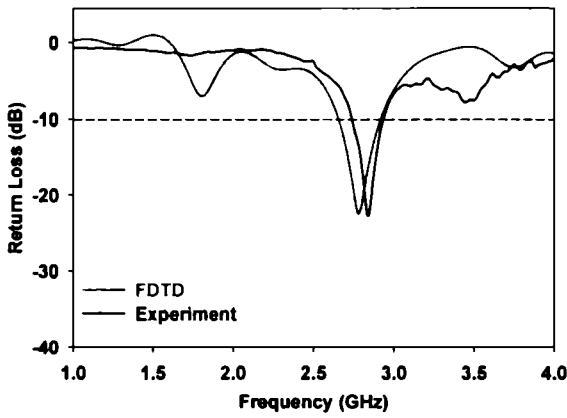


Figure 5.67 Return loss characteristics of the DRA at the optimum bandwidth position.
 feed line length = 3 cm large ground plane: 5x 4 sq cm
 DR-1 orientation: d-a-b $(d_x, d_y) = (0.28, 1.3)$ cm

The FDTD method predicts 269 MHz bandwidth (9.6%) at 2.7811 GHz in a band operating from 2.651 GHz to 2.92 GHz at the position $(d_x, d_y) = (0.28, 1.3)$ cm. A resonant mode at 2.845 GHz operating from 2.73 GHz to 2.94 GHz, exhibiting 210 MHz bandwidth (7.4%) is observed experimentally at the same position. The fractional difference between the experimentally measured and numerically computed resonant frequency is +2.2%.

The measured radiation patterns are broad in both the principal planes as shown in Figure 5.68. The radiation characteristics of the DRA are summarised in Table 5.34.

In the optimum resonant band centred at 2.845 GHz, the 3 cm fed DRA in the d-a-b orientation exhibits linear polarization along the longer dimension 'a' of the DR, along the feed axis. The average gain in the optimum resonant band is 6.7 dBi as shown in Figure 5.69.

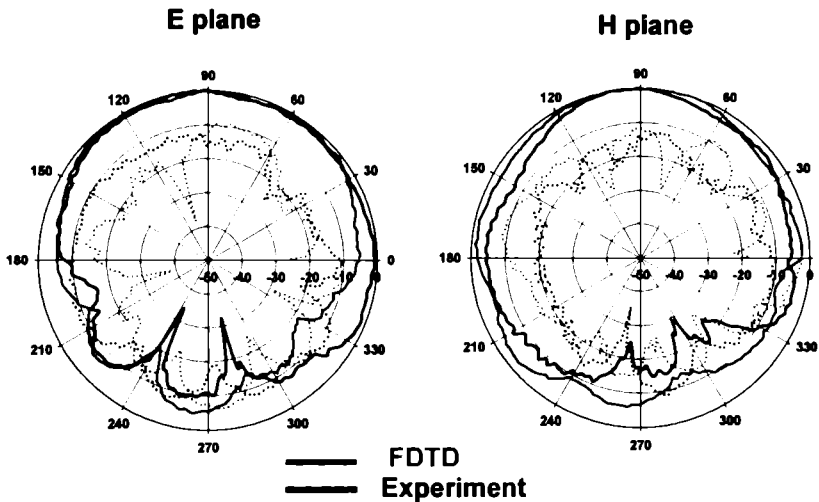


Figure 5.68 Radiation Pattern of the DRA at the optimum bandwidth position ($f = 2.845$ GHz)
 feed line length = 3 cm large ground plane: 5 x 4 sq cm
 DR-1 orientation : d-a-b $(d_x, d_y) = (0.28, 1.3)$ cm

	Half power beam width (degree)		On axis Front-to-Back Ratio (dB)		On axis Cross-Polarisation (dB)	
	E plane	H Plane	E plane	H plane	E plane	H plane
Theory	126	100	6	8	-13	-14
Experiment	176	58	15	17	-14	-19

Table 5.34 Radiation characteristics of the DRA at the optimum bandwidth position ($f = 2.845$ GHz)
 feed line length = 3 cm large ground plane: 5 x 4 sq cm
 DR-1 orientation : d-a-b $(d_x, d_y) = (0.28, 1.3)$ cm

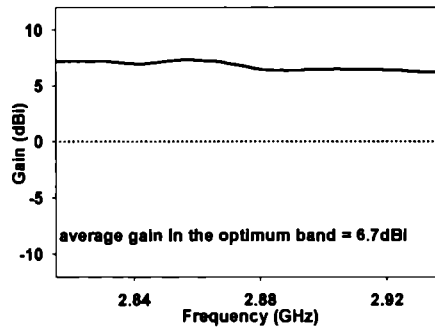


Figure 5.69 Gain of the DRA measured in the optimum band
 feed line length = 3 cm large ground plane: 5 x 4 sq cm
 DR-1 orientation : d-a-b $(d_x, d_y) = (0.28, 1.3)$ cm

Figure 5.70 shows the return loss and gain characteristics of the DRA measured at the optimum bandwidth position $[(d_x, d_y) = (0, 2.1)$ cm] when the ground plane is truncated at the end of the 3 cm feed. A low frequency resonant mode at 2.785 GHz operating from 2.702 GHz to 2.897 GHz exhibits 195 MHz bandwidth (7%). The DRA exhibits 5.1 dBi gain in the optimum resonant band. Thus the truncation of the ground plane results in a compact antenna configuration displaying good radiation characteristics.

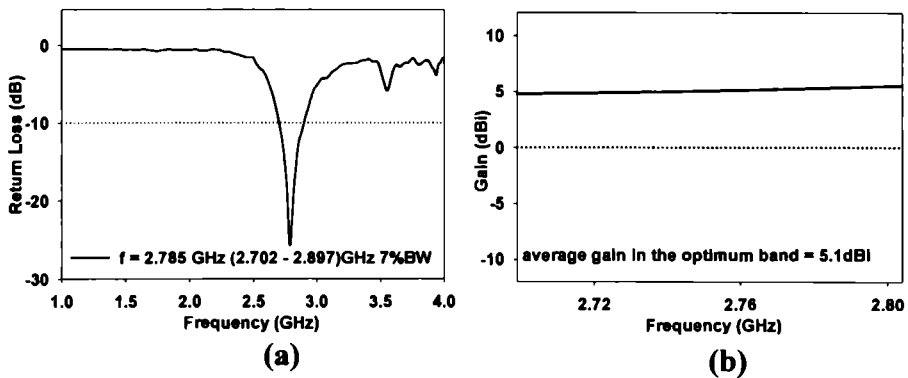


Figure 5.70 Characteristics of the DRA measured at the optimum bandwidth position
 (a) Return loss (b) Gain
 feed line length = 3 cm truncated ground plane: 3 x 4 sq cm
 DR-1 orientation : d-a-b $(d_x, d_y) = (0, 2.1)$ cm

The radiation patterns of the 3 cm line fed DRA measured in the truncated ground plane configuration are shown in Figure 5.71. The H plane pattern is broader than the E plane pattern. The radiation characteristics are summarised in Table 5.35.

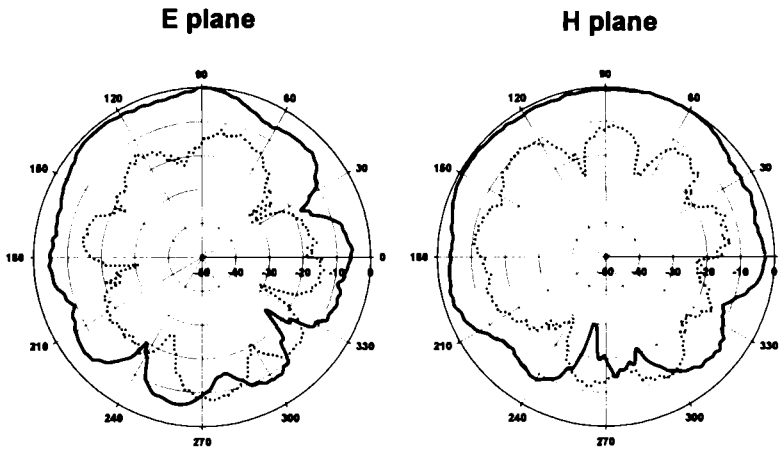


Figure 5.71 Radiation Pattern of the DRA measured at the optimum bandwidth position ($f = 2.785$ GHz)
 _____ co-polar cross-polar
 feed line length = 3 cm truncated ground plane: 3 x 4 sq cm
 DR-1 orientation : d-a-b (d_x, d_y) = (0,2.1) cm

Half power beam width (degree)		Front-to-Back Ratio along the Maxima (dB)		Cross-Polarisation along the Maxima (dB)	
E plane	H plane	E plane	H plane	E plane	H plane
70	126	10	19	-18	-16

Table 5.35 Radiation characteristics of the DRA measured at the optimum bandwidth position ($f = 2.785$ GHz)
 feed line length = 3 cm truncated ground plane: 3 x 4 sq cm
 DR-1 orientation : d-a-b (d_x, d_y) = (0,2.1) cm

Figure 5.72 illustrates the variation in resonant frequency and bandwidth of the DRA measured for increasing feed lengths. As the feed length is increased from 2 cm to 9 cm in the large ground plane configuration of the d-a-b orientation, the resonant frequency of the DRA at the optimum bandwidth position exhibits a variation from 2.65 GHz to 3.415 GHz. The 2:1 VSWR bandwidth varies from 5.1% to 10.3%. In the truncated ground plane configuration, the frequency varies from 2.53 GHz to 2.995 GHz, and the bandwidth varies from 2.8 % to 8.4 %.

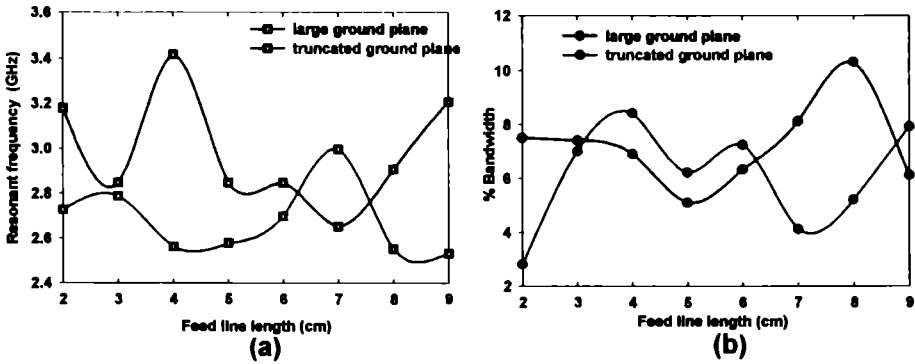


Figure 5.72 Variation in resonant behaviour of the DRA with feed length and ground plane dimensions at the optimum bandwidth position
 (a) Resonant frequency
 DR-1
 (b) % Bandwidth
 orientation : d-a-b

The return loss characteristics of the DRA in the d-a-b orientation, when excited by feed lengths ranging from 2 cm to 9 cm are summarised in Figure 5.73. Two resonant modes are observed at the optimum bandwidth position of the DRA excited by the 4 cm feed on a large ground plane. The lower mode exhibits lesser bandwidth with larger gain and the higher mode displays maximum bandwidth, though with lesser gain.

The experimental results suggest that the overall bandwidth performance is superior for the large ground plane configuration. However, a decision on the suitable configuration can be made only after the gain and radiation patterns are studied. The gain of the DRA in the d-a-b orientation, when excited by varying feed lengths and ground plane dimensions is shown in Figure 5.74.

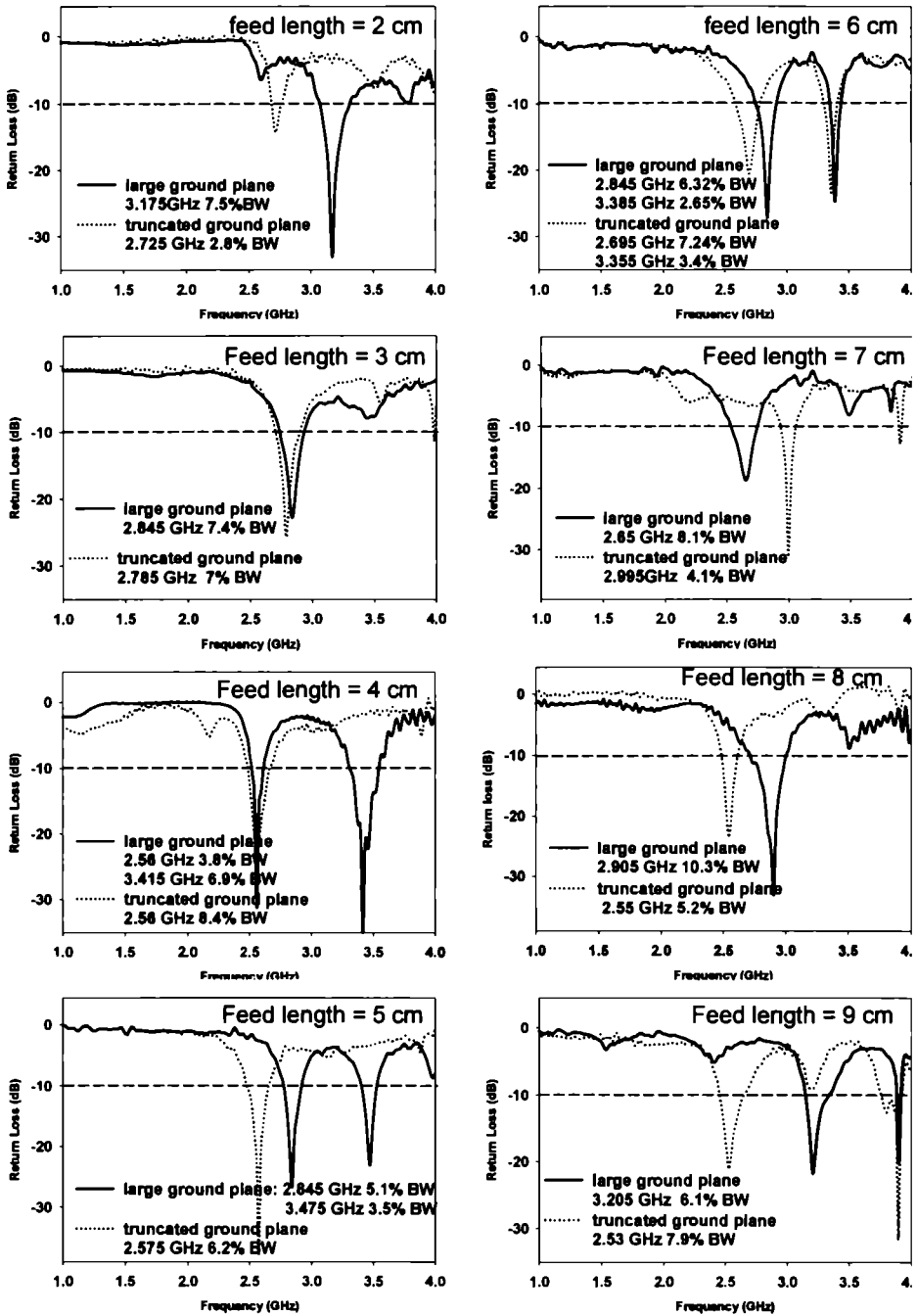


Figure 5.73 Return loss characteristics for varying feed lengths and ground plane dimensions measured at the optimum bandwidth position of the DRA DR-1 orientation : d-a-b

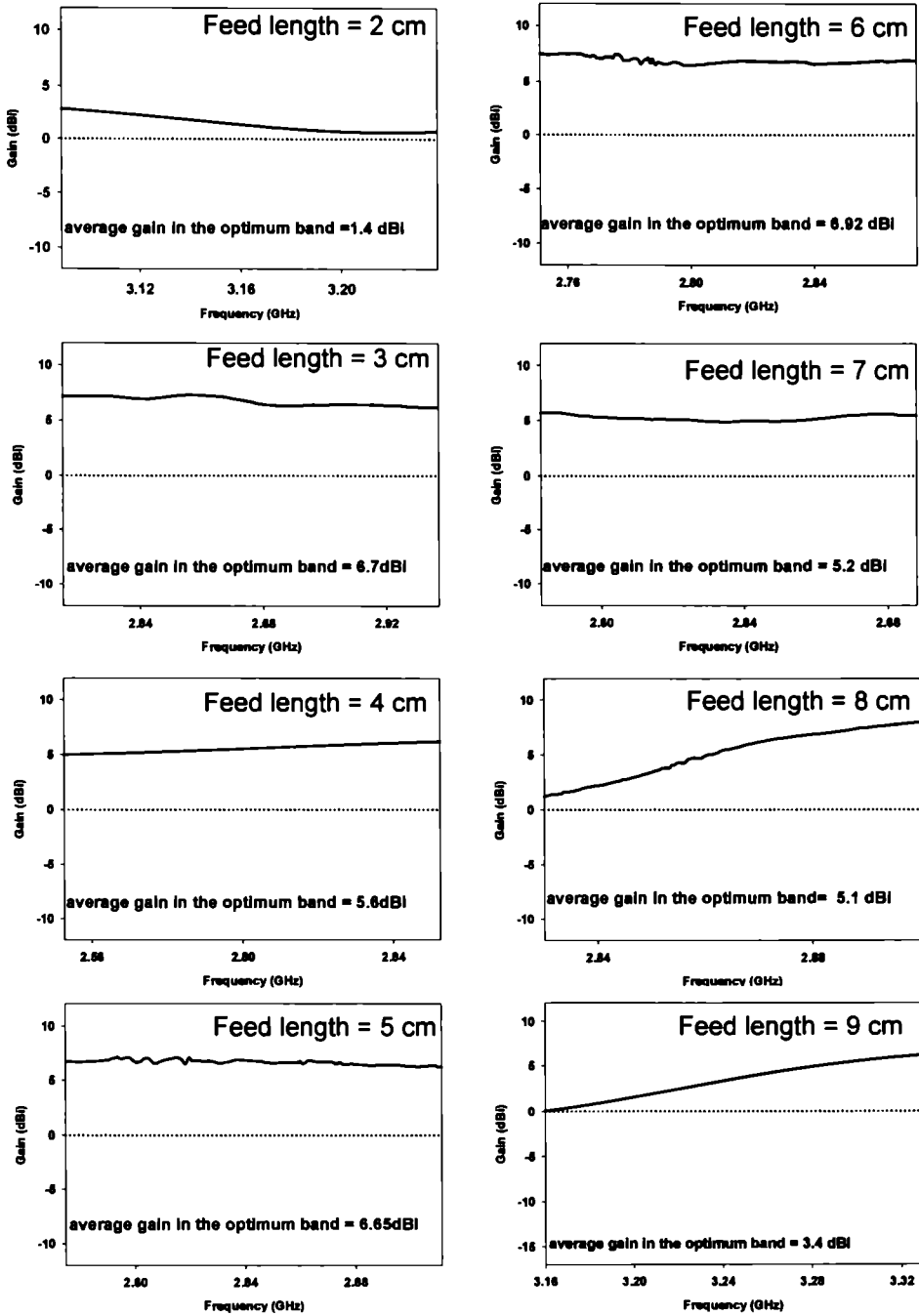


Figure 5.74(a) Gain of the DRA measured in the optimum band for varying feed lengths on a large ground plane orientation : d-a-b

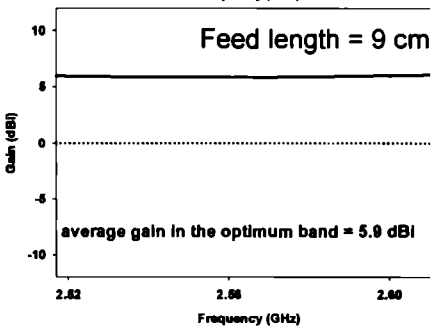
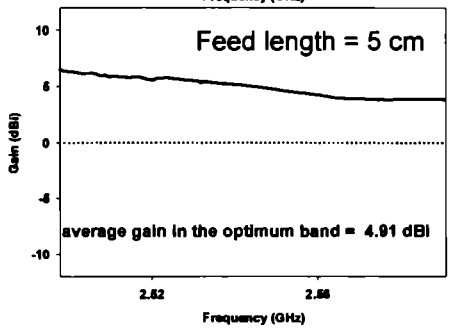
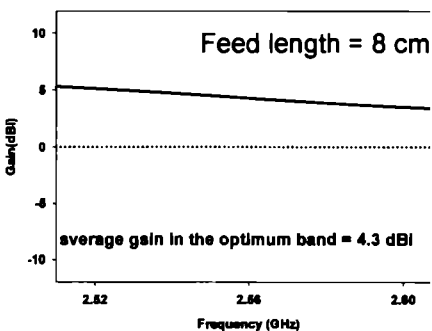
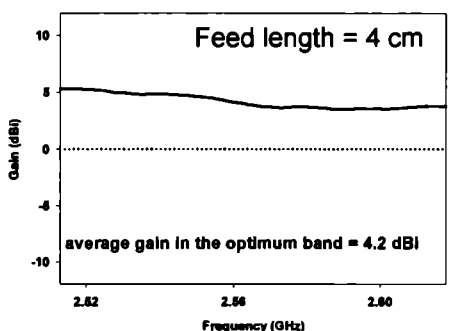
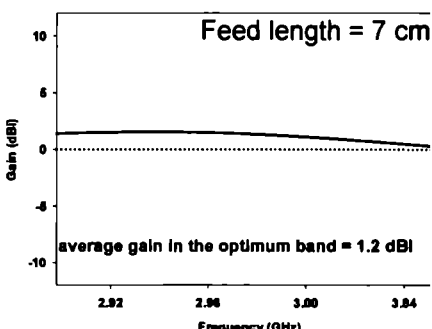
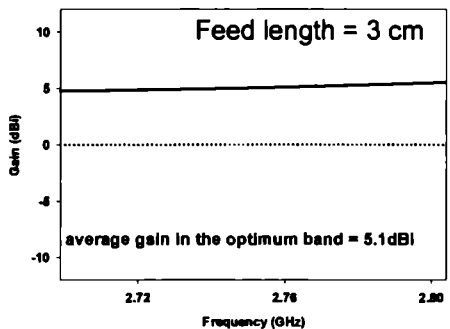
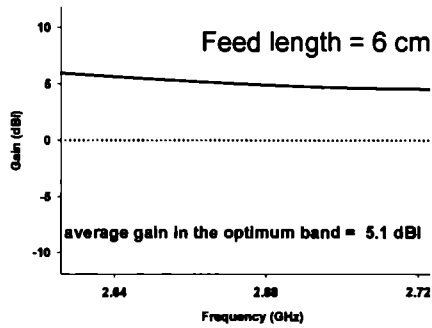
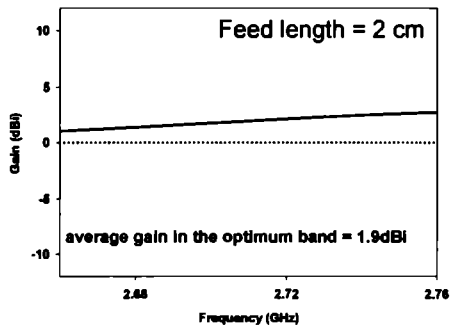


Figure 5.74(b) Gain of the DRA measured in the optimum band for vary feed lengths on a truncated ground plane DR-1 orientation : d-i

The variation of average gain in the optimum resonant band of the DRA for varying feed lengths is illustrated in Figure 5.75. The observations indicate that good gain is exhibited by the DRA in the d-a-b orientation when excited by all the feed lines in the large ground plane configuration, the 2 cm and 9 cm feed being exceptions. The gain performance deteriorates in the truncated ground plane configuration. The variation in radiation characteristics of the DRA with feed length is summarised in Table 5.36.

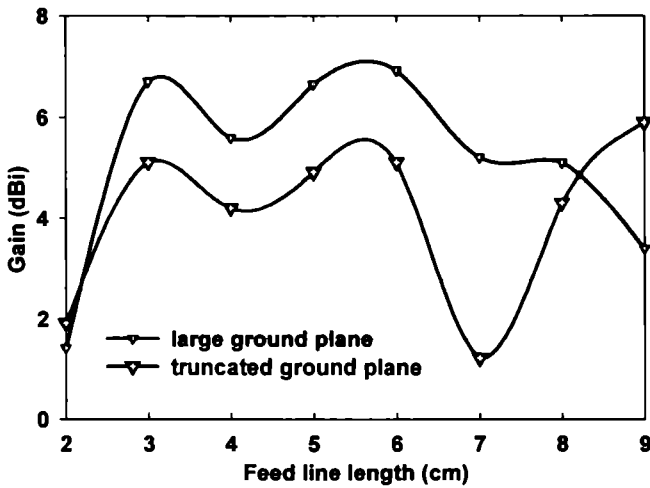


Figure 5.75 Variation in gain of the DRA with feed length and ground plane dimensions measured in the optimum band
DR-1 orientation: d-a-b

The principal plane radiation patterns are measured in the d-a-b orientation of the resonator for feeds varying in length from 2 cm to 9 cm. The patterns of the DRA excited by the 2 cm and 3 cm feeds in the large ground plane configuration were described earlier [Figures 5.57 and 5.68]. Figure 5.76 shows the principal plane patterns of the DRA excited by the 4 cm, 7 cm and 8 cm feeds. The characteristics obtained from the radiation pattern measurements are summed up in Table 5.37.

Feed Line length (cm)	Large Ground plane			Truncated Ground plane		
	Freq (GHz)	%BW	Avg gain (dBi)	Freq (GHz)	%BW	Avg gain (dBi)
2	3.175	7.5	1.4	2.725	2.8	1.9
3	2.845	7.4	6.7	2.785	7	5.1
4	2.56	3.8	5.6	2.56	8.4	4.2
5	2.845	5.1	6.65	2.575	6.2	4.91
6	2.845	6.32	6.92	2.695	7.24	5.1
7	2.65	8.1	5.2	2.995	4.1	1.2
8	2.905	10.3	5.1	2.55	5.2	4.3
9	3.205	6.1	3.4	2.53	7.9	5.9

Table 5.36 Variation in radiation characteristics of the DRA with feed length and ground plane dimensions measured at the optimum bandwidth position
DR-1 orientation: d-a-b

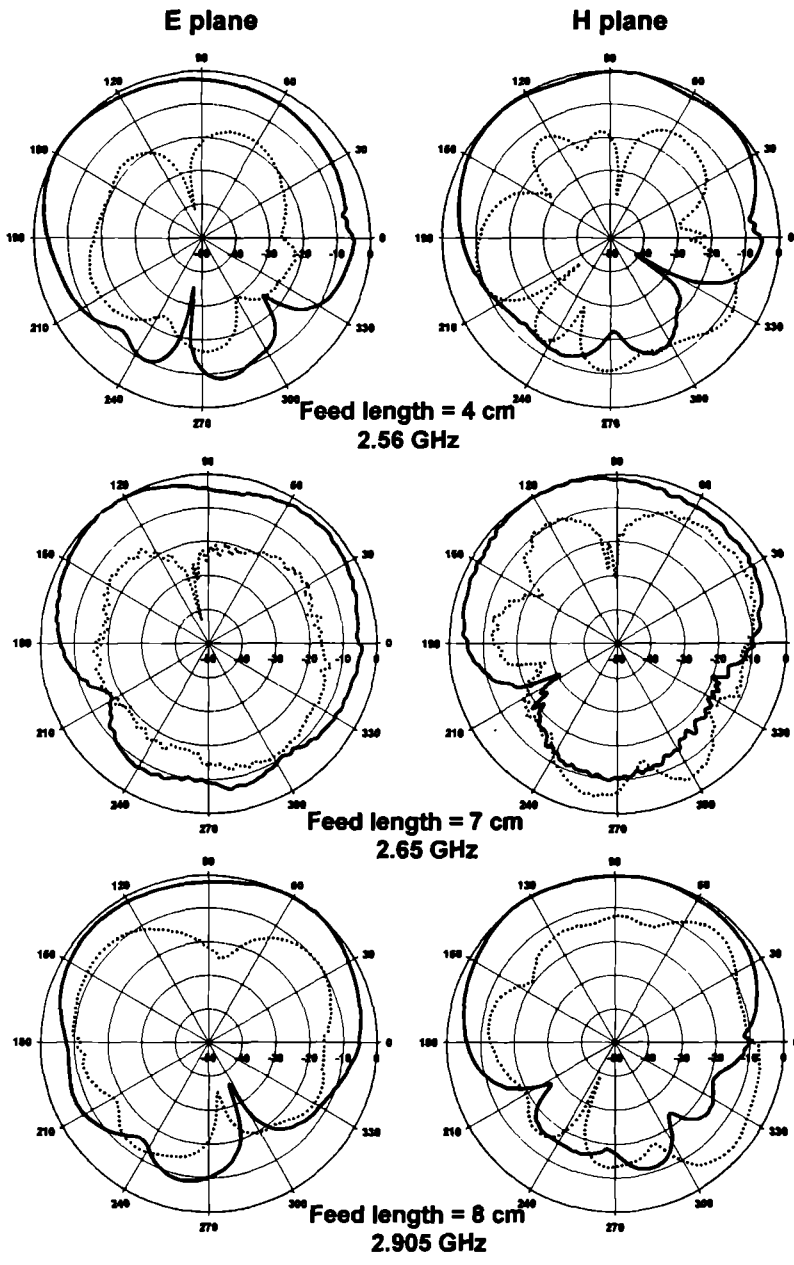


Figure 5.76 Radiation Pattern of the DRA for varying feed lengths measured at the optimum bandwidth position
 — co-polar cross-polar
 DR-1 large ground plane orientation : d-a-b

Feed Length (cm)	Half power beam width (degree)		Front-to-Back Ratio along the maxima (dB)		Cross-Polarisation along the maxima (dB)	
	E plane	H plane	E plane	H plane	E plane	H plane
2	50	80	13	6	-11	-28
3	176	58	15	17	-14	-19
4	94	136	14	12	-19	-38
5	70	104	10	17	-18	-30
6	70	126	10	19	-18	-16
7	62	88	10	14	-17	-9
8	134	130	15	19	-12	-15
9	75	40	6	17	-7	-4

Table 5.37 Radiation pattern characteristics of the DRA measured for varying feed lengths at the optimum bandwidth position
DR-1 large ground plane orientation : d-a-b

It is seen that the optimum bandwidth positions are not always symmetric with respect to the feed axis. The optimum position also varies with feed length and orientation. Figure 5.77 clearly illustrates the two positions of the DR in the d-a-b orientation at $d_x=d/2$ (the symmetrical position) and $d_x=0$ (DR edge lying along the feed axis). $d_x < d/2$ indicates a displacement to the left from the symmetrical position, and $d_x > d/2$ indicates a displacement to the right from the symmetrical position. Similarly, $0 < d_y < a$ indicates that the feed end lies within the DR. In the remaining positions ($d_y \geq a$), the configuration behaves like a DR loaded Microstrip line. Table 5.38 summarises the optimum bandwidth positions of the DR in the d-a-b orientation, when excited by feeds of varying lengths.

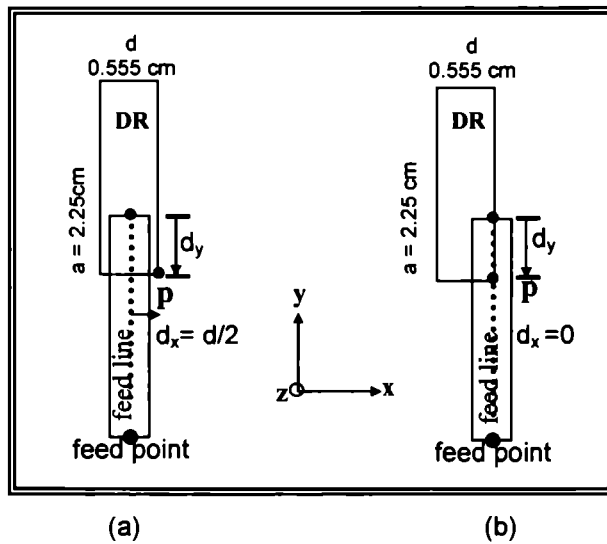


Figure 5.77 Lateral positions of the DR with respect to the feed axis (d_x, d_y) - distance of the DR vertex 'P' from the reference point along the x and y direction respectively
 DR-1 orientation: d-a-b
 (a) symmetrical (b) asymmetrical

Feed length (cm)	Ground plane ($l_g \times w_g$) sq cm	(d_x, d_y) cm
2	large (4 x 4)	0.25,1.5
	truncated (2 x 4)	0.28,1
3	large (5 x 4)	0.28,1.3
	truncated (3 x 4)	0,2.1
4	large (6 x 4)	0.5,2
	truncated (4 x 4)	0.2,3.2
5	large (7 x 4)	0,0.8
	truncated (5 x 4)	0.28,3.3
6	large (8 x 4)	0.28,1
	truncated (6 x 4)	0,3
7	large (9 x 4)	0.6,5.3
	truncated (7 x 4)	0.28,5.5
8	large (10 x 4)	0.28,0.5
	truncated (8 x 4)	0.28,3.2
9	large (11 x 4)	0.28,4.4
	truncated (9 x 4)	0.28,3.2

Table 5.38 The optimum bandwidth positions of the DR DR-1 orientation: d-a-b

5.1.3.10 Resonant behaviour of the DRA when the DR is placed symmetrically with respect to the feed axis

This section discusses the resonant behaviour of the DRA for varying feed lengths when the DR in the d-a-b orientation is placed symmetrically with respect to the feed axis at $(d_x, d_y) = (d/2, 0.5)$. Figure 5.78 illustrates the variation in resonant frequency and % bandwidth of the DRA with feed length.

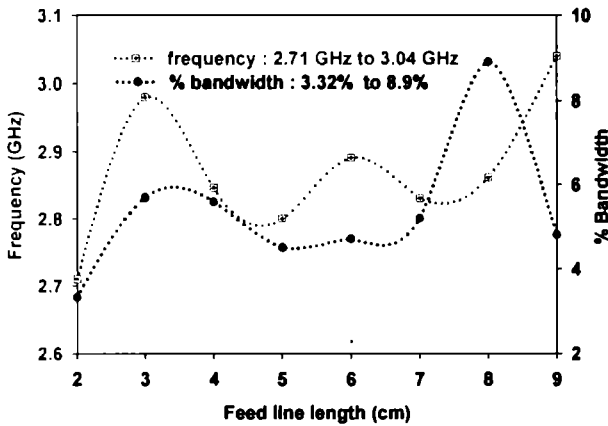


Figure 5.78 Variation in resonant frequency and % bandwidth of the DRA with feed length measured at a symmetrical position of the DR $[(d_x, d_y) = (d/2, 0.5)]$ cm large ground plane orientation : d-a-b DR-1

The varying feed lengths excite frequencies ranging from 2.71 GHz to 3.04 GHz, with an average bandwidth of 5.34%. Maximum bandwidth of 8.9% is exhibited by the 8 cm fed DRA at 2.86 GHz and the minimum bandwidth of 3.32% at 2.71 GHz by the 2 cm fed DRA. However, the low resonant frequency excited by the 2 cm feed results in a compact antenna configuration. The resonant characteristics are summarised in Table 5.39. The return loss characteristics for varying feed lengths are shown in Figure 5.79. Increase in feed length does not cause a significant change in the resonant frequency at this position of the DR. However, the bandwidth exhibits considerable variation as shown in Figures 5.78 and 5.79.

	Feed Length (cm)							
	2	3	4	5	6	7	8	9
Freq (GHz)	2.71	2.98	2.845	2.8	2.89	2.83	2.86	3.04
%BW	3.32	5.7	5.6	4.5	4.7	5.2	8.9	4.8

Table 5.39 Resonant behaviour of the DRA for varying feed lengths measured at a symmetrical position of the DR
 $(d_x, d_y) = (d/2, 0.5)$ cm large ground plane
 DR-1 orientation : d-a-b

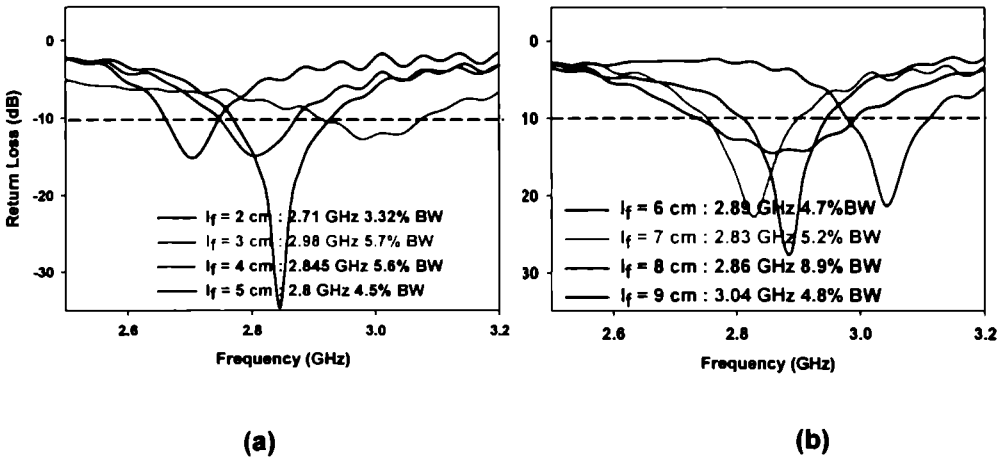


Figure 5.79 Return loss of the DRA for varying feed lengths measured at a symmetrical position of the DR
 (a) feed length = 2 cm to 5 cm (b) feed length = 6 cm to 9 cm
 large ground plane $(d_x, d_y) = (d/2, 0.5)$ cm
 DR-1 orientation: d-a-b

5.1.3.11 Salient features of the d-a-b orientation

The d-a-b orientation is noteworthy because of the low resonant frequencies excited as the DR is positioned at various locations upon the feed line. At 3.175 GHz, the 2 cm line fed DRA offers 58.5% size reduction with respect to a rectangular Microstrip antenna resonating at the same frequency. Table 5.36 and 5.37 sum up the characteristics of this orientation. In the large ground plane configuration, the varying feed line lengths excite frequencies in the S-band, providing an average gain of 5.12 dBi, and average 2:1 VSWR bandwidth of 6.82%. The 6 cm feed offers the maximum gain (6.92 dBi). The lower order mode excited by the 4 cm feed at the optimum bandwidth position has the lowest resonant frequency (2.56 GHz), while the maximum 2:1 VSWR bandwidth (10.3%) is provided by the 8 cm feed. The radiation patterns are generally broad - the average half-power beam width along the E plane and H plane being 91.4° and 95.3° respectively. The 8 cm line fed DRA offers the broadest radiation pattern with 134° and 130° half-power beam width respectively in the E and H planes [Figure 5.76].

The truncated ground plane configuration exhibits an average gain of 4.1 dBi and average 2:1 VSWR bandwidth of 6.1%. The overall performance is therefore comparable to that of the large ground plane configuration for most of the feed lengths unlike the a-b-d and b-a-d orientations. Also, this configuration acquires significance where the size of the antenna is of priority.

Investigations performed on the Dielectric Resonator Antenna incorporating the rectangular resonator sample DR-1 in the d-a-b orientation confirm the dependence of the antenna characteristics upon the feed length, ground plane dimensions and position of the DR. The performance of the DRA excited by Microstrip line feed of length 3 cm is noteworthy in lieu of its overall compactness, bandwidth and gain.

5.1.4 The d-b-a orientation

In comparison with the a-b-d, b-a-d and d-a-b orientations discussed in the previous sections, the d-b-a orientation is a relatively high profile orientation [aspect ratio=1.9], as explained in Section 5.1. Figure 5.80 illustrates the orientation.

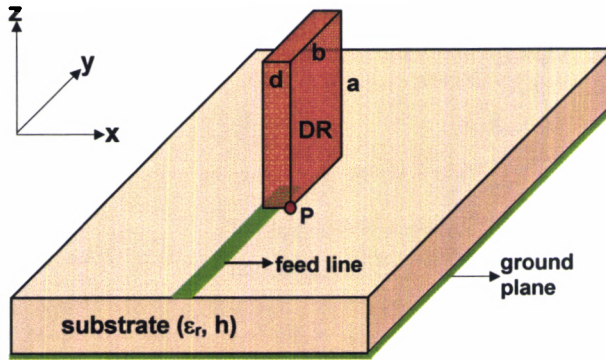


Figure 5.80 The d-b-a orientation of the Dielectric Resonator DR-1 $a \times b \times d = [2.25 \times 1.19 \times 0.555] \text{ cm}^3$
substrate: $\epsilon_r = 4.28$, $h = 0.16 \text{ cm}$

5.1.4.1 Return loss characteristics

The return loss characteristics are computed numerically employing the FDTD method and the position of the DR with respect to the feed line (d_x, d_y) is optimised for maximum 2:1 VSWR bandwidth. The numerical results are validated experimentally. Measurements are recorded for varying dimensions of the feed line and ground plane. Figure 5.81 shows the return loss characteristics of the DRA excited by the 2 cm feed. Theoretically the antenna is found to resonate at 3.2931 GHz in a band operating from 3.1239 GHz to 3.3842 GHz with 260 MHz bandwidth (7.9%) when placed at $(d_x, d_y) = (0.28, 1.3) \text{ cm}$. Two resonant modes are observed experimentally at 3.16 GHz and 3.4 GHz, operating from 3.079 GHz to 3.426 GHz in a band centred at 3.28 GHz, exhibiting 347 MHz bandwidth (10.6%). The polarization of both these modes is linear and is directed along the dimension 'b' of the resonator, parallel to the feed axis. The centre frequency of the experimentally

observed resonant band differs from the numerically computed frequency by -0.4% . The field distribution within the 2 cm fed DR in the d-b-a orientation at 3.2931 GHz is shown in Figure 5.82. The resonant mode is identified as TE_{210}^z through simulation using HFSS™. The resonant fields undergo two half-wave variations along dimension ‘a’ and one half-wave variation along dimension ‘b’. The fields remain constant along dimension ‘d’. FDTD theory and experiment also give similar results.

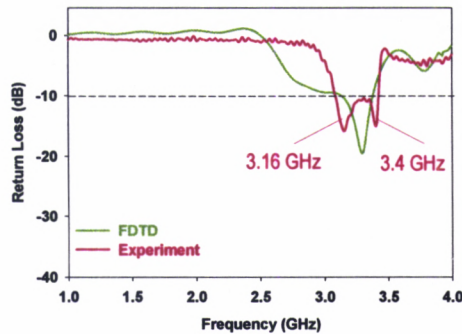


Figure 5.81 Return loss characteristics of the DRA at the optimum bandwidth position
 feed line length = 2 cm large ground plane: 4 x 4 sq cm
 DR-1 orientation : d-b-a (d_x, d_y) = (0.28, 1.3) cm

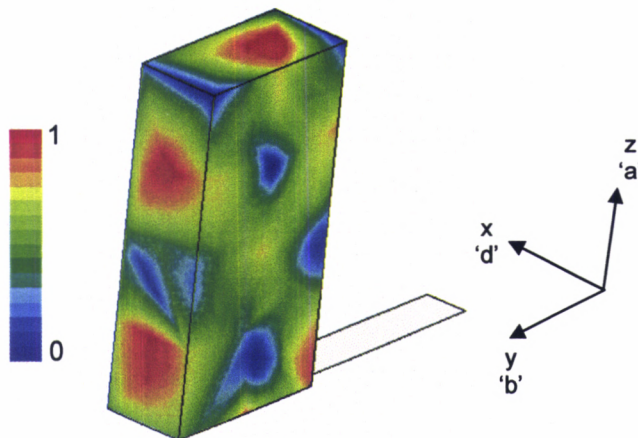


Figure 5.82 Simulated H field distribution within the DR at the optimum bandwidth position $f = 3.2931$ GHz
 feed line length = 2 cm large ground plane: 4 x 4 sq cm
 DR-1 orientation : d-b-a (d_x, d_y) = (0.28, 1.3) cm

At 3.28 GHz, the 2 cm fed DRA incorporating the resonator in the d-b-a orientation is found to possess 89% and 86.3% reduction in cross-section area with respect to a Rectangular and Circular Microstrip antenna designed to operate at the same frequency. Table 5.40 provides a comparison of the dimensions of different antennas operating at 3.28 GHz.

Antenna	Dimensions (cm)	Area (sq cm)
DRA in the d-b-a orientation	Length (d) = 0.555 Width (b) = 1.19	(d x b) 0.67
Rectangular Microstrip antenna	Length = 2.17 Width = 2.81	6.1
Circular Microstrip antenna	Radius = 1.245	4.87

Table 5.40 Dimensions of different antennas operating at 3.28 GHz

The truncation of the ground plane results in deterioration of the resonant behaviour of the DRA as shown in Figure 5.83. A resonant mode at 3.46 GHz operating from 3.43 GHz to 3.48 GHz exhibits a narrow bandwidth of 50 MHz (1.5%) at the position $(d_x, d_y) = (0.5, 1)$ cm.

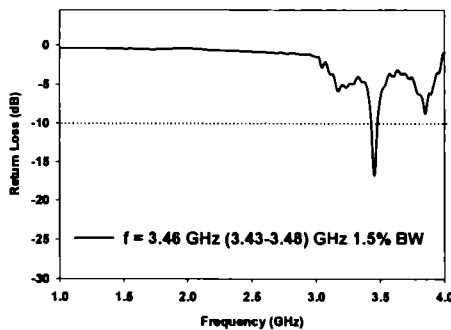


Figure 5.83 Return loss characteristics of the DRA measured at the optimum bandwidth position.
 feed line length = 2 cm truncated ground plane: 2x4 sq cm
 DR-1 orientation : d-b-a $(d_x, d_y) = (0.5, 1)$ cm

The variation in return loss characteristics with increasing feed lengths is illustrated in Figure 5.84. At the optimum bandwidth position, frequencies in the range 3.1 GHz to 3.325 GHz are excited by different feed lengths when the DR in the d-b-a orientation is placed on a large ground plane. The 4 cm feed excites the highest frequency and the 6 cm feed excites the lowest frequency. The 3 cm feed displays maximum bandwidth (15.4%). Minimum bandwidth (4.27%) is exhibited by the 4 cm feed. The average bandwidth observed in the d-b-a orientation on a large ground plane is 10.21%. When the DR is placed on a truncated ground plane, frequencies in the range 3.1 GHz to 3.46 GHz are excited by different feed lengths at the optimum bandwidth position. Highest frequency is excited by the 2 cm feed and the lowest frequency is excited by the 6 cm feed. Maximum (11.6%) and minimum (1.45%) bandwidth is exhibited by the 7 cm and 2 cm feeds respectively. The average bandwidth observed in the d-b-a orientation on a truncated ground plane is 6.77%.

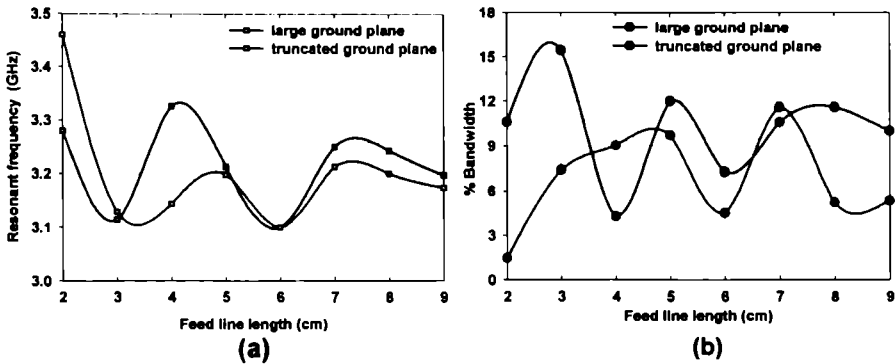


Figure 5.84 Variation in resonant behaviour of the DRA with feed length and ground plane dimensions measured at the optimum bandwidth position
 (a) Resonant frequency (b) % Bandwidth
 DR-1 orientation : d-b-a

5.1.4.2 Radiation Pattern

The principal plane radiation patterns are measured in the d-b-a orientation of the resonator for feed lengths varying from 2 cm to 9 cm. Figure 5.85 illustrates the principal plane patterns measured experimentally at both the resonant frequencies

(3.16 GHz and 3.4 GHz) in the optimum band of the 2 cm fed DRA in the d-b-a orientation. It is observed that the radiation patterns are broad throughout the operating band and have a broad coverage. This is highly suitable for Mobile Communication applications.

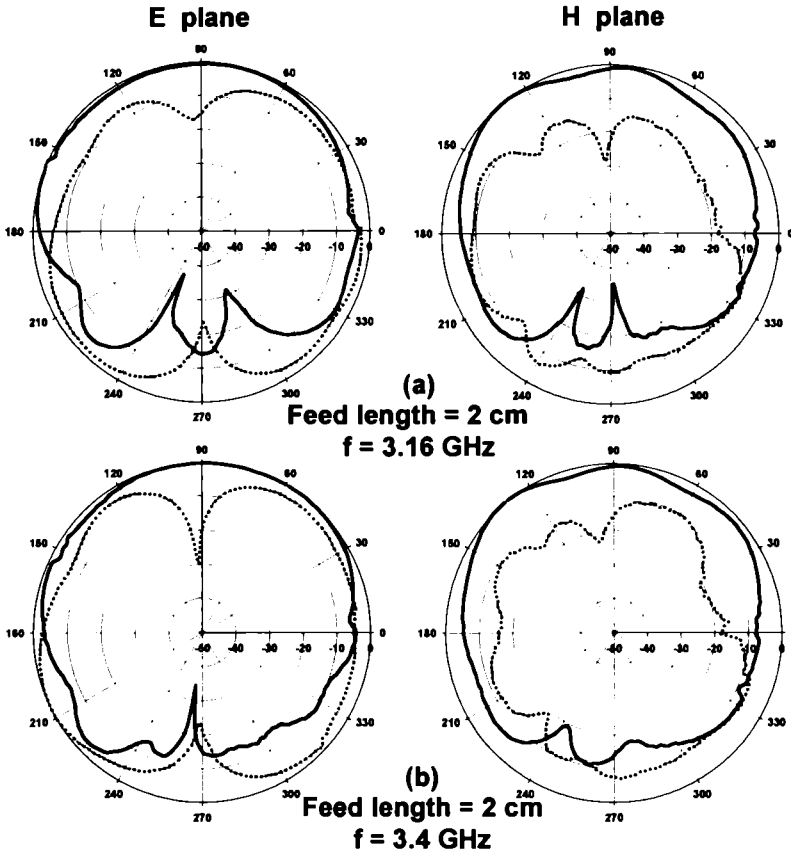


Figure 5.85 Radiation Pattern of the DRA measured at the optimum bandwidth position — co-polar cross-polar
 feed length = 2 cm large ground plane: 4×4 sq cm
 DR-1 orientation : d-b-a $(d_x, d_y) = (0.28, 1.3)$ cm
 (a) $f = 3.16$ GHz (b) $f = 3.4$ GHz

The radiation patterns of the 3 cm fed DRA also exhibit broad radiation coverage as shown in Figure 5.86. Table 5.41 summarises the radiation pattern characteristics of DRA excited by varying feed lengths.

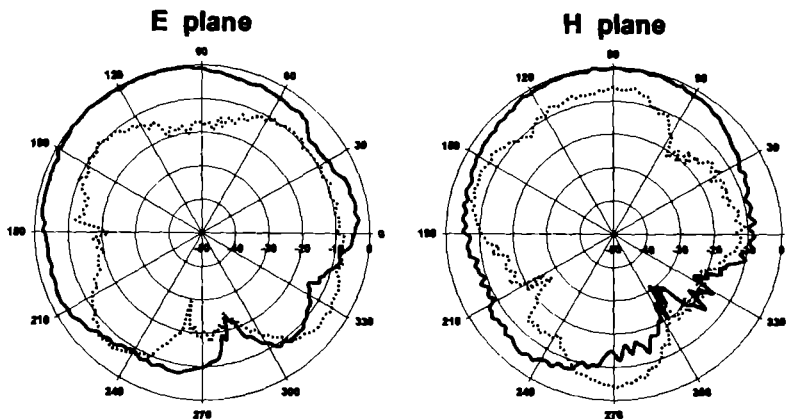


Figure 5.86 Radiation Pattern of the DRA measured at the optimum bandwidth position ($f = 3.115$ GHz)
 — co-polar cross-polar
 feed line length = 3 cm (d_x, d_y) = (0.25, 0.6) cm
 DR-1 orientation : d-b-a large ground plane: 5 x 4 cm

Feed Length (cm)	Half power beam width (degree)		Front-to-Back Ratio along the maxima (dB)		Cross-Polarisation along the maxima (dB)	
	E plane	H plane	E plane	H plane	E plane	H plane
2	159	90	12	10	-4	-17
3	102	90	9	16	-11	-8
4	38	86	9	7	-4	-11
5	66	84	14	6	-16	-14
6	58	104	6	7	-16	-13
7	84	28	10	16	-7	-11
8	62	62	8	5	-11	-14
9	24	42	13	9	-6	-21

Table 5.41 Radiation pattern characteristics of the DRA for varying feed lengths measured at the optimum bandwidth position
 DR-1 large ground plane orientation : d-b-a

5.1.4.3 Gain

The 2 cm line fed DRA in the d-b-a orientation of the resonator exhibits an average gain of 5.9 dBi and 4.74 dBi in the optimum resonant band when placed on a large ground plane and truncated ground plane respectively as shown in Figure 5.87. The variation in the average gain of the DRA in the optimum resonant band for varying feed lengths and ground plane dimensions is illustrated in Figure 5.88.

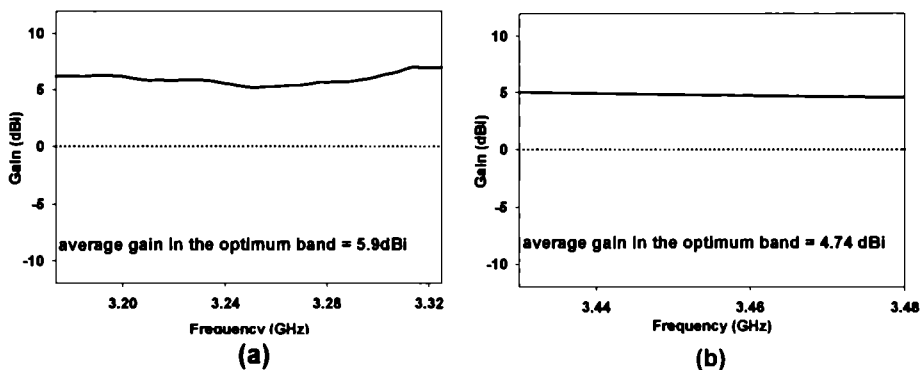


Figure 5.87 Gain of the DRA measured in the optimum band
 (a) large ground plane: 4 x 4 sq cm $(d_x, d_y) = (0.28, 1.3)$ cm
 (b) truncated ground plane: 2 x 4 sq cm $(d_x, d_y) = (0.5, 1)$ cm
 DR-1 feed line length = 2 cm orientation : d-b-a

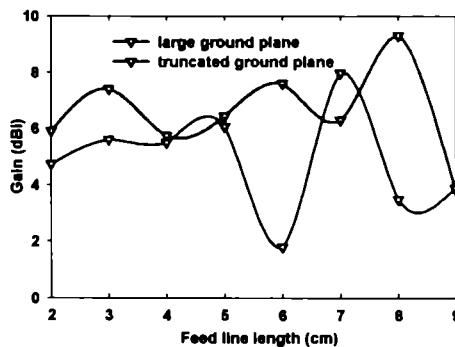


Figure 5.88 Variation in gain of the DRA with feed length and ground plane dimensions measured in the optimum band
 DR-1 orientation : d-b-a

Though the d-b-a orientation exhibits good gain when excited by different feed lengths, the large aspect ratio of the DR makes it attractive only in applications where the antenna footprint is not a major concern. The truncated ground plane configuration is attractive in view of its overall compactness. But, the resonant and radiation behaviour is found to deteriorate as the ground plane dimensions are reduced. Consequently this configuration will be useful in compact antenna structures where other compensation techniques can be employed to improve the antenna performance. The variation in radiation characteristics of the DRA with feed length and ground plane dimensions in the d-b-a orientation is summarised in Table 5.42.

Feed Line length (cm)	Large Ground plane			Truncated Ground plane		
	Freq (GHz)	%BW	Avg gain (dBi)	Freq (GHz)	%BW	Avg gain (dBi)
2	3.28	10.6	5.9	3.46	1.5	4.74
3	3.115	15.4	7.4	3.13	7.4	5.6
4	3.325	4.3	5.8	3.145	9.01	5.5
5	3.2125	12	6.4	3.1975	9.7	6.06
6	3.1	7.3	7.6	3.1	4.5	1.8
7	3.25	10.6	6.3	3.2125	11.6	7.97
8	3.2425	11.6	9.3	3.2	5.2	3.5
9	3.1975	10	3.9	3.175	5.32	3.9

Table 5.42 Variation in radiation characteristics of the DRA with feed length and ground plane dimensions measured at the optimum bandwidth position
DR-1 orientation: d-b-a

5.1.4.4 Resonant behaviour at different positions of the DR with respect to the feed

The resonant behaviour of the antenna when the DR in the d-b-a orientation is placed at discrete intervals of 0.25 cm along the x and y directions [$0.25 \leq d_x \leq 0.5$, $0.25 \leq d_y \leq 0.75$], on a 2 cm feed is discussed in this section. Figure 5.89 illustrates the return loss characteristics on a large ground plane at discrete positions of the DR. The resonant frequency varies from 3.565 GHz to 3.64 GHz and the 2:1 VSWR bandwidth in the dominant resonant band exhibit a variation from 0.4% to 3.96%.

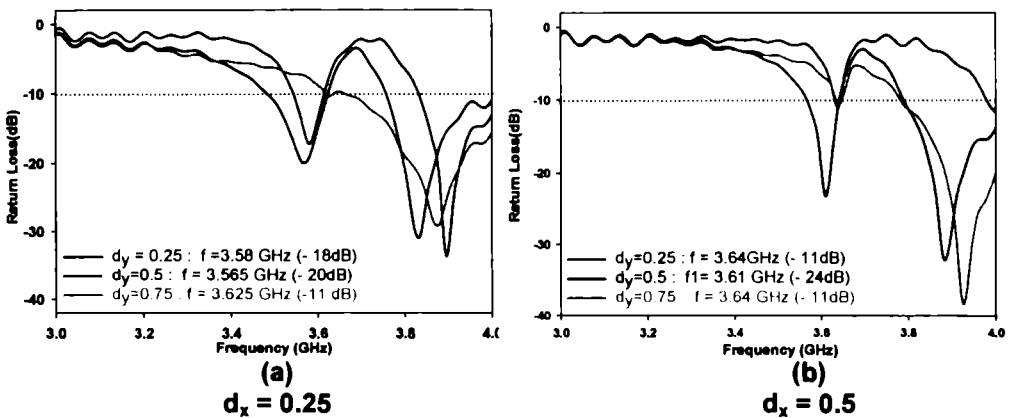


Figure 5.89 Return loss characteristics of the DRA at different d_y locations of the DR
 feed line length = 2 cm large ground plane: 4 x 4 sq cm
 DR-1 orientation : d-b-a

It is observed that the higher resonant modes exhibit considerably greater bandwidth (up to 8.8%). But at an intermediate position [$(d_x, d_y) = (0.28, 1.3)$ cm], two resonant modes at 3.16 GHz and 3.4 GHz combine to exhibit 10.6% bandwidth in a band centred at 3.28 GHz as described in Section 5.1.4.1 [Figure 5.81]. Figure 5.90 illustrates the dependence of the resonant frequency and bandwidth of the dominant mode on the position of the DR with respect to the feed line. The resonant behaviour of the DRA at the discrete positions in the d-b-a orientation is summarised in Table 5.43.

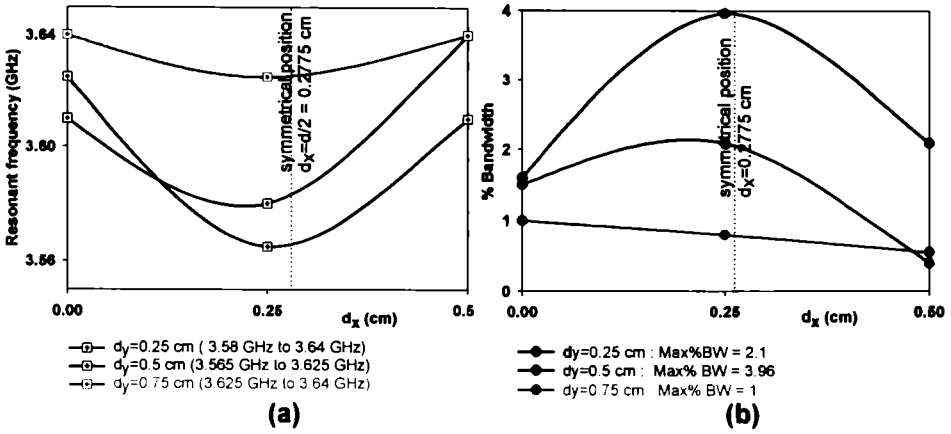


Figure 5.90 Variation in the resonant behaviour of the DRA measured with the position of the DR on the feed
 (a) Resonant frequency (b) % Bandwidth
 feed line length : 2 cm large ground plane: 4 x 4 sq cm
 DR-1 orientation: d-b-a

Resonant frequency (GHz)			
d_y (cm)	d_x (cm)		
	0	0.25	0.5
0.25	3.61	3.58	3.64
0.5	3.625	3.565	3.61
0.75	3.64	3.625	3.64

(a)

% bandwidth			
d_y (cm)	d_x (cm)		
	0	0.25	0.5
0.25	1.5	2.1	0.4
0.5	1.6	3.96	2.1
0.75	1	0.8	0.55

(b)

Table 5.43 Resonant behaviour of the DRA measured at various positions of the DR on the feed line
 (a) Resonant frequency (GHz)
 (b) % Bandwidth
 feed line length : 2 cm large ground plane: 4 x 4 sq cm
 DR-1 orientation: d-b-a

It is observed that for varying feed length and ground plane dimensions, the maximum bandwidth is not always obtained when the DR is placed symmetrically with respect to the feed [$d_x = d/2 = 0.2775$ cm]. Table 5.44 summarises the optimum bandwidth positions of the DR in the d-b-a orientation when excited by feeds of varying lengths.

Feed length (l_f) cm	Ground plane ($l_g \times w_g$) sq cm	(d_x, d_y) cm
2	large (4 x 4)	0.28, 1.3
	truncated (2 x 4)	0.5, 1
3	large (5 x 4)	0.25, 0.6
	truncated (3 x 4)	0, 1.7
4	large (6 x 4)	0.5, 2.4
	truncated (4 x 4)	0.25, 2
5	large (7 x 4)	0, 1.5
	truncated (5 x 4)	0.25, 3.9
6	large (8 x 4)	0.25, 4.5
	truncated (6 x 4)	0.25, 1.5
7	large (9 x 4)	0.25, 1.8
	truncated (7 x 4)	0.25, 4.3
8	large (10 x 4)	0, 1.2
	truncated (8 x 4)	0.25, 1.6
9	large (11 x 4)	0.25, 1.5
	truncated (9 x 4)	0.25, 4

Table 5.44 The optimum bandwidth positions of the DR DR-1 orientation: d-b-a

5.1.4.5 Resonant behaviour of the DRA when the DR is placed symmetrically with respect to the feed axis

This section discusses the resonant behaviour of the DRA for varying feed lengths when the DR in the d-b-a orientation is placed symmetrically with respect to the feed axis at $(d_x, d_y) = (d/2, 0.5)$ cm. Figure 5.91 illustrates the variation in resonant frequency and % bandwidth of the DRA with feed length at this position of the DR.

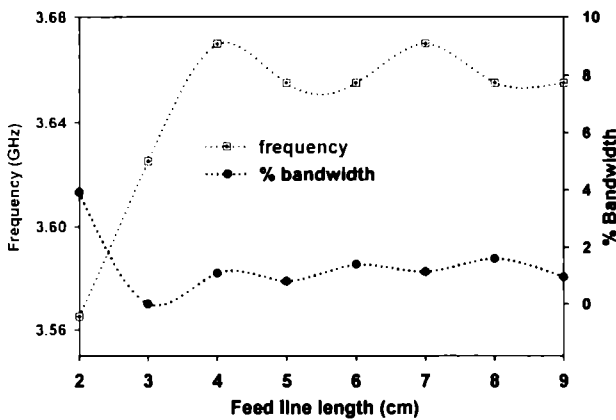


Figure 5.91 Variation in resonant frequency and % bandwidth of the DRA with feed length measured at a symmetrical position of the DR $(d_x, d_y) = (d/2, 0.5)$ cm large ground plane orientation : d-b-a DR-1

The varying feed lengths excite frequencies ranging from 3.565 GHz to 3.67 GHz, with an average bandwidth of 1.4%. The 3 cm feed fails to provide sufficient impedance matching to the resonant frequency at 3.625 GHz at this position. Maximum bandwidth of 3.92% is exhibited by the 2 cm fed DRA at 3.565 GHz. The observations indicate that the bandwidth performance of the DRA in the d-b-a orientation of the resonator placed at $[(d_x, d_y) = (d/2, 0.5)]$ is far inferior to that of the other orientations at the same position. Nevertheless, the influence of the feed length on the return loss characteristics is evident from Figure 5.91. The 2 cm fed DRA is preferred over the rest because of its overall compactness and moderate bandwidth.

5.1.4.6 Salient features of the d-b-a orientation

The d-b-a orientation is a relatively high profile orientation. Nevertheless, at 3.28 GHz the 2 cm fed DRA offers ~89% size reduction with respect to a Rectangular Microstrip Antenna resonating at the same frequency. Table 5.41 and Table 5.42 sum up the characteristics of this orientation. The varying feed line lengths excite frequencies in the S-band in the large ground plane configuration, providing an average gain of 6.6 dBi, and average 2:1 VSWR bandwidth of 10.2%. The 8 cm feed offers the maximum gain (9.3 dBi). The lowest resonant frequency (3.1 GHz) is excited by the 6 cm feed and the maximum 2:1 VSWR bandwidth (15.4%) is provided by the 3 cm feed. The 2 cm line fed DRA offers the broadest radiation pattern at 3.4 GHz with 159° and 90° half-power beam width respectively in the E and H planes [Figure 5.85(b)]. The truncated ground plane configuration exhibits an average gain of 4.8 dBi and average 2:1 VSWR bandwidth of 6.8% for varying feed lengths. The performance is therefore relatively inferior to that of the large ground plane configuration. However, it acquires significance where the size of the antenna is of priority.

The above investigations performed on the Dielectric Resonator Antenna incorporating the rectangular resonator sample DR-1 in the d-b-a orientation confirm the dependence of the antenna characteristics upon the feed length, ground plane dimensions and position of the DR. The performance of the DRA excited by Microstrip line feeds of length 2 cm and 3 cm is noteworthy in lieu of its overall compactness, bandwidth, gain and broad radiation pattern.

5.1.5 The a-d-b orientation

The a-d-b orientation has the second highest profile among the six possible orientations of the rectangular resonator [aspect ratio =2.14]. Figure 5.92 illustrates the orientation.

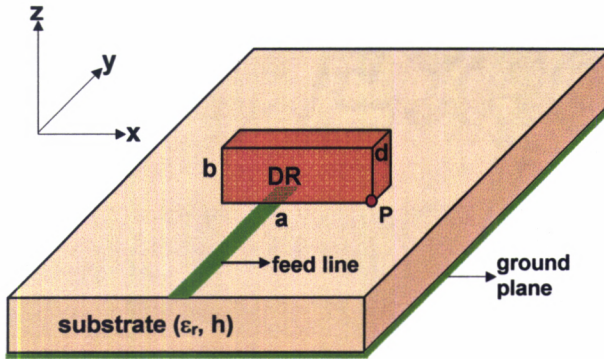


Figure 5.92 The a-d-b orientation of the Dielectric Resonator
 $a \times b \times d = [2.25 \times 1.19 \times 0.555] \text{ cm}^3$
 substrate: $\epsilon_r = 4.28$, $h = 0.16 \text{ cm}$

5.1.5.1 Return loss characteristics

The return loss characteristics are computed numerically employing the FDTD method and the position of the DR with respect to the feed line (d_x, d_y) is optimised for maximum 2:1 VSWR bandwidth. The numerical results are validated experimentally. Measurements are recorded for varying dimensions of the feed line and ground plane. Figure 5.93 shows the return loss characteristics of the DRA excited by the 2 cm feed. Theoretically the antenna is found to resonate at 3.6315 GHz in a band operating from 3.5665 GHz to 3.6793 GHz with 112.8 MHz bandwidth (3.1%) when placed at $(d_x, d_y) = (1.5, 0.25) \text{ cm}$. Two closely spaced resonant frequencies at 3.55 GHz and 3.685 GHz observed experimentally at this position combine together in a frequency band centred at 3.6175 GHz, operating from 3.479 GHz to 3.814 GHz, to provide 335 MHz bandwidth (9.3%). Both these modes are linearly polarized along the dimension 'd' of the resonator, parallel to the feed axis. The centre frequency of the experimental data differs from the numerically

predicted frequency by -0.38% . The field distribution within the 2 cm fed DR in the a-d-b orientation at 3.6315 GHz is shown in Figure 5.94. The resonant mode is identified as TE_{210}^z through simulation using HFSSTM. The resonant fields undergo two half-wave variations along dimension 'a' and one half-wave variation along dimension 'b'. The fields remain constant along dimension 'd'. FDTD theory and experiment also give similar results

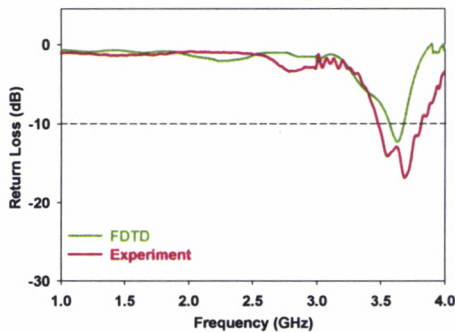


Figure 5.93 Return loss characteristics of the DRA at the optimum bandwidth position.
 feed line length = 2 cm large ground plane: 4 x 4 sq cm
 DR-1 orientation : a-d-b (d_x, d_y) = (1.5, 0.25) cm

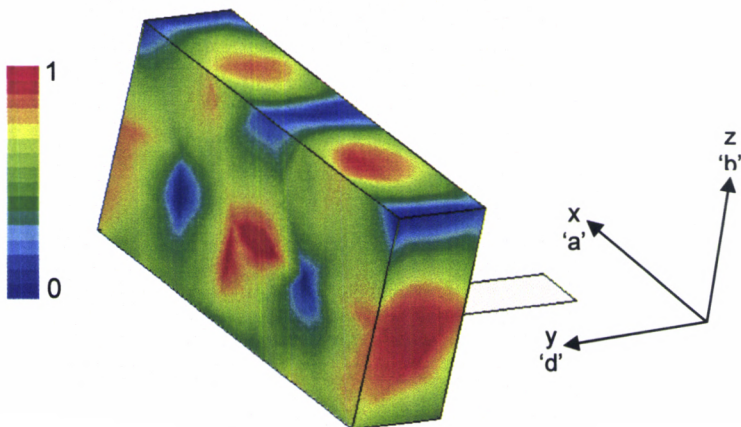


Figure 5.94 Simulated H field distribution within the DR at the optimum bandwidth position ($f = 3.6315$ GHz)
 feed line length = 2 cm large ground plane: 4x4 sq cm
 DR-1 orientation : a-d-b (d_x, d_y) = (1.5, 0.25) cm

At 3.6175 GHz, the 2 cm fed DRA incorporating the resonator in the a-d-b orientation is found to possess 75% and 68.5% reduction in the cross-section area with respect to a Rectangular and Circular Microstrip Antenna designed to operate at the same frequency. Table 5.45 provides a comparison of the dimensions of different antennas operating at 3.6175 GHz.

Antenna	Dimensions (cm)	Area (sq cm)
DRA in the a-d-b orientation	Length (a) = 2.25 Width (d) = 0.555	(a x d) 1.25
Rectangular Microstrip Antenna	Length = 1.9581 Width = 2.5520	4.997
Circular Microstrip Antenna	Radius = 1.125	3.98

Table 5.45 Dimensions of different antennas operating at 3.6175 GHz

Figure 5.95 illustrates the resonant behaviour of the DRA in the truncated ground plane configuration. A resonant mode at 3.565 GHz operating from 3.454 GHz to 3.615 GHz and exhibiting a bandwidth of 161 MHz (4.5%) is experimentally observed at $(d_x, d_y) = (1.125, 0.5)$ cm. The variation in return loss characteristics with increasing feed lengths is illustrated in Figure 5.96.

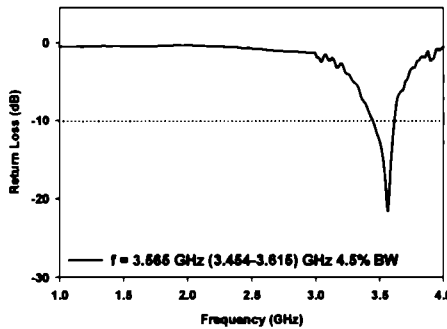


Figure 5.95 Return loss characteristics of the DRA measured at the optimum bandwidth position.
 feed line length = 2 cm truncated ground plane: 2x4 sqcm
 DR-1 orientation : a-d-b $(d_x, d_y) = (1.125, 0.5)$ cm

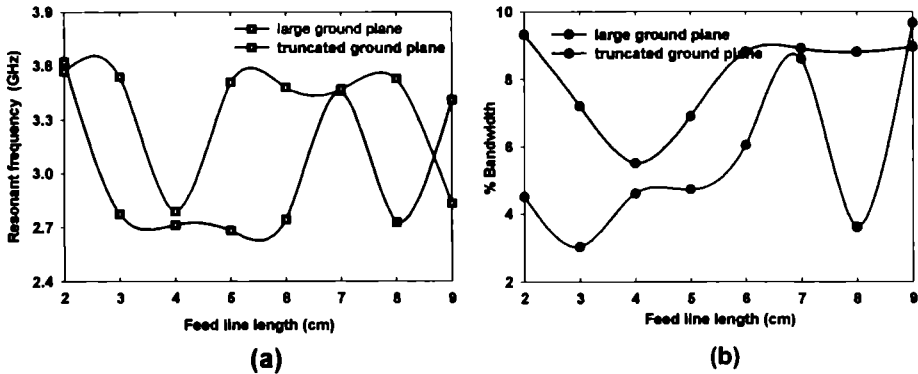


Figure 5.96 Variation in resonant behaviour of the dominant mode of the DRA with feed length and ground plane dimensions measured at the optimum bandwidth position
 (a) Resonant frequency (b) % Bandwidth
 DR-1 orientation : a-d-b

When the DR in the a-d-b orientation is placed on a large ground plane at the optimum bandwidth position, different feed lengths excite frequencies in the range 2.68 GHz - 3.6175 GHz. The 2 cm feed excites the highest frequency and the 5 cm feed excites the lowest frequency. The 2 cm feed displays maximum bandwidth (9.3%). Minimum bandwidth (5.5%) is exhibited by the 4 cm feed. The average bandwidth observed on a large ground plane is 8.04%.

Frequencies in the range 2.785 GHz to 3.565 GHz are excited by different feed lengths in the optimum bandwidth condition when the DR is placed on a truncated ground plane. Highest frequency is excited by the 2 cm feed and the lowest frequency is excited by the 4 cm feed. Maximum (9.65%) and minimum (3.02%) bandwidth is exhibited by the 9 cm and 3 cm feeds respectively. The average bandwidth observed in the a-d-b orientation on a truncated ground plane is 5.59%.

5.1.5.2 Radiation Pattern

The principal plane radiation patterns are measured in the a-d-b orientation of the resonator for feed lengths varying from 2 cm to 9 cm. Figure 5.97 illustrates the principal plane patterns measured experimentally at 3.6175 GHz in the optimum band of the 2 cm fed DRA in the a-d-b orientation. The pattern in both the planes are not as broad as that exhibited by the other orientations.

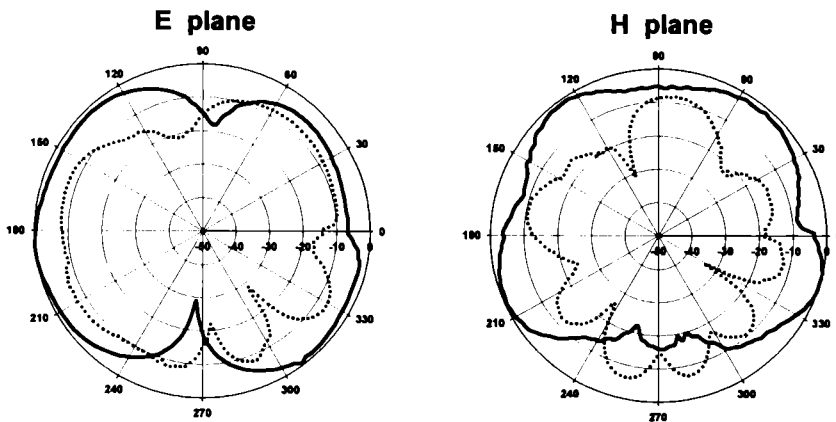


Figure 5.97 Radiation Pattern of the DRA at the optimum bandwidth position — co-polar cross-polar ($f = 3.6175$ GHz)
 feed line length = 2 cm (d_x, d_y) = (1.5, 0.25) cm
 DR-1 orientation: a-d-b large ground plane : 4x4 sq cm

The patterns of the DRA excited by the 3 cm, 5 cm and 8 cm feeds are shown in Figure 5.98. These antenna configurations with broad radiation coverage may find applications in Mobile Communications. The radiation pattern characteristics of the DRA excited by varying feed lengths are summarised in Table 5.46.

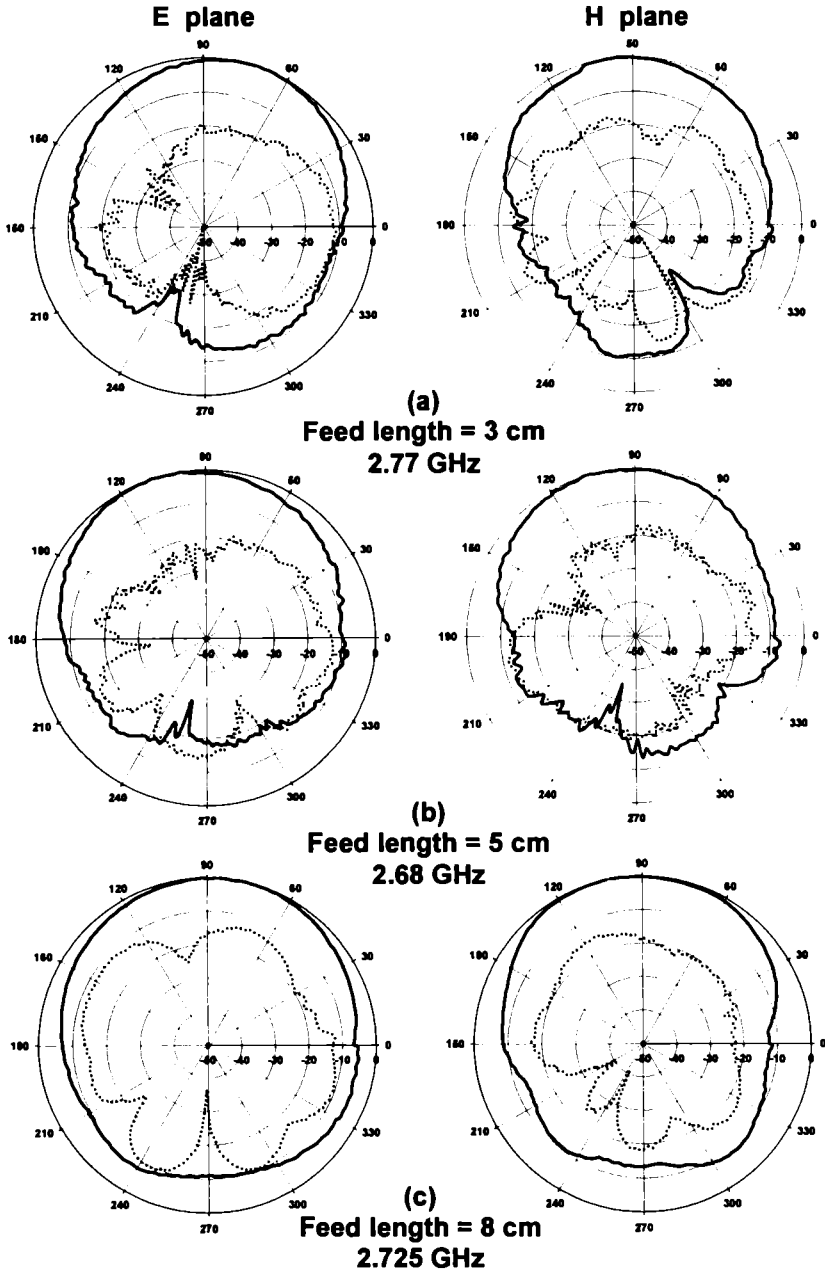


Figure 5.98 Radiation Pattern of the DRA for varying feed lengths at the optimum bandwidth position
orientation : a-d-b — co-polar cross-polar
DR-1 large ground plane

Feed Length (cm)	Half power beam width (degree)		Front-to-Back Ratio along the maxima (dB)		Cross-Polarisation along the maxima (dB)	
	E plane	H plane	E plane	H plane	E plane	H plane
2	108	30	7	8	-9	-13
3	76	74	28	11	-20	-19
4	148	60	15	11	-13	-24
5	82	80	18	15	-26	-20
6	70	126	10	19	-18	-16
7	52	34	13	11	-7	-7
8	104	92	11	13	-16	-17
9	54	22	2	2	-4	-12

Table 5.46 Radiation pattern characteristics of the DRA for varying feed lengths at the optimum bandwidth position
DR-1 large ground plane orientation : a-d-b

5.1.5.3 Gain

Figure 5.99 shows the gain characteristics of the 3 cm fed DRA in the a-d-b orientation of the resonator. The variation in the gain of the DRA in the optimum resonant band for varying feed lengths and ground plane dimensions is illustrated in Figure 5.100.

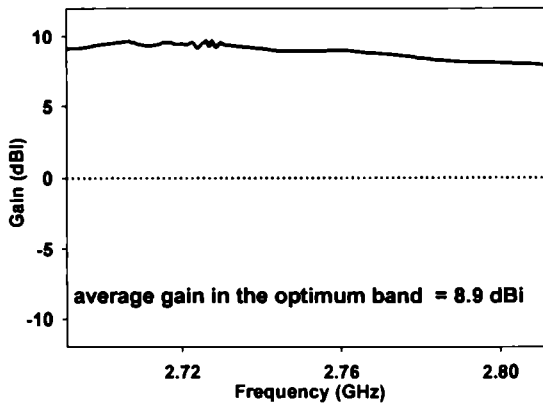


Figure 5.99 Gain of the DRA measured in the optimum band
 feed line length = 3 cm large ground plane : 5x4 sq cm
 DR-1 orientation : a-d-b $(d_x, d_y) = (0, 0.5)$ cm

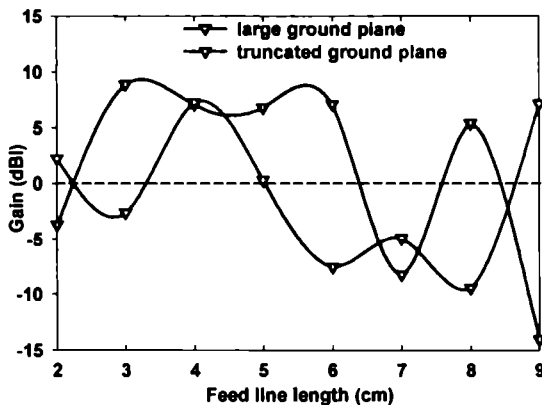


Figure 5.100 Variation in gain of the DRA with feed length and ground plane dimensions measured in the optimum band
 DR-1 orientation : a-d-b

Table 5.47 summarises the variation in radiation characteristics of the DRA with feed length and ground plane dimensions in the a-d-b orientation. It is observed that the overall radiation performance of the truncated ground plane configuration is inferior in comparison to that of the large ground plane configuration.

Feed Line length (cm)	Large Ground plane			Truncated Ground plane		
	Freq (GHz)	%BW	Avg gain (dBi)	Freq (GHz)	%BW	Avg gain (dBi)
2	3.6175	9.3	poor	3.565	4.5	poor
3	2.77	7.2	8.9	3.535	3.02	poor
4	2.71	5.5	7.1	2.785	4.6	7.25
5	2.68	6.9	6.8	3.505	4.72	poor
6	2.74	8.8	7.1	3.475	6.04	poor
7	3.455	8.9	poor	3.4675	8.6	poor
8	2.725	8.8	5.4	3.525	3.6	poor
9	3.4075	8.95	poor	2.83	9.65	7.15

Table 5.47 Variation in radiation characteristics of the DRA with feed length and ground plane dimensions at the optimum bandwidth position
DR-1 orientation: a-d-b

5.1.5.4 Resonant behaviour at different positions of the DR with respect to the feed

The resonant behaviour of the antenna at different positions of the DR in the a-d-b orientation is discussed in this section. The DR is placed at discrete intervals of 0.25 cm along the x and y directions on a 2 cm feed for the study [$0.25 \leq d_x \leq 2$, $0.25 \leq d_y \leq 0.75$]. Figure 5.101 illustrates the return loss characteristics for the a-d-b orientation on a large ground plane at different locations of the DR. A feature observed in this orientation (similar to d-a-b) is the presence of a low frequency mode at 2.78 GHz at certain positions of the DR, though it fails to achieve sufficient impedance matching. Stub matching may be attempted to improve the impedance matching of the lower resonant modes.

When the DR is placed laterally at $d_x = 0.5$ cm as shown in Figure 5.101(a), the second mode achieves better impedance matching at all d_y positions. The frequency of the second mode decreases to ~ 3.5 GHz when the DR is moved laterally to $d_x = 1$ cm.

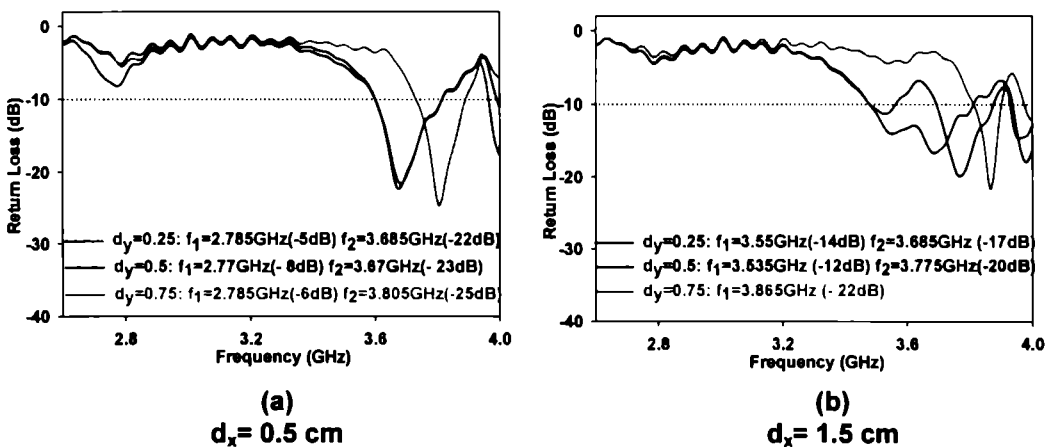


Figure 5.101 Return loss characteristics of the DRA measured at different d_y locations of the DR
 feed line length = 2 cm large ground plane: 4 x 4 sq cm
 DR-1 orientation : a-d-b

However, maximum bandwidth (9.3%) is observed in the frequency band centred at 3.6175 GHz (3.479 GHz – 3.814 GHz), when the DR is placed at $(d_x, d_y) = (1.5, 0.25)$ [Figure.5.101(b)]. Two resonant modes at 3.55 GHz and 3.685 GHz merge at this position of the DR as explained in Section 5.1.5.1 [Figure 5.93].

Figure 5.102 illustrates the shift in the resonant frequency and 2:1 VSWR bandwidth of the higher order mode, as the DR is located at different positions with respect to the feed. Table 5.48 summarises the resonant behaviour of the DRA in the a-d-b orientation. The frequency varies from 3.46 GHz to 3.865 GHz and the bandwidth exhibits a variation from 2% to 9.3%.

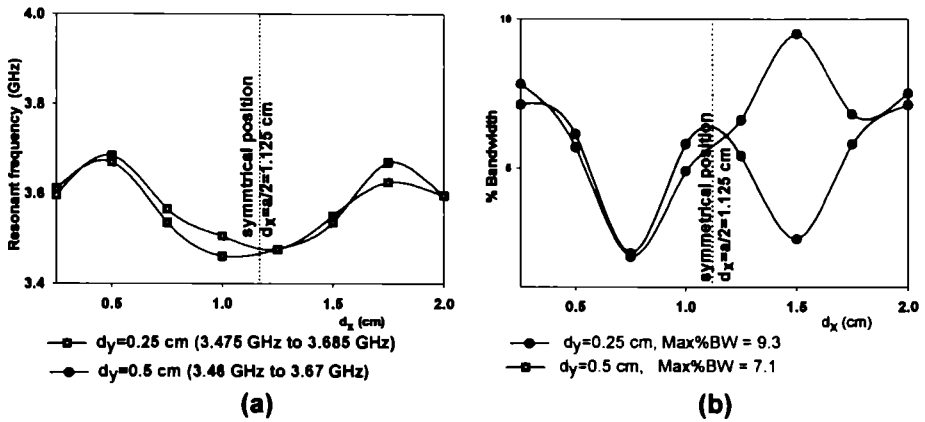


Figure 5.102 Measured variation in the resonant behaviour of the DRA with position of the DR on the feed
 (a) Resonant frequency (b) % Bandwidth
 feed line length : 2 cm large ground plane: 4 x 4 sq cm
 DR-1 orientation: a-d-b

From Figure 5.102 it is inferred that the positions of the DR corresponding to $d_x=1$ cm and 1.25 cm are ideal for exciting lower resonant frequencies (3.46-3.505 GHz) with moderate bandwidths (~7%). The optimum bandwidth positions of the DR in the a-d-b orientation, when excited by feeds of varying lengths are summarised in Table 5.49. It is observed that for varying feed length and ground plane dimensions, the maximum bandwidth is not always obtained when the DR is placed symmetrically with respect to the feed i.e, $d_x = a/2 = 1.125$ cm.

Resonant frequency (GHz)								
d _y (cm)	d _x (cm)							
	0.25	0.5	0.75	1	1.25	1.5	1.75	2
0.25	3.595	3.685	3.565	3.505	3.475	3.55	3.625	3.595
0.5	3.61	3.67	3.535	3.46	3.475	3.535	3.67	3.595
0.75	3.64	3.805	3.865	3.52	3.535	3.865	3.82	3.65

(a)

% Bandwidth								
d _y (cm)	d _x (cm)							
	0.25	0.5	0.75	1	1.25	1.5	1.75	2
0.25	7.8	5.7	2	4.9	6.6	9.3	6.7	7.5
0.5	7.1	6.13	2.12	5.8	5.4	2.6	7.5	7.1
0.75	2.2	4.4	3.1	-	-	2.3	3.1	-

(b)

Table 5.48 Resonant behaviour of the DRA measured at various positions of the DR on the feed line
(a) Resonant frequency (GHz)
(b) % Bandwidth
 feed line length : 2 cm large ground plane: 4 x 4 sq cm
 DR-1 orientation: a-d-b

Feed length (l_f) cm	Ground plane ($l_g \times w_g$) sq cm	(d_x, d_y) cm
2	large (4 x 4)	1.5, 0.25
	truncated (2 x 4)	1.125, 0.5
3	large (5 x 4)	0, 0.5
	truncated (3 x 4)	1, 2
4	large (6 x 4)	2, 2.5
	truncated (4 x 4)	1.4, 2.4
5	large (7 x 4)	1.5, 2.3
	truncated (5 x 4)	0.9, 1.8
6	large (8 x 4)	0.5, 2.5
	truncated (6 x 4)	1.125, 4.1
7	large (9 x 4)	1.125, 4
	truncated (7 x 4)	1.125, 4
8	large (10 x 4)	1.5, 5.2
	truncated (8 x 4)	1.125, 6.5
9	large (11 x 4)	1.125, 6.5
	truncated (9 x 4)	1.5, 2.2

Table 5.49 The optimum bandwidth positions of the DR
DR-1 orientation: a-d-b

5.1.5.5 Resonant behaviour of the DRA when the DR is placed symmetrically with respect to the feed axis

This section discusses the resonant behaviour of the DRA for varying feed lengths when the DR in the a-d-b orientation is placed symmetrically with respect to the feed axis at $(d_x, d_y) = (a/2, 0.5)$. Figure 5.103 illustrates the variation in resonant frequency and % bandwidth of the DRA with feed length at this position of the DR.

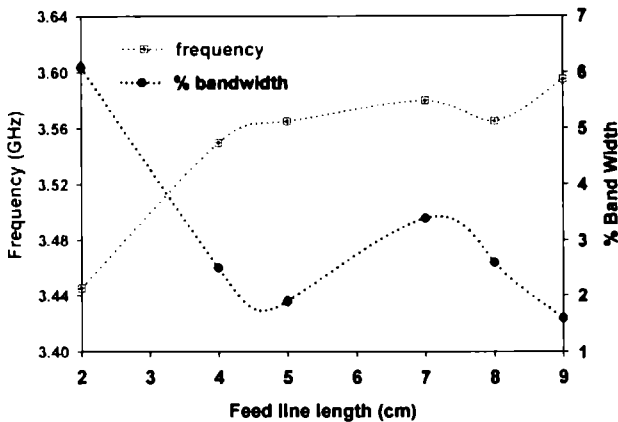


Figure 5.103 Variation in resonant frequency and % bandwidth of the DRA with feed length measured at a symmetrical position of the DR $[(d_x, d_y) = (a/2, 0.5)]$ cm large ground plane orientation : a-d-b DR-1

The varying feed lengths excite frequencies ranging from 3.445 GHz to 3.595 GHz with an average bandwidth of 3.02%. The 2 cm feed is attractive since it excites the lowest frequency with a maximum bandwidth of 6.1%, resulting in a compact antenna configuration. Minimum bandwidth of 1.6% at 3.595 GHz is exhibited by the 9 cm fed DRA. The 3 cm and 6 cm feed fail to excite resonance at this position. The influence of the feed length on the return loss characteristics is evident from Figure 5.103.

5.1.5.6 Salient features of the a-d-b orientation

The a-d-b orientation is a relatively high profile orientation. Nevertheless, at 3.6175 GHz the 2 cm fed DRA offers 75% size reduction with respect to a Rectangular Microstrip Antenna resonating at the same frequency. Table 5.46 and Table 5.47 sum up the characteristics of this orientation. The varying feed line lengths excite frequencies in the S-band, providing an average 2:1 VSWR bandwidth of 8.04%. The 3 cm feed offers the maximum gain (8.9 dBi). The lowest resonant frequency (2.68 GHz) is excited by the 5 cm feed and the maximum 2:1 VSWR bandwidth (9.3%) is provided by the 2 cm feed. The 3 cm line fed DRA also offers broad radiation patterns at 2.77 GHz with 76° and 74° half-power beam width respectively in the E and H planes [Figure 5.98(a)]. Though the truncated ground plane configuration exhibits an average 2:1 VSWR bandwidth of 6.7%, the overall gain performance is far inferior to that of the large ground plane configuration. Nevertheless, it acquires significance where the size of the antenna is of priority.

The above investigations performed on the Dielectric Resonator Antenna incorporating the rectangular resonator sample DR-1 in the a-d-b orientation confirm the dependence of the antenna characteristics upon the feed length, ground plane dimensions and position of the DR. The performance of the DRA excited by the 3 cm long Microstrip line feed is noteworthy in lieu of its overall compactness, low resonant frequency, good bandwidth, gain and broad radiation pattern.

5.1.6 Performance of the DRA in various orientations of the DR upon the feed line

A comparison of the performance of the DRA in various orientations of the DR upon the feed line is presented in this section. Figure 5.104 illustrates the variation in resonant frequency at the optimum bandwidth position of the DRA in different orientations, for varying lengths and ground plane dimensions.

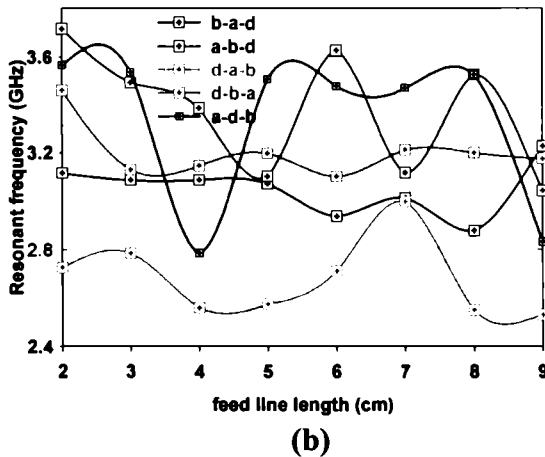
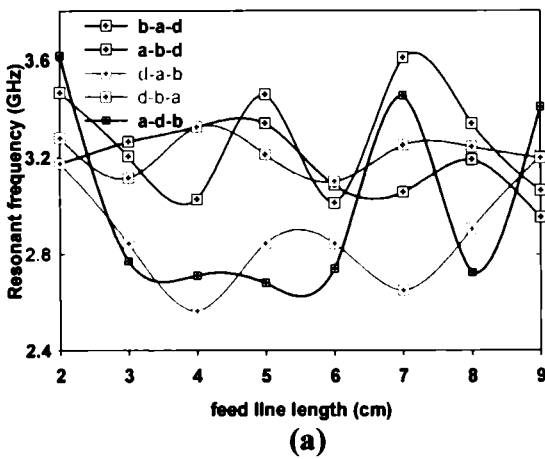
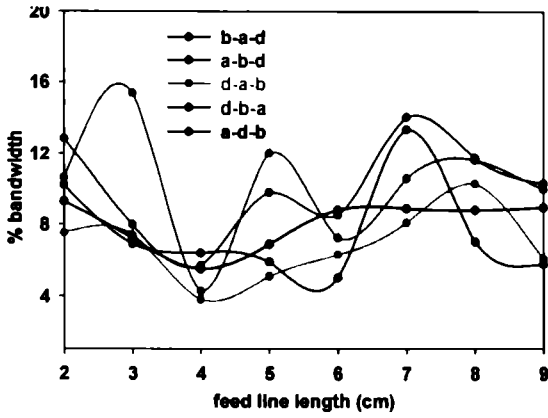
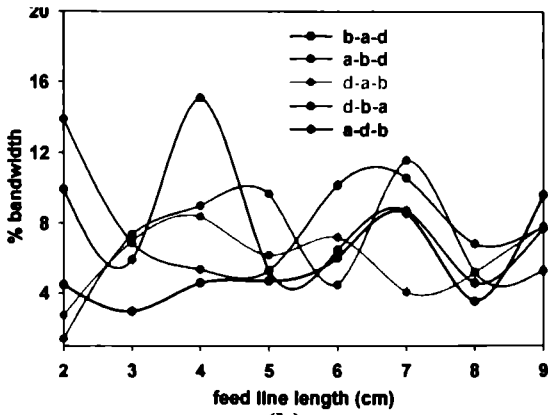


Figure 5.104 Variation in resonant frequency of the DRA with feed length for different orientations of DR-1 measured at the optimum bandwidth position
 (a) large ground plane (b) truncated ground plane

The variation in the maximum % bandwidth is illustrated in Figure 5.105. Table 5.50 and Table 5.51 summarise the resonant behaviour and average gain of the DRA excited by varying feed lengths in different orientations of the DR in the optimum resonant band.



(a)



(b)

Figure 5.105 Variation in % bandwidth of the DRA with feed length for different orientations of DR-1 measured at the optimum bandwidth position
 (a) large ground plane (b) truncated ground plane

Feed length (cm)	(a) large ground plane				
	b-a-d	a-b-d	d-a-b	d-b-a	a-d-b
2	3.175 10.2%	3.4675 12.9%	3.175 7.5%	3.28 10.6%	3.6175 9.3%
3	3.265 6.9%	3.205 7.96%	2.845 7.4%	3.115 15.4%	2.77 7.2%
4	3.325 6.4%	3.025 5.7%	2.56 3.8%	3.325 4.3%	2.71 5.55
5	3.34 5.9%	3.46 9.8%	2.845 5.1%	3.2125 12%	2.68 6.9%
6	3.085 5.02%	3.01 8.5%	2.845 6.32%	3.1 7.3%	2.74 8.8%
7	3.055 13.4%	3.61 14.1%	2.65 8.1%	3.25 10.6%	3.455 8.9%
8	3.19 7.05%	3.34 11.7%	2.905 10.3%	3.2425 11.6%	2.725 8.8%
9	2.95 5.8%	3.0625 10.3%	3.205 6.1%	3.1975 10%	3.4075 8.95%

Feed length (cm)	(b) truncated ground plane				
	b-a-d	a-b-d	d-a-b	d-b-a	a-d-b
2	3.115 9.95%	3.715 13.9%	2.725 2.8%	3.46 1.5%	3.565 4.5%
3	3.085 5.93%	3.49 6.9%	2.785 7%	3.13 7.4%	3.535 3.02%
4	3.085 15.1%	3.385 5.4%	2.56 8.4%	3.145 9.01%	2.785 4.6%
5	3.07 5.3%	3.1 5.3%	2.575 6.2%	3.1975 9.7%	3.505 4.72%
6	2.935 6.5%	3.625 10.2%	2.695 7.24%	3.1 4.5%	3.475 6.04%
7	3.01 8.73%	3.115 10.6%	2.995 4.1%	3.2125 11.6%	3.4675 8.6%
8	2.875 4.6%	3.525 6.9%	2.55 5.2%	3.2 5.2%	3.525 3.6%
9	3.2275 7.75%	3.04 7.8%	2.53 7.9%	3.175 5.32%	2.83 9.65%

Table 5.50 Resonant frequency (GHz) and % bandwidth of the DRA excited by varying feed lengths in different orientations of DR-1 measured at the optimum bandwidth position

Feed length (cm)	b-a-d	a-b-d	d-a-b	d-b-a	a-d-b
2	7.15	7.8	1.4	5.9	poor
3	8.7	7.05	6.7	7.4	8.9
4	6.1	7.4	5.6	5.8	7.1
5	7.4	6.5	6.65	6.4	6.8
6	7.5	8.02	6.92	7.6	7.1
7	5.3	6.7	5.2	6.3	poor
8	7.52	2.3	5.1	9.3	5.4
9	3.8	6.8	3.4	3.9	poor

(a)

Feed length (cm)	b-a-d	a-b-d	d-a-b	d-b-a	a-d-b
2	2.1	4.5	1.9	4.74	poor
3	6.2	7.8	5.1	5.6	poor
4	5.74	3.7	4.2	5.5	7.25
5	3.56	2.1	4.91	6.06	poor
6	4.5	6.42	5.1	1.8	poor
7	2.7	7.9	1.2	7.97	poor
8	4.82	3.5	4.3	3.5	poor
9	2.8	7.7	5.9	3.9	7.15

(b)

The low profile orientations [a-b-d, b-a-d and d-a-b] are suitable for compact antenna configurations. For varying feed lengths on a large ground plane, the b-a-d and a-b-d orientations display an average gain of ~ 6.7 dBi and 6.6 dBi in their optimum resonant bands, centred at ~ 3.17 GHz and 3.27 GHz, respectively [Table 5.51(a)]. The d-a-b orientation differs from the rest, displaying an average gain of 6.92 dBi in an optimum resonant band centred at a low frequency of ~ 2.8 GHz when excited by varying feed lengths fabricated on large ground planes [Figure 5.104(a)]. It is observed that the average bandwidth for varying feed lengths is greater than 7 % in all the above configurations as seen in Figure 5.105(a). The radiation patterns are generally broad as discussed in the previous sections. However, though the truncated ground plane configuration offers better size reduction, it exhibits reduced bandwidth [Figure 5.105(b)] and gain [Table 5.51(b)] for all orientations.

The high profile orientations [d-b-a and a-d-b] do not provide consistently good performance when excited by varying feed lengths. Therefore, it is inferred that the low profile orientations of the DR upon the Microstrip feed line fabricated on a large ground plane are suited for antenna applications.

The radiation performance of the DRA in five different orientations of the DR has been described in this chapter. It is noted that the b-d-a orientation of the DR does not excite any resonance within the DR in the observed frequency band (1-4 GHz), perhaps due to the largest aspect ratio ($a/d = 4.05$).

5.2 Radiation Characteristics of the Microstrip line fed Rectangular Dielectric Resonator Antenna incorporating DR-2 and DR-3

The investigations performed on a Microstrip line fed DRA incorporating the resonator sample DR-1 discussed in the previous sections indicate the significant influence of the orientation, position, feed line and ground plane dimensions on the performance of the antenna. The low profile orientations b-a-d, a-b-d and d-a-b are attractive in terms of the overall compactness of the antenna. The b-a-d and a-b-d orientations exhibit almost similar characteristics. However, the d-a-b orientation excites lower resonant frequencies with reasonable gain and bandwidth. This section describes the radiation characteristics of the DRA incorporating the Rectangular Dielectric Resonator samples DR-2 and DR-3. These samples are fabricated from the same ceramic material $\text{Ca}_5\text{Nb}_2\text{TiO}_{12}$ ($\epsilon_r = 48$), but are of different dimensions [DR-2 : $(3.4 \times 1.7 \times 0.555) \text{ cm}^3$ and DR-3 : $(3.4 \times 1.7 \times 1.1) \text{ cm}^3$]. The dimensions of the resonator sample are chosen so as to excite frequencies in the Mobile Communication bands. The behaviour of these DR samples is similar to that of the first sample (DR-1) envisaged in the previous sections. As such, only the salient features of the antenna are presented in this section.

The position of the DR with respect to the feed line was optimised for good bandwidth performance in the previous section. Nevertheless, the outcome of these investigations suggests that fine-tuning of the resonant frequency is achieved by selecting the suitable orientation and proper positioning of the resonator sample. The characteristics of the DRA in the b-a-d and d-a-b orientations of the resonator is discussed in this section. The lay out of the b-a-d and d-a-b orientation is described in Section 5.1.1 [Figure 5.1] and Section 5.1.3 [Figure 5.55] respectively.

5.2.1 Return Loss Characteristics

The measured return loss and impedance characteristics of the antenna are shown in Figure 5.106.

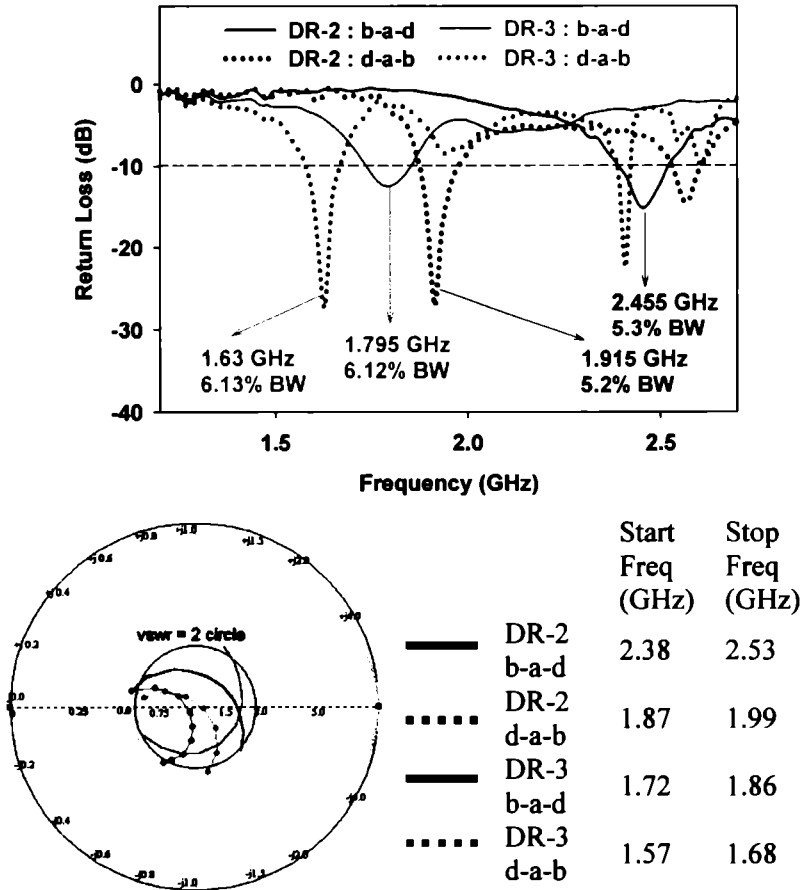


Figure 5.106 Measured return loss characteristics and impedance curve of the DRA
 (increasing frequency is in clockwise direction)
 feed length length : 7 cm ground plane : 9 cm x 4 cm

The DRA in the b-a-d orientation of the resonator DR-2 placed at $(d_x, d_y) = (0.74, 5.5)$ cm operates in a resonant band from 2.39 GHz to 2.52 GHz, centred at 2.455 GHz, offering 130 MHz bandwidth (5.3%). Hence this antenna configuration is

suitable for 2.4 GHz WLAN applications in the designated band (2.4-2.484 GHz). When the resonator sample DR-3 in the b-a-d orientation is placed at $(d_x, d_y) = (1, 4.2)$ cm, a resonant band centred at 1.795 GHz operates from 1.73 GHz to 1.84 GHz offering 110 MHz bandwidth (6.12%). This antenna configuration finds application in GSM 1800 (1710-1880 MHz) bands.

The d-a-b orientation gives rise to a lower resonant frequency. When the sample DR-2 is placed at $(d_x, d_y) = (0.25, 2.5)$ cm, a resonant band centred at 1.915 GHz operating from 1.87 GHz to 1.97 GHz, displaying 100 MHz bandwidth (5.25%) and covering the PCS 1900 (1.85-1.99 GHz) frequency band is observed. When the resonator sample DR-3 in the d-a-b orientation is placed at $(d_x, d_y) = (0.5, 5)$ cm, a resonant band centred at 1.63 GHz operates from 1.57 GHz to 1.67 GHz offering 100 MHz bandwidth (6.13%). This antenna configuration finds application in GPS (1.565-1.585 GHz) bands. The experimental data agree reasonably well with the FDTD predicted values as shown in Table 5.52.

orientation	DR	Experiment		FDTD		% error in freq
		Freq (GHz)	% BW	Freq (GHz)	% BW	
b-a-d	DR-2	2.455	5.3	2.42	4.13	+1.42
	DR-3	1.795	6.12	1.8	4.1	-0.3
d-a-b	DR-2	1.915	5.25	1.9	6.3	+0.78
	DR-3	1.63	6.13	1.6	4.7	+1.84

Table 5.52 Comparison of experimental and predicted results

5.2.2 Resonant mode

The resonant mode is identified through simulation using HFSS™. The field distribution within the DR in various antenna configurations is shown in Figure 5.107. TE_{208}^z resonant mode is observed within DR-2 resonating at 2.42 GHz in the b-a-d orientation [Fig.5.107(1)]. The resonant mode is TE_{180}^z in the d-a-b orientation of DR-2 at 1.9 GHz [Fig.5.107(2)].

When DR-3 is used as the radiating element, TE_{118}^z resonant mode is observed at 1.8 GHz in the b-a-d orientation[Fig.5.107(3)] and TE_{180}^z mode at 1.6 GHz in the d-a-b orientation[Fig.5.107(4)].

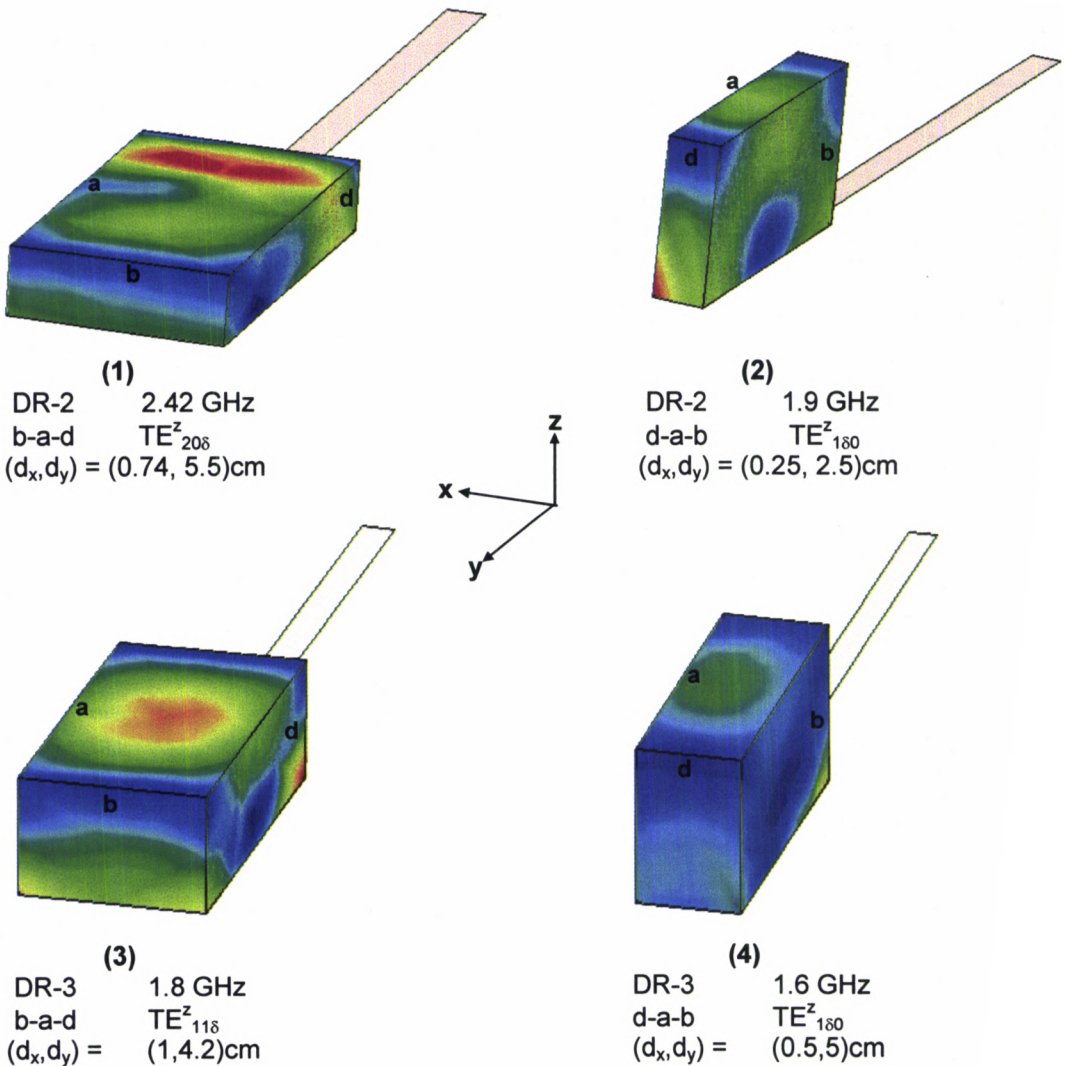


Figure 5.107 Simulated H field distribution within the DR in various antenna configurations incorporating DR-2 and DR-3
 feed line length : 7 cm ground plane : 9 x 4 sq cm

5.2.3 Compactness

Table 5.53 provides a comparison of the dimensions of antennas in different operating bands. The DRA offers good reduction in the cross-section area with respect to a rectangular and circular Microstrip antenna designed to operate in the same band.

Antenna	Cross sectional dimensions (cm)	Cross section area (sq cm)	Cross sectional dimensions (cm)	Cross section area (sq cm)
DR-2	b-a-d orientation 2.455 GHz		d-a-b orientation 1.915 GHz	
	Length (b) = 1.7 Width (a) = 3.4	(b x a) 5.78	Length (d) = 0.555 Width (a) = 3.4	(d x a) 1.89
Rect: Microstrip antenna	Length = 2.92 Width = 3.76	10.97	Length = 3.75 Width = 4.82	18.1
Circular Microstrip antenna	Radius = 1.6	8.04	Radius = 2.16	14.7
% area reduction with ref to:	Rectangular 47.3%	Circular 28.1%	Rectangular 89.5%	Circular 87.1%
DR-3	b-a-d orientation 1.795 GHz		d-a-b orientation 1.63 GHz	
	Length (b) = 1.7 Width (a) = 3.4	(b x a) 5.78	Length (d) = 1.1 Width (a) = 3.4	(d x a) 6.8
Rect: Microstrip antenna	Length = 4.01 Width = 5.14	20.6	Length = 4.4 Width = 5.7	25
Circular Microstrip antenna	Radius = 2.31	16.8	Radius = 2.55	20.4
% area reduction with ref to:	Rectangular 71.9%	Circular 65.6%	Rectangular 72.8%	Circular 66.7%

Table 5.53 Comparison of dimensions of the DRA with Microstrip antennas in similar operating bands

5.2.4 Radiation Pattern

The radiation patterns are broad in all the operating bands, confirming the suitability of the DRA for wireless communication applications. Figure 5.108 illustrates the principal plane radiation patterns of the antenna incorporating the resonator DR-2 in the b-a-d orientation. The 3 dB beamwidth is 67° and 118° in the E and H planes. The cross polarization along the boresight direction is better than -10 dB in both the planes.

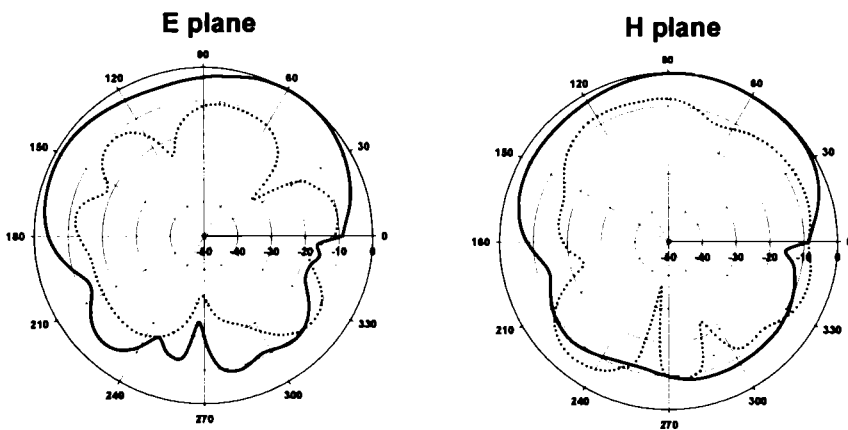


Figure 5.108 Radiation Pattern of the DRA measured at 2.455 GHz
 _____ co-polar cross-polar
 feed line length = 7cm ground plane : 9x 4 sq cm
 DR-2 orientation: b-a-d $(d_x, d_y) = (0.74, 5.5)$ cm

5.2.5 Gain

The antenna exhibits good gain in all the operating bands as listed in Table 5.54. The position of the DR with respect to the feed axis denoted as (d_x, d_y) is also indicated. The gain characteristics in the b-a-d orientation of DR-2, operating in the 2.4 GHz band is shown in Figure 5.109. The polarization is linear in all the configurations and oriented in a direction along the feed length.

orientation	b-a-d		d-a-b	
	DR-2	DR-3	DR-2	DR-3
(d _x ,d _y) cm	0.74,5.5	1,4.2	0.25,2.5	0.5,5
Centre freq (GHz)	2.455	1.795	1.915	1.63
Avg gain (dBi)	7.2	6.6	5.8	6.2

Table 5.54 Average gain measured in the operating band of various antenna configurations

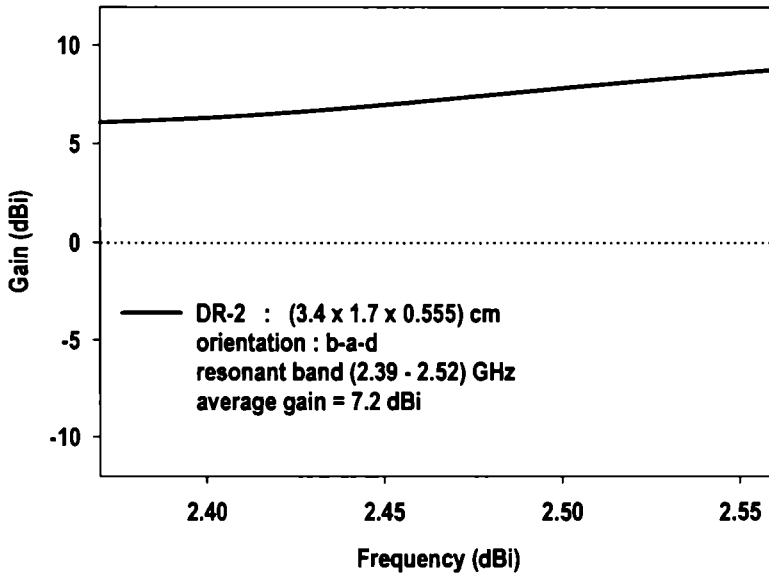


Figure 5.109 Average gain measured in the operating band of DR-2 centred at 2.455 GHz

Good bandwidth, broad radiation patterns and moderate gain highlight the significance of the above antenna configurations in Mobile Communication bands – GPS 1600, PCS 1900, GSM 1800 and 2.4 GHz WLAN.

5.3 Radiation Characteristics of the Microstrip line fed Rectangular Dielectric Resonator Antenna incorporating DR-4 and DR-5

The characteristics of the DRA incorporating the rectangular resonator samples DR-4 [1.85 x 1.7 x 0.85] cm³ and DR-5 [2.65 x 1.75 x 0.85] cm³, prepared using the ceramic material (Ba,Sr)₂Ti₉O₂₀ ($\epsilon_r = 34$) are presented in this section. The position of the DR is optimized for maximum bandwidth in the two low profile orientations a-b-d and d-a-b and the radiation characteristics are studied. This procedure is repeated for varying feed lengths.

5.3.1 Return Loss Characteristics

Figure 5.110 illustrates the measured variation in resonant frequency and % bandwidth of the DRA at the optimum bandwidth positions for varying feed lengths (l_f) on a ground plane of dimensions ($l_g \times w_g$), where ($l_g = l_f + 2$) cm and $w_g = 4$ cm.

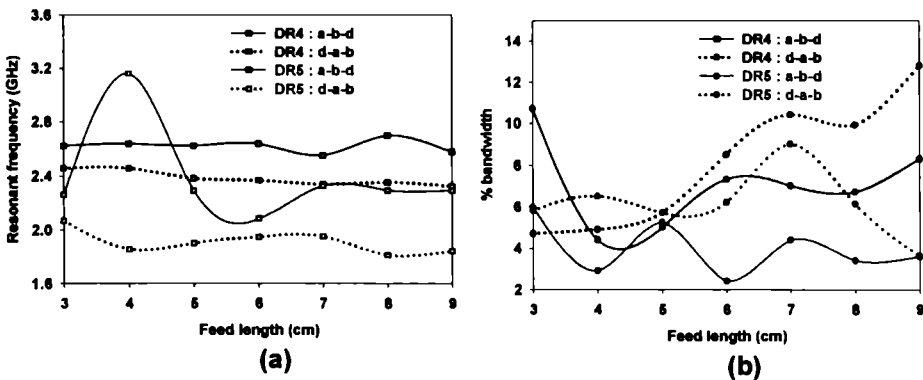


Figure 5.110 Variation in the resonant behaviour of the DRA with feed length (l_f) measured at the optimum bandwidth position
ground plane : $l_g = (l_f + 2)$ cm, $w_g = 4$ cm
(a) Resonant frequency (b) % Bandwidth

The average resonant frequency excited by the varying feed lengths in the a-b-d and d-a-b orientations of DR-4 is 2.62 GHz and 2.38 GHz. As in the previous cases, the d-a-b orientation excites resonant frequencies reduced by ~9.2% with respect to that excited by the b-a-d orientation. However, the average resonant frequency excited by the d-a-b orientation of DR-5 (1.9 GHz) is ~20% lower in comparison to that excited by the a-b-d orientation (2.39 GHz). It is thus inferred that the aspect ratio of the two DR samples is critical in determining the extent of frequency reduction. Table 5.55 differentiates the two resonator samples.

DR	a cm	b cm	d cm	aspect ratio (d/a)	freq reduction
DR-4	1.85	1.7	0.85	0.46	9.2%
DR-5	2.65	1.75	0.85	0.32	20 %

Table 5.55 Frequency reduction in the d-a-b orientation with respect to the a-b-d orientation for DR-4 and DR-5

The bandwidth variation illustrated in Figure 5.110 (b) shows an improvement in the bandwidth of the antenna with increase in feed length, when DR-4 is used. However, an increase in feed length results in an increase in the overall size of the antenna configuration. A trade-off between bandwidth and size is thus required.

The measured return loss and impedance characteristics of a 3 cm fed DRA incorporating the resonator sample DR-4 and DR-5 in the a-b-d and d-a-b orientation is illustrated in Figure 5.111. At the optimum bandwidth position $[(d_x, d_y) = (0.5, 1.75)]$, the DRA in the a-b-d orientation of the resonator DR-4 operates in a resonant band from 2.514 GHz to 2.795 GHz, centred at 2.62 GHz, offering 281 MHz bandwidth (10.7%). A resonant band centred at 2.26 GHz, operates from 2.202 GHz to 2.337 GHz offering 135 MHz bandwidth (5.97%) when the resonator sample DR-5 in the a-b-d orientation is placed at the optimum bandwidth position $[(d_x, d_y) = (2.4, 0.6)]$.

The d-a-b orientation gives rise to a lower resonant frequency. When the sample DR-4 is employed, a resonant band centred at 2.455 GHz, operating from 2.39 GHz to 2.505 GHz, displaying 115 MHz bandwidth (4.7%) and covering the 2.4 WLAN (2.4 – 2.484 GHz) frequency band is observed at $(d_x, d_y) = (0.5, 0.5)$. When the resonator sample DR-5 in the d-a-b orientation is positioned at $(d_x, d_y) = (0.4, 0.5)$, a resonant band centred at 2.065 GHz operates from 2 GHz to 2.12 GHz, offering 120 MHz bandwidth (5.8%) The experimental data agree reasonably well with the FDTD predicted values as shown in Table 5.56.

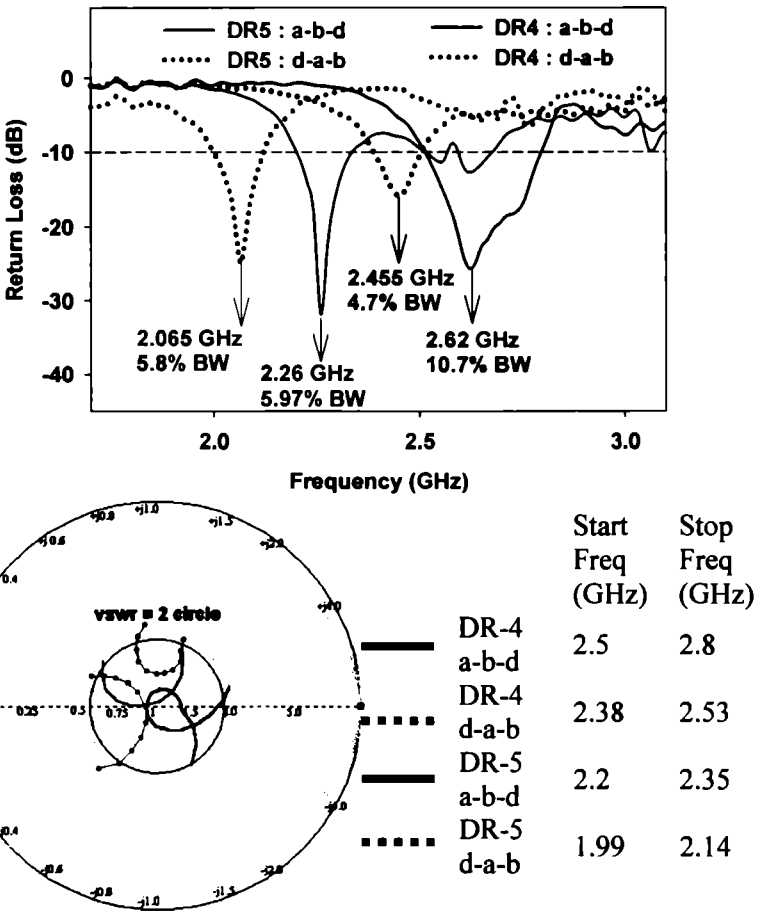


Figure 5.111 Measured return loss characteristics and impedance curve of the DRA at the optimum bandwidth position. (increasing frequency is in clockwise direction)
 feed line length : 3 cm ground plane : 5 x 4 sq cm

orientation	DR	Experiment		FDTD		% error in freq
		Freq (GHz)	% BW	Freq (GHz)	% BW	
a-b-d	DR-4	2.62	10.7	2.647	9.3	-1.03
	DR-5	2.26	5.97	2.224	4.3	+1.6
d-a-b	DR-4	2.455	4.7	2.432	5.1	+0.93
	DR-5	2.065	5.8	2.103	4.6	-1.8

Table 5.56 Comparison of experimental and predicted results

5.3.2 Resonant mode

The resonant mode is identified through simulation using HFSS™. The field distribution within the DR in various antenna configurations is shown in Figure 5.112. TE_{118}^z resonant mode is observed within DR-4 resonating at 2.647 GHz in the a-b-d orientation. At 2.432 GHz the resonant mode is TE_{180}^z in the d-a-b orientation of DR-4.

When DR-5 is used as the radiating element, the resonant mode is TE_{118}^z at 2.224 GHz in the a-b-d orientation and TE_{180}^z at 2.103 GHz in the d-a-b orientation.

5.3.3 Compactness

The DRA offers good reduction in the cross-section area with respect to a Rectangular and Circular Microstrip Antenna designed to operate at the same frequency. The area reduction in the d-a-b orientation is better than the a-b-d orientation because of the lower cross sectional area of the DR ($a > b > d$). Table 5.57 provides a comparison of the dimensions of antennas in the different operating bands.

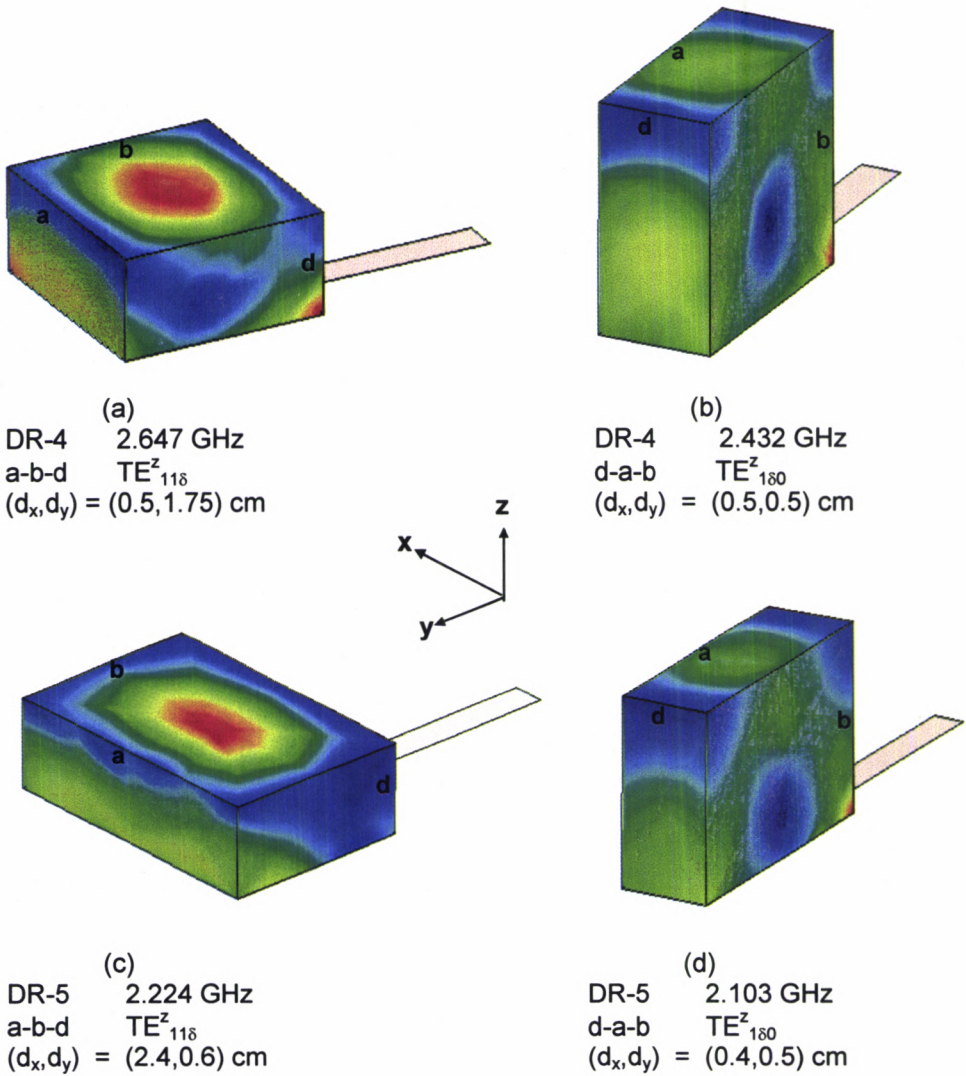


Figure 5.112 Simulated H field distribution within the DR in various antenna configurations
feed line length : 3 cm ground plane : 5x4 sq cm

Antenna	Cross sectional dimensions (cm)	Cross section area (sq cm)	Cross sectional dimensions (cm)	Cross section area (sq cm)
DR-4	a-b-d orientation 2.62 GHz		d-a-b orientation 2.455 GHz	
	Length (b) = 1.7 Width (a) = 1.85	(b x a) 3.145	Length (d) = 0.85 Width (a) = 1.85	(d x a) 1.5725
Rect: Microstrip antenna	Length = 2.73 Width = 3.52	9.61	Length = 2.92 Width = 3.76	10.97
Circular Microstrip antenna	Radius = 1.57	7.75	Radius = 1.6	8.04
% area reduction with ref: to	Rectangular 67.3%	Circular 59.4%	Rectangular 85.6%	Circular 80.4%
DR-5	a-b-d orientation 2.26 GHz		d-a-b orientation 2.065 GHz	
	Length (b) = 1.75 Width (a) = 2.65	(b x a) 4.64	Length (d) = 0.85 Width (a) = 2.65	(d x a) 2.25
Rect: Microstrip antenna	Length = 3.17 Width = 4.1	12.99	Length = 3.48 Width = 4.47	15.6
Circular Microstrip antenna	Radius = 1.83	10.5	Radius = 1.99	12.4
% area reduction with ref: to	Rectangular 64.3%	Circular 55.8%	Rectangular 85.6%	Circular 81.8%

Table 5.57 Comparison of dimensions of the DRA with Microstrip antennas in similar operating bands

5.3.4 Radiation Pattern

The radiation patterns are broad in all the operating bands. Figure 5.113 shows the principal plane radiation patterns of the antenna at 2.455 GHz, incorporating the resonator DR-4 in the d-a-b orientation. The 3 dB beamwidth is 94° and 150° in the E and H planes. The on-axis cross polarization is better than -14 dB in both the planes.

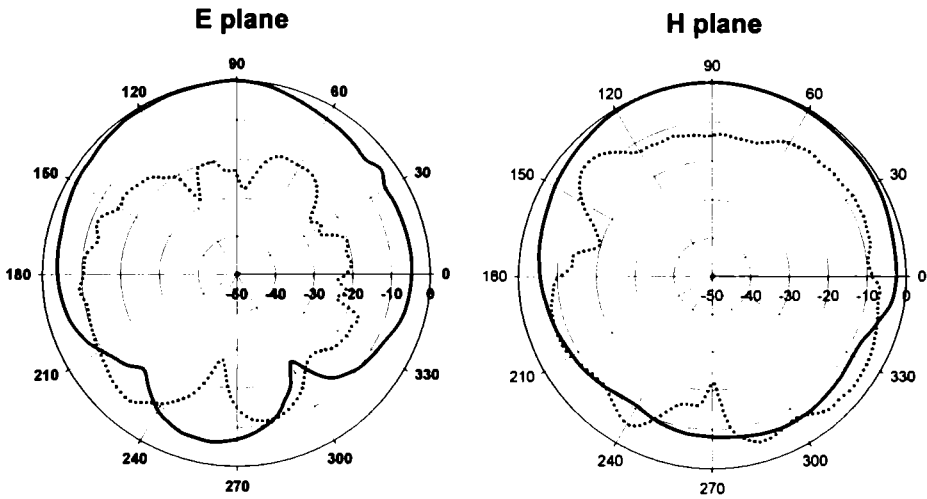


Figure 5.113 Radiation Pattern of the DRA measured at 2.455 GHz
 _____ co-polar cross-polar
 feed line length = 3 cm ground plane: 5x4 sq cm
 DR-4 orientation: d-a-b $(d_x, d_y) = (0.5, 0.5)$ cm

5.3.5 Gain

The antenna exhibits good gain in all the operating bands as listed in Table 5.58. The gain characteristics in the d-a-b orientation of DR-4, operating in the 2.4 GHz band is shown in Figure 5.114. The polarization is linear in all the configurations and oriented in a direction along the feed length.

orientation	a-b-d		d-a-b	
	DR-4	DR-5	DR-4	DR-5
(d _x ,d _y) cm	0.5,1.75	2.4,0.6	0.5,0.5	0.4,0.5
centre freq (GHz)	2.62	2.26	2.455	2.065
avg gain (dBi)	7.1	6.7	6.1	5.6

Table 5.58 Average gain measured in the operating band of various antenna configurations

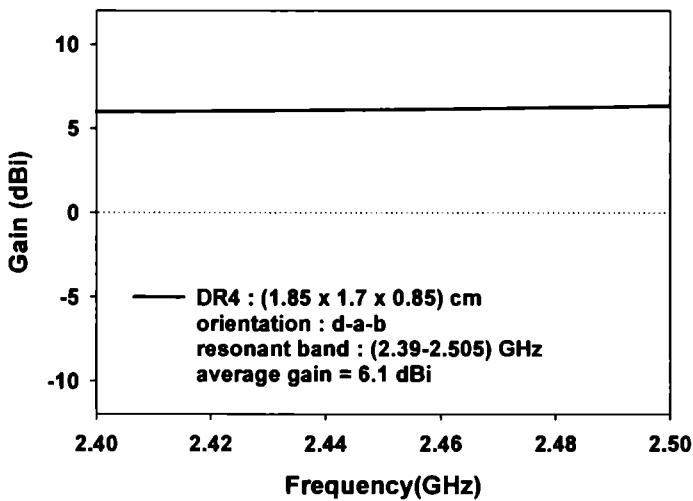


Figure 5.114 Average gain measured in the operating band of DR-4 centred at 2.455 GHz

The above investigations confirm the suitability of Rectangular DRA configurations for wireless communication applications. The antenna configuration is more compact than conventional patch antennas. Good bandwidth, broad radiation patterns and moderate gain are other attractive features.

5.4 Concluding remarks

Exhaustive experimental and theoretical investigations performed on various Rectangular Dielectric Antenna Configurations discussed in this chapter throw light on several significant parameters controlling the radiation performance of the antenna. Among the various orientations of the resonator, the low resonant frequency excited by the d-a-b orientation is noteworthy. Table 5.59 compares the performance of different DRA configurations in the d-a-b orientation.

DR	ϵ_r	a cm	b cm	d cm	Resonant frequency GHz	% BW	Gain dBi	(d_x, d_y) cm
DR-1	48	2.25	1.19	0.555	2.65	8.1	5.2	0.6,5.3
DR-2	48	3.4	1.7	0.555	1.915	5.25	5.8	0.25,2.5
DR-3	48	3.4	1.7	1.1	1.63	6.13	6.2	0.5,5
DR-4	34	1.85	1.7	0.85	2.335	10.4	6.2	0.5,5.8
DR-5	34	2.65	1.75	0.85	1.95	9	5.9	0.25,4

Table 5.59 Comparison of DRA configurations
orientation : d-a-b feed line length = 7 cm
ground plane : 9x4 sq cm

The resonant frequency is primarily decided by the permittivity of the material and the dimensions of the resonator, as is evident from Table 5.59. However, the feed length, the orientation of the DR and its position upon the feed line play a vital role in tuning the resonant frequency as described in the previous sections. It is observed that a Microstrip line fed Rectangular DRA acts as a compact antenna without deteriorating the radiation characteristics compared to an equivalent conventional Microstrip patch antenna. The DRA can thus serve as an excellent radiating element where antenna size is of concern.

5.5 Wideband Rectangular Dielectric Resonator Antenna for W-LAN applications

Antennas for W-LAN applications ought to be compact, exhibit wide impedance bandwidth and omni-directional radiation pattern. The Rectangular Dielectric Resonator sample DR-1 ($\epsilon_r = 48$) in the a-d-b orientation, excited by a 50 Ω Microstrip Line of length $l_f = 3$ cm and width $w_f = 0.3$ cm, top loaded by a stub of dimensions $l_s = 0.3$ cm and $w_s = 2.5$ cm, forming a symmetric T shaped feed, exhibits wide band characteristics. The Dielectric Resonator is placed at a distance $d_s = 2$ cm from the edge of the stub as shown in Figure 5.115.

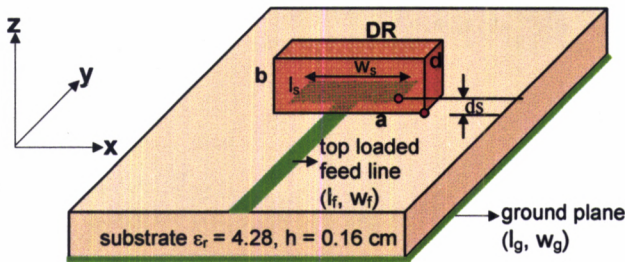


Figure 5.115. Lay out of the wide band DRA configuration
 $a \times b \times d = (2.25 \times 1.19 \times 0.555)$ cm³
 $l_f = 3$ cm $w_f = 0.3$ cm, $l_g = 7$ cm $w_g = 4$ cm
 $l_s = 0.3$ cm $w_s = 2.5$ cm, $d_s = 2$ cm

The measured return loss is plotted in Figure 5.116 (a). The 2:1 VSWR impedance bandwidth of the antenna configuration excited at 5.45 GHz in the band operating from 4.5685 GHz to 5.7469 GHz is 1.178 GHz (21.6%). The antenna thus provides a broad coverage of the 5.15 – 5.35 GHz band centred at 5.2 GHz for W-LAN application. The antenna exhibits an average gain of 5.6 dBi in the operating band as shown in Figure 5.116(b). The co-polar and cross-polar radiation characteristics of the antenna at different frequencies within the band viz. 4.9 GHz, 5.22 GHz and 5.5 GHz, corresponding to $d_s = 0.33\lambda$, 0.35λ and 0.37λ respectively are shown in Figure 5.117.

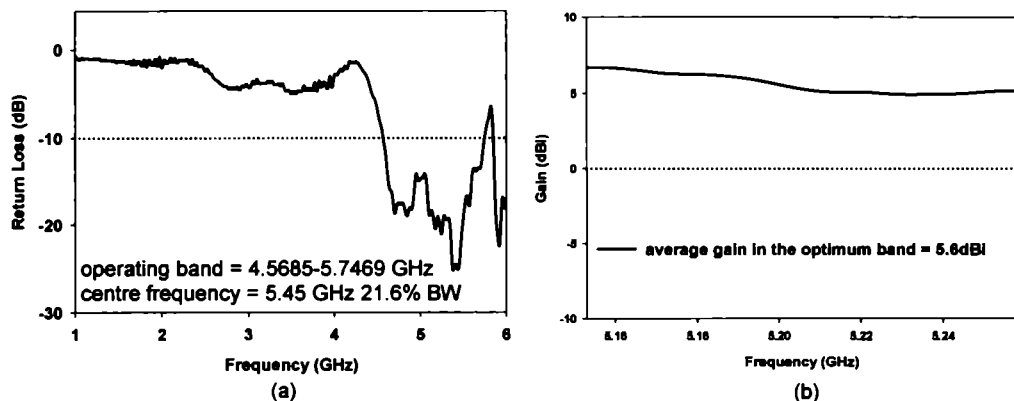


Figure 5.116 (a) Return loss characteristics of the wide band DRA
(b) Gain of the wideband DRA in the operating band

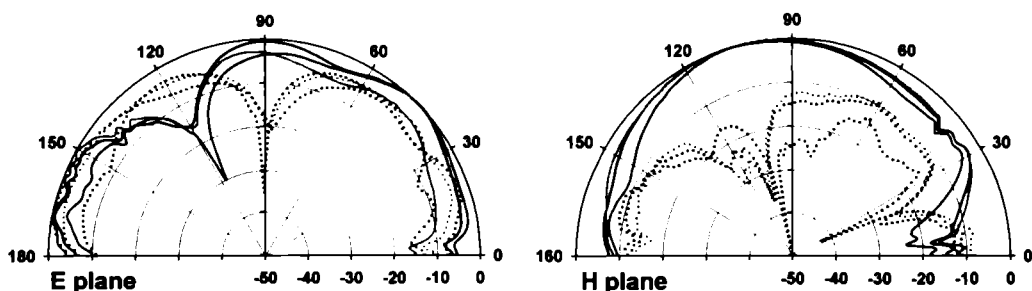


Figure 5.117. Radiation pattern of the wideband DRA at different frequencies in the operating band
 — co-polar cross-polar
 $f_1 = 4.9 \text{ GHz}$ $f_2 = 5.22 \text{ GHz}$ $f_3 = 5.5 \text{ GHz}$

Throughout the band the H plane patterns are broad, offering 3 dB beam widths of 60° , 42° and 50° respectively at the three frequencies shown in figure. However the E plane patterns are slightly distorted, probably due to the fact that the effect of the stub in the 2-element array formed by the DR and the stub is more prominent in the E-Plane radiation pattern taken in the y-z plane along the feed axis. It is evident from the patterns that the distance (d_s) between the stub and the DR is an important parameter deciding the radiation pattern of the array. It is therefore inferred that even though the radiation pattern is slightly distorted, the T shaped feeding technique offers large bandwidth with moderate gain.

Chapter 6

Conclusions

The conclusions drawn from the numerical computation and experimental investigations carried out on Rectangular Dielectric Resonator Antenna configurations are presented in this chapter. The salient features of the present system over other existing systems are examined. Suggestions for future work in the field are also provided.

6.1 Thesis Highlights

This chapter brings the thesis to a close by presenting the conclusions drawn from the outcome of the Numerical Computation and Experimental Observations of the radiation characteristics of a Microstrip excited Rectangular DRA. Chapter one introduced the topic of research. Various methods of computational electromagnetics for numerical analysis of antennas were also explained. Significant work in related areas were discussed in Chapter two. Chapter three described the characteristic features of the DRA, the scheme of work and experimental methodology. The fundamentals of the FDTD method and its adaptation to the problem were discussed in Chapter four. The essence of the thesis is Chapter five. This chapter presented the outcome of the Numerical Computation and Experimental Observations. Rectangular DRA configurations suitable for Mobile Communication applications were also proposed. Appendix A of the thesis presents a very high permittivity multi-band Eye shaped DRA. A Microstrip antenna with reduced radiation hazards, suitable for Mobile telephone handset applications is presented in Appendix B.

6.2 Inferences from Numerical Computation using FDTD method

The FDTD method models the propagation through the elements of the computational domain using the discrete form of Maxwell's equations. In the thesis the FDTD method is employed for the numerical computation of the radiation characteristics of the Microstrip excited Rectangular DRA. Chapter four describes the 3D-FDTD modeller for the antenna configuration. The use of a Gaussian pulse excitation enables characterization of the model over a broad frequency band. The input impedance (Z_{in}) is calculated from the ratio of the FFT of the voltage derived from the E field values over the entire time steps to the FFT of the current derived from the H field values. The experimentally plotted return loss characteristics

illustrated in Section 5.1.1.1 and the measured far field radiation patterns described in Section 5.1.1.2 are akin to the numerically predicted figures and those computed from the tangential field components defined in an aperture in the near field. Uniform gridding has been employed while modelling. The use of non-uniform gridding could improve the results further. However this calls for more complex modelling techniques. The FDTD method is thus found to be a viable alternative to the conventional theoretical modelling techniques. This is also an efficient computational tool in visualizing the EM field distribution within the DR as well. The numerically predicted resonant modes are identified experimentally and also through simulation using HFSS™ as illustrated in Section 5.1.1.5. The results are in good agreement.

6.3 Inferences from Experimental Observations

Experiments are performed using HP 8510C Vector Network Analyzer to validate the computed results. The geometry of the Rectangular DRA permits six different orientations upon the feed line as discussed in Chapter 3. A comprehensive summary of the exhaustive investigations conducted in all these orientations is presented in Section 5.1.6. Microstrip feed lines varying in length from 2 cm to 9 cm, have been used for the study. The minimum length of 2 cm was chosen for convenient mounting of the antenna on the ground plane. No significant improvement in radiation characteristics was observed when the length was increased beyond 8 cm. As a consequence, the study was limited to feed lengths in the range 2 – 9 cm. Nevertheless, an increase in feed length also results in an increase in the overall size of the antenna configuration.

The resonator sample DR-1 was used for the initial study. Among the six possible orientations, the b-a-d, a-b-d and d-a-b orientations are attractive by virtue of their low profile nature, resulting in compact antenna configurations. Though the d-b-a orientation exhibits good bandwidth and gain, this orientation may not be much sought after because of the larger aspect ratio. The a-d-b orientation displays good

bandwidth characteristics. However, the gain performance is not consistent for varying feed lengths. No resonance was observed in the b-d-a orientation in the frequency range under study (1-4 GHz), perhaps due to the large aspect ratio. Thus, the interest narrows down to the b-a-d, a-b-d and d-a-b orientations. The b-a-d and a-b-d orientations are the two orientations with the lowest profiles. In the large ground plane configuration their resonant behaviour is quite similar, but for some subtle differences as evident from Figures 5.104, 5.105 and Tables 5.50, 5.51. Nevertheless, the lower resonant frequencies at the optimum bandwidth position and the lower aspect ratio together make the b-a-d orientation more attractive between the two. The d-a-b orientation strikingly differs from the rest because of the lower range of resonant frequencies excited. As a result this orientation offers better size reduction in comparison to a conventional rectangular patch antenna operating at the same frequency. However when excited by the 2 cm feed, the low frequency resonant mode fails to obtain sufficient impedance matching, the optimum bandwidth being observed at 3.175 GHz. Stub matching is suggested as an alternative as explained in Section 5.1.3.8. The truncation of the ground plane results in reduced size of the antenna but deteriorates the gain, perhaps due to the increased back scattering. Consequently, this configuration is preferred where the overall size of the antenna is a major concern. Active circuitry may be incorporated to compensate for the reduced gain.

The DR was positioned at intervals of 0.25 cm along the feed line and also laterally, to ascertain the importance of the positioning of the DR. The return loss characteristics showed significant variation as illustrated in Section 5.1.1.8 for the b-a-d orientation. Similar studies were conducted on all the orientations as detailed in Sections 5.1.2.8, 5.1.3.8, 5.1.4.4 and 5.1.5.4. Numerous resonant modes were observed as the DR was positioned at discrete intervals of 0.25 cm. At certain positions, two closely spaced modes merged together displaying wideband characteristics. For example, the 10.2% bandwidth exhibited by the b-a-d orientation at the position $(d_x, d_y) = (0.5, 1.5)$, is due to the merging of two resonant modes at 3.04 GHz and 3.175 GHz. The dependence of the resonant frequency upon the DR

position was thus confirmed. The optimum bandwidth positions of the DR in the b-a-d orientation for varying feed lengths are listed in Table 5.14 of Section 5.1.1.9. Similar results for the other orientations are listed in Table 5.27 [Section 5.1.2.9], Table 5.38 [Section 5.1.3.9], Table 5.44 [Section 5.1.4.4] and Table 5.49 [Section 5.1.5.4].

The influence of the feed line length on the antenna properties was further confirmed by placing the antenna symmetrically to the feed line as described in Section 5.1.1.10 for the b-a-d orientation. Similar studies were conducted on other orientations also as detailed in Sections 5.1.2.10, 5.1.3.10, 5.1.4.5 and 5.1.5.5. Though the resonant frequency did not exhibit drastic variations with increasing feed lengths, significant changes were observed in the impedance characteristics as illustrated by the return loss curves. Based on the above conclusions drawn from the theoretical and experimental investigations, Rectangular DRA's suitable for Mobile Communication applications were developed using other resonator samples [DR-2 and DR-3] as described in Section 5.2 and 5.3.

6.4 Salient features of the Microstrip excited Rectangular Dielectric Resonator Antenna

The Microstrip excited Rectangular DRA investigated in this thesis is highly suitable for Mobile Communication applications. The antenna offers considerable size reduction in comparison to conventional Rectangular and Circular Microstrip patch antennas. More so, the compactness is achieved without causing deterioration of the radiation properties. Good bandwidth, broad radiation patterns and high gain are the salient features of this antenna. The simple geometry and ease of excitation using direct Microstrip line feed are added attractions. The antenna can thus effectively replace conventional patch antennas for use in Mobile Communication handsets. Resonant frequency in the desired band may be obtained by choosing suitable material parameters and dimensions of the DR.

6.5 Suggestions for future work

The results of the numerical computation show good agreement with experimental data. However in some orientations of the DR there are discrepancies. These are presumably due to the approximations in the numerical model. The problems for further investigations in continuation with the present work are listed below.

- ◆ Uniform gridding has been employed in the computational domain. Non-uniform gridding, if applied to the regions in the vicinity of the feed would model the excitation more accurately.
- ◆ Mur's first order ABC is used for the outer radiation boundary conditions. The use of Mur's second order ABC or Berenger's PML boundary conditions could be looked into.
- ◆ Direct Microstrip line feed coupling is used to excite the DR. Other feed configurations may be examined. The Coplanar waveguide feed is an alternative. This feed has the advantage of connecting series and shunt components on the same side of the substrate without via holes and is therefore attractive from the point of view of integrating the DRA with active circuitry.
- ◆ The Rectangular DRA presented in this thesis is linearly polarized. The feed configuration may be modified to obtain circular polarization.
- ◆ The effect of conductor strip grating on the walls of the DRA is an interesting field of work. This may find applications in Mobile telephone handsets where the radiation pattern needs to be modified so as to direct minimum radiation towards the user.

A compact very high permittivity eye – shaped Dielectric Resonator Antenna for multiband wireless applications

A very high permittivity ($\epsilon_r=100$) multi-band Dielectric Eye Resonator Antenna is presented. The compact antenna excited by a Microstrip line resonates at two frequencies centered at ~ 1.9 GHz and 2.3 GHz with identical polarization. The resonant behaviour of the antenna at different positions along the feed line is studied and optimized. Multiple resonances with the same polarization and broad radiation patterns suggest the suitability of the antenna for multi-band wireless applications.

A.1 Introduction

The development of numerous Mobile Communication systems has led to the increased demand for compact, efficient antennas. Small-integrated antennas play a significant role in the progress of the rapidly expanding military and commercial communications applications. Recently, with the booming wireless mobile communications market, the urgency to design compact, multi-band antennas is even more pronounced [1-3]. Dielectric Resonator Antenna (DRA) is attractive to antenna designers due to the excellent radiation characteristics [4-6]. An eye shaped Dielectric Resonator Antenna suitable for wireless applications is described in this section

A.2 Antenna Geometry

The eye shape is defined by the intersection of two circles of the same radius 3.15 cm with their centres displaced by a small distance $d=0.75$ cm, as shown in Figure A.1.

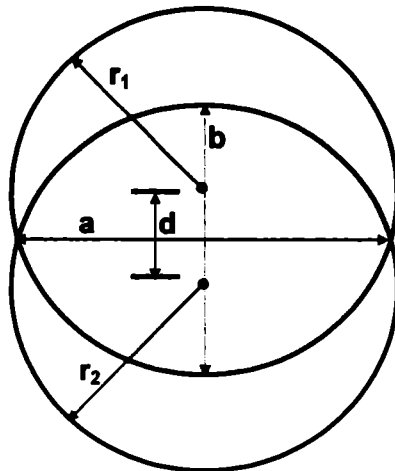


Figure A.1 Two identical circles of radius $r_1 = r_2 = r$ and centre -to - centre spacing d , intersecting to form the eye geometry.

a = major axis b = minor axis
 $r = 3.15$ cm, $d = 0.75$ cm, $a = 3.05$ cm, $b = 2.35$ cm

The DR is made of very high permittivity ($\epsilon_r=100$) ceramic material TiO_2 doped with 1 mole % Fe_2O_3 prepared using the conventional solid-state ceramic route. By virtue of its geometry, the DR can be placed in two orthogonal orientations upon the feed line, resulting in two different antenna configurations. Figure A.2 illustrates a schematic layout of the antenna.

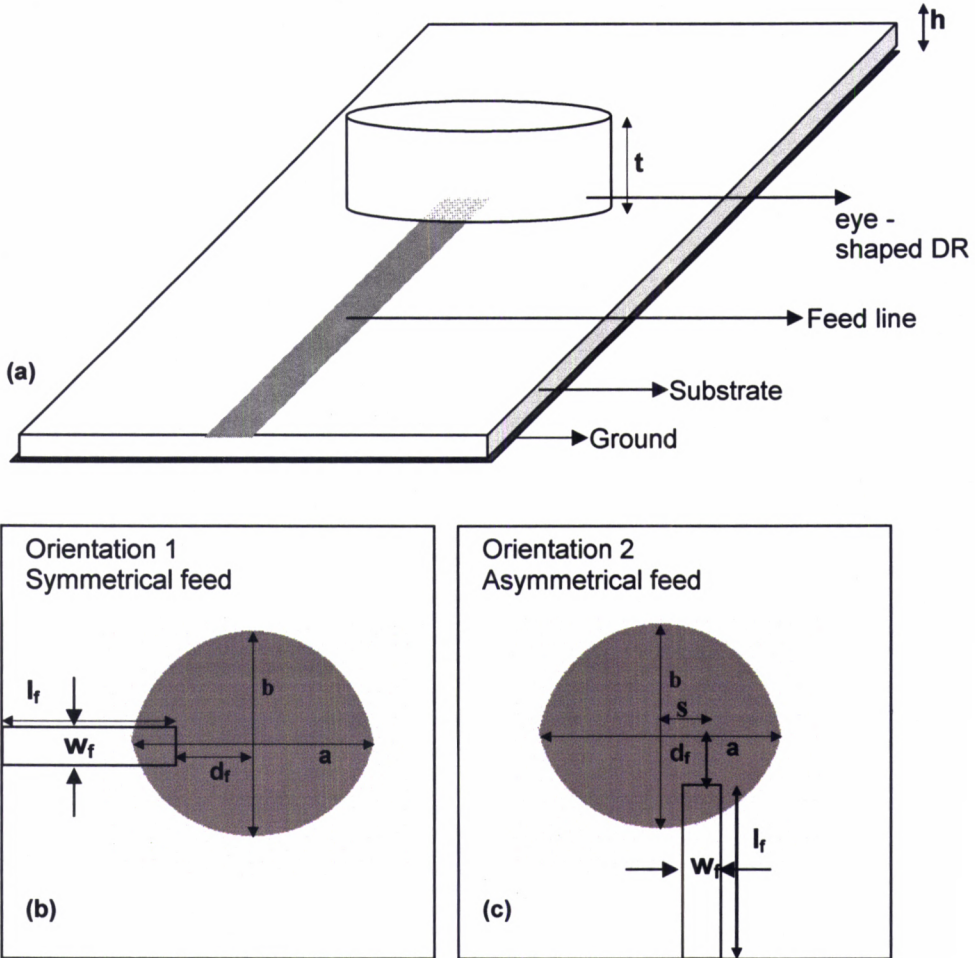


Figure A.2 The eye shaped DRA

- (a) Geometry
 (b) Top view of orientation 1 : $d_f = 1.25$ cm
 (c) Top view of orientation 2 : $d_f = 0.6$ cm, $s = 0.75$ cm
 $h=0.16$ cm, $t=0.75$ cm
 $a = 3.05$ cm, $b = 2.35$ cm, $l_f = 3.5$ cm, $w_f = 3$ cm
 ground plane dimensions : 7×7 sq cm

Dual band operation is obtained by exciting various resonant modes of the eye shaped DR using a direct 50Ω Microstrip line feed of length 3.5 cm fabricated on FR4 substrate ($\epsilon_r=4.28$, $h=0.16$ cm). The DR is moved along the feed line and its position is optimized for maximum bandwidth. The measurements are repeated for the orthogonal orientation of the DR upon the feed line.

A.3 Experimental results

Numerous resonant modes of the DRA are observed, the prominent being the bands centered at ~ 1.9 GHz and ~ 2.3 GHz. The return loss characteristics at the optimum bandwidth position of the DR in the two orientations is plotted in Figure A.3.

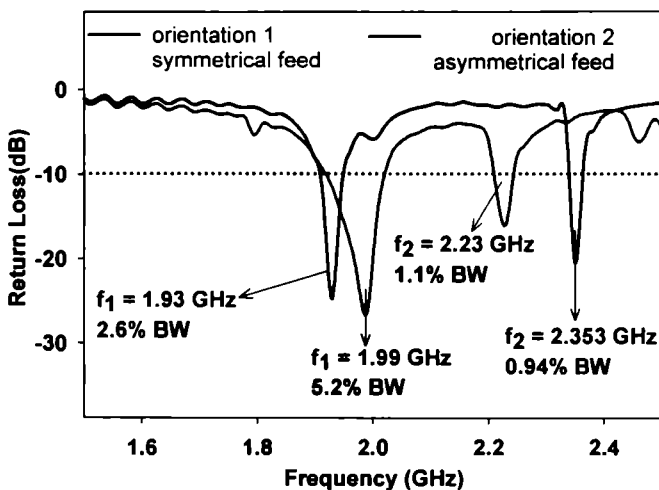


Figure A.3 Reflection characteristics of the eye shaped DRA measured at the optimum bandwidth position
ground plane dimensions : 7×7 sq cm
orientation 1: $d_r = 1.25$ cm
orientation 2: $d_r = 0.6$ cm, $s = 0.75$ cm

The 2:1 VSWR bandwidth exhibited by the antenna in orientation 1 of the symmetrically fed DR is 2.6% and 0.94% at 1.93 GHz and 2.353 GHz respectively. In orientation 2, maximum bandwidth is exhibited by the antenna for the

asymmetrical positions of the DR upon the feed line. Here the bandwidth is 5.2% and 1.1% at 1.99 GHz and 2.23 GHz respectively. Figure A.4. illustrates the gain of the antenna measured in the lower resonant band of the two orientations. The measured gain of the antenna is 8.57 dBi and 9 dBi in the two orientations respectively. However the higher band exhibits lesser gain.

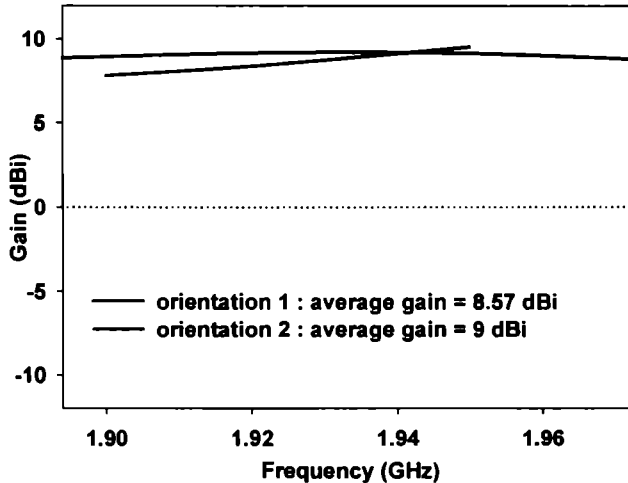


Figure A.4 Gain of the eye shaped DRA measured in the lower resonant band
 ground plane dimensions : 7 x 7 sq cm
 orientation 1: $d_r = 1.25$ cm
 orientation 2: $d_r = 0.6$ cm, $s = 0.75$ cm

The measured radiation patterns in the lower operating band of the DRA is shown in Figure A.5. The patterns are reasonably broad in both E and H Planes in both the orientations, indicating the usefulness of the antenna in wireless applications. The E plane and H plane 3 dB beam width of the antenna is 98° and 94° in orientation 1 and 122° and 102° in orientation 2 respectively. Though the antenna exhibits broad radiation patterns in the upper resonant band, the gain is less in comparison with the lower band. Nevertheless, incorporating active components into the circuitry can provide gain enhancement, thereby enabling efficient use of the upper operating band as well. The antenna exhibits linear polarization in both the bands. The antenna is

compact in geometry, with considerable reduction in area when compared to a standard rectangular / circular patch operating at the same frequency as shown in Table.A.1

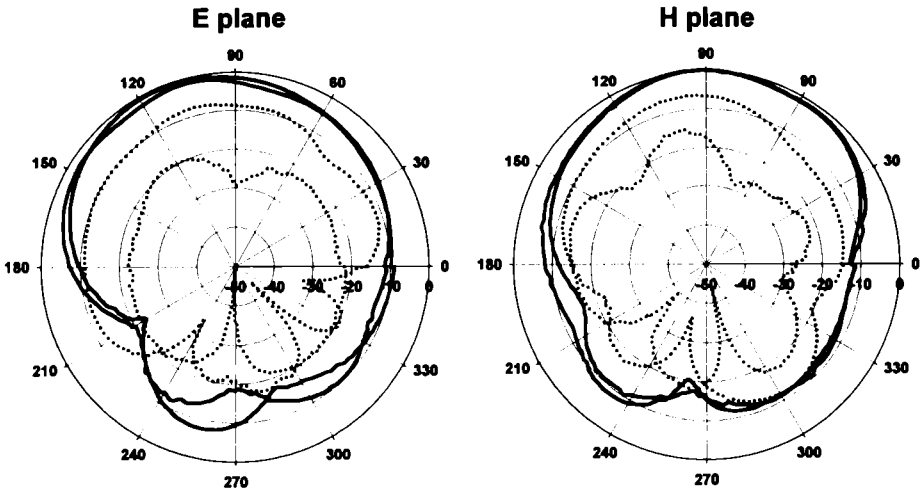


Figure A.5. Radiation pattern of the eye shaped DRA in the two orientations of the resonator
 _____ co-polar cross-polar
 orientation 1 : $f = 1.93$ GHz: $d_r = 1.25$ cm
 orientation 2 : $f = 1.99$ GHz (d_r, s)=(0.6, 0.75)cm

Resonant frequency	Dimensions (cm)		
	Eye DRA	Rectangular Patch antenna	Circular Patch antenna
1.9 GHz	$a=3.05$ $b=2.35$ $t=0.75$	length = 3.78 width = 4.86 area = 18.4 sq cm	radius = 2.235 area = 15.7 sq cm
2.3 GHz	area = 11.48 sq cm	length = 3.12 width = 4.01 area = 12.5 sq cm	radius = 1.77 area = 9.84 sq cm

Table A.1 Comparison of the dimensions of the eye – shaped DRA with standard Microstrip patch antennas operating in the same band

A.4 Conclusions

The very high permittivity ($\epsilon_r=100$) eye shaped DRA exhibits multiband resonances centered at ~ 1.9 GHz and 2.3 GHz. Two different orientations of the DR discussed here displays moderate bandwidth, broad radiation patterns and good gain in the lower resonant band. The above features make the antenna highly suitable for Mobile Communication applications.

References

1. N.Chiba, T.Amano and H. Iwasaki, "Dual-frequency planar antenna for handsets," *Electron.Lett.*, vol.34, no.25, pp.2362-2363, 10 Dec 1998.
2. Yong-Xin Guo, M.Y.W.Chia and Z.N.Chen, "Miniature built-in quad-band antennas for mobile handsets," *IEEE Antennas and wireless propagat.letters*, vol.2, pp. 30-32, 2003.
3. D.S.Yim, J.Kim and S.O.Park, "Novel wideband internal chip antenna for PCS / IMT-2000 Dual-band applications," *Microwave Opt Technol Lett.*, vol.40, no.4, pp. 324-326, 20 Feb 2004.
4. A.Petosa, A.Ittipiboon, Y.M.M.Antar, D.Roscoe and M.Cuhaci, "Recent Advances in Dielectric Resonator Antenna Technology," *IEEE Antennas Propag. Mag*, vol.40, no.3, pp. 35-48, June 1998.
5. Jung-Ick Moon and Seong-Ook Park, "Dielectric Resonator Antenna for dual band PCS/IMT-2000," *Electron.Lett.*, vol.36, no.12, pp.1002-1003, 8 June 2000.
6. D.Cormos, A.Laisne, R.Gillard, F.Le Bolzer and C.Nicolas, "Compact Dielectric Resonator Antenna for WLAN applications," *Electron.Lett.*, vol.39, no.7, pp.588-590, 3 April 2003.

Microstrip Antenna with reduced radiation hazards for Mobile telephone handset applications

A novel antenna configuration comprising of two Circular Microstrip Antennas placed back to back and separated by a thickness comparable to a typical mobile handset is presented. The antennas resonate in the fundamental TM_{11} and the higher order TM_{21} mode, producing a radiation pattern with a quiet zone in the quadrant facing the user.

B.1 Introduction

The monopole antenna has been the dominant radiating element in mobile telephones by virtue of its omnidirectional radiation pattern, large bandwidth and low cost. But the need for a more compact, lightweight antenna makes the Microstrip antenna an ideal substitute for mobile terminals [1]. Also while in use, the handset is placed close to the head of the user within the near field zone of the antenna where most of the electromagnetic energy is stored rather than radiated. This results in considerable amount of user exposure to the RF power. The energy absorbed in the head is proportional to the square of the magnetic field strength at the location of the tissue [2]. The mass energy absorption (referred to as the Specific absorption rate -SAR) is limited to 1.6W/Kg averaged over 1 gram of tissue [3]. In general, large absorption values correlate with poor radiation performance. A mobile telephone antenna must therefore, not only radiate at full strength in order to communicate properly with the base station transmitters, but also reduce the power density incident upon the user.

B.2 Design and Experimental details

The antenna configuration comprising of two Circular Microstrip Antennas (CMA's) is placed back-to-back on either side of the handset of thickness 'd' as shown in Figure B.1. Both the antennas are excited in phase and amplitude using a 3 dB power divider, with the CMA resonating in the higher order TM_{21} mode placed on the side of the handset facing the user and the CMA resonating in the fundamental TM_{11} mode placed on the opposite side, away from the user. The antennas are mounted in such a way so as to match the polarization. The CMA resonating in the fundamental TM_{11} mode radiates a broad side directed beam, whereas the higher order TM_{02} and TM_{21} modes radiate with a null in the broadside direction [4]. However, the area of a TM_{21} mode CMA is nearly 35% less than that of a TM_{02} mode CMA. Hence this mode is used in obtaining the null in the radiation pattern, thereby forming a silent zone where the user's head is safely located.

The antennas are designed for a resonant frequency of 2 GHz and fabricated on a substrate of relative permittivity $\epsilon_r = 4.28$ and thickness $h=0.16$ cm. The TM_{11} and TM_{21} mode CMA's of radii $r_1 = 2.02$ cm and $r_2 = 3.38$ cm respectively, are fed at radial distances of $\rho_1 = 0.7$ cm and $\rho_2 = 2$ cm. Finite ground planes of radii 2.2 cm and 3.5 cm respectively are used for the above antennas.

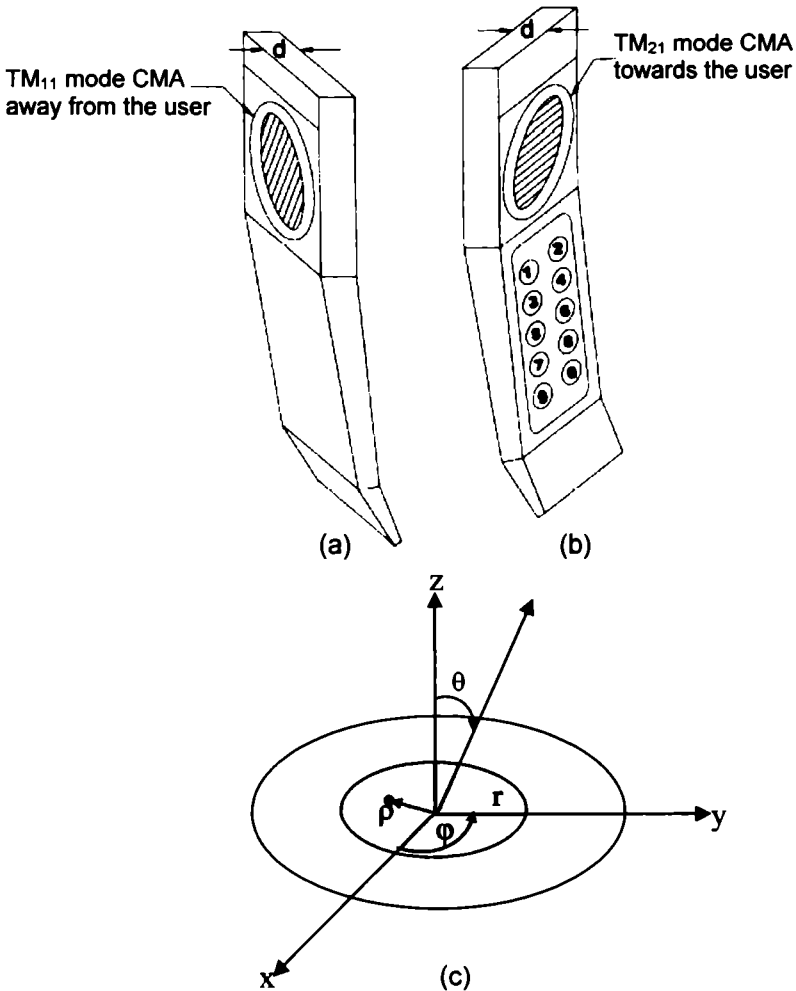


Figure B.1 The back-to-back antenna configuration
 (a) Back view (b) front view
 (c) Geometry of the Microstrip antenna element

The return loss characteristics of the individual antennas along with that of the combined set up is shown in Figure B.2. It is observed that the TM_{11} and TM_{21} CMA's operate in the same frequency band centred at ~ 2.01 GHz displaying 1.4% and 1.3% bandwidth respectively. The combined antenna configuration gives a bandwidth of 4.7%. The radiation pattern of the antenna along $\phi = 0^\circ, 45^\circ, 90^\circ$ and 135° planes are shown in Figure B.3 (a).

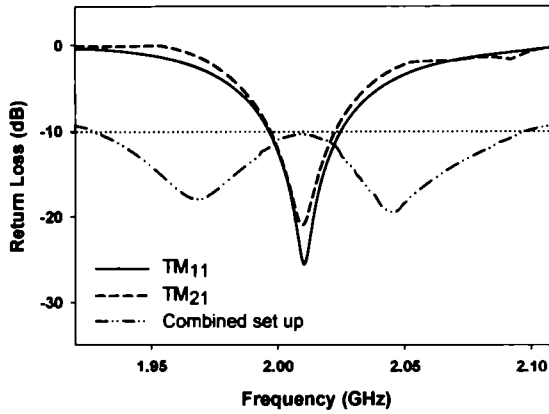


Figure B.2 Return loss characteristics of the back-to-back antenna configuration

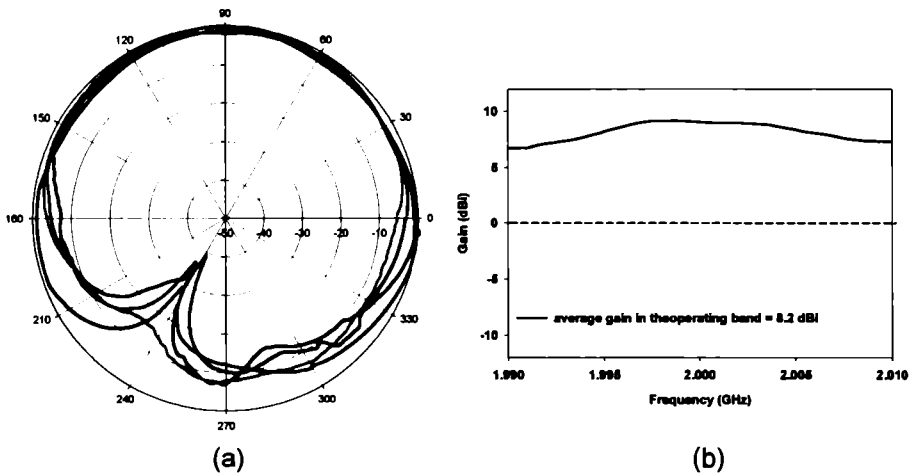


Figure B.3 Radiation characteristics of the back-to-back antenna configuration

(a) Radiation Pattern (b) Gain
 ——— $\phi = 0^\circ$ ——— $\phi = 90^\circ$
 ——— $\phi = 45^\circ$ ——— $\phi = 135^\circ$

The figure indicates considerable reduction in radiation intensity in the quadrant facing the user [$\theta=180^\circ$ to 270°]. The suitability of the antenna configuration for Mobile telephone handsets is thus confirmed. Proper spacing, excitation phase and amplitude of TM_{11} and TM_{21} mode CMA's can trim the radiation pattern further. The combined antenna configuration exhibits good gain in the operating band as shown in Figure B.3 (b). This may be due to the constructive interference between the back lobe and front lobe of the CMA's.

B.3 Conclusions

A compact Microstrip antenna configuration suitable for Mobile telephone handsets is presented. The radiation characteristics of this novel configuration shows reduced radiation intensity in the region facing the user's head.

References

1. A.Serrano-Vaello and D.Sanchez-Hernandez, "Printed antennas suitable for dual-band GSM/DCS 1800 mobile handsets," *Electron.Lett.*, vol.34, no.2, pp.140-141, January 1988.
2. R.Y.Tay, Q.Balzano and N.Kuster, "Dipole configurations with strongly improved radiation efficiency for hand-held transceivers," *IEEE Trans. Antennas Propagation*, vol.46, no.6, pp.798-806, June 1998.
3. Gianluca Lazzi, Shyam S.Patnaik, Cynthia.M.Furse and Om.P.Gandhi, "Comparison of FDTD Computed and measured radiation patterns of commercial mobile telephones in presence of the human head," *IEEE Trans. Antennas Propagat.*, vol 46, no.6, pp. 943-944, June 1998.
4. L.Shafai and A.A.Kishk, "Analysis of Circular Microstrip Antennas," *Handbook of Microstrip Antennas*, James.J.R & Hall.P.S., vol.1, London, U.K: Peter Peregrinus, pp.45 – 110, 1989.

LIST OF PUBLICATIONS OF THE AUTHOR

International Journal

1. **S.Mridula**, Jacob George and P.Mohanana, "Microstrip Antenna for Mobile Telephone Handset with reduced radiation hazards," **Microwave and Optical Technology letters**, Vol.23, No. 6, pp. 370 – 372, December 20 1999.
2. Binu Paul, **S. Mridula**, C.K.Aanandan and P.Mohanana, "A new Microstrip Patch Antenna for Mobile Communications and Bluetooth applications," **Microwave and Optical Technology letters**, Vol.33, No.4, pp. 285 – 286, May 20 2002.
3. **S.Mridula**, Sreedevi.K.Menon, B.Lethakumary, Binu Paul, C.K.Aanandan and P.Mohanana, "Planar L–Strip fed broadband Microstrip Antenna," **Microwave and Optical Technology letters**, Vol. 34, No.2, pp 115-117, July 20 2002.
4. **S.Mridula**, Sreedevi.K.Menon, P.Mohanana, P.V.Bijumon and M.T.Sebastian, "Characteristics of a Microstrip excited high permittivity Rectangular Dielectric Resonator Antenna," **Microwave and Optical Technology letters**, Vol. 40, No.4, pp 316-318, February 20 2004.
5. Binu Paul, **S.Mridula**, P.Mohanana, P.V.Bijumon and M.T.Sebastian, "A compact very-high-permittivity Dielectric-eye Resonator Antenna for multiband wireless applications," **Microwave and Optical Technology letters**, Vol. 43, No.2, pp.118-121, October 20 2004.
6. Rohith.K.Raj, Manoj Joseph, Binu Paul, **S.Mridula** and P.Mohanana, "A printed compact coplanar antenna," Paper communicated to **IEEE Microwave and Wireless Component Letters**.

International Conference

1. **S.Mridula**, Jacob George and P.Mohanana, "A compact Mobile Telephone Handset Antenna," Proc. **Second International Conference on Information, Communication and Signal Processing (ICICS'99)**, Nanyang Technological University, Singapore, December 7-10 1999.
2. **S.Mridula**, Binu Paul, C.K.Aanandan and P.Mohanana, "Octagon Shaped Microstrip Patch Antenna for dual band applications," Proc. **IEEE Antennas and Propagation Society International Symposium, Texas**, July 16-21 2002.
3. **S.Mridula**, Sreedevi.K.Menon, K.Vasudevan, P.Mohanana, P.V.Bijumon and M.T.Sebastian, "Microstrip fed compact Rectangular Dielectric Resonator Antenna," Proc. **First International Conference on Microwaves, Antennas, Propagation and Remote Sensing (ICMARS 2003)**, International Centre for Radio Science, Jodhpur, December 15-19 2003.
4. **S.Mridula**, Sreedevi.K.Menon, Binu Paul, C.K.Aanandan K.Vasudevan, P.Mohanana P.V.Bijumon and M.T.Sebastian, "Experimental investigations on a Microstrip fed compact Rectangular Dielectric Resonator Antenna," Proc. **International Conference on Computers and Devices for Communication (CODEC–04)**, Institute of Radio Physics and Electronics, University of Calcutta, January 1-3 2004.

5. Binu Paul, **S.Mridula**, Sreedevi.K.Menon, C.K.Aanandan, P.Mohanan, P.V.Bijumon and M.T.Sebastian, "Time Domain Analysis of a Microstrip Line excited compact Rectangular Dielectric Resonator Antenna," Proc. **20th Annual Review of Progress in Applied Computational Electromagnetics (ACES-04)**, Syracuse, NewYork, April 19-23 2004.
[Paper presented]
6. **S. Mridula**, Binu Paul, Sreedevi.K.Menon, C.K.Aanandan, P.Mohanan, P.V.Bijumon and M.T.Sebastian "Wideband Rectangular Dielectric Resonator Antenna for W-LAN applications," Proc. **IEEE Antennas and Propagation Society International Symposium**, Monterey, June 20-25 2004
7. Binu Paul, **S.Mridula**, C.K.Aanandan, K.Vasudevan and P.Mohanan, "Electromagnetically Coupled Dual Port, Dual Band, Octagonal Patch Antenna," Proc. **IEEE International conference on Personal Wireless Communication (ICPWC 2005)**, New Delhi, January 23-25 2005.
8. **S.Mridula**, Binu Paul, K.Vasudevan P.Mohanan, P.V.Bijumon and M.T.Sebastian, "Rectangular Dielectric Resonator Antenna configurations for Mobile Communication applications," accepted for poster presentation at **URSI GA 2005**, New Delhi, October 2005.
9. Binu Paul, **S.Mridula**, C.K.Aanandan, K.Vasudevan and P.Mohanan, "Octagonal Microstrip Patch Antenna for dual band applications," accepted for poster presentation at **URSI GA 2005**, New Delhi, October 2005.

Citation – International Journal

1. 4 Citations on the paper:
S.Mridula, Jacob George and P.Mohanan, "Microstrip Antenna for Mobile Telephone Handset with reduced radiation Hazards," **Microwave and Optical Technology letters**, Vol. 23, No. 6, December 20 1999, pp. 370 – 372.
Source – www.isinet.com/iso/products/citation
2. Comments on the paper:
Binu Paul, **S. Mridula**, C.K.Aanandan and P.Mohanan, "A Microstrip Patch Antenna for Mobile Communications and Bluetooth Applications," **Microwave and Optical Technology letters**, Vol.33, No.4, pp. 285-286, May 20 2002.
Microwaves and RF, R&D round up column, pp. 54, August 2002.

National Conference

1. **S.Mridula**, Jacob George, K.Vasudevan and P.Mohanan, "Low radiation hazard Microstrip Antenna for Mobile telephone handset," Proc. **Zonal Seminar on Modern Trends in Personal Communication**, IETE Cochin, pp. 30-32, May 4-5 1999.
[Paper presented]
2. **S.Mridula**, G.S.Binoy, C.K.Aanandan, K.Vasudevan and P.Mohanan, "Multilayer Bowtie Microstrip Antenna," Proc. **National Conference on Technology Convergence for Information, Communication, and Entertainment (NICE 2001)**, IETE Cochin, pp. 195–199, February 23-24 2001.
[Paper presented]

3. I.Shyju Mon, Binu Paul, **S.Mridula**, C.K.Aanandan, K.Vasudevan and P.Mohanan, "Rectangular Microstrip Antenna for Mobile Communications and Bluetooth Applications," Proc. **National Conference on Microwaves, Antennas and Propagation (MICROWAVE 2001)**, Jaipur, pp. 24-26, November 2-4 2001.
4. **S.Mridula**, Binu Paul, I.Shyju Mon, C.K.Aanandan and P.Mohanan, "Dual Polarized Electromagnetically coupled Microstrip Antenna," Proc. **National Conference on Microwaves, Antennas and Propagation (MICROWAVE 2001)**, Jaipur, pp. 145-147, November 2-4 2001.
5. **S.Mridula**, Binu Paul, C.K.Aanandan, K.Vasudevan and P.Mohanan, "Dual Band Octagonal Patch Antenna suitable for PCS and Bluetooth Applications," Proc. **Interactive Integrated Technological Advancement-Recent Trends (IITART)**, College of Engineering, Trivandrum, pp. 88-95, July 5-6 2002. [Paper presented]
6. Binu Paul, **S.Mridula**, C.K.Aanandan and P.Mohanan, "Dual Band Octagonal Patch Antenna," Proc. **National Symposium on Antennas and Propagation (APSYM 2002)**, Cochin, pp. 245-248, December 9-11 2002.
7. Binu Paul, **S.Mridula**, C.K.Aanandan, K.Vasudevan and P.Mohanan, "Time domain analysis of Octagonal Microstrip Patch Antenna by conformal FDTD method," Proc. **National Symposium on Antennas and Propagation (APSYM 2004)**, Cochin, pp. 117-121, December 21-23 2004.
8. **S.Mridula**, Binu Paul, C.K.Aanandan, H.Sreemoolanadhan, V.Chandrasekaran and P.Mohanan, "Rectangular Dielectric Resonator Antenna for 2.4 GHz W-LAN Applications," Proc. **National Symposium on Antennas and Propagation (APSYM 2004)**, Cochin, pp. 215-218, December 21-23 2004. [Paper presented]

RESUME OF THE AUTHOR

MRIDULA.S

Research Scholar
Department of Electronics
Cochin University of Science and Technology
Kochi – 682 022, INDIA
Phone: 91-484-2576418
E-mail: mridula@cusat.ac.in

Objective:

To involve in research activities in the field of Mobile Communication antennas, Numerical Modelling techniques and Biological effects of Microwaves.

Education:

M.Tech Electronics
Specialization: Microwave and Radar Electronics
Cochin University of Science and Technology (1999)
Score: 82.9% - First class with Distinction and First Rank

B. Tech Electronics and Communication
College of Engineering, Trivandrum
Kerala University (1988)
Score: 77.9% - First class with Distinction

Academic Honours:

Recipient of the **K.G. Nair Endowment Gold Medal** for securing First Rank in the M.Tech Electronics Examination conducted by the Cochin University of Science and Technology in July 1999.

Research Experience:

Worked as project associate in the UGC Major research project entitled, "Development of a compact Microstrip Antenna with reduced radiation hazards suitable for use in Mobile Communication handsets" from July 2003 – January 2005.

Principal investigator of the DST-SERC FAST TRACK Project entitled, "Design, development and analysis of a compact Microstrip antenna with reduced radiation hazards towards the human head", October 2004 onwards [Rs.4.02 Lakhs].

Participation in National / International Conferences:

Participated and presented research papers at 4 National conferences and at the '20th Annual Review of Progress in Applied Computational Electromagnetics (ACES - 04)', held at Syracuse University, Syracuse, New York during April 19-23 2004.

Publications:

International Journal : 5
International Conference : 9
National Conference : 8

Citation:

Comments on the paper:

Binu Paul, **S. Mridula**, C.K.Aanandan and P.Mohanan, "A Microstrip Patch Antenna for Mobile Communications and Bluetooth Applications," **Microwave and Optical Technology letters**, Vol.33, No.4, pp. 285-286, May 20 2002.

Microwaves and RF, R&D round up column, pp. 54, August 2002.

Computer Proficiency:

C, MATLAB
Simulation Software: IE3D, Fidelity, Microwave Studio, HFSS

Work experience:

15+ years teaching experience

Lecturer in Electronics (27.6.1990 – 6.7.1999)
Institute of Human Resource Development (IHRD)
Govt. of Kerala

Lecturer in Electronics (7.7.1999 onwards)
Division of Electronics and Communication Engineering
School of Engineering
Cochin University of Science and Technology, Kochi – 682 022

Membership in Professional bodies:

Life member- Indian Society for Technical Education (ISTE)
Life member- Institute of Electronics and Telecommunication Engineers (IETE)

INDEX

-
- A
- a-b-d orientation 184, 218
 Absorbing Boundary Condition 118, 121
 Accuracy 11, 111, 125, 126, 127, 146,
 148, 159, 185, 194, 220
 a-d-b orientation 262, 276
 Analytical techniques 10
 Antar 18, 19, 20, 21, 63, 65, 66, 67, 68,
 69, 70, 83, 104, 105, 107, 316
 Antenna 3
 Antenna Applications 6
 Antenna Design Parameters 6
 Aspect ratio 143
- B
- b-a-d orientation 144, 183
 Balanis 22, 107
 Bandwidth 5, 6, 12, 20, 25, 27, 28, 29,
 30, 31, 32, 33, 34, 35, 36, 37,
 39, 40, 41, 42, 43, 44, 45, 46,
 47, 48, 52, 54, 55, 56, 63, 64,
 67, 79, 84, 86, 278, 283, 289, 291, 299
 b-a-d 146, 155, 157, 161, 173
 a-b-d 185, 190, 192, 196, 208
 d-a-b 220, 224, 226, 228, 236
 d-b-a 249, 251, 252, 258
 a-d-b 263, 264, 265, 272, 275
 b-d-a orientation 281
 Beam width 177, 213, 243, 254, 268
 Berenger 122, 138
 Boundary conditions 118
 Broadband dielectric antenna 5
- C
- Cell size 123, 125, 126, 132
 Central differences 112
 Compactness 154, 189, 223, 286, 292
 Computational domain 132
 Computational Electromagnetics 10
 Courant-Friedrichs-Lewy Stability criterion
 127
- D
- Cross polarization 177, 213, 243,
 254, 268
- d-a-b orientation 219, 248
 d-b-a orientation 249, 261
 Dielectric antennas 4
 Dielectric Constant 78, 94
 Dielectric excited antenna 5
 Dielectric interface 121
 Dielectric loaded antenna 5
 Dielectric Resonator 37, 77
 Rectangular DR samples 92
 Dielectric Resonator Antenna 5, 38, 75
 Eye shaped DRA 311
 Rectangular DRA 86, 141
- E
- Electromagnetic modelling 11
 Esselle 21, 43, 53, 66, 71
 Excitation techniques
 Aperture coupled 42, 89
 Coaxial Probe 39, 88
 Coplanar wave guide 46, 90
 Microstrip line 47, 90
 Expert systems 10
- F
- Far field computation 134
 Finite Difference Time Domain Method
 17, 49, 111
 Flow chart 123
 3D FDTD modeller 131
 Field distribution 150, 188, 222, 250,
 263, 285, 293
 Finite Element Method 14
 Fourier transform 127, 134
 Frequency bands 9
 Front to back ratio 177, 213, 243, 254, 268
-

- G**
- Gain
 b-a-d 148, 174, 175, 176
 a-b-d 187, 209, 210, 211
 d-a-b 222, 238, 239, 240
 d-b-a 255
 a-d-b 269
Gain-transfer method 101
Gaussian pulse 128
GPS 9, 284, 288
Grid lay out 132
GSM 9, 284, 288
- H**
- HFSS 153, 188, 222, 250, 263, 284, 292
- I**
- Input impedance 134
Ittipiboon 18, 19, 20, 21, 42, 51, 63, 64,
65, 66, 67, 68, 69, 70, 105, 106, 107,
139, 316
- K**
- Kajfez 64, 66, 69, 72, 104
Kishk 21, 39, 41, 49, 54, 55, 56, 63, 64,
66,69, 70, 72, 73, 105, 322
Kranenburg 46, 47, 67, 68
- L**
- Leap-frog time integration 116
Length of the feed line 98
Leubbers 130, 139
Long 64, 65, 104
Luk 19, 20, 21, 22, 45, 46, 48, 50, 51, 58,
62, 64, 65, 66, 67, 68, 69, 70, 71, 105,
106, 107
- M**
- MATLAB 131
Maxwell's equations 11, 12, 86, 112
Measurement techniques 100
 Gain 101
 Radiation pattern 101
 Resonant frequency 100
Method of Moments 12, 13
Mobile Communication 6
 Handset antennas 27
Modes 83, 137, 149
- Mongia 18, 19, 39, 40, 42, 49, 51, 63, 64,
65, 66, 68, 69, 70, 86, 104, 106, 107
Mur's ABC 121
- N**
- Network analyser 81, 100
Numerical techniques 10, 49
- O**
- Optimum bandwidth positions
180,215,245,259,274
Orientation of the DR 96
- P**
- PCS 1900 9, 284, 288
Perfect Electric Conductor (PEC) 119
Perfect Magnetic Conductor (PMC) 120
Perfectly Matched Layer (PML) 122
Polarization 148, 187, 221
Position of the DR 96, 179, 214, 244
- Q**
- Quality Factor 79
- R**
- Radiation characteristics of the DRA
 b-a-d 176,177
 a-b-d 211,213
 d-a-b 241,243
 d-b-a 254,256
 a-d-b 268,270
 Salient features 306
Radiation hazards 303, 317, 323, 326
Radiation Patterns 147,186, 220, 252,
266, 287, 295
Raj Mittra 22, 52, 71, 72, 106, 139
Return loss characteristics
 b-a-d 146,172
 a-b-d 185,207
 d-a-b 220,237
 d-b-a 250
 a-d-b 263
Richtmyer 37, 62, 77, 104
- S**
- Scheme of Work 92
Sheen 104, 116, 138
Source modelling 127

Stability 37, 78, 80, 91, 126
Stub matching 229

T

Taflove 17, 21, 22, 126, 139
Temperature Coefficient 81
Time step 16, 17, 115, 119, 123, 125,
126, 127, 128, 135
Transmission Line Matrix 16
Truncated ground plane 154, 157, 189,
192, 224, 226

W

W-LAN applications 298

Y

Yee 17, 22, 38, 83, 112, 116, 117, 119,
120, 121, 126, 138
Yee lattice 112

Z

Zimmerman 139